

**Stability of Finite Element Solutions to
Maxwell's Equations in Frequency Domain**

Von der Fakultät für Geowissenschaften, Geotechnik und Bergbau
der Technischen Universität Bergakademie Freiberg

genehmigte

DISSERTATION

zur Erlangung des akademischen Grades

doctor rerum naturalium

(Dr. rer. nat.)

vorgelegt

von Dipl.-Geophys. Christoph Schwarzbach

geboren am 31. Oktober 1977 in Görlitz

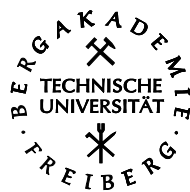
Gutachter: Prof. Dr. Klaus Spitzer, Freiberg
Prof. Dr. Peter Weidelt, Braunschweig
Prof. Dr. Eldad Haber, USA

Tag der Verleihung: 10. August 2009

Dissertation

Stability of Finite Element Solutions to Maxwell's Equations in Frequency Domain

Christoph Schwarzbach



This dissertation has been submitted in partial satisfaction of the requirements for the degree of *doctor rerum naturalium* (Dr. rer. nat.) in Geophysics and approved by the Faculty of Geosciences, Geoengineering and Mining of the Technische Universität Bergakademie Freiberg, Germany.

Assessors: Prof. Dr. Klaus Spitzer, Freiberg
Prof. Dr. Peter Weidelt, Braunschweig
Prof. Dr. Eldad Haber, USA

Doctorate awarded on August 10, 2009.

Published electronically by Universitätsbibliothek 'Georgius Agricola', Technische Universität Bergakademie Freiberg, Agricolastraße 10, 09599 Freiberg/Sachsen, Germany, 2009.

Contents

1	Introduction	1
2	Boundary value problems	7
2.1	Fundamentals	7
2.1.1	Basic notation	7
2.1.2	Maxwell's equations	8
2.2	Derived systems	12
2.2.1	Simple approach – The E -field formulation	13
2.2.2	The kernel of the curl-operator	15
2.2.3	Mixed approach – The E - V formulation	18
2.3	The weak form	20
2.4	A change of coordinates	25
2.5	Anisotropy	26
3	The finite element method	31
3.1	Finite elements for Maxwell's equations	31
3.2	Derivation of the system of linear equations	44
3.2.1	Geometric decomposition	44
3.2.2	Finite dimensional function spaces	44
3.2.3	Trial functions	46
3.2.4	Test functions	46
3.3	An <i>a posteriori</i> error indicator	49
3.4	Implementation	51
3.4.1	The finite element kernel	52
3.4.2	The finite element software suite	56
3.5	Numerical experiments	59
3.5.1	Matrix condition number	59
3.5.2	A symmetric matrix scaling	59
3.5.3	Iterative or direct solvers?	61
3.5.4	Compatible polynomial spaces for the E - V formulation	65
3.5.5	Low frequency stability	67
4	Enhanced concepts	83
4.1	Scattered field problems	83

Contents

4.1.1	The boundary value problem	84
4.1.2	The weak form	85
4.1.3	Finite element solution	87
4.1.4	Incident fields	88
4.2	Absorbing boundaries – The perfectly matched layer	89
4.2.1	Construction of a perfectly matched layer	91
4.2.2	Properties of a uniaxial PML	97
4.2.3	The PML in three dimensions – An example	109
5	Application – Marine controlled source electromagnetics	113
5.1	Canonical disk model	114
5.2	Seafloor topography	121
6	Summary and outlook	131
	Appendices	135
A	Formulary	135
A.1	Vector identities	135
A.2	Integral identities	136
B	The mixed dielectric and conductive media case	137
C	Removing a non-trivial normal cohomology space	140
C.1	The continuous problem	140
C.2	The discrete problem	145
C.3	Numerical experiments	149
D	Sensitivity calculation	161
E	Plane wave within a horizontally stratified earth	164
	Bibliography	167

Chapter 1

Introduction

Electromagnetic methods in geophysics cover a broad frequency spectrum. Ordered by increasing frequency they comprise direct current, low induction number, induction and wave propagation methods, irrespective of a time-harmonic or transient time characteristic. The thesis presents the theoretical framework for the numerical solution of time-harmonic, or frequency domain, Maxwell's equations using the finite element method. Yet, transient, or time domain, problems could easily be taken into account by Fourier synthesis of a number of frequency domain problems. Restriction to the time-harmonic case directs the focus on the properties of the particular finite element types which are used to spatially approximate the electromagnetic fields. These elements would also form the basis for the spatial semi-discretization of time-dependent problems. However, the delicacies of time stepping schemes are avoided here.

The intention of the practical part of this work was to provide a flexible and powerful all-purpose solver for the Maxwell system. Accordingly, the problem formulation is carried out in an as general as possible way. The finite element method has been chosen amongst the existing numerical methods which compute an approximate solution to Maxwell's equations. It provides the greatest flexibility regarding model geometry, the option for a higher order spatial approximation and a rigorous framework for the treatment of virtually arbitrary constitutive parameter distributions. Early applications of the finite element method to frequency domain electromagnetic problems in the geophysical literature date back to the 1970s and 80s (Coggon, 1971; Reddy, Rankin, and Phillips, 1977; Pridmore, Hohmann, Ward, and Sill, 1981; Mur and Hoop, 1985). With the advent of more powerful computers, the development of sophisticated direct solvers for systems of linear equations, and the request for a greater geometrical flexibility the finite element method has recently regained attention (Mogi, 1996; Zanolubi, Jin, Donepudi, and Chew, 1999; Zyserman and Santos, 2000; Badea, Everett, Newman, and Biro, 2001; Mitsuhata and Uchida, 2004). The implemental overhead required for the treatment of unstructured meshes, higher order spatial approximations and a general representation of constitutive parameters, boundary values and source terms goes at the expense of an intricate software design. However, these features are supported by the finite element method. In contrast to that, the finite difference method (Mackie, Madden, and Wannamaker, 1993; Newman and Alumbaugh, 1995; Smith, 1996) is far easier implemented but is restricted to tensor product grids and to piecewise constant constitutive parameters. Usually, it is only derived with spatial approximations of first or second order. The finite volume method potentially provides the same flexibility as the finite element method. However, applications to

geophysical problems reported in the literature (Haber, Ascher, Aruliah, and Oldenburg, 2000; Haber and Ascher, 2001; Weiss and Constable, 2006) only involve structured grids and piecewise constant parameter distributions. Quite recently, a subgridding technique has been proposed by Haber and Heldmann (2007) as a generalization. The integral equation method (Hohmann, 1975; Weidelt, 1975; Wannamaker, Hohmann, and SanFilipo, 1984; Newman, Hohmann, and Anderson, 1986; Wannamaker, 1991; Xiong and Tripp, 1997; Avdeev, Kuvshinov, Pankratov, and Newman, 1997) provides a somehow complementary approach to the finite element, finite difference and finite volume methods. Its strength is found in the solution for a possibly complex shaped anomalous parameter distribution within a simple background medium. However, its scope of application is limited in comparison to the finite element method. In order to complete the picture of numerical methods, the finite difference time domain method needs to be mentioned. As a finite difference method it is subject to the same restrictions as the frequency domain counterpart. If the time stepping is carried out by an explicit scheme, the finite difference time domain method allows for a very memory efficient implementation as it does not require storage and solution of a system of linear equations like frequency domain solvers. The finite difference time domain method is consequently the most popular approach for time dependent problems (Adhidjaja and Hohmann, 1989; Wang and Tripp, 1996; Roberts and Daniels, 1997; Chen, Chew, and Oristaglio, 1997; Teixeira, Chew, Straka, Oristaglio, and Wang, 1998; Bergmann, Robertsson, and Holliger, 1998).

Numerical simulation of most of the geophysical methods in frequency domain typically involves a number of frequencies which may cover a range of several decades. This especially holds if for example the transient of a time-domain method both at early and late times or the wave propagation of a broad spectrum radar signal for several cycles of the dominating frequency is to be computed by Fourier synthesis. A couple of conflicting interests have to be considered when a numerical algorithm is designed. A simulation involves the solution of a boundary value problem that models the relevant physical phenomena. Although all boundary value problems describing geophysical methods are naturally posed on an infinite domain the numerical solution requires that the computational domain is finite and bounded. An artificial boundary is introduced which defines the computational domain. Boundary conditions need to be posed on the artificial boundary such that the field computed on the truncated domain resembles the solution of the boundary value problem on the original, infinite domain as much as possible. These boundary conditions typically approximate the behavior of the electromagnetic field at infinity. Their approximation error is consequently a function of the distance between the artificial boundary and the sources within the computational domain. In order to keep this approximation error small the artificial boundary should be placed as far away as possible from any sources. Distance is best expressed in terms of either wavelength for wave propagation dominated applications or skin depth for induction dominated applications and consequently depends on frequency. While the boundary can be considered far away for higher frequencies this might not be true for lower frequencies. If a model is constructed for a range of frequencies the overall size of the domain is determined by the lowest frequency considered. The mesh size, i. e., the smallest element size is determined by the highest frequency because it corresponds with the smallest wavelength or skin depth that needs

to be resolved by the mesh. The product of mesh and domain size determines the computational effort in terms of the number of unknowns. Limited computational resources now impose severe constraints on the useful frequency range which can be treated by one domain size at once. This is especially true for three-dimensional problems where the mesh and domain size scale with the third power of length. An optimum mesh with respect to both distance to the boundary and element size can only be constructed for a single frequency. Multiple frequencies either require a proportional increase of numerical effort or give rise to a loss of accuracy at either end of the spectrum considered.

The increase of numerical effort might be balanced if the solution for a number of frequencies can be computed using the same domain and mesh faster than by separate domain and mesh sizes. A saving of simulation time is first of all linked with the overhead of creating the model, generating a mesh and assembling the system of linear equations. Special cases of boundary problems furthermore allow for an efficient solution of the system of linear equations for multiple frequencies (Druskin and Knizhnerman, 1999; Zanolubi et al., 1999; Börner, Ernst, and Spitzer, 2008) when the factorization of the system matrix for one frequency can be reused. For practical applications the trade-off between the saving of computational time by exploiting common data structure, increase of domain and mesh size as well as loss of accuracy needs to be carefully considered.

The main focus of this work lies on a numerically stable solution of Maxwell's equations for a single domain size with a fixed spatial discretization and for multiple frequencies. It is instructive to consider the static case as the limiting case of low frequencies. However, the approximate nature of boundary conditions mentioned previously should be kept in mind. A solution stable at low frequencies requires that an appropriate subset of differential equations is chosen from the Maxwell system and is supplemented by suitable boundary conditions. This stability consideration regards the continuous side, the formulation of the boundary value problem in terms of the electromagnetic fields as functions of space prior to any numerical approximation. The discrete side involves the application of the finite element method in order to derive a system of linear equations. Its solution expresses an approximation of the spatial distribution of the electromagnetic field by a finite number of degrees of freedom. The condition number of the coefficient matrix of the linear equation system is used as an experimental indicator for stability of the discrete problem. While the usable lower frequency limit is determined by the choice of the correct boundary value problem and the approximation error of the truncated domain boundary conditions, the upper frequency limit is governed by approximation errors of the finite spatial discretization, ultimately by the Nyquist wavelength of the mesh.

The boundary value problem can be stated in a number of different ways. A system of first order partial differential equations involving both the electric field E and the magnetic field H was solved by Mackie et al. (1993) and Zyserman and Santos (2000). If one of the fields is eliminated the vector Helmholtz equation in terms of E or H emerges which is a partial differential equation of second order. Solution of the vector Helmholtz equation in terms of E has been carried out, e. g., by Newman and Alumbaugh (1995) and Mogi (1996) and will also be the first attempt pursued

here. Other formulations can be stated in terms of the magnetic vector and the electric scalar potential (A - ϕ method; Haber et al., 2000; Badea et al., 2001), and in terms of the electric vector and the magnetic scalar potential (T - Ω method; Mitsuhata and Uchida, 2004). These two potential formulations are especially suited for low frequency problems. They involve a scalar field which will be introduced in a similar fashion here in order to augment the vector Helmholtz equation in terms of E and to stabilize the BVP for low frequencies. The resulting formulation will be called the E - V formulation. While the mixed potential formulations in terms of A and ϕ or T and Ω require both the vector and the scalar field, the scalar field of the E - V formulation can as well be dropped at higher frequencies if stabilisation is not required.

The E - V formulation suggested here is considered a partial novelty in that it is a generalisation of the E - p formulation of Demkowicz and Vardapetyan (1998). In particular, the E - V formulation (a) uses a different scaling for the scalar field and the equation of continuity; (b) introduces a zeroth-order term for V in order to account for a wider range of boundary conditions; and (c) takes into account inhomogeneous boundary conditions. In addition, a slightly transformed set of field quantities and constitutive parameters is put forward which makes use of the vacuum wavenumber instead of frequency. This approach realizes a concept which penetrates the theoretical and practical work of this thesis and can be summarized as follows:

‘Devise a formulation of the boundary value problem which reduces to its discretized form as a system of linear equations such that the coefficient matrix is symmetric, is scaled appropriately for all frequencies, and only requires a minimum of algebraic manipulation prior to solving the system.’

Based on either the E -field formulation or the E - V formulation a software package has been implemented as the practical part of this work. It encompasses a number of features and a flexibility the combination of which is, to the best of the author’s knowledge, so far unparalleled to any existing geophysical software. For example, Mogi (1996) and Mitsuhata and Uchida (2004) only consider structured meshes with linear hexahedral elements. Badea et al. (2001) present a finite element solution based on unstructured tetrahedral meshes but only with a piecewise linear approximation. They only consider isotropic parameters and neglect displacement currents. All the three papers mentioned use a set of equations different from the one considered here.

The ensued software suite gathers the following benefits:

1. Treatment of the full set of frequency domain Maxwell’s equations. All three constitutive parameters magnetic permeability, electric permittivity and electric conductivity are, in general, assumed to be non-zero, inhomogeneous and anisotropic. They are consequently expressed as piecewise polynomial matrix functions.
2. Optional use of the E -field formulation or the E - V formulation. The E - V formulation stabilizes the classical vector Helmholtz equation in terms of the electric field for low frequencies.
3. Optional use of a total field or a scattered field formulation. Incident fields are predefined for

a point electric or point magnetic dipole in a homogeneous fullspace as well as for a plane wave in a horizontally stratified earth.

4. Implementation of the anisotropic complex frequency shifted perfectly matched layer (CFS PML; Berenger, 1994; Kuzuoglu and Mittra, 1996). Definition on input by a complex coordinate stretching.
5. Support of unstructured hexahedral or tetrahedral meshes for a maximum of geometric flexibility.
6. Vector finite element approximation with piecewise polynomials of practically arbitrary order.
7. Implementation of an *a posteriori* error indicator which can guide adaptive mesh refinement, i. e., automatic mesh generation.
8. XML input file format with a self-explanatory structure.

The general design of the software allows for the simulation of almost every electromagnetic method used in geophysics. It supports the direct simulation of frequency domain methods and the simulation of time domain methods by combination with a Fast Fourier Transform (FFT).

The features of the finite element software suite of this thesis can well be compared to those of the commercial product COMSOL Multiphysics® which has reached its competitive state only recently. In order to perform the same numerical modelling using, e. g., the scattered field approach, COMSOL Multiphysics® nevertheless requires an additional piece of work which is already an integral part of the software presented here, namely, the definition of the incident fields. Implementational and design details of the software are partially hidden to the users of COMSOL Multiphysics® but can potentially be looked at in the source code of this thesis' software. Due to its availability as a package of C++/Fortran source code the software is more easily ported to different computing facilities, in particular to distributed memory architectures, than it is possible with any commercial software product.

In accordance with the practical part of the thesis its written part collects and documents the theoretical background of the software. The presented work has been written with the intention of promoting the understanding of the mathematical and numerical methods to the interested geophysicist reader. Its outline is as follows.

The derivation of the boundary value problems from Maxwell's equations with particular attention to the low frequency stability aspect as well as the derivation of their weak form equivalents are described in Chapter 2. The weak form serves as the basis for the finite element method which is described in Chapter 3. A brief summary of the particular finite element spaces and types is given, which are required for the discretization of the electromagnetic field quantities. It is followed by the derivation of the discrete boundary value problem, i. e., the system of linear equations. Some implementation details of the emerged collection of finite element software tools precede the description of the experimental part. Numerical tests have been carried out which were

designed to provide empirical evidence for the theoretical stability considerations of Chapter 2. The influence of the non-trivial nullspace of the curl-curl operator on the matrix condition seems to be considered evident throughout the literature since it is rarely demonstrated by example. This effect is illustrated here by a carefully designed series of numerical tests which are instructive in order to make this link clear.

The boundary value problem formulations introduced in Chapters 2 and 3 constitute a quite straightforward approach to the simulation of geophysical problems. It provides the framework required for the stability considerations and at the same time avoids an overly complex notation. Chapter 4 extends the model setup by two more sophisticated concepts. The so-called scattered field formulation improves the accuracy of the computed total field by assuming part of the field, the incident field, known, and by approximating only the other part, the scattered field, numerically. Furthermore, the famous perfectly matched layer (PML; Berenger, 1994) is introduced which provides a means to reduce the influence of the approximate boundary conditions on truncated domains at least for wave propagation phenomena. The PML properties are defined by the means of a continuous coordinate stretching function. This function is usually approximated by a piecewise constant, i. e., a discontinuous function. In contrast to the wealth of finite difference codes a well-designed finite element code can thoroughly treat the continuous stretching function. The benefit of doing that is demonstrated by an example. Finally, the application of the emerged finite element software suite to two marine controlled source electromagnetics (CSEM) problems is described in Chapter 5. Treatment of seafloor topography by unstructured tetrahedral meshes when simulating marine CSEM has not been reported in the geophysical literature so far. The thesis gives a first example of this. Chapter 6 finishes the thesis with a summary and an outlook.

Chapter 2

Boundary value problems of electromagnetic wave propagation – The continuous case

2.1 Fundamentals

It is convenient to start this chapter by introducing some notation that will be used throughout the remainder of this work.

2.1.1 Basic notation

While most boundary value problems in geophysics do not have natural boundaries but rather involve the whole space \mathbb{R}^3 , the numerical approximation of solutions will require a domain of finite volume. Therefore, the following considerations are restricted to the case of a finite domain $\Omega \subsetneq \mathbb{R}^3$.

The domain Ω is subdivided into a number of non-overlapping subdomains Ω_i , $\Omega = \bigcup_i \overline{\Omega}_i$ and $\Omega_i \cap \Omega_j = \emptyset$ for $i \neq j$ (Figure 2.1), such that within each subdomain constitutive parameters and source terms are continuous functions of space. Discontinuities have to coincide with interfaces between subdomains. The interface is denoted by $\Sigma_{i,j} = \overline{\Omega}_i \cap \overline{\Omega}_j$. On each interface $\Sigma_{i,j}$ the normal vector \mathbf{n} is defined to point from domain Ω_i to domain Ω_j . The normal vector makes the interface direction dependent, i. e., interchanging the indices turns the normal vector in the opposite direction and $\Sigma_{i,j} = -\Sigma_{j,i}$. The jump of a function $u(\mathbf{r})$ across the interface $\Sigma_{i,j}$ will be expressed by the short hand notation

$$[u(\mathbf{r})]_{\Sigma_{i,j}} = u^+(\mathbf{r}) - u^-(\mathbf{r}), \quad \mathbf{r} \in \Sigma_{i,j}, \quad \text{where} \quad (2.1a)$$

$$u^+(\mathbf{r}) = \lim_{\delta \rightarrow 0} u(\mathbf{r} + \delta \mathbf{n}) \quad \text{and} \quad (2.1b)$$

$$u^-(\mathbf{r}) = \lim_{\delta \rightarrow 0} u(\mathbf{r} - \delta \mathbf{n}). \quad (2.1c)$$

The boundary of Ω is denoted by $\Gamma = \partial\Omega$. It is decomposed into a number of non-overlapping parts Γ_i , $\Gamma = \bigcup_i \Gamma_i$ and $\Gamma_i \cap \Gamma_j = \emptyset$ for $i \neq j$, such that the data of boundary conditions are smooth functions on each boundary part. In particular, different types of boundary conditions will be posed on different boundary parts.

Note that the indices i, j of subdomains and boundary parts are independent of each other. Usually, the meaning of an index variable can be derived from the context. A more elaborate

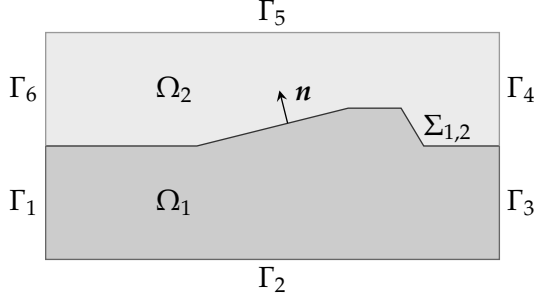


Figure 2.1: Notation for a domain Ω which is subdivided into two subdomains. The boundary Γ consists of six parts.

indexing scheme is sacrificed for simplicity of notation. A similar problem arises with the use of i as an index variable and as the imaginary unit $i = \sqrt{-1}$. Since index variables will only appear as subscripts and the imaginary unit as a factor the correct meaning should be clear from the context.

Finally, some basic mathematical notation: The real part of a complex number $c \in \mathbb{C}$ is denoted by $\Re\{c\}$ or c_{\Re} ; the imaginary part by $\Im\{c\}$ or c_{\Im} ; the magnitude, absolute value or modulus by $|c|$ or $\text{mod}\{c\}$; and the angle, phase or argument by $\arg\{c\}$. The Kronecker symbol is defined by

$$\delta_{i,j} = \begin{cases} 1 & i = j, \\ 0 & i \neq j. \end{cases} \quad (2.2)$$

2.1.2 Maxwell's equations

All electromagnetic phenomena are described by the system of Maxwell's equations,

$$\text{curl } \mathbf{E} = -\dot{\mathbf{B}}, \quad \text{Faraday's law,} \quad (2.3a)$$

$$\text{curl } \mathbf{H} = \mathbf{j} + \dot{\mathbf{D}}, \quad \text{Maxwell-Ampère's law,} \quad (2.3b)$$

$$\text{div } \mathbf{B} = 0, \quad \text{Gauss's magnetic law,} \quad (2.3c)$$

$$\text{div } \mathbf{D} = \rho, \quad \text{Gauss's electric law,} \quad (2.3d)$$

which link electric field \mathbf{E} , magnetic field \mathbf{H} , electric flux density \mathbf{D} , magnetic flux density \mathbf{B} , electric current density \mathbf{j} and electric charge density ρ . All field quantities are functions of space and time. As usual, the dot denotes the time derivative. The system of partial differential equations is completed by the set of constitutive relations

$$\mathbf{B} = \boldsymbol{\mu} * \mathbf{H}, \quad (2.3e)$$

$$\mathbf{D} = \boldsymbol{\varepsilon} * \mathbf{E}, \quad (2.3f)$$

$$\mathbf{j} = \mathbf{j}_s + \boldsymbol{\sigma} * \mathbf{E}, \quad \text{Ohm's law,} \quad (2.3g)$$

where the symbol $*$ denotes convolution in time and \mathbf{j}_s an impressed current density. For inhomogeneous, anisotropic and dispersive media the electric permittivity $\boldsymbol{\varepsilon}$, the magnetic permeability $\boldsymbol{\mu}$ and the electric conductivity $\boldsymbol{\sigma}$ are symmetric tensors that depend on space and time.

The time dependency of all quantities can be removed if equations (2.3) are Fourier transformed. Using the Fourier transform defined by

$$E(\mathbf{r}, \omega) = \frac{1}{2\pi} \int_{-\infty}^{\infty} E(\mathbf{r}, t) e^{-i\omega t} dt \quad (2.4)$$

for the electric field and similarly for all other fields, Maxwell's equations in frequency domain read

$$\text{curl } \mathbf{E} = i\omega \mathbf{B}, \quad (2.5a)$$

$$\text{curl } \mathbf{H} = \mathbf{j} - i\omega \mathbf{D}, \quad (2.5b)$$

$$\text{div } \mathbf{B} = 0, \quad (2.5c)$$

$$\text{div } \mathbf{D} = \rho. \quad (2.5d)$$

The convolution in the time domain constitutive relations reduces to a product in frequency domain,

$$\mathbf{B} = \mu \mathbf{H}, \quad (2.5e)$$

$$\mathbf{D} = \epsilon \mathbf{E}, \quad (2.5f)$$

$$\mathbf{j} = \mathbf{j}_s + \sigma \mathbf{E}. \quad (2.5g)$$

The usage of the same symbols for time and frequency domain quantities is ambiguous. However, it is restricted to this section. Only the frequency domain quantities will be considered throughout the remainder of this work.

Continuity equation

The Maxwell system (2.5) involves the two vector differential operators curl and div. It is well known that the identity $\text{div curl } \mathbf{u} \equiv 0$ holds for any smooth vector field \mathbf{u} . Using this vector identity, Gauss's magnetic law can be derived from Faraday's law for non-zero frequencies ω . The static case $\omega = 0$, however, requires that Gauss's magnetic law is enforced explicitly since it cannot be derived from the other equations in that case.

Similarly, the divergence of Maxwell-Ampère's law produces

$$\text{div } \mathbf{j} - i\omega \text{div } \mathbf{D} = 0. \quad (2.6)$$

Gauss's electric law turns out to be independent and cannot be derived from the other equations even for non-zero frequencies. Combining this equation with Gauss's electric law results in the well-known continuity equation

$$\text{div } \mathbf{j} - i\omega \rho = 0 \quad (2.7)$$

which establishes a relation between volumetric charge density and current density.

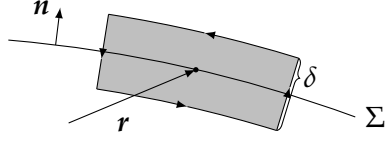


Figure 2.2: Area of integration around a surface point $\mathbf{r} \in \Sigma$ for application of Stokes' theorem.

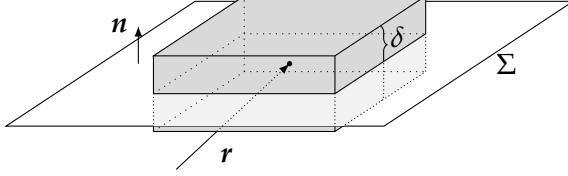


Figure 2.3: Volume of integration around a surface point $\mathbf{r} \in \Sigma$ for application of Gauss' theorem.

Continuity conditions

The partial differential equations given above are only valid if the functions involved are sufficiently smooth. Conditions concerning the smoothness of the electromagnetic field quantities can be derived from Maxwell's equations directly. For this purpose the field behavior is examined at a point on an arbitrary surface Σ (Nolting, 1997).

First, consider Faraday's and Maxwell-Ampère's law. Integrating these equations over an area perpendicular to the surface (Figure 2.2), using Stokes' theorem and making the edge perpendicular to the surface infinitely small ($\delta \rightarrow 0$) leads to the continuity of the tangential electric and magnetic field components

$$[\mathbf{n} \times \mathbf{E}]_{\Sigma} = \mathbf{0}, \quad (2.8a)$$

$$[\mathbf{n} \times \mathbf{H}]_{\Sigma} = \mathbf{j}_f. \quad (2.8b)$$

\mathbf{j}_f is an impressed surface current density which flows only within the surface. It is imperative that \mathbf{j}_f satisfies $\mathbf{n} \cdot \mathbf{j}_f = 0$. If $\mathbf{n} \cdot \mathbf{j}_f \neq 0$, equation (2.8b) is not an equality since $\mathbf{n} \cdot (\mathbf{n} \times \mathbf{H}) = 0$ for any \mathbf{H} .

Second, integrating Gauss' electric and magnetic laws, equation (2.6) as well as the continuity equation over a volume around the surface point (Figure 2.3), invoking Gauss' theorem, and making the height of the volume perpendicular to the surface infinitely small ($\delta \rightarrow 0$) finally results in the conditions

$$[\mathbf{n} \cdot \mathbf{B}]_{\Sigma} = 0, \quad (2.8c)$$

$$[\mathbf{n} \cdot \mathbf{D}]_{\Sigma} = \rho_f, \quad (2.8d)$$

$$[\mathbf{n} \cdot \mathbf{j} - i\omega \mathbf{n} \cdot \mathbf{D}]_{\Sigma} = 0, \quad (2.8e)$$

$$[\mathbf{n} \cdot \mathbf{j}]_{\Sigma} = i\omega \rho_f \quad (2.8f)$$

which enforce the continuity of the normal fluxes. ρ_f denotes a surface charge. Similar to the underlying differential equations only two of the three continuity conditions (2.8d) to (2.8f) involving \mathbf{D} , \mathbf{j} and ρ_f are independent of each other.

The continuity conditions of the flux density normal components can partially be derived from those of the tangential field components. More precisely, equation (2.8c) can be derived from equation (2.8a) by applying the *surface divergence* (Monk, 2003). If the surface is smooth enough the surface divergence div_Γ of the tangential electric field is related to the normal component of the curl of the electric field by equation (A.1i) given in Appendix A. For non-zero frequencies, Faraday's law yields the final form of equation (2.8c). Application of the surface divergence to equation (2.8b) and making use of equation (2.8e) reveals another restriction on the surface current density. Its surface divergence $\text{div}_\Gamma \mathbf{j}_f$ has to vanish in order to make equations (2.8b) and (2.8e) compatible. Note that the volume divergence of the surface current density is not well-defined since \mathbf{j}_f could only be extended to the vicinity of the surface by employing the Dirac delta distribution in the surface normal direction.

Summarizing, the normal component of the electric and magnetic field across a surface is discontinuous if the constitutive parameters are discontinuous even if there is no surface charge. Similarly, the tangential components of the electric and magnetic flux density as well as of the electric current density are discontinuous if the constitutive parameters are discontinuous even if there is no surface current density.

These observations motivate the subdivision of domain Ω into subdomains Ω_i (section 2.1.1) according to the smoothness of constitutive parameters and source terms. In particular, surface currents or charges are restricted to the interface between subdomains. Maxwell's equations are only enforced within the subdomains Ω_i . At the interface $\Sigma_{i,j}$ between two adjacent subdomains Ω_i and Ω_j , the system of partial differential equations is supplemented by the continuity conditions derived above.

Boundary conditions

The solution to a system of partial differential equations is not uniquely defined unless some appropriate boundary conditions are posed on Γ . The boundary is divided into two parts, Γ_e and Γ_h . These symbols are chosen according to the prescription of the tangential components of either the electric or magnetic field.

Boundary conditions can be grouped into two classes. The first class treats the boundary just as an interface between the interior and the exterior domain where the fields in the exterior domain are assumed known. Consequently, the continuity conditions (2.8) are reinterpreted as boundary conditions. If the known exterior fields are marked by subscript 0, the boundary conditions require that

$$\mathbf{n} \times \mathbf{E} = \mathbf{n} \times \mathbf{E}_0, \quad (2.9a)$$

$$\mathbf{n} \cdot \mathbf{B} = \mathbf{n} \cdot \mathbf{B}_0 \quad (2.9b)$$

on Γ_e and

$$\mathbf{n} \times \mathbf{H} = \mathbf{j}_f + \mathbf{n} \times \mathbf{H}_0, \quad (2.9c)$$

$$\mathbf{n} \cdot \mathbf{D} = \rho_f + \mathbf{n} \cdot \mathbf{D}_0, \quad (2.9d)$$

$$\mathbf{n} \cdot (\mathbf{j} - i\omega\mathbf{D}) = \mathbf{n} \cdot (\mathbf{j}_0 - i\omega\mathbf{D}_0), \quad (2.9e)$$

$$\mathbf{n} \cdot \mathbf{j} = i\omega\rho_f + \mathbf{n} \cdot \mathbf{j}_0 \quad (2.9f)$$

on Γ_h . \mathbf{n} denotes the outer normal vector on Γ . It is important to understand that the exterior fields have to be a valid solution of Maxwell's equations. Sorting the equations into the two sections for Γ_e and Γ_h is not arbitrary. Indeed, \mathbf{E} and \mathbf{B} are mutually linked by Faraday's law; \mathbf{H} , \mathbf{j} and \mathbf{D} are mutually linked by Maxwell-Ampère's law.

The class of boundary conditions (2.9) contains two special cases. If $\mathbf{E}_0 = \mathbf{0}$ and $\mathbf{B}_0 = \mathbf{0}$ equations (2.9a) and (2.9b) describe the surface of a *perfect electric conductor* (PEC). The analogous choice for the magnetic field, equations (2.9c) to (2.9f) with $\mathbf{H}_0 = \mathbf{0}$, $\mathbf{D}_0 = \mathbf{0}$, $\mathbf{j}_0 = \mathbf{0}$, $\mathbf{j}_f = \mathbf{0}$ and $\rho_f = 0$, is called a *perfect magnetic conductor* (PMC) despite the fact that there is no magnetic conductivity.

The second class of boundary conditions originates in the solution of boundary value problems posed on an infinite domain. The solution is required to satisfy a Sommerfeld radiation condition infinitely far away from sources. This condition is usually approximated on the boundary of a truncated, finite domain by a so-called *absorbing boundary condition* (ABC). Here, only the lowest order ABC will be considered. A plane wave proportional to $e^{ik\mathbf{n}\cdot\mathbf{r}}$, i. e., travelling into the direction of \mathbf{n} with wavenumber k , passes the ABC boundary without reflection if

$$\mathbf{n} \times \mathbf{E} + \mathbf{n} \times (\boldsymbol{\kappa} (\mathbf{n} \times \mathbf{H})) = \mathbf{0}, \quad (2.10a)$$

$$\mathbf{n} \cdot \mathbf{B} = 0 \quad (2.10b)$$

on Γ_e and

$$\mathbf{n} \times \mathbf{H} + \mathbf{n} \times (\boldsymbol{\lambda} (\mathbf{n} \times \mathbf{E})) = \mathbf{0}, \quad (2.10c)$$

$$\mathbf{n} \cdot (\mathbf{j} - i\omega\mathbf{D}) = 0 \quad (2.10d)$$

on Γ_h . Note that \mathbf{n} denotes both the outer normal vector on the boundary and the propagation direction of the plane wave. The wavenumber k depends on \mathbf{n} for anisotropic media (section 2.5). Therefore, the coefficients $\boldsymbol{\kappa} = k(\boldsymbol{\sigma} - i\omega\boldsymbol{\varepsilon})^{-1}$ and $\boldsymbol{\lambda} = k(\omega\boldsymbol{\mu})^{-1}$ are tensors which respectively have the dimension of an electromagnetic admittance or impedance.

The scalar equations (2.10b) and (2.10d) are independent of the vector equations (2.10a) and (2.10c). Indeed, taking the surface divergence of the vector equations yields another set of scalar boundary conditions

$$i\omega\mathbf{n} \cdot \mathbf{B} + \mathbf{n} \cdot \text{curl}(\boldsymbol{\kappa} (\mathbf{n} \times \mathbf{H})) = 0 \quad \text{on } \Gamma_e \text{ and} \quad (2.10e)$$

$$\mathbf{n} \cdot (\mathbf{j} - i\omega\mathbf{D}) + \mathbf{n} \cdot \text{curl}(\boldsymbol{\lambda} (\mathbf{n} \times \mathbf{E})) = 0 \quad \text{on } \Gamma_h. \quad (2.10f)$$

2.2 Derived systems

The constitutive equations can be inserted into the partial differential equations in order to eliminate \mathbf{B} , \mathbf{D} and \mathbf{j} . Then, the vector fields \mathbf{E} and \mathbf{H} and the scalar field ρ have to satisfy all of the following

partial differential equations

$$\operatorname{curl} E - i\omega\mu H = 0, \quad (2.11a)$$

$$\operatorname{curl} H - (\sigma - i\omega\varepsilon)E = j_s, \quad (2.11b)$$

$$\operatorname{div} \mu H = 0, \quad (2.11c)$$

$$\operatorname{div} \varepsilon E - \rho = 0, \quad (2.11d)$$

$$\operatorname{div} (\sigma - i\omega\varepsilon)E = -\operatorname{div} j_s, \quad (2.11e)$$

$$\operatorname{div} \sigma E - i\omega\rho = -\operatorname{div} j_s \quad (2.11f)$$

given the impressed current density j_s . These equations are repeated in Table 2.1 which also gives an overview of the corresponding interface and boundary conditions. For compactness of notation the boundary conditions (2.9) and (2.10) have been combined. However, one should always keep in mind that either the external fields or κ and λ are to be set zero. The normal flux ABCs (2.10e) and (2.10f), which are consistent to the tangential field ABCs (2.10a) and (2.10c), are preferred to equations (2.10b) and (2.10d). There is no ABC contribution to the normal flux boundary conditions (2.9d) and (2.9f) in terms of the induced current density or the displacement current density only because the ABC involves the sum of both current densities.

Obviously, this collection of equations contains redundancies as, e. g., the continuity equation can be derived from Faraday's law and the electric Gauss's law. One aim of this section is to derive appropriate subsets of equations which constitute a well posed boundary value problem. The other goal is to eliminate the magnetic field and to reformulate the boundary value problems in terms of the electric field only. While the original Maxwell system is of first order, the derived system of partial differential equations will be of second order. It is expected that the reduction of the number of unknowns implies less computational effort when solving the boundary value problem numerically.

2.2.1 Simple approach – The E -field formulation

Comparing the number of equations and unknowns, a plausible approach is to select the two vector partial differential equations involving the curl of the electric and magnetic field and to drop the equations involving the divergence of the corresponding flux densities. According to this choice only continuity and boundary conditions are taken into account which involve the fields and to drop those conditions which involve their flux densities (Table 2.1, second and fourth row). Let $\omega \neq 0$. Then, Faraday's law can be used to express the magnetic field in terms of the curl of the electric field. The resulting boundary value problem amounts to finding the electric field E such that

$$\operatorname{curl} (\mu^{-1} \operatorname{curl} E) - i\omega(\sigma - i\omega\varepsilon)E = i\omega j_s \quad \text{on } \Omega_i, \quad (2.12a)$$

$$[n \times E]_\Sigma = 0 \quad \text{on } \Sigma_{i,j}, \quad (2.12b)$$

$$\left[n \times \mu^{-1} \operatorname{curl} E \right]_\Sigma = i\omega j_f \quad \text{on } \Sigma_{i,j}, \quad (2.12c)$$

PDEs defined on Ω_i	continuity condition on $\Sigma_{i,j}$	boundary condition on Γ_i
$\text{curl } E - i\omega\mu H = 0$	$[n \times E]_\Sigma = 0$	$n \times (E + (\kappa(n \times H))) = n \times E_0$
$\text{div } \mu H = 0$	$[n \cdot \mu H]_\Sigma = 0$	$n \cdot (i\omega\mu H + \text{curl}(\kappa(n \times H))) = n \cdot \text{curl } E_0$
$\text{curl } H - (\sigma - i\omega\varepsilon) E = j_s$	$[n \times H]_\Sigma = j_f$	$n \times (H + (\lambda(n \times E))) = j_f + n \times H_0$
$\text{div } \varepsilon E - \rho = 0$	$[n \cdot \varepsilon E]_\Sigma - \rho_f = 0$	$n \cdot \varepsilon E - \rho_f = n \cdot D_0$
$\text{div}(\sigma - i\omega\varepsilon) E = -\text{div } j_s$	$[n \cdot (\sigma - i\omega\varepsilon) E]_\Sigma = -[n \cdot j_s]_\Sigma$	$n \cdot ((\sigma - i\omega\varepsilon) E + \text{curl}(\lambda(n \times E))) = n \cdot (\text{curl } H_0 - j_s)$
$\text{div } \sigma E - i\omega\rho = -\text{div } j_s$	$[n \cdot \sigma E]_\Sigma - i\omega\rho_f = -[n \cdot j_s]_\Sigma$	$n \cdot \sigma E - i\omega\rho_f = n \cdot j_0$

Table 2.1: Tabular lookup of all partial differential equations (PDEs) as well as interface and boundary conditions of the Maxwell system. Each line contains the partial differential equation and its derived interface and boundary conditions involving the same physical quantity, from top to bottom, the electric field, the magnetic flux density, the magnetic field, the electric flux density, the complex current density and the current density.

$$\mathbf{n} \times \mathbf{E} = \mathbf{n} \times \mathbf{E}_0 \quad \text{on } \Gamma_e \text{ and} \quad (2.12d)$$

$$\mathbf{n} \times \boldsymbol{\mu}^{-1} \operatorname{curl} \mathbf{E} + i\omega \mathbf{n} \times (\boldsymbol{\lambda} (\mathbf{n} \times \mathbf{E})) = i\omega \mathbf{j}_f + i\omega \mathbf{n} \times \mathbf{H}_0 \quad \text{on } \Gamma_h. \quad (2.12e)$$

Only boundary condition (2.9a) has been chosen for Γ_e in order to obtain a Dirichlet boundary condition. The absorbing boundary condition is expressed by equation (2.10c) and combined with equation (2.9c) into a mixed ($\boldsymbol{\lambda} \neq 0$) or Neumann ($\boldsymbol{\lambda} = 0$) boundary condition on Γ_h . The boundary value problem (2.12) only involves one vector valued function to be determined. Once the electric field is computed the magnetic field and all flux densities can be derived using Maxwell's equations.

Let \mathbf{E} a solution of boundary value problem (2.12) and smooth enough such that the divergence of equation (2.12a) can be taken. Since $\operatorname{div} \operatorname{curl} \mathbf{u} \equiv 0$, the electric field has been shown to also satisfy

$$-i\omega \operatorname{div} (\boldsymbol{\sigma} - i\omega \boldsymbol{\epsilon}) \mathbf{E} = i\omega \operatorname{div} \mathbf{j}_s, \quad (2.13)$$

i. e., one form of the continuity equation times $i\omega$. The electric field *implicitly* satisfies the continuity equation as it is not enforced explicitly as part of the boundary value problem formulation.

However, there is one conceptional weakness of this formulation which is pointed at by the assumption that $\omega \neq 0$: The limit $\omega \rightarrow 0$ renders the boundary value problem (2.12) ill-posed as uniqueness of the solution can only be proven for non-zero frequencies. From a computational point of view this limit will turn out to cause numerical instabilities at low but far from zero frequencies. Therefore, it is instructive to study the null-space of boundary value problem (2.12) with $\omega = 0$ which is essentially the kernel of the curl-operator subject to particular boundary conditions.

2.2.2 The kernel of the curl-operator

The nullspace, or kernel, of boundary value problem (2.12) with $\omega = 0$ is spanned by functions which satisfy the boundary value problem with homogeneous source and boundary terms, i. e., a vanishing right hand side,

$$\operatorname{curl} (\boldsymbol{\mu}^{-1} \operatorname{curl} \mathbf{E}) = \mathbf{0} \quad \text{on } \Omega_i, \quad (2.14a)$$

$$[\mathbf{n} \times \mathbf{E}]_{\Sigma} = \mathbf{0} \quad \text{on } \Sigma_{i,j}, \quad (2.14b)$$

$$\left[\mathbf{n} \times \boldsymbol{\mu}^{-1} \operatorname{curl} \mathbf{E} \right]_{\Sigma} = \mathbf{0} \quad \text{on } \Sigma_{i,j}, \quad (2.14c)$$

$$\mathbf{n} \times \mathbf{E} = \mathbf{0} \quad \text{on } \Gamma_e \text{ and} \quad (2.14d)$$

$$\mathbf{n} \times \boldsymbol{\mu}^{-1} \operatorname{curl} \mathbf{E} = \mathbf{0} \quad \text{on } \Gamma_h. \quad (2.14e)$$

Note that the zeroth order term of the mixed boundary condition on Γ_h vanishes since $\lim_{\omega \rightarrow 0} i\omega \boldsymbol{\lambda} = 0$. Due to the vector identity $\operatorname{curl} \operatorname{grad} u \equiv \mathbf{0}$, the field $\mathbf{E} = \operatorname{grad} V$ expressed as the gradient of any scalar function $V \in H^1(\Omega)$ satisfies the partial differential equation, the continuity conditions as well as the Neumann boundary condition on Γ_h . The Dirichlet boundary condition additionally requires that $\mathbf{n} \times \operatorname{grad} V = \mathbf{0}$ on Γ_e . This is equivalent to $V = \text{const.}$ on Γ_e .

Chapter 2 Boundary value problems

In order to render the boundary value problem (2.12) well-defined for the static limit, i. e, stable for low frequencies the kernel just described has to be removed. Therefore, the continuity equation and its corresponding interface and boundary conditions, which had been dropped previously, are taken into account. From the three partial differential equations coming into question, Gauss' electric law and the two forms of the continuity equation, equation (2.13) is chosen because it is the divergence condition consistent with the vector Helmholtz equation (2.12a). Unfortunately, this choice introduces a severe restriction. The electrical conductivity σ has to be assumed non-zero in all of Ω . If σ vanishes, equation (2.13) is trivial for $\omega = 0$. The case of a dielectric requires that Gauss' electric law is enforced. However, combination of two different divergence conditions, the continuity equation where $\sigma \neq 0$ and Gauss' electric law where $\sigma = 0$, leads to difficulties when deriving the weak form. The discussion of this issue is deferred to Appendix B.

Now, the source-free, static boundary value problem (2.14a) to (2.14e) is augmented by the set of conditions

$$\operatorname{div} \sigma \mathbf{E} = 0 \quad \text{on } \Omega_i, \quad (2.14f)$$

$$[\mathbf{n} \cdot \sigma \mathbf{E}]_{\Sigma} = 0 \quad \text{on } \Sigma_{i,j}, \quad (2.14g)$$

$$\mathbf{n} \cdot \sigma \mathbf{E} = 0 \quad \text{on } \Gamma_h. \quad (2.14h)$$

The solutions of the non-augmented problem, $\mathbf{E} = \operatorname{grad} V$ with $V = \text{const.}$ on Γ_e , are now reduced to those which solve the following boundary value problem:

Search $V \in H^1(\Omega)$ such that

$$\operatorname{div} \sigma \operatorname{grad} V = 0 \quad \text{on } \Omega_i, \quad (2.15a)$$

$$[V]_{\Sigma} = 0 \quad \text{on } \Sigma_{i,j}, \quad (2.15b)$$

$$[\mathbf{n} \cdot \sigma \operatorname{grad} V]_{\Sigma} = 0 \quad \text{on } \Sigma_{i,j}, \quad (2.15c)$$

$$V = \text{const.} \quad \text{on } \Gamma_e, \quad (2.15d)$$

$$\mathbf{n} \cdot \sigma \operatorname{grad} V = 0 \quad \text{on } \Gamma_h. \quad (2.15e)$$

Existence and uniqueness of solutions of this boundary value problem depend on the topology of the domain as well as of the Dirichlet and Neumann boundaries. For simplicity the domain Ω is assumed to be connected. This will rarely be a restriction for geophysical model settings. Concerning the different types of boundary conditions, consider first the case of a non-empty, connected Dirichlet boundary Γ_e . The boundary condition $V = C$ on Γ_e , $C \in \mathbb{C}$ fixed, renders $V = C$ in Ω the unique solution of boundary value problem (2.15). The kernel of boundary value problem (2.14a) to (2.14e) in terms of the electric field is spanned by the gradient of V . Because the gradient of the constant V vanishes the augmented boundary value problem (2.14a) to (2.14h) has a trivial nullspace and, provided existence, a unique solution \mathbf{E} .

The same argument holds for the second case of an empty Dirichlet boundary. Even though V as a solution of boundary value problem (2.15) with $\Gamma_e = \emptyset$ is not determined uniquely, the solution is nevertheless a constant, $V = C$ in Ω where $C \in \mathbb{C}$ is not fixed.

A complication arises with the third case of a disconnected Dirichlet boundary. Let $\Gamma_e = \Gamma_{e,1} \cup \dots \cup \Gamma_{e,J}$ where each of the Dirichlet boundary patches $\Gamma_{e,j}$, $j = 1, \dots, J$, is a connected part of Γ_e but different patches $\Gamma_{e,i}$ and $\Gamma_{e,j}$, $i \neq j$, are not connected with each other. Then any solution of boundary value problem (2.15) with $V = C_j$ on $\Gamma_{e,j}$, $j = 1, \dots, J$ will satisfy $\mathbf{n} \times \text{grad } V = \mathbf{0}$, i. e., $V = \text{const.}$ on Γ_e . If, and only if, $C_i = C_j$ for all $i, j = 1, \dots, J$ the potential V is constant and its gradient is zero. In general, V and its gradient do not vanish. Consequently, only part of the kernel of the curl-operator has been removed by the additional equations (2.14f) to (2.14h), namely all functions $\mathbf{E} = \text{grad } V$, $V \in H^1(\Omega)$, $V = 0$ on Γ_e . They span an infinite dimensional function space whose orthogonal complement using the $H_{\text{curl}}(\Omega)$ inner product is called the cohomology space (Monk, 2003)

$$K_N := \left\{ V_i \in H^1(\Omega) : \text{div } \sigma \text{ grad } V_i = 0 \text{ in } \Omega \text{ and } V_i = \delta_{i,j} \text{ on } \Gamma_{e,j}, \right. \\ \left. i = 1, \dots, J-1, j = 1, \dots, J \right\}. \quad (2.16)$$

The normal cohomology space is finite dimensional and of dimension $J - 1$. K_N is empty if Γ_e consists of exactly one connected, possibly empty part. The physical interpretation of K_N can easily be derived from its definition. K_N represents the static electric field which is caused by electric potential differences between $J > 1$ disconnected Dirichlet boundary patches where $V = C_j$ on $\Gamma_{e,j}$, $j = 1, \dots, J$. Since the cause is a potential *difference*, the dimension of K_N must be $J - 1$ if there are J boundary patches. The normal cohomology space could be annihilated by imposing $J - 1$ additional boundary conditions on Γ_e , corresponding to the dimension of K_N . The discussion of one possible way of treating a non-empty normal cohomology space is deferred to Appendix C. For the sake of simplicity the case of a disconnected Dirichlet boundary is excluded from the following considerations. This assumption is satisfied if the domain Ω has no holes, and if the outer boundary does not contain disconnected parts where a Dirichlet boundary condition is imposed. If Ω contains holes, only mixed or Neumann boundary conditions are admitted on their boundary. This assumption precludes, e. g., modelling the surface of buried metallic objects by a perfectly electric conducting (PEC) boundary condition.

Note that the restrictions concerning the topology of the computational domain and the assumption of a non-vanishing electric conductivity apply only to the augmented boundary value problem. The \mathbf{E} -field formulation (2.12) is not subject to these restrictions but suffers from the low frequency instability.

Returning to the non-static case, the boundary value problem (2.12) is augmented by the continuity equation (2.13) which is now enforced *explicitly*. Along with this condition, which involves electric current and electric flux densities, also the corresponding continuity and boundary conditions have to be taken into account. The augmented boundary value problem reads

$$\text{curl} \left(\boldsymbol{\mu}^{-1} \text{curl } \mathbf{E} \right) - i\omega(\boldsymbol{\sigma} - i\omega\boldsymbol{\varepsilon})\mathbf{E} = i\omega\mathbf{j}_s \quad \text{on } \Omega_i, \quad (2.17a)$$

$$- \text{div}(\boldsymbol{\sigma} - i\omega\boldsymbol{\varepsilon})\mathbf{E} = \text{div } \mathbf{j}_s \quad \text{on } \Omega_i, \quad (2.17b)$$

$$[\mathbf{n} \times \mathbf{E}]_{\Sigma} = \mathbf{0} \quad \text{on } \Sigma_{i,j}, \quad (2.17c)$$

$$\left[\mathbf{n} \times \mu^{-1} \text{curl } \mathbf{E} \right]_{\Sigma} = i\omega \mathbf{j}_f \quad \text{on } \Sigma_{i,j}, \quad (2.17d)$$

$$-[\mathbf{n} \cdot (\sigma - i\omega\epsilon)\mathbf{E}]_{\Sigma} = [\mathbf{n} \cdot \mathbf{j}_s]_{\Sigma} \quad \text{on } \Sigma_{i,j}, \quad (2.17e)$$

$$\mathbf{n} \times \mathbf{E} = \mathbf{n} \times \mathbf{E}_0 \quad \text{on } \Gamma_e, \quad (2.17f)$$

$$\mathbf{n} \times \mu^{-1} \text{curl } \mathbf{E} + i\omega \mathbf{n} \times (\lambda (\mathbf{n} \times \mathbf{E})) = i\omega \mathbf{n} \times \mathbf{H}_0 + i\omega \mathbf{j}_f \quad \text{on } \Gamma_h \text{ and } (2.17g)$$

$$\mathbf{n} \cdot (\sigma - i\omega\epsilon) \mathbf{E} + \mathbf{n} \cdot \text{curl} (\lambda (\mathbf{n} \times \mathbf{E})) = \mathbf{n} \cdot \text{curl } \mathbf{H}_0 - \mathbf{n} \cdot \mathbf{j}_s \quad \text{on } \Gamma_h. \quad (2.17h)$$

It is important to distinguish the three source fields in boundary conditions (2.17g) and (2.17h). While \mathbf{j}_s denotes the impressed current density which is prescribed in the interior of Ω , \mathbf{H}_0 is an external magnetic field, and \mathbf{j}_f is the surface current density only defined on Γ_h with $\mathbf{n} \cdot \mathbf{j}_f = 0$ and $\text{div}_{\Gamma_h} \mathbf{j}_f = 0$.

Now, there are four scalar partial differential equations to determine three components of the electric field vector. To resolve this apparent ambiguity the boundary value problem can be augmented by introducing a scalar field V as a fourth, unknown function (Jiang, Wu, and Povinelli, 1996). The extension of the boundary value problem is constructed such that it is equivalent to the original boundary value problem (2.17) and the electric field retains its values. This implies that V is introduced as a dummy variable which has to vanish in Ω .

2.2.3 Mixed approach – The E - V formulation

The extended boundary value problem amounts to finding the electric field \mathbf{E} and the scalar field V such that

$$\begin{aligned} \text{curl} \left(\mu^{-1} \text{curl } \mathbf{E} \right) - i\omega (\sigma - i\omega\epsilon) \mathbf{E} \\ + (\sigma - i\omega\epsilon) \text{grad } V = i\omega \mathbf{j}_s \end{aligned} \quad \text{on } \Omega_i, \quad (2.18a)$$

$$- \text{div} (\sigma - i\omega\epsilon) \mathbf{E} - \gamma V = \text{div } \mathbf{j}_s \quad \text{on } \Omega_i, \quad (2.18b)$$

$$[\mathbf{n} \times \mathbf{E}]_{\Sigma} = \mathbf{0} \quad \text{on } \Sigma_{i,j}, \quad (2.18c)$$

$$[V]_{\Sigma} = 0 \quad \text{on } \Sigma_{i,j}, \quad (2.18d)$$

$$\left[\mathbf{n} \times \mu^{-1} \text{curl } \mathbf{E} \right]_{\Sigma} = i\omega \mathbf{j}_f \quad \text{on } \Sigma_{i,j}, \quad (2.18e)$$

$$[\mathbf{n} \cdot (\sigma - i\omega\epsilon) \mathbf{E}]_{\Sigma} = [\mathbf{n} \cdot \mathbf{j}_s]_{\Sigma} \quad \text{on } \Sigma_{i,j}, \quad (2.18f)$$

$$[\mathbf{n} \cdot (\sigma - i\omega\epsilon) \text{grad } V]_{\Sigma} = 0 \quad \text{on } \Sigma_{i,j}, \quad (2.18g)$$

$$\mathbf{n} \times \mathbf{E} = \mathbf{n} \times \mathbf{E}_0 \quad \text{on } \Gamma_e, \quad (2.18h)$$

$$V = 0 \quad \text{on } \Gamma_e, \quad (2.18i)$$

$$\begin{aligned} \mathbf{n} \times \mu^{-1} \operatorname{curl} \mathbf{E} + i\omega \mathbf{n} \times (\boldsymbol{\lambda} (\mathbf{n} \times \mathbf{E})) \\ - \mathbf{n} \times (\boldsymbol{\lambda} (\mathbf{n} \times \operatorname{grad} V)) = i\omega \mathbf{n} \times \mathbf{H}_0 + i\omega \mathbf{j}_f \quad \text{on } \Gamma_h, \end{aligned} \quad (2.18j)$$

$$\mathbf{n} \cdot (\boldsymbol{\sigma} - i\omega \boldsymbol{\varepsilon}) \mathbf{E} + \mathbf{n} \cdot \operatorname{curl} (\boldsymbol{\lambda} (\mathbf{n} \times \mathbf{E})) = \mathbf{n} \cdot \operatorname{curl} \mathbf{H}_0 - \mathbf{n} \cdot \mathbf{j}_s \quad \text{on } \Gamma_h, \quad (2.18k)$$

$$\mathbf{n} \cdot (\boldsymbol{\sigma} - i\omega \boldsymbol{\varepsilon}) \operatorname{grad} V - \mathbf{n} \cdot \operatorname{curl} (\boldsymbol{\lambda} (\mathbf{n} \times \operatorname{grad} V)) = 0 \quad \text{on } \Gamma_h. \quad (2.18l)$$

The additional term $(\boldsymbol{\sigma} - i\omega \boldsymbol{\varepsilon}) \operatorname{grad} V$ in equation (2.18a) is chosen as the symmetric counterpart of $-\operatorname{div} (\boldsymbol{\sigma} - i\omega \boldsymbol{\varepsilon}) \mathbf{E}$. Similarly, $-\mathbf{n} \times (\boldsymbol{\lambda} (\mathbf{n} \times \operatorname{grad} V))$ in equation (2.18j) is the symmetric counterpart of $-\operatorname{div}_{\Gamma_h} (\mathbf{n} \times (\boldsymbol{\lambda} (\mathbf{n} \times \mathbf{E}))) = \mathbf{n} \cdot \operatorname{curl} (\boldsymbol{\lambda} (\mathbf{n} \times \mathbf{E}))$ in equation (2.18k). These symmetry considerations assume, of course, that the tensors $\boldsymbol{\sigma}$, $\boldsymbol{\varepsilon}$ and $\boldsymbol{\lambda}$ are symmetric. The interpretation of symmetry for the system of partial differential equations will become more evident when the weak form of the boundary value problem is derived in section 2.3. The underlying objective of deriving a symmetric formulation is to obtain a symmetric finite element system matrix when the boundary value problem is discretized. Symmetric matrices require less memory to be stored than non-symmetric ones.

The parameter γ in equation (2.18b) is either a scalar, non-negative function of space or chosen to vanish, $\gamma \equiv 0$. Taking the divergence of equation (2.18a) and inserting equation (2.18b) shows that V implicitly satisfies

$$-\operatorname{div} ((\boldsymbol{\sigma} - i\omega \boldsymbol{\varepsilon}) \operatorname{grad} V) - i\omega \gamma V = 0 \quad \text{on } \Omega_i, \quad (2.19a)$$

$$[V]_{\Sigma} = 0 \quad \text{on } \Sigma_{i,j}, \quad (2.19b)$$

$$[\mathbf{n} \cdot (\boldsymbol{\sigma} - i\omega \boldsymbol{\varepsilon}) \operatorname{grad} V]_{\Sigma} = 0 \quad \text{on } \Sigma_{i,j}, \quad (2.19c)$$

$$V = 0 \quad \text{on } \Gamma_e \text{ and} \quad (2.19d)$$

$$\mathbf{n} \cdot (\boldsymbol{\sigma} - i\omega \boldsymbol{\varepsilon}) \operatorname{grad} V - \mathbf{n} \cdot \operatorname{curl} (\boldsymbol{\lambda} (\mathbf{n} \times \operatorname{grad} V)) = 0 \quad \text{on } \Gamma_h. \quad (2.19e)$$

Only if $V \equiv 0$ is the unique solution of boundary value problem (2.19), the boundary value problem (2.18) will have a unique solution (\mathbf{E}, V) where \mathbf{E} is also a solution of boundary value problem (2.17). Consequently, γ has to be chosen such that it is not a solution of the eigenvalue problem

$$\operatorname{div} \left(\left(\boldsymbol{\varepsilon} + \frac{i}{\omega} \boldsymbol{\sigma} \right) \operatorname{grad} V \right) = \gamma V \quad (2.20)$$

subject to the boundary conditions (2.19d) and (2.19e). The eigenvalues λ of the differential operator on the left hand side of (2.20) are situated in the third quadrant of the complex plane including the negative real axis and the origin, $\Re\{\lambda\} \leq 0$ and $\Im\{\lambda\} \leq 0$, if the tensors $\boldsymbol{\varepsilon}$ and $\boldsymbol{\sigma}$ have positive eigenvalues. Therefore, the choice $\Re\{\gamma\} > 0$ or $\Im\{\gamma\} > 0$ guarantees that boundary value problem (2.19) only has the trivial solution for any set of homogeneous boundary conditions.

If γ is chosen to vanish, equation (2.19a) is not a Helmholtz-like but a Laplace-like equation. In this particular case, Γ_e has to be assumed non-empty. If Γ_e is empty, any constant V will satisfy the boundary value problem and non-uniqueness renders it ill-posed. Note that this is a problem which originates from introducing V as a dummy variable and not from the kernel of the curl-operator. The kernel is spanned by the gradient of V which is trivial for constant but non-zero V .

A similar set of equations has been suggested by Demkowicz and Vardapetyan (1998) where a scalar variable p is introduced and interpreted as a Lagrange multiplier. Their set of equations, however, differs from the one presented here by a different scaling of the scalar variable $V = i\omega p$, by a factor of $i\omega$ in front of the continuity equation as well as by considering only the case of $\gamma = 0$, a non-empty Γ_e and homogeneous boundary conditions. They further prove for the dielectric case ($\sigma = 0$) that their E - p formulation has a unique solution which is uniformly stable for $\omega \rightarrow 0$. This result is derived by choosing a suitable norm which involves a factor of ω^2 for the term $\|\text{grad } p\|$. If this factor is modified for the case of conductive media ($\sigma \neq 0$) and included into the scalar field the definition $V = i\omega p$ naturally arises. For symmetry reasons the factor $i\omega$ is also removed from the continuity equation. Only this choice guarantees that neither the term $(\sigma - i\omega\epsilon) \text{grad } V$ in equation (2.18a) nor the continuity equation (2.18b) do not vanish if the limit $\omega \rightarrow 0$ is taken.

2.3 The weak form

So far, the physics of electromagnetic phenomena has been mathematically described by a system of partial differential equations, continuity conditions and boundary conditions. This description was naturally derived from Maxwell's equations in differential form. However, it suffers from a number of inconveniences. First, if point sources, such as an electric or magnetic dipole, are to be modelled, the source term is not a classical function any more but a distribution, the Dirac delta distribution. This leads to the questions how to 'interpret' the partial differential equation and which function space to choose the solution from. Second, the second order partial differential equation requires the electric field to be differentiable twice while the original Maxwell system requires only the first derivative to be defined. The third point is merely a trifle in that the splitting of the domain into subdomains with smooth constitutive parameters and coupling the solution of the partial differential equations defined on each subdomain by continuity conditions is not very elegant.

All these conditions can be relaxed by introducing the weak form of the boundary value problem. In addition, the weak form is the basis for the method of finite elements which will be presented in Chapter 3.

The notion of 'weak' in mathematical terminology means that something is interpreted in the sense of an inner product. If two quantities u and f are equal in the weak sense, only their inner products with a test function v are required to be equal, $(u, v) = (f, v)$, for every possible choice of v .

In the case of the boundary value problems considered here, the inner product is the usual L_2 inner product of complex valued scalar or vector functions,

$$(u, v)_{L_2(\Omega)} := \int_{\Omega} \bar{v} u \, d^3r \quad \text{and} \quad (\mathbf{u}, \mathbf{v})_{L_2(\Omega)} := \int_{\Omega} \bar{\mathbf{v}} \cdot \mathbf{u} \, d^3r. \quad (2.21)$$

The partial differential equations of the boundary value problem are interpreted in the weak sense, i. e., the inner product is applied to the partial differential equations. Formally, the inner product

is taken on the whole domain Ω with test functions defined on the whole of Ω . Since the partial differential equations are only defined on the subdomains and $\bar{\Omega} = \bigcup_{i=1}^n \bar{\Omega}_i$ the integration is split into the sum over all n subdomains.

The E -field formulation

Let Φ be a test function defined on Ω . Then, equation (2.12a) reads in the weak sense as

$$\sum_{i=1}^n \int_{\Omega_i} \bar{\Phi} \cdot \left(\text{curl} \left(\mu^{-1} \text{curl} E \right) - i\omega(\sigma - i\omega\epsilon)E \right) d^3r = \sum_{i=1}^n \int_{\Omega_i} \bar{\Phi} \cdot (i\omega j_s) d^3r \quad (2.22)$$

The first integral on the left hand side involving the curl can be transformed using Green's theorem (A.3*) (Appendix A.2)

$$\begin{aligned} \int_{\Omega_i} \bar{\Phi} \cdot \text{curl} \left(\mu^{-1} \text{curl} E \right) d^3r \\ = \int_{\Omega_i} \text{curl} \bar{\Phi} \cdot \left(\mu^{-1} \text{curl} E \right) d^3r + \int_{\partial\Omega_i} \bar{\Phi} \cdot \left(\mathbf{n} \times \left(\mu^{-1} \text{curl} E \right) \right) d^2r \end{aligned} \quad (2.23)$$

where \mathbf{n} is the outer normal vector on $\partial\Omega_i$. The boundary of Ω_i is composed of an outer boundary part $\Gamma_i = \Gamma \cap \partial\Omega_i$ and an inner boundary part $\partial\Omega_i \setminus \Gamma_i = \bigcup_{j \neq i} \Sigma_{i,j}$ which is the union of all interfaces with adjacent subdomains Ω_j . Consider first all inner boundary integrals. If the normal vector \mathbf{n} on $\Sigma_{i,j}$ is defined to point from Ω_i to Ω_j , the following holds

$$\begin{aligned} \sum_{i=1}^n \int_{\partial\Omega_i \setminus \Gamma_i} \bar{\Phi} \cdot \left(\mathbf{n} \times \left(\mu^{-1} \text{curl} E \right) \right) d^2r &= \sum_{\substack{i,j=1 \\ i \neq j}}^n \int_{\Sigma_{i,j}} \bar{\Phi} \cdot \left(\mathbf{n} \times \left(\mu^{-1} \text{curl} E \right) \right) d^2r \\ &= \sum_{\substack{i,j=1 \\ i < j}}^n \int_{\Sigma_{i,j}} \bar{\Phi} \cdot \left[\mathbf{n} \times \left(\mu^{-1} \text{curl} E \right) \right]_{\Sigma} d^2r \\ &= \sum_{\substack{i,j=1 \\ i < j}}^n \int_{\Sigma_{i,j}} \bar{\Phi} \cdot (i\omega j_f) d^2r \end{aligned} \quad (2.24)$$

where $[\cdot]$ again denotes the jump across the interface. The last equality follows from the continuity condition (2.12c). Second, the outer boundary integrals

$$\sum_{i=1}^n \int_{\Gamma_i} \bar{\Phi} \cdot \left(\mathbf{n} \times \left(\mu^{-1} \text{curl} E \right) \right) d^2r = - \sum_{i=1}^n \int_{\Gamma_i} (\mathbf{n} \times \bar{\Phi}) \cdot \left(\mu^{-1} \text{curl} E \right) d^2r \quad (2.25)$$

are transformed using the boundary conditions. For $\Gamma_i \cap \Gamma_e$ the Dirichlet boundary condition in terms of the electric field $\mathbf{n} \times E = \mathbf{n} \times E_0$ will be enforced explicitly as an *essential* boundary condition. Therefore, the test function has to be chosen such that $\mathbf{n} \times \Phi = \mathbf{0}$ and the corresponding

Chapter 2 Boundary value problems

boundary integral vanishes. For $\Gamma_i \cap \Gamma_h$ the boundary condition (2.12e) enters the integrals as a *natural* boundary condition. This leaves

$$\begin{aligned} \sum_{i=1}^n \int_{\Gamma_i} \bar{\Phi} \cdot \left(\mathbf{n} \times \left(\mu^{-1} \operatorname{curl} \mathbf{E} \right) \right) d^2r \\ = i\omega \int_{\Gamma_h} \left(\mathbf{n} \times \bar{\Phi} \right) \cdot \left(\lambda \left(\mathbf{n} \times \mathbf{E} \right) \right) d^2r + i\omega \int_{\Gamma_h} \bar{\Phi} \cdot \left(\mathbf{j}_f + \mathbf{n} \times \mathbf{H}_0 \right) d^2r. \end{aligned} \quad (2.26)$$

Finally, the sum of subdomain integrals in equations (2.22) and (2.23) can be collected into a single integral over the whole domain. Choosing the trial and test functions from appropriate spaces such that all integrals are well-defined the weak form of the boundary value problem reads:

Search $\mathbf{E} \in \mathcal{U}$ such that

$$\begin{aligned} \int_{\Omega} \operatorname{curl} \bar{\Phi} \cdot \left(\mu^{-1} \operatorname{curl} \mathbf{E} \right) d^3r - i\omega \int_{\Omega} \bar{\Phi} \cdot \left((\sigma - i\omega\epsilon) \mathbf{E} \right) d^3r + i\omega \int_{\Gamma_h} \left(\mathbf{n} \times \bar{\Phi} \right) \cdot \left(\lambda \left(\mathbf{n} \times \mathbf{E} \right) \right) d^2r \\ = i\omega \int_{\Omega} \bar{\Phi} \cdot \mathbf{j}_s d^3r - i\omega \sum_{\substack{i,j=1 \\ i < j}}^n \int_{\Sigma_{i,j}} \bar{\Phi} \cdot \mathbf{j}_f d^2r - i\omega \int_{\Gamma_h} \bar{\Phi} \cdot \left(\mathbf{j}_f + \mathbf{n} \times \mathbf{H}_0 \right) d^2r \end{aligned} \quad (2.27a)$$

for all $\Phi \in \mathcal{U}_0$. The spaces of test and trial functions are defined by

$$\mathcal{U}_0 = \{ \Phi \in H_{\operatorname{curl}}(\Omega) : \mathbf{n} \times \Phi = \mathbf{0} \text{ on } \Gamma_e \} \quad (2.27b)$$

$$\mathcal{U} = \{ \mathbf{E} \in H_{\operatorname{curl}}(\Omega) : \mathbf{n} \times \mathbf{E} = \mathbf{n} \times \mathbf{E}_0 \text{ on } \Gamma_e \} \quad (2.27c)$$

where

$$H_{\operatorname{curl}}(\Omega) = \{ \mathbf{E} \in (L_2(\Omega))^3 : \operatorname{curl} \mathbf{E} \in (L_2(\Omega))^3 \} \quad (2.27d)$$

is the space of functions with a well-defined curl.

Note that this choice of function spaces justifies the merging of the subdomain integrals above. Furthermore, this choice enforces the continuity condition (2.12b) which has not been used when deriving the weak form of boundary value problem (2.12). One can show that vector functions with well-defined curl must have continuous tangential components (Nédélec, 1980).

The E-V formulation

The derivation of the weak form of the mixed boundary value problem (2.18) proceeds in a similar way. Application of a vector test function Φ to the vector Helmholtz equation (2.18a) now produces additional integrals involving $\operatorname{grad} V$,

$$\int_{\Omega} \bar{\Phi} \cdot \left((\sigma - i\omega\epsilon) \operatorname{grad} V \right) d^3r \quad \text{and} \quad - \int_{\Gamma_h} \left(\mathbf{n} \times \bar{\Phi} \right) \cdot \left(\lambda \left(\mathbf{n} \times \operatorname{grad} V \right) \right) d^2r.$$

2.3 The weak form

In addition to the vector test function Φ a scalar test function ϕ is introduced in order to form the inner product with the continuity equation (2.18b) on Ω ,

$$-\sum_{i=1}^n \int_{\Omega_i} \bar{\phi} \operatorname{div} (\sigma - i\omega\epsilon) E \, d^3r - \sum_{i=1}^n \int_{\Omega_i} \bar{\phi} \gamma V \, d^3r = \sum_{i=1}^n \int_{\Omega_i} \bar{\phi} \operatorname{div} j_s \, d^3r. \quad (2.28)$$

Another Green's theorem (A.2) is now applied to shift the differential operator to the test function.

$$\begin{aligned} & - \int_{\Omega_i} \bar{\phi} \operatorname{div} (j_s + (\sigma - i\omega\epsilon) E) \, d^3r \\ &= \int_{\Omega_i} \operatorname{grad} \bar{\phi} \cdot (j_s + (\sigma - i\omega\epsilon) E) \, d^3r - \int_{\partial\Omega_i} \bar{\phi} \mathbf{n} \cdot (j_s + (\sigma - i\omega\epsilon) E) \, d^2r. \end{aligned} \quad (2.29)$$

Splitting the surface integrals into subdomain interface and boundary contributions, and applying the interface and boundary conditions for all subdomains, the surface integrals are transformed according to

$$\begin{aligned} & - \sum_{i=1}^n \int_{\partial\Omega_i} \bar{\phi} \mathbf{n} \cdot (j_s + (\sigma - i\omega\epsilon) E) \, d^2r \\ &= - \sum_{i=1}^n \int_{\Gamma_i} \bar{\phi} \mathbf{n} \cdot (j_s + (\sigma - i\omega\epsilon) E) \, d^2r - \sum_{\substack{i,j=1 \\ i < j}}^n \int_{\Sigma_{i,j}} \bar{\phi} [\mathbf{n} \cdot (j_s + (\sigma - i\omega\epsilon) E)]_{\Sigma} \, d^2r \\ &= - \int_{\Gamma_h} \bar{\phi} \mathbf{n} \cdot \operatorname{curl} (\mathbf{H}_0 - \lambda (\mathbf{n} \times \mathbf{E})) \, d^2r \\ &= - \int_{\Gamma_h} \operatorname{grad} \bar{\phi} \cdot (\mathbf{n} \times (\mathbf{H}_0 - \lambda (\mathbf{n} \times \mathbf{E}))) \, d^2r - \int_{\partial\Gamma_h} \bar{\phi} \boldsymbol{\tau} \cdot (\mathbf{H}_0 - \lambda (\mathbf{n} \times \mathbf{E})) \, dr \\ &= - \int_{\Gamma_h} \operatorname{grad} \bar{\phi} \cdot (\mathbf{n} \times \mathbf{H}_0) \, d^2r - \int_{\Gamma_h} (\mathbf{n} \times \operatorname{grad} \bar{\phi}) \cdot (\lambda (\mathbf{n} \times \mathbf{E})) \, d^2r. \end{aligned} \quad (2.30)$$

In order to make the boundary integrals vanish on Γ_e , the test functions have to satisfy $\phi = 0$ on Γ_e . The last but one step follows from a form of Stoke's theorem for surface integrals (A.4). Here, $\boldsymbol{\tau}$ is defined by $\boldsymbol{\tau} = \mathbf{n} \times \boldsymbol{\nu}$ as the unit tangential vector on $\partial\Gamma_h$ and $\boldsymbol{\nu}$ as the unit outer normal vector on $\partial\Gamma_h$. The contour integral vanishes if Γ_h is empty or if it consists of closed surfaces only, i. e., if $\partial\Gamma_h$ is empty. If Γ_h contains open surfaces its boundary $\partial\Gamma_h$ coincides with $\partial\Gamma_e$. In this case, the contour integral vanishes because $\phi = 0$ on Γ_e .

Collecting everything and combining the subdomain integrals yields the weak form of the mixed boundary value problem:

Chapter 2 Boundary value problems

Search $\mathbf{E} \in \mathcal{U}$ and $V \in \mathcal{V}$ such that

$$\begin{aligned} & \int_{\Omega} \operatorname{curl} \bar{\Phi} \cdot (\mu^{-1} \operatorname{curl} \mathbf{E}) d^3r - i\omega \int_{\Omega} \bar{\Phi} \cdot ((\sigma - i\omega\epsilon)\mathbf{E}) d^3r + \int_{\Omega} \bar{\Phi} \cdot ((\sigma - i\omega\epsilon) \operatorname{grad} V) d^3r \\ & + i\omega \int_{\Gamma_h} (\mathbf{n} \times \bar{\Phi}) \cdot (\lambda(\mathbf{n} \times \mathbf{E})) d^2r - \int_{\Gamma_h} (\mathbf{n} \times \bar{\Phi}) \cdot (\lambda(\mathbf{n} \times \operatorname{grad} V)) d^2r \\ & = i\omega \int_{\Omega} \bar{\Phi} \cdot \mathbf{j}_s d^3r - i\omega \sum_{\substack{i,j=1 \\ i < j}}^n \int_{\Sigma_{i,j}} \bar{\Phi} \cdot \mathbf{j}_f d^2r - i\omega \int_{\Gamma_h} \bar{\Phi} \cdot (\mathbf{j}_f + \mathbf{n} \times \mathbf{H}_0) d^2r \end{aligned} \quad (2.31a)$$

for all $\Phi \in \mathcal{U}_0$ and

$$\begin{aligned} & \int_{\Omega} \operatorname{grad} \bar{\phi} \cdot ((\sigma - i\omega\epsilon)\mathbf{E}) d^3r - \int_{\Omega} \bar{\phi} \gamma V d^3r - \int_{\Gamma_h} (\mathbf{n} \times \operatorname{grad} \bar{\phi}) \cdot (\lambda(\mathbf{n} \times \mathbf{E})) d^2r \\ & = - \int_{\Omega} \operatorname{grad} \bar{\phi} \cdot \mathbf{j}_s d^3r + \int_{\Gamma_h} \operatorname{grad} \bar{\phi} \cdot (\mathbf{n} \times \mathbf{H}_0) d^2r \end{aligned} \quad (2.31b)$$

for all $\phi \in \mathcal{V}_0$. The spaces of test and trial functions are defined by

$$\mathcal{U}_0 = \{\Phi \in H_{\operatorname{curl}}(\Omega) : \mathbf{n} \times \Phi = \mathbf{0} \text{ on } \Gamma_e\}, \quad (2.31c)$$

$$\mathcal{U} = \{\mathbf{E} \in H_{\operatorname{curl}}(\Omega) : \mathbf{n} \times \mathbf{E} = \mathbf{n} \times \mathbf{E}_0 \text{ on } \Gamma_e\}, \quad (2.31d)$$

$$\mathcal{V}_0 = \{\phi \in H_1(\Omega) : \phi = 0 \text{ on } \Gamma_e\}, \quad (2.31e)$$

$$\mathcal{V} = \mathcal{V}_0 \quad (2.31f)$$

where

$$H_{\operatorname{curl}}(\Omega) = \{\mathbf{E} \in (L_2(\Omega))^3 : \operatorname{curl} \mathbf{E} \in (L_2(\Omega))^3\}, \quad (2.31g)$$

$$H_1(\Omega) = \{V \in L_2(\Omega) : \operatorname{grad} V \in L_2(\Omega)\} \quad (2.31h)$$

are the spaces of functions with a well-defined curl and gradient, respectively.

\mathcal{V} and \mathcal{V}_0 are only identical because V is assumed zero on Γ_e . In general, these spaces would differ by inhomogeneous Dirichlet boundary values for V .

In the classical formulation the boundary value problem that V implicitly satisfies had been derived by taking the divergence of the augmented vector Helmholtz equation. The equivalent procedure for the weak form consists of choosing particular test functions $\Phi = \operatorname{grad} \phi$, $\phi \in \mathcal{V}_0$. This choice is valid since $\operatorname{grad} \phi \in \mathcal{U}_0$. Combining the variational integrals (2.31a) with $\Phi = \operatorname{grad} \phi$ and (2.31b) results in the following boundary value problem:

Search $V \in \mathcal{V}$ such that

$$\begin{aligned} & \int_{\Omega} \operatorname{grad} \bar{\phi} \cdot ((\sigma - i\omega\epsilon) \operatorname{grad} V) d^3r - i\omega \int_{\Omega} \bar{\phi} \gamma V d^3r \\ & - \int_{\Gamma_h} (\mathbf{n} \times \operatorname{grad} \bar{\phi}) \cdot (\lambda(\mathbf{n} \times \operatorname{grad} V)) d^2r = 0 \end{aligned} \quad (2.32)$$

for all $\phi \in \mathcal{V}_0$.

2.4 A change of coordinates

The integrals $\int_{\Sigma_{i,j}} \text{grad } \bar{\phi} \cdot \mathbf{j}_f d^2r$ and $\int_{\Gamma_h} \text{grad } \bar{\phi} \cdot \mathbf{j}_f d^2r$ which constitute potential source terms have been dropped because they express the weak form of the surface divergence which vanishes by assumption on \mathbf{j}_f , namely, $\mathbf{n} \cdot \mathbf{j}_f$ and $\text{div}_{\Gamma_h} \mathbf{j}_f = 0$. The variational integral (2.32) is the weak equivalent of boundary value problem (2.19). This could be shown by partial integration using Green's theorem (A.2).

As pointed out in the previous section, the mixed boundary value problem has been devised such that it produces a symmetric pattern. This pattern can be observed from the variational form (2.31a), (2.31b). For the integrals involving pairs of vector or scalar functions, (Φ, E) and (ϕ, V) , symmetry means that Φ can be interchanged with E and ϕ with V without changing the integral. This holds except for complex conjugation if the constitutive parameter tensors are symmetric. Similarly, all integrals involving the mixed pair $(\Phi, \text{grad } V)$ in (2.31a) have, except for complex conjugation, identical counterparts in (2.31b) which involve the mixed pair $(\text{grad } \phi, E)$.

2.4 A change of coordinates

Not least seen from an æsthetic point of view the natural choice of time as the fourth coordinate is not very satisfactory. Space and time coordinates have different physical dimensions, the SI units meter and second (Bureau international des poids et mesures (BIPM), 2006). Along with this difference, the numerical values of the coordinates involved may differ by orders of magnitude. This can be expressed by the fundamental relationship between space and time $x = ct$ of a wave travelling with speed c which is in the order of 3×10^8 m/s. The numerical values can be made more equal and the physical units identical if vacuum wavelength is used as the fourth coordinate instead of time. Maxwell's equations are rewritten using the following transform

$$t \mapsto \lambda = ct \quad (2.33)$$

where $c = 299\,792\,458$ m/s is the vacuum speed of light. A list of corresponding physical quantities is given in Table 2.2. This coordinate transform preserves the electric and magnetic field, current density and electric conductivity. All other quantities change both their magnitude and their unit. Working with either set is theoretically equivalent. From the numerical perspective the wavelength set might be advantageous as it scales all four coordinates to the same level.

As an example consider the two governing partial differential equations of this work with vacuum constitutive parameters

$$\text{curl} (\mu_0^{-1} \text{curl } E) - \omega^2 \varepsilon_0 E = 0, \quad (2.34a)$$

$$i\omega \text{div } \varepsilon_0 E = 0 \quad (2.34b)$$

and their plane wave solution $E \propto \exp(ik \cdot \mathbf{r})$ where $|k|^2 = \omega^2 \mu_0 \varepsilon_0 = k_0^2$. Analyzing the magnitude of the terms of the partial differential equations reveals that

$$|\text{curl} (\mu_0^{-1} \text{curl } E)| = k_0^2 / \mu_0 = \omega^2 \varepsilon_0, \quad (2.35a)$$

$$|\omega^2 \varepsilon_0 E| = \omega^2 \varepsilon_0 \quad \text{and} \quad (2.35b)$$

time		wavelength	
quantity	unit	quantity	unit
t	s	$\lambda = ct$	m
ω	1/s	$k_0 = \omega/c$	1/m
μ_0	Vs/Am	$Z_0 = c\mu_0$	V/A
$\varepsilon_0 = 1/(c^2\mu_0)$	As/Vm	$Y_0 = c\varepsilon_0 = 1/Z_0$	A/V
$\varepsilon = \varepsilon_0\varepsilon_r$	As/Vm	$\tilde{\varepsilon} = c\varepsilon = Y_0\varepsilon_r$	A/V
$\mu = \mu_0\mu_r$	Vs/Am	$\tilde{\mu} = c\mu = Z_0\mu_r$	V/A
σ	A/Vm	$\tilde{\sigma} = \sigma$	A/Vm
E	V/m	$\tilde{E} = E$	V/m
H	A/m	$\tilde{H} = H$	A/m
D	As/m ²	$\tilde{D} = cD$	A/m
B	Vs/m ²	$\tilde{B} = cB$	V/m
j	A/m ²	$\tilde{j} = j$	A/m ²
ρ	As/m ³	$\tilde{\rho} = c\rho$	A/m ²

Table 2.2: Equivalent physical quantities for Maxwell's equations using time or wavelength as the fourth coordinate.

$$|i\omega \operatorname{div} \varepsilon_0 E| = \omega k_0 \varepsilon_0, \quad (2.35c)$$

i. e., the first and second partial differential equation differ by a factor of $\omega/k_0 = c$. This potentially leads to problems if the system of partial differential equations is discretized and the resulting system of linear equations is solved numerically. If, however, the wavelength set of equations is used, the partial differential equations appear in the same order of magnitude. The three terms of

$$\operatorname{curl} (Z_0^{-1} \operatorname{curl} E) - k_0^2 Y_0 E = 0 \quad \text{and} \quad (2.36a)$$

$$ik_0 \operatorname{div} Y_0 E = 0 \quad (2.36b)$$

evaluate to the same value,

$$|\operatorname{curl} (Z_0^{-1} \operatorname{curl} E)| = k_0^2 / Z_0 = k_0^2 Y_0, \quad (2.37a)$$

$$|k_0^2 Y_0 E| = k_0^2 Y_0 \quad \text{and} \quad (2.37b)$$

$$|ik_0 \operatorname{div} Y_0 E| = k_0^2 Y_0. \quad (2.37c)$$

2.5 Anisotropy

In Chapter 4 the system of Maxwell's equations will be extended to the so-called perfectly matched layer (PML) equations with anisotropic constitutive parameters. Therefore, it is instructive to make

a couple of remarks on anisotropic media. It is well known (Landau and Lifschitz, 1980) that a beam of light that traverses optically anisotropic crystals, such as quartz or calcite, is split into two polarizations with different refractive indices/phase velocities (birefringence). The *ordinary* ray is polarized perpendicular to the axis of anisotropy, the *extraordinary* ray parallel. Let μ , ϵ and σ be symmetric tensors of full rank, homogeneous in \mathbb{R}^3 . A plane wave is a solution of source free Maxwell's equations

$$\text{curl} \left(\mu^{-1} \text{curl} E \right) + i\omega(\sigma - i\omega\epsilon)E = 0, \quad (2.38a)$$

$$\text{div}(\sigma - i\omega\epsilon)E = 0 \quad (2.38b)$$

which can be expressed by

$$E = \hat{E} e^{ikn \cdot r} \quad (2.39)$$

where the unit vector $n = (n_x, n_y, n_z)$ defines the propagation direction. Insertion of the plane wave solution (2.39) into Maxwell's equations reduces the differential operators to vector products,

$$\text{curl} E = ikn \times E, \quad (2.40a)$$

$$\text{div}(\sigma - i\omega\epsilon)E = n \cdot (\sigma - i\omega\epsilon)E \quad (2.40b)$$

where, of course, σ and ϵ have to be assumed constant. Equations (2.40b) and (2.38b) reveal that the electric current density and the electric flux density are polarized perpendicular to the propagation direction. The same holds for the magnetic flux density which can be shown by taking the dot product of n with equation (2.40a),

$$n \cdot B = i\omega n \cdot \text{curl} E = -\omega k n \times E = 0 \quad (2.41)$$

The magnetic field can be derived by combining Faraday's law and equation (2.40a),

$$H = (i\omega\mu)^{-1} \text{curl} E = k(\omega\mu)^{-1} n \times E. \quad (2.42)$$

This relation forms the basis of the absorbing boundary condition (2.10c) introduced in section 2.1 which is just the cross product of n with equation (2.42).

In order to determine the parameters \hat{E} and k in equation (2.39) it is useful to write the vector cross product as a matrix-vector product

$$n \times E = NE \quad (2.43a)$$

where

$$N = \begin{pmatrix} 0 & -n_z & n_y \\ n_z & 0 & -n_x \\ -n_y & n_x & 0 \end{pmatrix}. \quad (2.43b)$$

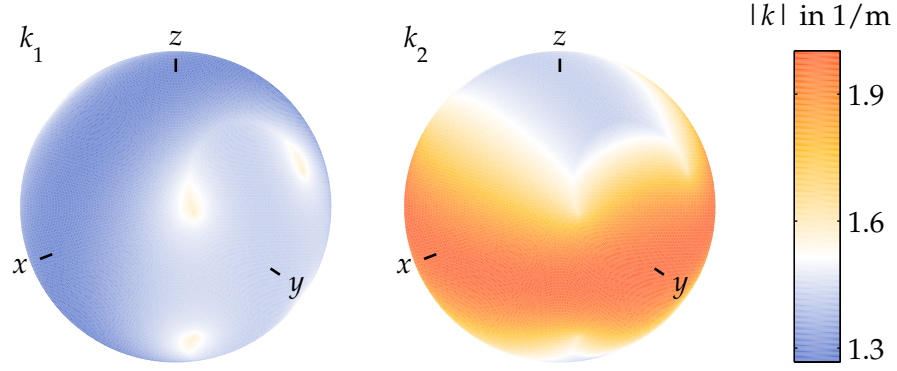


Figure 2.4: Projection of the wavenumbers of an arbitrary anisotropic medium on the unit sphere as a function of the direction of propagation.

The matrix N is skew symmetric, its rank is 2 and its null space is spanned by \mathbf{n} , i. e., $N\mathbf{n} = 0$ and $\mathbf{n}^T N = 0$. Now, inserting the plane wave solution (2.39) into equation (2.38a) yields an eigenvalue problem

$$A\hat{\mathbf{E}} = \lambda\hat{\mathbf{E}} \quad (2.44a)$$

in terms of eigenvectors $\hat{\mathbf{E}}$ and eigenvalues $\lambda = i\omega/k^2$ where

$$A = (\sigma - i\omega\varepsilon)^{-1} N \mu^{-1} N. \quad (2.44b)$$

Since $A\mathbf{n} = 0$, $\lambda_1 = 0$ is an eigenvalue with a corresponding eigenvector $\hat{\mathbf{E}}_1 = \alpha\mathbf{n}$ where $\alpha \in \mathbb{C}$ is an arbitrary constant. Equation (2.38b) further requires that

$$\mathbf{n}^T(\sigma - i\omega\varepsilon)\hat{\mathbf{E}} = 0. \quad (2.45)$$

This leads to $\alpha = 0$, i. e., the eigenpair $(\lambda_1, \hat{\mathbf{E}}_1)$ is trivial. The other two eigenvalues λ_2 and λ_3 are non-trivial. Their corresponding eigenvectors can be shown to satisfy equation (2.45) by left-multiplying equation (2.44a) with $\mathbf{n}^T(\sigma - i\omega\varepsilon)$:

$$\begin{aligned} \lambda \mathbf{n}^T(\sigma - i\omega\varepsilon)\hat{\mathbf{E}} &= \mathbf{n}^T(\sigma - i\omega\varepsilon)A\hat{\mathbf{E}} \\ &= \mathbf{n}^T(\sigma - i\omega\varepsilon)(\sigma - i\omega\varepsilon)^{-1} N \mu^{-1} N \hat{\mathbf{E}} \\ &= \mathbf{n}^T N \mu^{-1} N \hat{\mathbf{E}} \\ &= 0. \end{aligned} \quad (2.46)$$

In general, λ_2 and λ_3 need not be equal and depend on the propagation direction \mathbf{n} (Figure 2.4). All eigenvalues can be obtained from equation (2.44a) by setting the determinant of $A - \lambda I$ equal to zero. This yields a cubic polynomial in λ . The first root $\lambda_1 = 0$ separates; λ_2 and λ_3 are the solutions of a quadratic equation. If $\lambda_2 \neq \lambda_3$, two distinct plane wave solutions exist that have different linear polarizations defined by the two corresponding eigenvectors $\hat{\mathbf{E}}_2$ and $\hat{\mathbf{E}}_3$. If $\lambda_2 = \lambda_3$,

any linear combination of \hat{E}_2 and \hat{E}_3 is a plane wave solution where the polarization can be linear in an arbitrary direction or elliptical.

As a special case consider constitutive parameters that follow the same anisotropy pattern. Let $\mu = \mu M^{-1}$, $\varepsilon = \varepsilon M^{-1}$ and $\sigma = \sigma M^{-1}$ where $M \in \mathbb{C}^{3 \times 3}$ is a symmetric tensor of full rank. Then the matrix A reads

$$A = \frac{1}{\mu(\sigma - i\omega\varepsilon)} MNMN \quad (2.47)$$

In order to analyze its eigenvalues it is sufficient to consider an arbitrary tensor M and a particular direction of propagation \mathbf{n} or the corresponding matrix N . Let $\mathbf{n} = (0, 0, 1)^T$. Then a straightforward calculation yields

$$\begin{aligned} \det(A - \lambda I) &= \frac{1}{\mu^3(\sigma - i\omega\varepsilon)^3} \det(MNMN - \lambda^* I) \\ &= -\lambda^* (\lambda^* + m_{11}m_{22} - m_{12}^2)^2 \\ &= 0 \end{aligned} \quad (2.48)$$

where $\lambda^* = \lambda\mu(\sigma - i\omega\varepsilon)$. Therefore, A has one trivial eigenvalue

$$\lambda_1 = 0 \quad (2.49a)$$

and a duplicate eigenvalue

$$\lambda_2 = \lambda_3 = \frac{m_{12}^2 - m_{11}m_{22}}{\mu(\sigma - i\omega\varepsilon)}. \quad (2.49b)$$

This means that a plane wave travels within this special medium with speed and damping irrespective of its polarization. However, the wavenumber depends on the direction of propagation as for another $\mathbf{n} = (1, 0, 0)^T$ the duplicate eigenvalue is

$$\lambda_2 = \lambda_3 = \frac{m_{23}^2 - m_{22}m_{33}}{\mu(\sigma - i\omega\varepsilon)}. \quad (2.49b^*)$$

Chapter 3

The finite element method for electromagnetic wave propagation – The discrete problem

The boundary value problems of electromagnetic wave propagation which have been described in the previous chapter can be solved analytically only in very simple cases. In general, numerical methods are required to compute an approximate solution, preferably to a desired accuracy. Like other numerical methods the finite element method reduces the boundary value problem to a system of linear equations. Its solution gives an approximate solution to the original boundary value problem. The quality of the numerical solution ought to be checked by quantifying the discretization and solution errors in order to iteratively improve the approximation until an desired accuracy is obtained.

The finite element method approximates the function space from which the solution is taken. Therefore, the first section of this chapter will introduce the particular finite element spaces and types which are used to discretize the physical quantities occurring in Maxwell's equations. The second section describes the steps involved in reducing the boundary value problems from Chapter 2, the continuous case, to a system of linear equations, the discrete problem. An *a posteriori* error estimator is briefly summarized in section 3.3. Implementation issues of the finite element solver are outlined in section 3.4. Finally, the properties of the coefficient matrix of the system of linear equations are examined in section 3.5. In particular, the effect of the E -field and the E - V formulations on the matrix condition number for varying frequencies will be shown.

The finite element method with all its technical details is a too vast subject to be described in full length here. For a comprehensive description the reader is referred to standard textbooks (Ciarlet, 1978; Girault and Raviart, 1986; Jin, 1993; Monk, 2003). Moreover, an existing finite element library has served as a basis for further software development (section 3.4). Therefore, implementation details of particular finite element types are only of marginal concern and will be skipped. This chapter will consequently give but a brief overview over the main ingredients of the finite element method with particular emphasis on the application to Maxwell's equations.

3.1 Finite elements for Maxwell's equations

One, if not the, characteristic feature of the finite element method is the fact that it approximates function spaces. Two of these function spaces have been introduced in Chapter 2 where the electric

u	$H.(\Omega)$	χ_i	$\mathcal{P}.(\Omega)$	u_h
V	$H_1(\Omega)$	ϕ_i	$\mathcal{P}_1(\Omega)$	V_h
\mathbf{E}, \mathbf{H}	$H_{\text{curl}}(\Omega)$	Φ_i	$\mathcal{P}_{\text{curl}}(\Omega)$	$\mathbf{E}_h, \mathbf{H}_h$
$\mathbf{B}, \mathbf{D}, \mathbf{j}$	$H_{\text{div}}(\Omega)$	Ψ_i	$\mathcal{P}_{\text{div}}(\Omega)$	$\mathbf{B}_h, \mathbf{D}_h, \mathbf{j}_h$
ρ	$H_0(\Omega)$	ψ_i	$\mathcal{P}_0(\Omega)$	ρ_h

Table 3.1: Summary of symbols used to denote the electromagnetic fields, the function spaces they are chosen from and their corresponding finite element basis functions. The symbols in the head line are used as a shorthand notation for the symbols in either of the lines below.

field was chosen from the space of functions with well-defined curl and the auxiliary scalar field from the space of functions with well-defined gradient. The rationale behind this choice was the objective to make the integrals of the variational problems well-defined. As a nice byproduct of interpreting the differential equations in the weak sense the continuity conditions have been absorbed into the function spaces. Elements of $H_{\text{curl}}(\Omega)$ have continuous tangential components and elements of $H_1(\Omega)$ are globally continuous.

There is a pattern hidden behind this choice of function spaces which can be extended to the other electromagnetic field quantities. For Maxwell's equations to be well-defined in the weak sense the fields are chosen according to

$$V \in H_1(\Omega), \quad H_1(\Omega) = \{u \in L_2(\Omega) : \text{grad } u \in L_2(\Omega)\}, \quad (3.1a)$$

$$\mathbf{E}, \mathbf{H} \in H_{\text{curl}}(\Omega), \quad H_{\text{curl}}(\Omega) = \{\mathbf{u} \in (L_2(\Omega))^3 : \text{curl } \mathbf{u} \in (L_2(\Omega))^3\}, \quad (3.1b)$$

$$\mathbf{B}, \mathbf{D}, \mathbf{j} \in H_{\text{div}}(\Omega), \quad H_{\text{div}}(\Omega) = \{\mathbf{u} \in (L_2(\Omega))^3 : \text{div } \mathbf{u} \in (L_2(\Omega))^3\}, \quad (3.1c)$$

$$\rho \in H_0(\Omega), \quad H_0(\Omega) = \{u \in L_2(\Omega)\}. \quad (3.1d)$$

Two additional function spaces have been introduced: The space of functions with well-defined divergence $H_{\text{div}}(\Omega)$ is used to describe flux densities. $H_0(\Omega) \equiv L_2(\Omega)$ describes discontinuous scalar fields. While elements of $H_{\text{div}}(\Omega)$ have a continuous normal component, elements of $H_0(\Omega)$ are not subject to any continuity conditions.

For brevity, the short hand notation $H.(\Omega)$ will be used in the following to denote one of the spaces $H_1(\Omega)$, $H_{\text{curl}}(\Omega)$, $H_{\text{div}}(\Omega)$ and $H_0(\Omega)$. Similarly, the corresponding fields will be denoted by u , irrespective of u representing a scalar or a vector. This is summarized in the first two columns of Table 3.1.

The four function spaces are complex Hilbert spaces. As such they are equipped with the inner products

$$(u, v)_{H_1(\Omega)} = \int_{\Omega} \bar{u} v d^3r + \int_{\Omega} \text{grad } \bar{u} \cdot \text{grad } v d^3r, \quad (3.1e)$$

3.1 Finite elements for Maxwell's equations

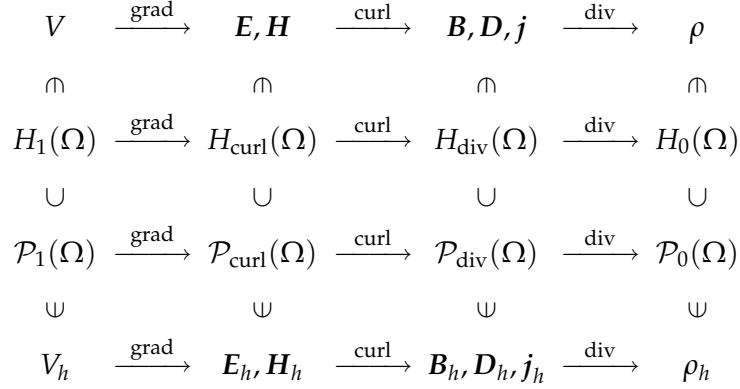


Figure 3.1: Framework of function spaces and physical fields for Maxwell's equations excluding boundary conditions.

$$(\mathbf{u}, \mathbf{v})_{H_{\text{curl}}(\Omega)} = \int_{\Omega} \bar{\mathbf{u}} \cdot \mathbf{v} \, d^3r + \int_{\Omega} \text{curl } \bar{\mathbf{u}} \cdot \text{curl } \mathbf{v} \, d^3r, \quad (3.1f)$$

$$(\mathbf{u}, \mathbf{v})_{H_{\text{div}}(\Omega)} = \int_{\Omega} \bar{\mathbf{u}} \cdot \mathbf{v} \, d^3r + \int_{\Omega} \text{div } \bar{\mathbf{u}} \, \text{div } \mathbf{v} \, d^3r, \quad (3.1g)$$

$$(u, v)_{H_0(\Omega)} = \int_{\Omega} \bar{u} v \, d^3r \quad (3.1h)$$

and norms

$$\|u\|_{H(\Omega)} = \left((u, u)_{H(\Omega)} \right)^{1/2}. \quad (3.1i)$$

Recalling the variational problems of Chapter 2 the fields were actually chosen from subspaces of $H(\Omega)$ which additionally take into account the essential boundary conditions. In order to illustrate the general concept of the finite element method it is sufficient to consider just the spaces $H(\Omega)$. The following discussion thus strictly applies only to the case of an infinite domain Ω or a finite domain with natural boundary conditions. The technical details involved in treating essential boundary conditions are left to more comprehensive mathematical works on the finite element method.

The four classes of fields (3.1a) to (3.1d) can be logically arranged in a sequence such that its entries are connected by the three differential operators gradient, curl and divergence apart from a factor of $\pm i\omega$. This is schematically depicted in the topmost line of Figure 3.1. The next line shows the sequence of the corresponding function spaces which are also linked by the three differential operators. Their operation is at first interpreted just as a mapping from one space to the other. At a closer look, the sequence turns out to be a so-called *exact sequence*. In an exact sequence the image of one operator equals the kernel of the following operator. This translates in particular to the well-known vector identities $\text{curl grad } u \equiv \mathbf{0}$ for all $u \in H_1(\Omega)$ and $\text{div curl } \mathbf{u} \equiv 0$ for all $\mathbf{u} \in H_{\text{curl}}(\Omega)$.

The transition from the upper half of Figure 3.1 to the lower half is the step that the finite element method takes. The infinite dimensional function spaces $H(\Omega)$ are approximated by finite dimensional subspaces which will be denoted by $\mathcal{P}(\Omega)$. While an infinite dimensional function space is intractable to numerical computation the finite element spaces $\mathcal{P}(\Omega)$ provide the framework within which a numerical approximation to the solution of the variational problems of Chapter 2 can practically be computed. In particular, the finite element space is spanned by a finite number of basis functions. The basis functions of $\mathcal{P}_1(\Omega)$, $\mathcal{P}_{\text{curl}}(\Omega)$, $\mathcal{P}_{\text{div}}(\Omega)$ and $\mathcal{P}_0(\Omega)$ will respectively be denoted by the symbols ϕ_i , Φ_i , Ψ_i and ψ_i (Table 3.1).

Members of the finite element spaces $\mathcal{P}(\Omega)$ are equipped with a subscript indicating the dependency on some discretization parameter h . h for example denotes the smallest edge length or the diameter of the inscribed sphere of the smallest element of the geometric decomposition of Ω into elements, shortly the *mesh*.

The finite element spaces $\mathcal{P}(\Omega)$ are constructed such that (a) they are subspaces of $H(\Omega)$, i. e., they satisfy the same continuity conditions, (b) their members are piecewise polynomial (hence symbol \mathcal{P}), (c) their basis functions have a small support, and (d) they form an exact sequence. Conditions (a) and (b) give rise to the following definition:

$$\mathcal{P}_1(\Omega) = \{u_h \in H_1(\Omega) : u_h|_K \text{ polynomial of degree } p < \infty\} \quad (3.2a)$$

$$\mathcal{P}_{\text{curl}}(\Omega) = \{\mathbf{u}_h \in H_{\text{curl}}(\Omega) : \mathbf{u}_h|_K \text{ polynomial of degree } p < \infty\} \quad (3.2b)$$

$$\mathcal{P}_{\text{div}}(\Omega) = \{\mathbf{u}_h \in H_{\text{div}}(\Omega) : \mathbf{u}_h|_K \text{ polynomial of degree } p < \infty\} \quad (3.2c)$$

$$\mathcal{P}_0(\Omega) = \{u_h \in H_0(\Omega) : u_h|_K \text{ polynomial of degree } p < \infty\} \quad (3.2d)$$

The shorthand notation $u_h|_K$ denotes the restriction of u_h onto element K . The notion of an element needs to be made more precise.

As the name of the method suggests, the function spaces $\mathcal{P}(\Omega)$ are constructed from building blocks which are called *finite elements*. According to Ciarlet (1978), a finite element can be defined as the triple $(K, \mathcal{P}(K), \mathcal{A})$ which consists of

- a geometric domain K , e. g., a tetrahedron or a hexahedron,
- a space of functions $\mathcal{P}(K)$ on K , e. g., polynomials in the three spatial variables x, y, z of degree 1, 2, etc., and
- a set of linear functionals $\{\mathcal{A}_i\}_{i=1}^n$ which are called *degrees of freedom*.

If the element is *unisolvant*, any function $u_h \in \mathcal{P}(K)$ can be written as

$$u_h(\mathbf{r}) = \sum_{i=1}^n \mathcal{A}_i(u) \chi_i(\mathbf{r}) \quad (3.3)$$

for $\mathbf{r} \in K$ where $\{\chi_i\}_{i=1}^n$ is a basis of $\mathcal{P}(K)$ and $n = \dim \mathcal{P}(K)$. The degrees of freedom are the linear coefficients of the basis function expansion of u_h in $\mathcal{P}(K)$. While the elements u_h of the

3.1 Finite elements for Maxwell's equations

	vertex	edge	face	volume
$\mathcal{P}_1(\Omega)$	×	×	×	×
$\mathcal{P}_{\text{curl}}(\Omega)$		×	×	×
$\mathcal{P}_{\text{div}}(\Omega)$			×	×
$\mathcal{P}_0(\Omega)$				×

Table 3.2: Depending on the continuity requirements of the function space the degrees of freedom are associated with different parts of an element. For example, the degrees of freedom of a curl-conforming finite element are associated with either edges, faces or volume, but not with vertices.

polynomial space $\mathcal{P}(K)$ can be scalar or vector valued, the degrees of freedom are scalars in any case. Note that unisolvence implies

$$\mathcal{A}_i(\chi_j) = \delta_{i,j} \quad (3.4)$$

for $i, j = 1, \dots, n$. The degrees of freedom are typically associated with one of the geometric entities of an element, with either a vertex, an edge, a face or the volume. Depending on which function space is considered, some entities cannot be used in order to define the degrees of freedom unambiguously. This is summarized in Table 3.2.

Two major classes of degrees of freedom are commonly used. They realize the mapping of a function $u_h \in \mathcal{P}(K)$ onto the set of complex numbers \mathbb{C} either by evaluating u_h pointwise or by computing a weighted integral of u_h over the geometric entity. The second choice involves one-, two-, or three-dimensional integrals performed along an edge, across the face or over the volume of the element. The degree of freedom thus defined is sometimes called a *moment* (Nédélec, 1980).

The degrees of freedom of the vector finite element space $\mathcal{P}_{\text{curl}}(K)$ reduce the vector field \mathbf{u}_h to a scalar value by taking the dot product with the tangential vector along an edge or with one of the two tangential vectors of a face. Similarly, the dot product of \mathbf{u}_h with the face normal vector is formed for $\mathbf{u}_h \in \mathcal{P}_{\text{div}}(K)$. Interior degrees of freedom, i. e., those associated with the volume, reduce the vector field \mathbf{u}_h to a scalar by computing the dot product with one of the three linearly independent vectors spanning the \mathbb{R}^3 .

The global function space $\mathcal{P}(\Omega)$ is basically constructed by patching together finite elements and respecting global continuity conditions. Therefore, the domain Ω is subdivided into n_e elements such that $\bigcup_{k=1}^{n_e} K_k = \Omega$ and $\bigcap_{k=1}^{n_e} K_k = \emptyset$. Denote the basis functions and degrees of freedom local to element K_k by $\{\chi_{i_k}^k\}_{i_k=1}^{n_k}$ and $\{\mathcal{A}_{i_k}^k\}_{i_k=1}^{n_k}$ and the global counterparts by $\{\chi_i\}_{i=1}^n$ and $\{\mathcal{A}_i\}_{i=1}^n$. Now, the crucial step is the design of a discrete mapping between local indices $i_k = 1, \dots, n_k$ and global indices $i = i(k, i_k) = 1, \dots, n$ such that

- the local basis function $\chi_{i_k}^k$ forms part of the global basis function χ_i , i. e., $\chi_i(\mathbf{r}) = \chi_{i_k}^k(\mathbf{r})$ for $\mathbf{r} \in K_k, k = 1, \dots, n_e$,
- the global basis functions satisfy the global continuity conditions, and
- $\mathcal{A}_i = \mathcal{A}_{i_k}^k$.

The mapping $(i_k, k) \mapsto i$ is surjective and, in general, not bijective. If more than one element contribute to a global basis function there are several local indices i_{k_1}, i_{k_2}, \dots which map to the same global index i . This property has an important consequence: If the global degrees of freedom are to be defined unambiguously, the local degrees of freedom which are mapped to the same global degree of freedom need to evaluate to the same value. For this reason, they cannot be defined on all geometric entities of an element as shown in Table 3.2.

Assuming that the elements are unisolvent and the degrees of freedom have been defined unambiguously, any function $u_h \in \mathcal{P}(\Omega)$ can be expressed by

$$u_h(\mathbf{r}) = \sum_{i=1}^n \mathcal{A}_i(u_h) \chi_i(\mathbf{r}) \quad (3.3^*)$$

for all $\mathbf{r} \in \Omega$ where, now, $\{\chi_i\}_{i=1}^n$ is the basis of $\mathcal{P}(\Omega)$ and $n = \dim \mathcal{P}(\Omega)$. u_h and χ_i can be scalar or vector valued functions according to Table 3.1.

The linear functionals \mathcal{A}_i are not restricted to functions from $\mathcal{P}(\Omega)$ but can also be applied to any function $u \in H(\Omega)$. Then,

$$u_h(\mathbf{r}) = \sum_{i=1}^n \mathcal{A}_i(u) \chi_i(\mathbf{r}) \quad (3.3^\dagger)$$

defines an *interpolant* of $u \in H(\Omega)$ in $\mathcal{P}(\Omega)$, i. e., u is sampled by the n degrees of freedom \mathcal{A}_i , $i = 1, \dots, n$, and interpolated by piecewise polynomial functions χ_i . Equation (3.3[†]) can alternatively be interpreted as a *projection* of function u from $H(\Omega)$ onto its subspace $\mathcal{P}(\Omega)$. The interpolant u_h is more regular than the original u because u_h is piecewise polynomial, $u_h|_K \in C^\infty(K)$.

The last design criterion which needs to be discussed is the exact sequence property. As an example, consider the mixed problem of Chapter 2 and the approximation of $V_h \in \mathcal{P}_1(\Omega)$ and $E_h \in \mathcal{P}_{\text{curl}}(\Omega)$. On the one hand, $\mathcal{P}_1(\Omega)$ has to be chosen large enough such that its gradient contains the kernel of the curl-operator in $\mathcal{P}_{\text{curl}}(\Omega)$. On the other hand, $\mathcal{P}_1(\Omega)$ has to be chosen small enough such that its gradient is contained in the kernel of the curl-operator in $\mathcal{P}_{\text{curl}}(\Omega)$. This property will be demonstrated by an example in section 3.4.

The nature of the vector finite element spaces $\mathcal{P}_{\text{curl}}(\Omega)$ and $\mathcal{P}_{\text{div}}(\Omega)$ reveals a strange and unexpected behavior which deserves some extra comments. Due to the exact sequence property of those two function spaces the magnetic flux B_h computed from a finite element approximation of $E_h \in \mathcal{P}_{\text{curl}}(\Omega)$ by $B_h = (i\omega)^{-1} \text{curl } E_h$ is an element of $\mathcal{P}_{\text{div}}(\Omega)$, i. e., B_h satisfies the correct physical continuity conditions. In contrast to that, the complex electric current density $\tilde{j}_h = (\sigma + i\omega\varepsilon)E_h$ is not guaranteed to possess continuous normal components, i. e., $\tilde{j}_h \notin \mathcal{P}_{\text{div}}(\Omega)$. This is even and especially true for the case of homogeneous and isotropic constitutive parameters when $\tilde{j}_h = (\sigma + i\omega\varepsilon)E_h \in \mathcal{P}_{\text{curl}}(\Omega)$ [sic]. Similarly, the magnetic field computed by $H_h = (i\omega\mu)^{-1} \text{curl } E_h \notin \mathcal{P}_{\text{curl}}(\Omega)$. In order to obtain $\tilde{j}_h \in \mathcal{P}_{\text{div}}(\Omega)$ and $H_h \in \mathcal{P}_{\text{curl}}(\Omega)$ either a variational formulation in terms of the magnetic field analogous to those given in Chapter 2 has to be solved or the quantities computed using the constitutive laws have to be projected onto the desired function spaces. The second way has been used by Beck and Hiptmair (1999) to devise an error indicator (section 3.3).

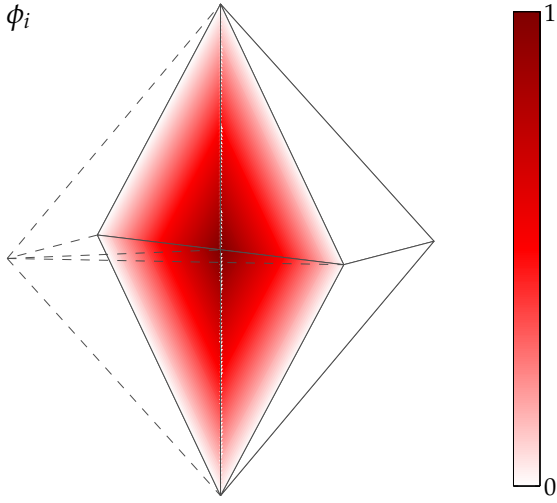


Figure 3.2: Part of a tetrahedral mesh and a piecewise linear basis function ϕ_i with well-defined gradient which is associated with the common vertex of the eight tetrahedra. The support of ϕ_i only consists of the eight tetrahedra shown.

Before turning to the finite element solution of the variational problems of Chapter 2, basis functions for $\mathcal{P}_1(\Omega)$, $\mathcal{P}_{\text{curl}}(\Omega)$, $\mathcal{P}_{\text{div}}(\Omega)$ and $\mathcal{P}_0(\Omega)$ need to be exemplified and their interpolation properties be discussed.

The Lagrange element is the standard finite element type which is used to approximate functions from $H_1(\Omega)$, i. e., scalar functions which are globally continuous. Its name is due to the fact that the projection of a function $u \in H_1(\Omega)$ onto $\mathcal{P}_1(K)$ is exactly the Lagrange interpolating polynomial of u on K . In the case of the linear Lagrange element, the basis functions of $\mathcal{P}_1(\Omega)$ can be associated with the vertices of the mesh. An example is shown in Figure 3.2. ϕ_i varies linearly between one at the vertex shared by all the eight tetrahedra shown and zero at the opposite faces. ϕ_i is continuous at the interfaces between the elements and vanishes on all other than the eight tetrahedra shown. The degree of freedom \mathcal{A}_i corresponding to basis function ϕ_i just evaluates the function it is applied to at vertex i .

Vector finite elements have been invented in order to meet the peculiar continuity requirements of vector fields from $H_{\text{curl}}(\Omega)$ and $H_{\text{div}}(\Omega)$. They are known as Nédélec elements (Nédélec, 1980, 1986), edge or Whitney elements (Bossavit, 1998). The denomination edge element strictly applies only to the linear curl-conforming vector element whose degrees of freedoms are the tangential component of the field along each edge of the element. Application of differential geometry arguments to physical problems by Whitney (1957) lead to the name Whitney element. The mathematical foundation for the families of curl- and divergence-conforming finite elements used today was laid by Nédélec in 1980. The practical problem of constructing sets of higher order polynomials in $\mathcal{P}_{\text{curl}}(K)$ and $\mathcal{P}_{\text{div}}(K)$ have been addressed in a number of later works (Graglia, Wilton, and Peterson, 1997; Amrouche, Bernardi, Dauge, and Girault, 1998; Andersen and Volakis, 1998; Webb, 1999; Hiptmair, 2001, 2002).

Examples of basis functions from the lowest order curl- and divergence-conforming elements are

shown in Figures 3.3 and 3.5. In this case of a linear polynomial, the basis functions can respectively be associated with the common edge and face of neighboring elements. The corresponding degrees of freedom reduce to the tangential field component along the edge midpoint and the normal field component at the face center, respectively, which are multiplied by the edge length and face area if the degrees of freedom are defined as moments. Figures 3.4 and 3.6 illustrate that only the tangential or normal component is continuous at element interfaces, as required by the global continuity conditions. The other vector component is not forced to be continuous and will, except for special cases, be discontinuous. As a consequence, any function $\mathbf{u}_h \in \mathcal{P}_{\text{curl}}(\Omega)$ is *multi-valued* if evaluated on vertices or edges shared by more than one element because its normal component depends on the element the field is actually evaluated on. Similarly, any function $\mathbf{u}_h \in \mathcal{P}_{\text{div}}(\Omega)$ is multi-valued if evaluated on vertices, edges or faces shared by more than one element because its tangential components depend on the element the field is actually evaluated on.

From a practical point of view the field and, possibly, derived quantities like its derivate are often to be evaluated at special points of interest within Ω . Then, the question naturally turns up if it is advisable to place these points in the interior of elements in order to circumvent the problem of multi-valued fields at element interfaces. Because the field components are distributed over the element interpolation is always required to compute the complete field vector. The effect of this interpolation procedure is demonstrated in Figures 3.7 and 3.8. Two instances of a vector field are projected onto the finite element spaces $\mathcal{P}_{\text{curl}}(\Omega)$ and $\mathcal{P}_{\text{div}}(\Omega)$ according to equation (3.3[†]). The finite element spaces are built from four hexahedral elements with piecewise linear basis functions. In order to simplify visualization only a horizontal slice is shown where the vertical field components are assumed to be zero. The degree of freedom \mathcal{A}_i evaluates \mathbf{u} at point \mathbf{r}_i . Therefore, they are best characterized by the product of $\mathcal{A}_i\{\mathbf{u}\}$ with the corresponding basis function Φ_i or Ψ_i evaluated just at \mathbf{r}_i . The interpolant \mathbf{u}_h can then be constructed by linear interpolation between the field components on parallel edges and superposition of orthogonal field components.

For the examples shown, the interpolation error is smaller at the midpoint of each cell than at the points on the element boundaries. Note that at point \mathbf{r}_i where the degree of freedom \mathcal{A}_i is defined the error is by construction orthogonal to the basis function $\Phi_i(\mathbf{r}_i)$ or $\Psi_i(\mathbf{r}_i)$.

Comparison with the Yee-cell

If hexahedral elements of lowest degree, a piecewise linear approximation of the electric field $\mathbf{E}_h \in \mathcal{P}_{\text{curl}}(\Omega)$ and of the magnetic flux density $\mathbf{B}_h \in \mathcal{P}_{\text{div}}(\Omega)$ is used, the corresponding degrees of freedom show a remarkable similarity with the famous Yee cell (Yee, 1966). The Yee cell is a particular staggered grid arrangement of field components which is used to derive a finite difference discretization of Maxwell's equations. The electric field and magnetic flux density vector components are not considered at one single point but distributed over the edges and faces of the cell as shown in Figure 3.9. Placing the tangential electric field components at the midpoints of edges and the normal magnetic flux density components at the centers of faces adequately reproduces the correct physical continuity conditions. At the same time, the finite difference discretization of the curl-operator is easily derived. If the degrees of freedom of the finite element

3.1 Finite elements for Maxwell's equations

approximation of lowest order are defined pointwise, they coincide with the same components of the fields at exactly the same locations within the cell. Unlike the finite difference method where the computation of field values at arbitrary points $\mathbf{r} \in \Omega$ requires the *ad hoc* definition of a suitable interpolation operator, the finite element method provides this interpolation *per construction*. The i -th degree of freedom/field component associated with the common edge or face of adjacent elements contributes to the interpolated field with a weight defined by the corresponding i -th finite element basis function. Two example basis functions which would be used for a staggered grid like in Figure 3.9 are shown in Figures 3.10 and 3.11. Φ_i is the basis/weight function for the tangential electric field component defined on the common edge of the four hexahedra in Figure 3.10; Ψ_i is the basis/weight function for the normal magnetic flux density component defined on the common face of the two hexahedra in Figure 3.11.

A discontinuous element is required to approximate scalar functions from $H_0(\Omega)$. The lowest order basis consists of n_e functions where n_e is the number of elements and $\psi_i(\mathbf{r}) = \delta_{i,j}$ for $\mathbf{r} \in K_j$, $i, j = 1, \dots, n_e$. Note that the lowest order basis functions of the previous types had been piecewise linear. The discontinuous element only allows for degrees of freedom associated with the element volume. This element is not of further interest and only mentioned here to complete the description of the function space and finite element complex for the Maxwell system.

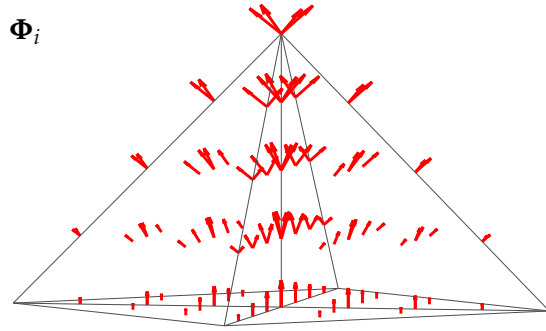


Figure 3.3: Part of a tetrahedral mesh and a piecewise linear, curl-conforming basis function Φ_i which is associated with the common edge of the four tetrahedra. The support of Φ_i only consists of the four tetrahedra shown.

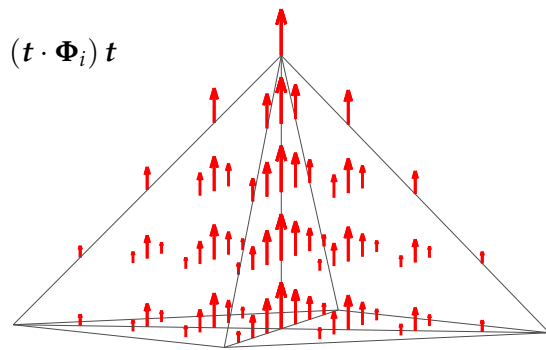


Figure 3.4: Tangential component of Φ_i with respect to the edge it is associated to. The tangential component is continuous and constant along the edge for a piecewise linear, curl-conforming basis function. t denotes the unit edge tangential vector.

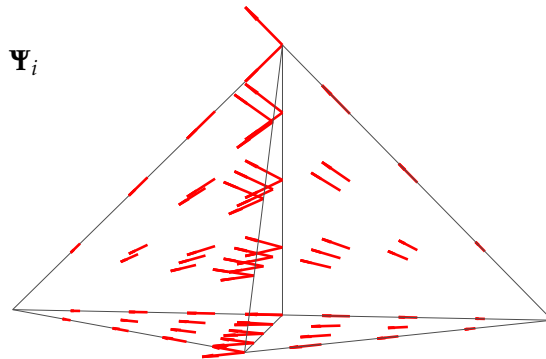


Figure 3.5: Part of a tetrahedral mesh and a piecewise linear, div-conforming basis function Ψ_i which is associated with the common face between the two tetrahedra. The support of Ψ_i only consists of the two tetrahedra shown.

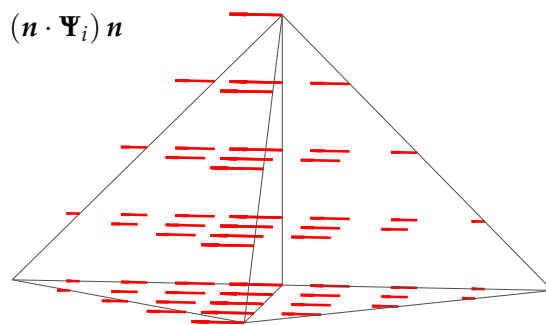


Figure 3.6: Normal component of Ψ_i with respect to the face it is associated to. The normal component is continuous and constant on the face for a piecewise linear, div-conforming basis function. n denotes the unit face normal vector.

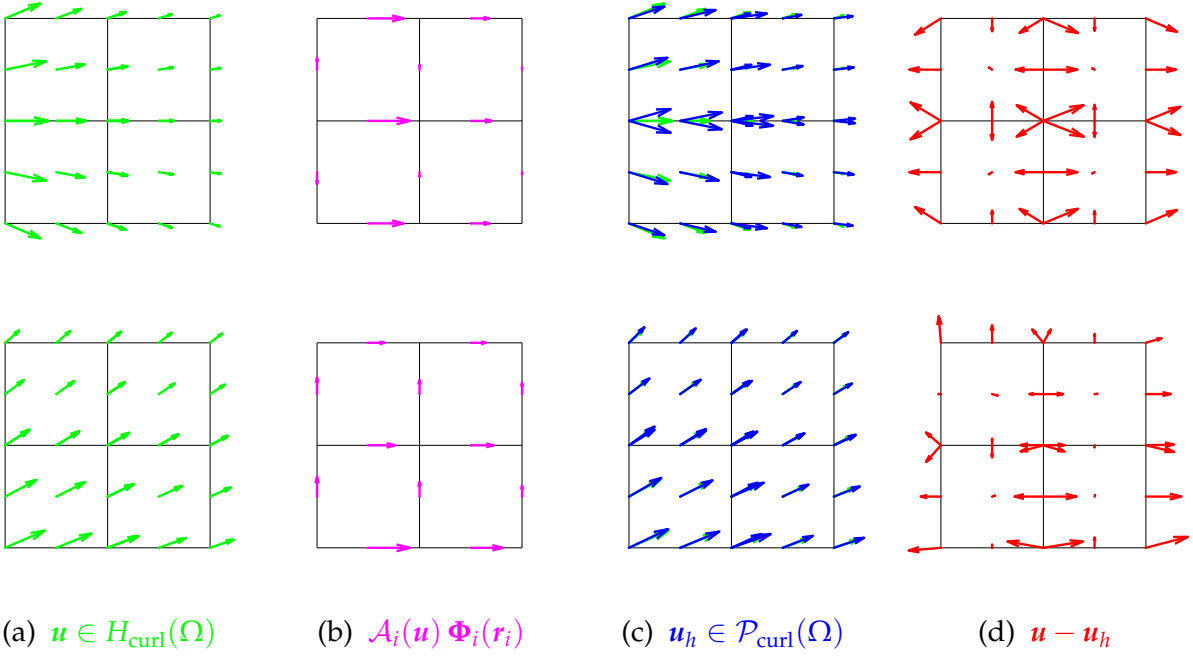


Figure 3.7: Projection of two instances of a vector field $\mathbf{u} \in H_{\text{curl}}(\Omega)$ (a), first and second line, onto a curl-conforming finite element space $\mathcal{P}_{\text{curl}}(\Omega)$ with linear vector elements. (b) Degrees of freedom $\mathcal{A}_i(\mathbf{u}) \Phi_i(\mathbf{r}_i)$. (c) Interpolant $\mathbf{u}_h(\mathbf{r}) = \sum_i \mathcal{A}_i(\mathbf{u}) \Phi_i(\mathbf{r})$ (blue) and original vector field \mathbf{u} (green). (d) Interpolation error $\mathbf{u} - \mathbf{u}_h$. The arrows of each subplot are scaled individually.

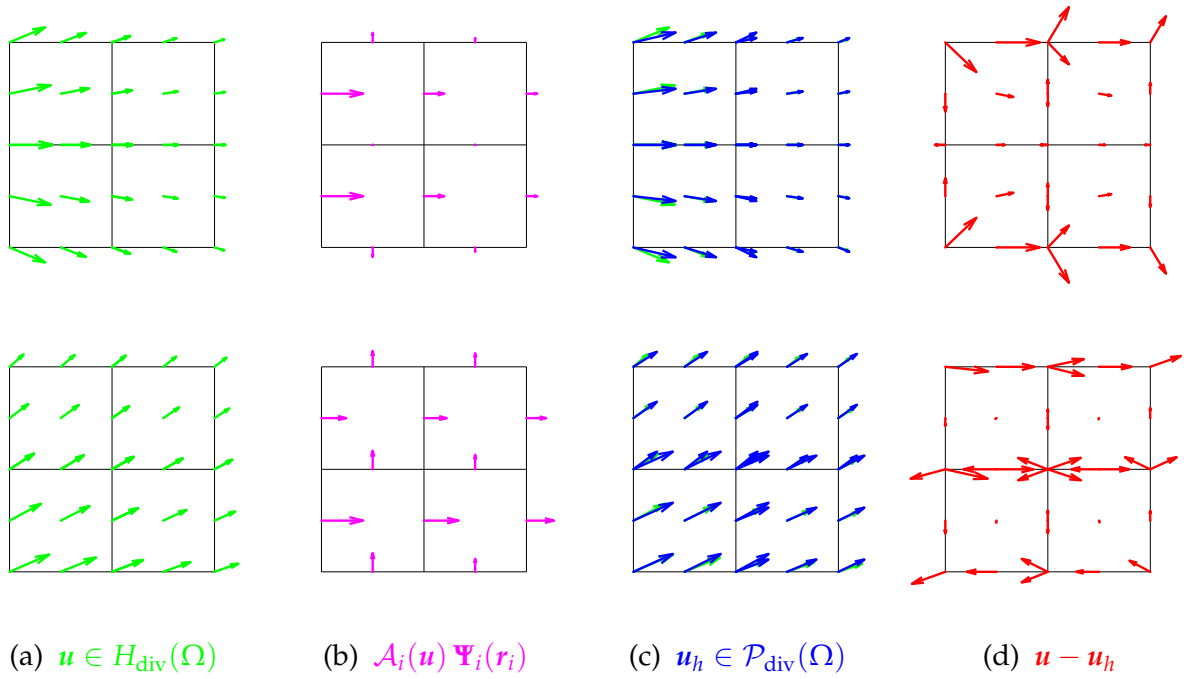


Figure 3.8: Projection of two instances of a vector field $\mathbf{u} \in H_{\text{div}}(\Omega)$ (a), first and second line, onto a divergence-conforming finite element space $\mathcal{P}_{\text{div}}(\Omega)$ with linear vector elements. (b) Degrees of freedom $\mathcal{A}_i(\mathbf{u}) \Psi_i(\mathbf{r}_i)$. (c) Interpolant $\mathbf{u}_h(\mathbf{r}) = \sum_i \mathcal{A}_i(\mathbf{u}) \Psi_i(\mathbf{r})$ (blue) and original vector field \mathbf{u} (green). (d) Interpolation error $\mathbf{u} - \mathbf{u}_h$. The arrows of each subplot are scaled individually.

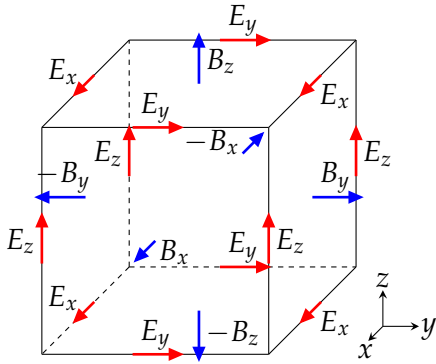


Figure 3.9: Location of field components within a Yee cell. If degrees of freedom of the linear curl/divergence-conforming finite element are defined pointwise, they reduce to exactly the same values.

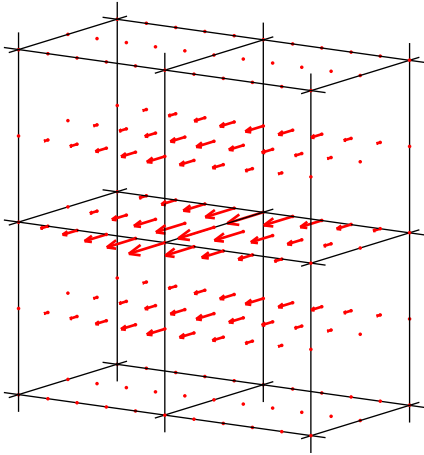


Figure 3.10: Part of a hexahedral mesh and a piecewise linear, curl-conforming basis function Φ_i which is associated with the common edge of the four hexahedra. The support of Φ_i only consists of the four hexahedra shown.

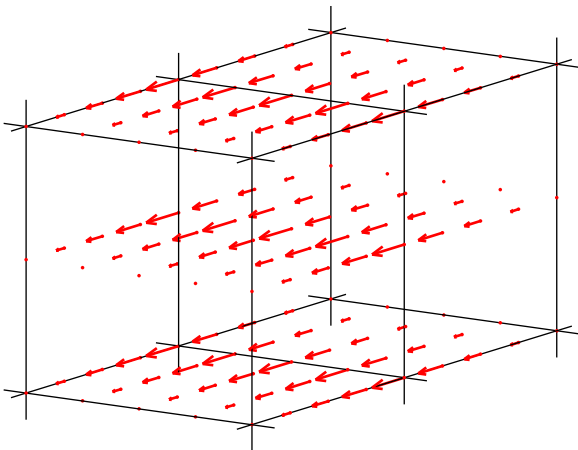


Figure 3.11: Part of a hexahedral mesh and a piecewise linear, div-conforming basis function Ψ_i which is associated with the common face between the two hexahedra. The support of Ψ_i only consists of the two hexahedra shown.

3.2 Derivation of the system of linear equations

A numerical approximation of the solution of the variational problems (2.27) and (2.31) or, equivalently, of the classical boundary value problems (2.12) and (2.18) is obtained by the method of finite elements. The finite element method reduces the boundary value problem to a system of linear equations. Its derivation can be logically subdivided into four steps which are described separately in the following four subsections.

3.2.1 Geometric decomposition

The domain Ω is decomposed into simple geometrical elements, e. g., tetrahedra or hexahedra. If Ω consists of several subdomains the elemental decomposition has to respect the subdomain interfaces. Standard mesh generators create tetrahedral or hexahedral meshes with planar (linear) elements. Curved interfaces or boundaries are then approximated by piecewise linear faces. This geometrical approximation will introduce errors to the numerical solution which can be reduced by refining the mesh at curved features. Another possibility is the use of curved elements which approximate a curved geometry by a quadratic polynomial.

In general, the geometric decomposition produces subdomains $\Omega_{i,h}$, boundaries $\Gamma_{e,h}$ and $\Gamma_{h,h}$ as well as interfaces $\Sigma_{i,j,h}$ which depend on the grid size h and do not necessarily coincide with the original domains, boundaries and interfaces. For ease of notation the symbols of the continuous case will be used for the discrete case throughout the remainder of this chapter. It should be kept in mind that this is only valid for polyhedral subdomains, i. e., subdomains bounded by planar faces.

3.2.2 Finite dimensional function spaces

The trial and test functions of the continuous boundary value problems (2.27) and (2.31) are chosen from subspaces of the two function spaces $H_{\text{curl}}(\Omega)$ and $H_1(\Omega)$. The fundamental step of the finite element method is to approximate these infinite dimensional function spaces by finite dimensional function spaces $\mathcal{P}_{\text{curl}}(\Omega)$ and $\mathcal{P}_1(\Omega)$ of elementwise polynomial functions. Consequently, the spaces of trial and test functions \mathcal{U} , \mathcal{V} and \mathcal{U}_0 , \mathcal{V}_0 also become finite dimensional and will be supplied by a subscript h . Now, the variational problem is stated in terms of functions from \mathcal{U}_h , \mathcal{V}_h and $\mathcal{U}_{h,0}$, $\mathcal{V}_{h,0}$.

The E-field formulation

Search $E_h \in \mathcal{U}_h$ such that

$$\begin{aligned} & \int_{\Omega} \text{curl } \overline{\Phi}_h \cdot \left(\mu^{-1} \text{curl } E_h \right) d^3r - i\omega \int_{\Omega} \overline{\Phi}_h \cdot ((\sigma - i\omega\epsilon) E_h) d^3r \\ & + i\omega \int_{\Gamma_h} (\mathbf{n} \times \overline{\Phi}_h) \cdot (\lambda (\mathbf{n} \times E_h)) d^2r \end{aligned}$$

3.2 Derivation of the system of linear equations

$$= i\omega \int_{\Omega} \bar{\Phi}_h \cdot \mathbf{j}_s d^3r - i\omega \sum_{\substack{i,j=1 \\ i < j}}^n \int_{\Sigma_{ij}} \bar{\Phi}_h \cdot \mathbf{j}_f d^2r - i\omega \int_{\Gamma_h} \bar{\Phi}_h \cdot (\mathbf{j}_f + \mathbf{n} \times \mathbf{H}_0) d^2r \quad (3.5a)$$

for all $\Phi_h \in \mathcal{U}_{h,0}$. The spaces of test and trial functions are defined by

$$\mathcal{U}_{h,0} = \{ \Phi_h \in \mathcal{P}_{\text{curl}}(\Omega) : \mathbf{n} \times \Phi_h = \mathbf{0} \text{ on } \Gamma_e \}, \quad (3.5b)$$

$$\mathcal{U}_h = \{ E_h \in \mathcal{P}_{\text{curl}}(\Omega) : \mathbf{n} \times E_h = \mathbf{n} \times E_0 \text{ on } \Gamma_e \} \quad (3.5c)$$

where

$$\mathcal{P}_{\text{curl}}(\Omega) = \{ E_h \in (L_2(\Omega))^3 : \text{curl } E_h \in (L_2(\Omega))^3, E_h|_K \text{ polynomial} \} \quad (3.5d)$$

is the space of elementwise polynomial functions with a well-defined curl.

The E-V formulation

Search $E_h \in \mathcal{U}_h$ and $V_h \in \mathcal{V}_h$ such that

$$\begin{aligned} & \int_{\Omega} \text{curl } \bar{\Phi}_h \cdot (\mu^{-1} \text{curl } E_h) d^3r - i\omega \int_{\Omega} \bar{\Phi}_h \cdot ((\sigma - i\omega\epsilon) E_h) d^3r \\ & + \int_{\Omega} \bar{\Phi}_h \cdot ((\sigma - i\omega\epsilon) \text{grad } V_h) d^3r + i\omega \int_{\Gamma_h} (\mathbf{n} \times \bar{\Phi}_h) \cdot (\lambda (\mathbf{n} \times E_h)) d^2r \\ & - \int_{\Gamma_h} (\mathbf{n} \times \bar{\Phi}_h) \cdot (\lambda (\mathbf{n} \times \text{grad } V_h)) d^2r \\ & = i\omega \int_{\Omega} \bar{\Phi}_h \cdot \mathbf{j}_s d^3r - i\omega \sum_{\substack{i,j=1 \\ i < j}}^n \int_{\Sigma_{ij}} \bar{\Phi}_h \cdot \mathbf{j}_f d^2r - i\omega \int_{\Gamma_h} \bar{\Phi}_h \cdot (\mathbf{j}_f + \mathbf{n} \times \mathbf{H}_0) d^2r \end{aligned} \quad (3.6a)$$

for all $\Phi_h \in \mathcal{U}_{h,0}$ and

$$\begin{aligned} & \int_{\Omega} \text{grad } \bar{\phi}_h \cdot ((\sigma - i\omega\epsilon) E_h) d^3r - \int_{\Omega} \bar{\phi}_h \gamma V_h d^3r - \int_{\Gamma_h} (\mathbf{n} \times \text{grad } \bar{\phi}_h) \cdot (\lambda (\mathbf{n} \times E_h)) d^2r \\ & = - \int_{\Omega} \text{grad } \bar{\phi}_h \cdot \mathbf{j}_s d^3r + \int_{\Gamma_h} \text{grad } \bar{\phi}_h \cdot (\mathbf{n} \times \mathbf{H}_0) d^2r \end{aligned} \quad (3.6b)$$

for all $\phi_h \in \mathcal{V}_{h,0}$. The spaces of test and trial functions are defined by

$$\mathcal{U}_{h,0} = \{ \Phi_h \in \mathcal{P}_{\text{curl}}(\Omega) : \mathbf{n} \times \Phi_h = \mathbf{0} \text{ on } \Gamma_e \}, \quad (3.6c)$$

$$\mathcal{U}_h = \{ E_h \in \mathcal{P}_{\text{curl}}(\Omega) : \mathbf{n} \times E_h = \mathbf{n} \times E_0 \text{ on } \Gamma_e \}, \quad (3.6d)$$

$$\mathcal{V}_{h,0} = \{ V_h \in \mathcal{P}_1(\Omega) : V_h = 0 \text{ on } \Gamma_e \}, \quad (3.6e)$$

$$\mathcal{V}_h = \mathcal{V}_{h,0} \quad (3.6f)$$

where

$$\mathcal{P}_{\text{curl}}(\Omega) = \{ E_h \in (L_2(\Omega))^3 : \text{curl } E_h \in (L_2(\Omega))^3, E_h|_K \text{ polynomial} \}, \quad (3.6g)$$

$$\mathcal{P}_1(\Omega) = \{V_h \in L_2(\Omega) : \text{grad } V_h \in L_2(\Omega), V_h|_K \text{ polynomial}\} \quad (3.6h)$$

are the spaces of elementwise polynomial functions with a well-defined curl and gradient, respectively.

3.2.3 Trial functions

A set of basis functions $\{\Phi_i\}_{i=1}^N$ is constructed for $\mathcal{P}_{\text{curl}}(\Omega)$. The electric field can then be expanded as a linear combination of these basis functions,

$$E_h(\mathbf{r}) = \sum_{i=1}^N E_i \Phi_i(\mathbf{r}). \quad (3.7)$$

The basis functions are sorted such that the set $\{\Phi_i\}_{i=1}^n$, $n \leq N$, forms a basis of $\mathcal{U}_{h,0}$. Since $\mathcal{P}_{\text{curl}}(\Omega)$ is finite dimensional, $n \leq N < \infty$. The coefficients E_i of the remaining basis functions Φ_i , $i = n+1, \dots, N$, have to be fixed in order to ensure $E_h \in \mathcal{U}_h$, i. e., to enforce the inhomogeneous Dirichlet boundary conditions by choosing

$$E_i = \mathcal{A}_i\{E_0\}. \quad (3.8)$$

\mathcal{A}_i acts as a linear operator which maps the vector field $E_0(\mathbf{r})$ onto the scalar valued degrees of freedom E_i , $i = n+1, \dots, N$.

Similarly, a set of basis functions $\{\phi_i\}_{i=1}^M$ is constructed for $\mathcal{P}_1(\Omega)$. The scalar field can then be expanded as a linear combination of these basis functions,

$$V_h(\mathbf{r}) = \sum_{i=1}^M V_i \phi_i(\mathbf{r}). \quad (3.9)$$

The basis functions are sorted such that the set $\{\phi_i\}_{i=1}^m$, $m \leq M$, forms a basis of $\mathcal{V}_{h,0}$, i. e., $\phi_i = 0$ on Γ_e for $i = 1, \dots, m$. Since $\mathcal{P}_1(\Omega)$ is finite dimensional, $m \leq M < \infty$. The coefficients V_i of the remaining basis functions ϕ_i , $i = m+1, \dots, M$, for which $\phi_i \neq 0$ on Γ_e holds, have to be fixed in order to ensure $V_h \in \mathcal{V}_h$, i. e., to enforce the Dirichlet boundary condition. $V_h = 0$ on Γ_e requires that $V_i = 0$, $i = m+1, \dots, M$.

3.2.4 Test functions

The variational integrals (3.5a) and (3.6a) have to be tested against all functions $\Phi_h \in \mathcal{U}_{h,0}$, the variational integrals (3.6b) against all functions $\phi_h \in \mathcal{V}_{h,0}$. This is equivalent to testing against all basis functions Φ_j , $j = 1, \dots, n$ and ϕ_j , $j = 1, \dots, m$, respectively, because $\{\Phi_i\}_{i=1}^n$ forms a basis of $\mathcal{U}_{h,0}$ and $\{\phi_i\}_{i=1}^m$ forms a basis of $\mathcal{V}_{h,0}$.

The E-field formulation

Inserting the trial function (3.7) into the variational form (3.5a) and taking the j -th basis function Φ_j as the test function produces the j -th row of a system of linear equations in terms of the unknown

3.2 Derivation of the system of linear equations

linear coefficients E_i ,

$$\sum_{i=1}^n a_{j,i} E_i = f_j, \quad j = 1, \dots, n, \quad (3.10a)$$

where

$$\begin{aligned} a_{j,i} = & \int_{\Omega} \text{curl } \bar{\Phi}_j \cdot \left(\mu^{-1} \text{curl } \Phi_i \right) d^3r - i\omega \int_{\Omega} \bar{\Phi}_j \cdot ((\sigma - i\omega\varepsilon) \Phi_i) d^3r \\ & + i\omega \int_{\Gamma_h} (\mathbf{n} \times \bar{\Phi}_j) \cdot (\lambda (\mathbf{n} \times \Phi_i)) d^2r, \end{aligned} \quad (3.10b)$$

$$\begin{aligned} f_j = & i\omega \int_{\Omega} \bar{\Phi}_j \cdot \mathbf{j}_s d^3r - i\omega \sum_{\substack{i,j=1 \\ i < j}}^n \int_{\Sigma_{i,j}} \bar{\Phi}_j \cdot \mathbf{j}_f d^2r - i\omega \int_{\Gamma_h} \bar{\Phi}_j \cdot (\mathbf{j}_f + \mathbf{n} \times \mathbf{H}_0) d^2r \\ & - \sum_{i=n+1}^N a_{j,i} E_i. \end{aligned} \quad (3.10c)$$

The complete system of linear equations reads in matrix notation as follows

$$\begin{pmatrix} a_{1,1} & \dots & a_{1,n} \\ \vdots & & \vdots \\ a_{n,1} & \dots & a_{n,n} \end{pmatrix} \begin{pmatrix} E_1 \\ \vdots \\ E_n \end{pmatrix} = \begin{pmatrix} f_1 \\ \vdots \\ f_n \end{pmatrix} \quad (3.10d)$$

or, even shorter,

$$AE = f \quad (3.10e)$$

with coefficient matrix $A \in \mathbb{C}^{n \times n}$ and column vectors $E, f \in \mathbb{C}^n$.

If the basis functions $\Phi_i, i = 1, \dots, n$, are real valued and if the tensors μ, σ and ε are symmetric, $a_{j,i} = a_{i,j}$ holds for all $i, j = 1, \dots, n$, i.e., $A = A^T$. Therefore, the coefficient matrix in (3.10d) or (3.10e) is quadratic, complex and symmetric, but not Hermitian.

The E-V formulation

Inserting the trial functions (3.7) and (3.9) into the variational forms (3.6a) and (3.6b), and taking the j -th basis function Φ_j and ϕ_j , respectively, as the test function produces the j -th row of a system of linear equations in terms of the unknown linear coefficients E_i and V_i ,

$$\sum_{i=1}^n a_{j,i}^{(\Phi,\Phi)} E_i + \sum_{i=1}^m a_{j,i}^{(\Phi,\phi)} V_i = f_j^{(\Phi)}, \quad j = 1, \dots, n, \quad (3.11a)$$

$$\sum_{i=1}^n a_{j,i}^{(\phi,\Phi)} E_i + \sum_{i=1}^m a_{j,i}^{(\phi,\phi)} V_i = f_j^{(\phi)}, \quad j = 1, \dots, m, \quad (3.11b)$$

Chapter 3 The finite element method

where

$$a_{j,i}^{(\Phi,\Phi)} = \int_{\Omega} \text{curl } \bar{\Phi}_j \cdot (\mu^{-1} \text{curl } \Phi_i) d^3r - i\omega \int_{\Omega} \bar{\Phi}_j \cdot ((\sigma - i\omega\varepsilon) \Phi_i) d^3r \\ + i\omega \int_{\Gamma_h} (\mathbf{n} \times \bar{\Phi}_j) \cdot (\lambda (\mathbf{n} \times \Phi_i)) d^2r, \quad (3.11c)$$

$$a_{j,i}^{(\Phi,\phi)} = \int_{\Omega} \bar{\Phi}_j \cdot ((\sigma - i\omega\varepsilon) \text{grad } \phi_i) d^3r - \int_{\Gamma_h} (\mathbf{n} \times \bar{\Phi}_j) \cdot (\lambda (\mathbf{n} \times \text{grad } \phi_i)) d^2r, \quad (3.11d)$$

$$a_{j,i}^{(\phi,\Phi)} = \int_{\Omega} \text{grad } \bar{\phi}_j \cdot ((\sigma - i\omega\varepsilon) \Phi_i) d^3r - \int_{\Gamma_h} (\mathbf{n} \times \text{grad } \bar{\phi}_j) \cdot (\lambda (\mathbf{n} \times \Phi_i)) d^2r, \quad (3.11e)$$

$$a_{j,i}^{(\phi,\phi)} = - \int_{\Omega} \bar{\phi}_j \gamma \phi_i d^3r \quad (3.11f)$$

and

$$f_j^{(\Phi)} = i\omega \int_{\Omega} \bar{\Phi}_j \cdot \mathbf{j}_s d^3r - i\omega \sum_{\substack{i,j=1 \\ i < j}}^n \int_{\Sigma_{i,j}} \bar{\Phi}_j \cdot \mathbf{j}_f d^2r - i\omega \int_{\Gamma_h} \bar{\Phi}_j \cdot (\mathbf{j}_f + \mathbf{n} \times \mathbf{H}_0) d^2r \\ - \sum_{i=n+1}^N a_{j,i}^{(\Phi,\Phi)} E_i - \sum_{i=m+1}^M a_{j,i}^{(\Phi,\phi)} V_i, \quad (3.11g)$$

$$f_j^{(\phi)} = - \int_{\Omega} \text{grad } \bar{\phi}_j \cdot \mathbf{j}_s d^3r + \int_{\Gamma_h} \text{grad } \bar{\phi}_j \cdot (\mathbf{n} \times \mathbf{H}_0) d^2r \\ - \sum_{i=n+1}^N a_{j,i}^{(\phi,\Phi)} E_i - \sum_{i=m+1}^M a_{j,i}^{(\phi,\phi)} V_i \quad (3.11h)$$

The complete system of linear equation reads in matrix notation as follows

$$\begin{pmatrix} a_{1,1}^{(\Phi,\Phi)} & \dots & a_{1,n}^{(\Phi,\Phi)} & a_{1,1}^{(\Phi,\phi)} & \dots & a_{1,m}^{(\Phi,\phi)} \\ \vdots & & \vdots & \vdots & & \vdots \\ a_{n,1}^{(\Phi,\Phi)} & \dots & a_{n,n}^{(\Phi,\Phi)} & a_{n,1}^{(\Phi,\phi)} & \dots & a_{n,m}^{(\Phi,\phi)} \\ a_{1,1}^{(\phi,\Phi)} & \dots & a_{1,n}^{(\phi,\Phi)} & a_{1,1}^{(\phi,\phi)} & \dots & a_{1,m}^{(\phi,\phi)} \\ \vdots & & \vdots & \vdots & & \vdots \\ a_{m,1}^{(\phi,\Phi)} & \dots & a_{m,n}^{(\phi,\Phi)} & a_{m,1}^{(\phi,\phi)} & \dots & a_{m,m}^{(\phi,\phi)} \end{pmatrix} \begin{pmatrix} E_1 \\ \vdots \\ E_n \\ V_1 \\ \vdots \\ V_m \end{pmatrix} = \begin{pmatrix} f_1^{(\Phi)} \\ \vdots \\ f_n^{(\Phi)} \\ f_1^{(\phi)} \\ \vdots \\ f_m^{(\phi)} \end{pmatrix}, \quad (3.11i)$$

or, even shorter,

$$\begin{pmatrix} A^{(\Phi,\Phi)} & A^{(\Phi,\phi)} \\ A^{(\phi,\Phi)} & A^{(\phi,\phi)} \end{pmatrix} \begin{pmatrix} E \\ V \end{pmatrix} = \begin{pmatrix} f^{(\Phi)} \\ f^{(\phi)} \end{pmatrix} \quad (3.11j)$$

with submatrices $A^{(\Phi,\Phi)} \in \mathbb{C}^{n \times n}$, $A^{(\Phi,\phi)} \in \mathbb{C}^{n \times m}$, $A^{(\phi,\Phi)} \in \mathbb{C}^{m \times n}$, $A^{(\phi,\phi)} \in \mathbb{C}^{m \times m}$ and column vectors $E, f^{(\Phi)} \in \mathbb{C}^n$, $V, f^{(\phi)} \in \mathbb{C}^m$. $A^{(\Phi,\Phi)}$ is identical with the coefficient matrix A of the E -field

formulation (3.10e) and represents the operator $\text{curl } \mu^{-1} \text{curl} - i\omega (\sigma - i\omega \varepsilon)$ (plus boundary conditions). The rectangular matrices $A^{(\phi, \Phi)}$ and $A^{(\Phi, \phi)}$ are respectively the discrete version of the operator $\text{div} (\sigma - i\omega \varepsilon)$ and of the gradient multiplied by the complex conductivity, $(\sigma - i\omega \varepsilon) \text{grad}$. $A^{(\phi, \phi)}$ is a γ -weighted mass matrix.

If the basis functions Φ_i , $i = 1, \dots, n$, and ϕ_i , $i = 1, \dots, m$, are real valued and if the tensors μ , σ and ε are symmetric, $a_{j,i}^{(\Phi, \Phi)} = a_{i,j}^{(\Phi, \Phi)}$ holds for all $i, j = 1, \dots, n$ and $a_{j,i}^{(\phi, \phi)} = a_{i,j}^{(\phi, \phi)}$ for all $i, j = 1, \dots, m$, i.e., $A^{(\Phi, \Phi)} = (A^{(\Phi, \Phi)})^T$ and $A^{(\phi, \phi)} = (A^{(\phi, \phi)})^T$. In addition, the mixed form matrix subblocks satisfy $a_{j,i}^{(\Phi, \phi)} = a_{i,j}^{(\phi, \Phi)}$ for all $i = 1, \dots, n$ and $j = 1, \dots, m$, i.e., $A^{(\Phi, \phi)} = (A^{(\phi, \Phi)})^T$. Therefore, the coefficient matrix in (3.11i) or (3.11j) is quadratic, complex and symmetric, but not Hermitian.

Symmetry had been a design criterion while constructing the low-frequency stabilized boundary value problem. The final coefficient matrix of the E - V formulation now proves to have the same symmetry property like that of the E -field formulation. The motivation for preserving this feature is that only the upper or lower triangular part of symmetric matrices needs to be stored in memory. This saves half of the resources which would be required to store a non-symmetric matrix in memory. Moreover, a matrix factorization can be performed with less operational costs and requires considerably less storage as well.

3.3 An a posteriori error indicator

Careful numerical treatment of any boundary value problem completes the computation of the actual solution by a suitable error estimation. Error estimators for Maxwell's equation are non-trivial and the topic of active research (Demkowicz, 2003; Monk, 2003; Nicaise and Creusé, 2003; Braess and Schöberl, 2008; Izsák, Harutyunyan, and Vegt, 2008). A large class of error estimators rely on the solution of the same boundary value problem on meshes of different coarseness or using different sets of polynomial basis functions (Verfürth, 1996; Ainsworth and Oden, 2000). Another approach has been followed here. The local error indicator of Beck and Hiptmair (1999) was chosen as a pragmatic solution. It was most easily implemented using the available software tools. However, it is emphasized that this choice does not claim to be the best, most accurate or fastest. On the contrary, computation of this error indicator is rather expensive as it involves assembly and solution of a global system of linear equations of the same size like the original boundary value problem, yet with a real coefficient matrix. Therefore, the error estimator is calculated faster than the boundary value problem solution but only by a factor of two to three. Using an error indicator instead of a more rigorous error estimator is sufficient if the estimated error is 'only' used to guide iterative mesh refinement.

The concept of the local error indicator of Beck and Hiptmair (1999) relies on the approximation of the magnetic field in different function spaces. If the electric field is calculated such that $E_h \in \mathcal{P}_{\text{curl}}(\Omega)$, its curl is well-defined and $(i\omega)^{-1} \text{curl } E_h = B_h \in \mathcal{P}_{\text{div}}(\Omega)$. Since $\mu \in (L_2(\Omega))^{(3 \times 3)}$, the magnetic field $H_h = \mu^{-1} B_h \in (L_2(\Omega))^3$ has in general neither continuous tangential nor normal

Chapter 3 The finite element method

components. Evidently, $\mathbf{H}_h \notin \mathcal{P}_{\text{curl}}(\Omega)$. To this end,

$$\mathbf{E}_h = \sum_{i=1}^N E_i \boldsymbol{\Phi}_i, \quad (3.12a)$$

$$\mathbf{H}_h = (i\omega\mu)^{-1} \sum_{i=1}^N E_i \text{curl } \boldsymbol{\Phi}_i. \quad (3.12b)$$

Equation (3.12b) expresses the magnetic field by the classical form of Faraday's law. Its weak form reads:

Search $\hat{\mathbf{H}}_h \in \mathcal{P}_{\text{curl}}(\Omega)$ such that

$$i\omega \int_{\Omega} \overline{\boldsymbol{\Phi}} \cdot \hat{\mathbf{H}}_h d^3r = \int_{\Omega} \overline{\boldsymbol{\Phi}} \cdot (\mu^{-1} \text{curl } \mathbf{E}_h) d^3r \quad (3.13)$$

holds for all $\boldsymbol{\Phi} \in \mathcal{P}_{\text{curl}}(\Omega)$.

Insertion of equation (3.12a) and

$$\hat{\mathbf{H}}_h = \sum_{i=1}^N \hat{H}_i \boldsymbol{\Phi}_i \quad (3.14)$$

yields a system of linear equations

$$\sum_{i=1}^N \hat{a}_{j,i} \hat{H}_i = \hat{f}_j \quad (3.15a)$$

where

$$\hat{a}_{j,i} = i\omega \int_{\Omega} \overline{\boldsymbol{\Phi}}_j \cdot \boldsymbol{\Phi}_i d^3r, \quad (3.15b)$$

$$\hat{f}_j = \sum_{i=1}^n E_i \int_{\Omega} \overline{\boldsymbol{\Phi}}_j \cdot (\mu^{-1} \text{curl } \boldsymbol{\Phi}_i) d^3r. \quad (3.15c)$$

Since the basis functions are real valued the coefficient matrix is real, symmetric and independent of constitutive parameters and frequency. Additionally, one can show that the matrix is positive definite. The solution of the system of linear equations with a complex right hand side can be carried out independently for the real and the imaginary part in real arithmetic.

Using the two magnetic field approximations $\mathbf{H}_h \in (L_2(\Omega))^3$ and $\hat{\mathbf{H}}_h \in \mathcal{P}_{\text{curl}}(\Omega)$, a local error estimator is defined for each element K by

$$\eta_K = \int_K \overline{(\hat{\mathbf{H}}_h - \mathbf{H}_h)} \cdot (\mu (\hat{\mathbf{H}}_h - \mathbf{H}_h)) d^3r. \quad (3.16)$$

This can be written in more explicit form as

$$\begin{aligned}
\eta_K = & \sum_{i,j=1}^N \overline{\hat{H}_j} \left(\int_K \overline{\Phi_j} \cdot (\mu \Phi_i) d^3r \right) \hat{H}_i \\
& + \frac{1}{i\omega} \sum_{i,j=1}^N \overline{\hat{H}_j} \left(\int_K \overline{\Phi_j} \cdot \text{curl } \Phi_i d^3r \right) E_i \\
& - \frac{1}{i\omega} \sum_{i,j=1}^N \overline{E_j} \left(\int_K \overline{(\mu^{-1} \text{curl } \Phi_j)} \cdot (\mu \Phi_i) d^3r \right) \hat{H}_i \\
& + \frac{1}{\omega^2} \sum_{i,j=1}^N \overline{E_j} \left(\int_K \overline{(\mu^{-1} \text{curl } \Phi_j)} \cdot \text{curl } \Phi_i d^3r \right) E_i.
\end{aligned} \tag{3.16*}$$

The first summand is a finite element approximation of the magnetic field energy within element K ,

$$\mathcal{M}_K = \int_K \overline{\hat{H}_h} \cdot (\mu \hat{H}_h) d^3r. \tag{3.17}$$

This fact motivates the introduction of μ in definition (3.16). The third integral in (3.16*) reduces to $\int_K \overline{\text{curl } \Phi_j} \cdot \Phi_i d^3r$ if μ is real valued. For each element K the summation has to be carried out only over the degrees of freedom E_i and \hat{H}_i local to element K .

η_K strongly depends on the element size as well as on the field energy pertaining to element K . Therefore, the normalized local error estimator

$$\hat{\eta}_K = \frac{\eta_K}{\mathcal{M}_K} \tag{3.18}$$

is introduced as an alternative to η_K . Application of either η_K or $\hat{\eta}_K$ as a guide for mesh refinement will lead to different meshes. If the field energy varies by orders of magnitude within the computational domain $\hat{\eta}_K$ will potentially be large where the energy is small while η_K will be large where the energy is large as well. Computational examples illustrating the application of the error indicator are given in Chapter 5.

3.4 Implementation

In order to perform actual computations, the systems of linear equations presented in sections 3.2 and 3.3 need to be assembled and solved using suitable software. This section will give an overview over the tools which have been implemented as the practical part of this thesis' work.

There are a couple of commercial software products available which can solve frequency domain Maxwell's equations, such as ANSYS Multiphysics^{®1}, COMSOL Multiphysics^{®2}, CST Studio

¹<http://www.ansys.com>; last visited on March 31, 2009

²<http://comsol.com>; last visited on March 31, 2009

Suite^{TM,3} or SuperNEC^{TM,4}. Apart from being commercial products they suffer from at least two other inconveniences: First, provided as a black box solver their source code is not available. Experimental research is restricted to the use of available interfaces. Mathematical and structural details, which may be of interest to the research user, are not always documented sufficiently. Second, portability to larger machines is scarcely given but unavoidable if three-dimensional, real world problems are to be tackled. However, commercial products have one important advantage. A graphical user interface as well as convenient post-processing tools are included as a standard and make the software ready and easy to use. This advantage is not considered to balance the disadvantages. For a maximum of transparency and flexibility an approach has been followed that makes use of libraries which are either open source or freely available for academic research purposes.

3.4.1 The finite element kernel

The kernel of the ensued finite element software suite is provided by the finite element library FEMSTER⁵ (Rieben, 2004; Castillo, Rieben, and White, 2005). The version dated from June 11, 2003, has been downloaded, extended and tailored to the demands of the thesis' work. In the meantime, FEMSTER has undergone rework at the Lawrence Livermore National Laboratory, has become part of the project EMSolve⁶ and is not available for download anymore.

Since FEMSTER is written in C++ (Stroustrup, 1997) all further software development has been carried out using the same programming language. Major changes of FEMSTER involved complex number support and the extension by interfaces for mesh input, linear equation solvers and function classes which handle constitutive parameters, source terms and boundary values.

The assembly of the system of linear equations is the central task of a finite element software. Given the mesh, constitutive parameters, source terms, boundary values, a set of basis functions and degrees of freedom, the integrals defining the matrix coefficients and right hand side contributions of equations (3.10) or (3.11) need to be evaluated. This task is performed by the interaction between a number of C++ classes. Figure 3.12 gives a graphical overview of the most important classes involved. They are mostly abstract base classes which provide uniform interfaces and hide the implementation of, e. g., particular basis functions or element types. Classes provided by FEMSTER are enclosed by the green box. All the classes can be arranged hierarchically. The lines connecting the classes do not indicate inheritance but the relation that the higher level class makes use of the lower level class.

Level 1 comprises the building blocks which hold all information needed to evaluate the integrals for an individual element. Class `Element3D` describes the geometry of a tetrahedral, hexahedral

³<http://www.cst.com>; last visited on March 31, 2009

⁴<http://www.supernec.com>; last visited on March 31, 2009

⁵<http://www.llnl.gov/casc/femster>; retrieved on February 17, 2005; last visited on April 2, 2007

⁶https://www-eng.llnl.gov/emsolve/emsolve_home.html; last visited on March 31, 2009

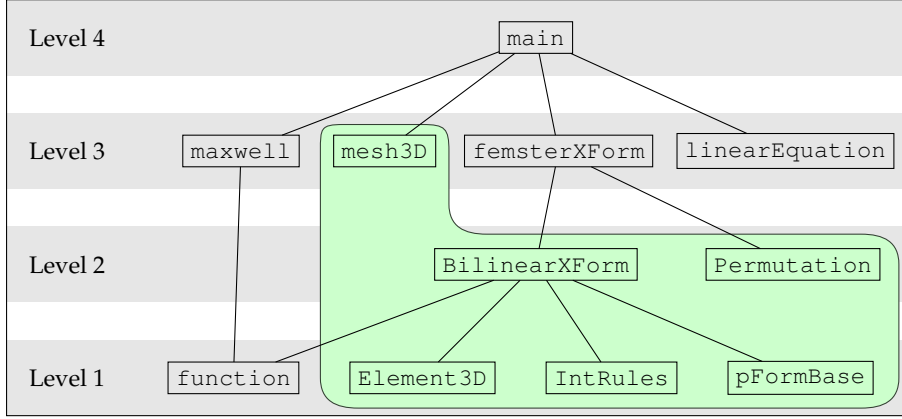


Figure 3.12: Overview of the main C++ classes hierarchy. The original FEMSTER classes are enclosed in the green box.

or prismatic element. It performs the transformation between the global and local coordinate system. The Jacobian of this coordinate transform is required because integration is performed on the reference tetrahedron, hexahedron or prism. Numerical integration rules are implemented for each reference element in class `IntRules`. They are further subdivided into one-, two-, or three-dimensional rules, according to integration along an edge, across a face or over a volume. Class `pFormBase` contains the sets of polynomial basis functions and degrees of freedom. It implements the four finite element spaces $\mathcal{P}_1(K)$, $\mathcal{P}_{\text{curl}}(K)$, $\mathcal{P}_{\text{div}}(K)$ and $\mathcal{P}_0(K)$ introduced in section 3.1 where K is either a hexahedron, a tetrahedron or a prism. The degrees of freedom associated to each set of polynomials is defined pointwise in order to compute degrees of freedom quickly. This deviates from the classical definition of degrees of freedom as moments, i. e., weighted integrals as introduced by Nédélec (1980) for vector finite elements. The last building block `function` provides a unified interface to scalar, vector or tensor valued functions on Ω , i. e., the mapping of $\mathbf{r} \in \mathbb{R}^3$ onto \mathbb{R} , \mathbb{C} , \mathbb{R}^3 , \mathbb{C}^3 , $\mathbb{R}^3 \times \mathbb{R}^3$ or $\mathbb{C}^3 \times \mathbb{C}^3$. Constitutive parameters, source terms and boundary values are represented by objects of classes derived from `function`.

Level 2 class `BilinearXForm` combines all information from the four Level 1 classes and evaluates the integrals. It subsumes implementations involving the different polynomial basis function types from $\mathcal{P}_1(K)$, $\mathcal{P}_{\text{curl}}(K)$, $\mathcal{P}_{\text{div}}(K)$ and $\mathcal{P}_0(K)$ as well as mixed forms and surface integrals. They are summarized in Table 3.3. The resulting element matrices and vectors are computed with respect to a local coordinate system. This fact needs to be considered for vector finite elements where the basis functions are vector-valued. The basis function associated with the common face of two elements is constructed from a vector-valued polynomial on each element such that the normal or tangential component is continuous. Within the local coordinate system of each element, i. e., using a local numbering of nodes, edges and faces, the normal or tangential vectors of the face are not guaranteed to match. Therefore, a global numbering is required which allows for the definition

Bilinear0Form	$\int_K \phi_j \eta \phi_i d^3r$	$\int_K \text{grad } \phi_j \cdot (\boldsymbol{\eta} \text{grad } \phi_i) d^3r$
Bilinear1Form	$\int_K \boldsymbol{\Phi}_j \cdot (\boldsymbol{\eta} \boldsymbol{\Phi}_i) d^3r$	$\int_K \text{curl } \boldsymbol{\Phi}_j \cdot (\boldsymbol{\eta} \text{curl } \boldsymbol{\Phi}_i) d^3r$
Bilinear2Form	$\int_K \boldsymbol{\Psi}_j \cdot (\boldsymbol{\eta} \boldsymbol{\Psi}_i) d^3r$	$\int_K \text{div } \boldsymbol{\Psi}_j (\eta \text{div } \boldsymbol{\Psi}_i) d^3r$
Bilinear3Form	$\int_K \psi_j \eta \psi_i d^3r$	
Bilinear01Form	$\int_K \text{grad } \phi_j \cdot (\boldsymbol{\eta} \boldsymbol{\Phi}_i) d^3r$	
Bilinear12Form	$\int_K \text{curl } \boldsymbol{\Phi}_j \cdot (\boldsymbol{\eta} \boldsymbol{\Psi}_i) d^3r$	
Bilinear23Form	$\int_K \text{div } \boldsymbol{\Psi}_j (\eta \psi_i) d^3r$	
SurfaceBilinear0Form	$\int_F \phi_j \eta \phi_i d^2r$	
SurfaceBilinear1Form	$\int_F (\mathbf{n} \times \boldsymbol{\Phi}_j) \cdot (\boldsymbol{\eta} (\mathbf{n} \times \boldsymbol{\Phi}_i)) d^2r$	
SurfaceBilinear2Form	$\int_F (\mathbf{n} \cdot \boldsymbol{\Phi}_j) (\eta (\mathbf{n} \cdot \boldsymbol{\Phi}_i)) d^2r$	

Table 3.3: Summary of the integrals implemented in the classes subsumed under `BilinearXForm`. η and $\boldsymbol{\eta}$ are used as placeholders which denote a scalar or tensor function of space. K is an element volume and F one of the element's faces.

of unique face normal and edge tangential vectors. Class `Permutation` provides a mapping between the local and the global numbering. This mapping is used to permute the local matrices and vectors including possible changes of sign if the orientation has to be switched. Furthermore, the definition of unique face normal and edge tangential vectors guarantees that the degrees of freedom associated with edges or faces are uniquely defined and do not depend on the element they are evaluated on.

Level 3 class `femsterXForm` is basically a wrapper around the Level 2 classes `BilinearXForm` and `Permutation`. It provides the element matrices and vectors ready for insertion into the global system matrix and right hand side vectors. Some technical details which are connected with the different types of functions derived from class `function` are implemented in `femsterXForm` in order to hide them from the user level Level 4.

Class `maxwell` is a container which collects all physics parameters defined in the physics input file and stores them internally as objects of class `function`. Constitutive parameters, source terms and boundary values are associated with volumes, faces, edges and vertices using an integer attribute ID. This ID corresponds to the ID which is attributed to each volume, face, edge or vertex in the mesh handler class `mesh3D`. These two classes supply the actual data for the solution of a particular boundary value problem.

The system of linear equations is stored and solved using class `linearEquation`. Given an element matrix or vector and a local to global mapping of degrees of freedom, the coefficients are

summed at their respective places within the global system matrix and vector during assembly stage. Subsequently, the system can be solved using one of the solver methods which is interfaced or implemented.

- PARDISO⁷ (Schenk, Gärtner, and Fichtner, 2000; Schenk and Gärtner, 2004, 2006) is a direct solver which is available as a dynamic link library, free for academic research purposes. PARDISO is designed for shared memory architectures and parallelized using OpenMPTM (OpenMP Architecture Review Board, 2008).
- MUMPS⁸ (Amestoy, Duff, and L'Excellent, 2000; Amestoy, Duff, Koster, and L'Excellent, 2001; Amestoy, Guermouche, L'Excellent, and Pralet, 2006) is a public domain direct solver package which is available as a bundle of source code files. MUMPS is designed for distributed memory architectures and parallelized using the MPI (Message Passing Interface Forum, 2008).
- An implementation of the coupled two-term quasi-minimum residual (QMR) method of Freund and Nachtigal (1994) is built into the software package. This iterative solver is currently implemented only in a sequential version. Optionally, a Jacobi preconditioner can be applied.

All three implementations rely on storing the matrix in compressed sparse row (CSR) format (Dongarra, 2000).

Level 4 contains `main` as a placeholder for a number of executables. They comprise the different tasks arising during the solution of a boundary value problem.

`mesh2bin` converts meshes from ASCII to binary format.

`femSolve` computes the finite element solution of the boundary value problem.

`errorEst` computes an *a posteriori* error indicator.

`meshMark` marks elements for mesh refinement given the error indicator.

`postEval` evaluates the computed finite element approximation at given points $\mathbf{r} \in \Omega$ and computes derived quantities if requested.

While all of them need access to the mesh through class `mesh3D`, the classes `maxwell` and `femsterXForm` are only needed by `femSolve`, `errorEst` and `postEval`. Systems of linear equations are solved only with `femSolve` and `errorEst`. These five programs form the computational core of the finite element software suite whose remaining components are described in the following section.

⁷<http://www.pardiso-project.org>; last visited on March 31, 2009

⁸<http://graal.ens-lyon.fr/MUMPS>; last visited on March 31, 2009

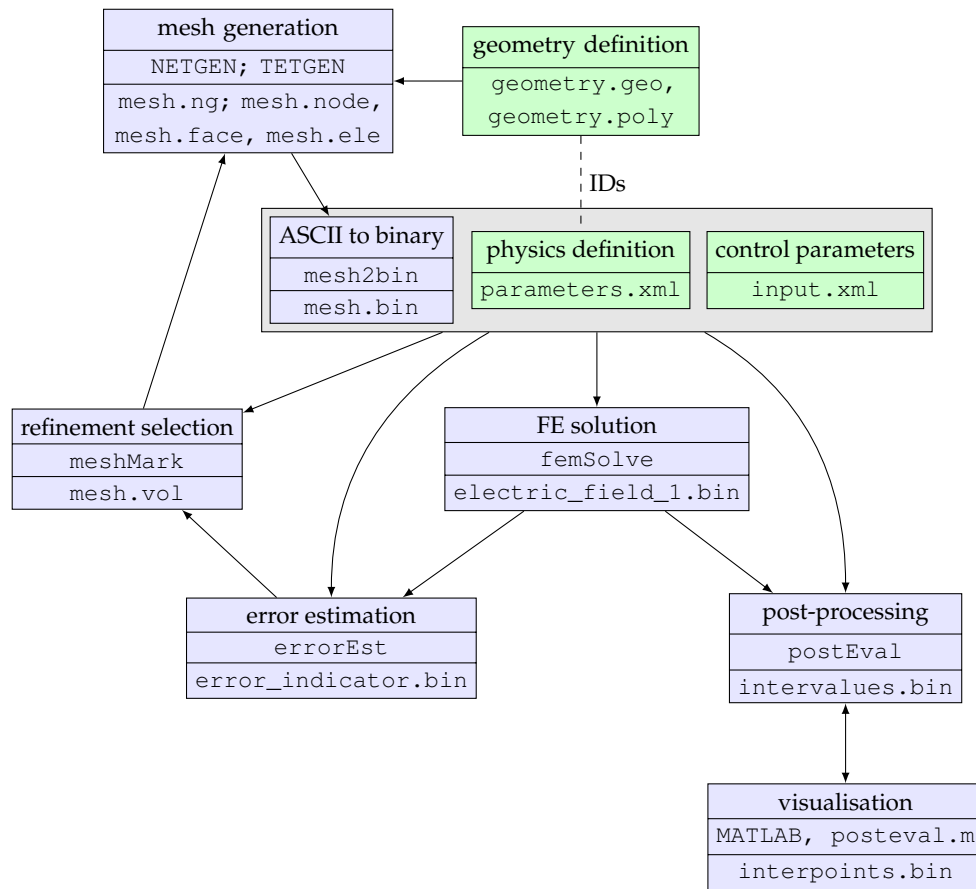


Figure 3.13: Flowchart of the finite element software suite. Green boxes indicate user defined input data, blue boxes actions of one of the software tools. Input files required by the actual finite element programs are enclosed in a grey box.

3.4.2 The finite element software suite

Figure 3.13 gives an overview of all components of the finite element software suite in form of a flowchart. Each of the programs executes one of the steps into which the solution of a boundary value problem can be subdivided. The computation of the finite element solution involves generating a mesh, assembling the system of linear equations and solving the system. Visualizing the solution, computing derived physical quantities and quantifying the solution error are classified as post-processing tasks. Data exchange between the programs is performed by storing the data in files.

Input/output files

The data of the boundary value problem consist of the geometry, physics settings and other control parameters. They form the input required by the finite element solver in order to compute a

finite element approximation to the boundary value problem solution. The three components are separately stored in files.

The format of the *geometry file* is determined by the mesh generator. The geometry can be logically subdivided into sets of vertices, edges, faces and volumes. The volumes coincide with the subdomains of Ω , i. e., constitutive parameters are continuous within each volume/subdomain. Moreover, Ω is decomposed such that each face as a part of the boundary $\partial\Omega$ is subject to one well-defined boundary condition with smooth boundary values. Integer values (IDs) are associated with each geometrical entity. They are transferred to the output files of the mesh generators and create the link between geometry and physics settings during finite element matrix assembly and post-processing.

Therefore, the geometric entity IDs are referred to in the *physics parameter file*. This file contains the physics parameters definition, constitutive parameters for each volume and boundary face as well as boundary condition data. Control parameters, such as the finite element base polynomial degree, parameter file name, iterative solver parameters, etc. are stored in another *control parameter file*. Since the physics settings can be formulated by a number of frequency independent quantities, the frequency or frequency range for which the finite element solution is to be computed is also part of the control parameter file.

The format of two parameter files has been decided to follow the Extensible Markup Language (XML) Standard (Bray, Paoli, Sperberg-McQueen, Maler, and Yergeau, 2006). XML documents are stored in ASCII format and can be edited using either standard text or special XML editors. They follow a tree structure whose leaves can be given intuitive names. Therefore, the XML file should be self-explanatory. In addition, comments can be provided virtually anywhere without invalidating the data structure. These benefits are bought at the expense of using interface routines from an external library to read or write XML files. Libxml2 (Veillard, 1999) is freely available under the terms of the MIT License.

ASCII files are suitable for user generated input files storing a small or moderate amount of information. The *output files* generated by the mesh generator and, in particular, by the finite element solver and post-processing programs contain a considerably larger amount of data. They are consequently stored in binary form. Communication between different tools of the finite element software suite is based on binary files mainly for speed reasons. Binary files are not only smaller than ASCII files storing the same data with the same precision. Input and output routines for binary files are also considerably faster than those for ASCII files. However, transparency is sacrificed for speed. The data stored within a binary file can only be accessed using executables or functions which are tailored to read a particular binary file type.

Mesh generation

A mesh generator is used to divide the geometry, defined in the geometry file, into tetrahedral or hexahedral elements. Given a previously generated mesh, the mesh generator is also required to refine parts or all of the mesh. The finite element suite provides input routines for a number of

mesh formats.

The mesh is handled within the finite element software by a C++ class `mesh3D`. It includes an input method which reads tetrahedral or hexahedral meshes from an ASCII file. This file format will be called native. Hexahedral meshes can be easily constructed for cuboidal domains from a tensor product grid. A MATLAB[®] function `fdgrid.m` has been written which creates such a mesh in the native mesh format.

Class `mesh3D` contains input methods for meshes stored in the native formats of NETGEN⁹ (Schöberl, 2008) and of TETGEN¹⁰ (Si, 2007). Both programs generate tetrahedral meshes and store them in formatted ASCII files. NETGEN and TETGEN are provided as stand-alone programs and as a collection of linkable interface routines. Following the stratagem of a modular software structure the stand-alone programs are used to generate the mesh in a step separated from the finite element tools.

All ASCII mesh formats can be converted to a binary file format using `mesh2bin`. This step accelerates reading larger meshes during finite element assembly and post-processing, especially if the mesh is to be read several times.

Finite element solution

The two programs `femSolve` and `errorEst` perform the central tasks of computing the finite element solution of the boundary value problem as well as an elementwise error indicator. Given the error estimation `meshMark` generates an input file for the mesh generator which in turn refines the mesh locally.

Visualization

MATLAB[®] has been chosen as the visualization tool. It provides the required plotting facilities and allows scripting the plot process. MATLAB[®] forms the only commercial component of the finite element software suite. Lack of equivalent alternatives and widespread availability seem to justify this choice.

Visualization of any physical field quantity requires interaction between MATLAB[®] as the display front-end and `postEval`. `postEval` evaluates the computed finite element solution and computes the requested field at a number of points given. Communication between MATLAB[®] and `postEval` is again performed via binary files. A MEX interface has been discarded for compatibility issues.

⁹<http://www.hpfem.jku.at/netgen>; retrieved on April 30, 2008; last visited on March 31, 2009

¹⁰<http://tetgen.berlios.de>; retrieved on October 7, 2008; last visited on March 31, 2009

3.5 Numerical experiments

Using the finite element software tools of the previous section, a number of numerical experiments has been carried out in order to investigate and illustrate the properties of the finite element matrix. The first part of this section examines aspects related to the solution of the system of linear equations. Second, the compatibility of polynomial spaces for the E - V formulation will be demonstrated. Finally, empirical evidence for the stability considerations of Chapter 2 will be provided. Therefore, the low frequency behavior of the solution of the different boundary value problem formulations is examined by a comprehensive test suite. For all experiments, the matrix condition number has been used as an experimental indicator which can point out possible problems when solving the discrete boundary value problem.

3.5.1 Matrix condition number

The susceptibility of the solution of a linear equation system to errors in the data, introduced, e. g., by inevitable rounding errors of computer arithmetics when computing the coefficients and solving the system, is related to the condition number κ of the coefficient matrix A . It is defined by $\kappa = \|A\| \|A^{-1}\|$ with an arbitrary matrix norm.

Computation of the 1-norm matrix condition number can be appended easily to the process of solving the system of linear equations directly. By using a 1-norm estimator (Higham and Tisseur, 2000), direct computation of A^{-1} can be avoided. Only a number of additional linear equation system solves are required which is computationally inexpensive once the matrix A has been factorized.

3.5.2 A symmetric matrix scaling

The finite element matrix entries depend on the element size and the constitutive parameters. If these quantities vary largely over the domain Ω , the columns and rows of A may have norms differing by orders of magnitude. Low frequency simulations for models including both air and earth, for example, lead to such badly scaled systems of linear equations.

Combination of different partial differential equations into one system leads to another scaling issue. Consider the two partial differential equations

$$\begin{aligned} \operatorname{curl} \left(\mu^{-1} \operatorname{curl} E \right) - i\omega(\sigma - i\omega\epsilon)E \\ + \alpha(\sigma - i\omega\epsilon) \operatorname{grad} V = i\omega j_s, \end{aligned} \quad (3.19a)$$

$$-\alpha \operatorname{div} (\sigma - i\omega\epsilon)E - \alpha^2 \gamma V = \alpha \operatorname{div} j_s \quad (3.19b)$$

which are identical to equations (2.18a) and (2.18b) except for the scaling parameter $\alpha \in \mathbb{C}$, $\alpha \neq 0$. The system of linear equations derived using the equation of continuity and the scalar field V both

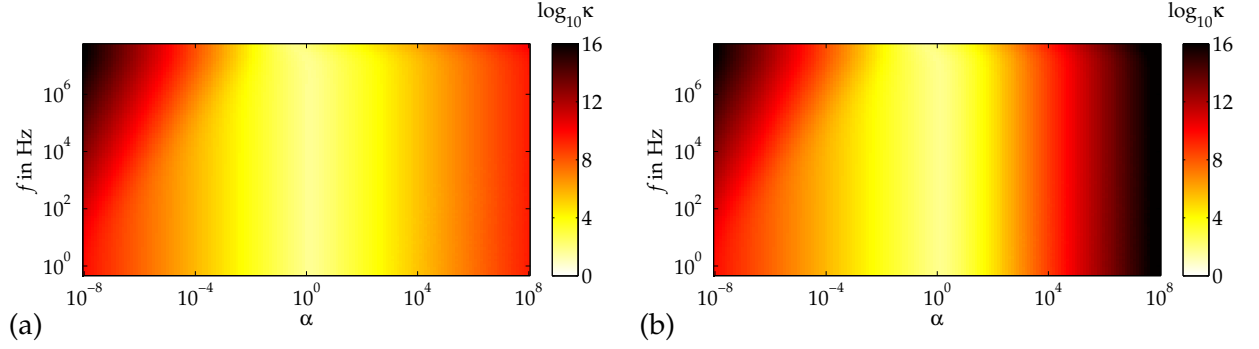


Figure 3.14: The 1-norm matrix condition number κ heavily depends on the parameter α which scales the equation of continuity relatively to the vector Helmholtz equation. V solves (a) Laplace's ($\gamma = 0$), (b) Helmholtz's equation ($\gamma = \sigma - i\omega\epsilon$).

scaled by α reads in block matrix notation as

$$\begin{pmatrix} A(\Phi, \Phi) & \alpha A(\Phi, \phi) \\ \alpha A(\phi, \Phi) & \alpha^2 A(\phi, \phi) \end{pmatrix} \begin{pmatrix} E \\ V \end{pmatrix} = \begin{pmatrix} f(\Phi) \\ \alpha f(\phi) \end{pmatrix}. \quad (3.20)$$

The electric field degrees of freedom E are independent of α because the system is equivalent to a symmetrically scaled system with a left and right block diagonal scaling matrix $\text{diag}(1, 1/\alpha)$. The transformation $\alpha V \mapsto V$ has no effect on E because V vanishes per construction. From the numerical point of view, the solution of the system of linear equations very well depends on the choice of α . Extreme values lead to a system which is even singular to working precision. Figure 3.14 gives an example: The 1-norm matrix condition number κ is computed for a simple test model. The domain $\Omega = [-1, 1]^3 \text{ m}^3$ is covered by a homogeneous medium with $\sigma = 0.01 \text{ S/m}$, $\epsilon_r = 8$, $\mu_r = 1$. A homogeneous Dirichlet boundary condition is posed on all boundary faces. Finite element matrices are computed for the frequency range $5.18 \times 10^{-1} \text{ Hz}$ to $5.18 \times 10^7 \text{ Hz}$. The upper bound is the Nyquist frequency for the material and tensor product grid considered which consists of 2^3 hexahedral elements of edge length 1 m. Base functions of polynomial degree 2 have been used.

Figure 3.14 shows that the optimum value of α is in the order of unity and independent of frequency. This is only true for the very simple test case of a homogeneous medium with the grid size used. In general, the optimum choice of α is not evident, namely for highly heterogeneous media and meshes.

In order to account for all these scaling issues, a preconditioner is applied to the system of linear equations which preserves symmetry of the coefficient matrix. Ruiz (2001) proposes an iterative scheme which calculates two diagonal matrices R and C such that $\tilde{A} = RAC$ has unit column and row norms. If A is symmetric, $R = C$. After computing the solution of the scaled system $\tilde{A}\tilde{x} = \tilde{b}$, where $\tilde{b} = Rb$, the solution of the original system is obtained from $x = C^{-1}\tilde{x}$. The inverse of the diagonal matrix C can be computed easily.

3.5.3 Iterative or direct solvers?

The matrix properties have great impact on how the system of linear equations can be solved. The matrices defined by equations (3.10b) and (3.11c) to (3.11f) are sparse, complex valued, symmetric and indefinite, i. e., they can have eigenvalues with positive and negative real parts. Regularity has to be assumed, of course, and should be a consequence of (a) a well-posed boundary value problem and (b) a well-designed finite element discretization.

Two different approaches for the solution of a system of linear equations can be distinguished, direct and iterative methods. A direct solver computes the solution in a fixed number of operations which is largely independent of the particular values of the nonzero entries of the matrix as long as the matrix satisfies all assumptions on regularity, symmetry and definiteness. Direct solvers first factorize the matrix into a lower and an upper triangular matrix. The solution is thus reduced to the solution of two systems with triangular matrices and can be performed easily by forward elimination and back-substitution. The direct solvers implemented in MUMPS and PARDISO both exploit sparsity and symmetry of the matrix. Reordering algorithms are applied to the matrix prior to the factorization in order to reduce fill-in, i. e., to minimize storage and floating point operations. Once the factorization is computed the solution for a number of right hand sides can be obtained rather cheaply. This advantage, compared to iterative solvers, goes at the expense of storing the matrix factors.

If the problem is too large to be solved by direct methods iterative solvers can be considered as an alternative. They only require computation of matrix-vector products involving the coefficient matrix. Depending on the particular member chosen from the large family of Krylov-subspace methods (Barret et al., 1994; Saad, 1996) a number of auxiliary vectors need to be stored. This largely depends on the matrix properties. As the matrix is indefinite the most efficient conjugate gradient (CG) method is not applicable. The generalized minimum residual (GMRES) method is the most general Krylov-subspace algorithm which can be applied to any matrix. It requires storage of as many vectors as iterations till convergence. This prohibitive storage requirement can be relaxed by restarting the method. The quasi-minimum residual (QMR) method best meets the matrix properties considered here. Only a couple of auxiliary vectors need to be stored. Matrix symmetry can be exploited in order to reduce storage and operational costs. A symmetric QMR variant with coupled two-term recurrences (Freund and Nachtigal, 1994) has been implemented. This solver has previously shown good performance in context with the finite difference/finite volume discretization of low-frequency electromagnetic problems (Weiss and Constable, 2006).

Unfortunately, the performance of the QMR algorithm with matrices arising from the finite element discretization turns out to be poor. A satisfactory rate of convergence can only be obtained if a suitable preconditioner is applied to the system of linear equations. The Jacobi preconditioner as used by Weiss and Constable (2006) does not significantly accelerate convergence. An incomplete Cholesky factorization of the symmetric positive definite mass matrix proved to give acceptable results if partial fill-in is admitted in the matrix factors. However, computation of the factorization is expensive and the need to store the matrix factors partially reduces the advantage of the iterative

method to tackle larger problem sizes.

In order to investigate the different convergence rates of the QMR method for finite difference or finite element discretized problems a small test case has been devised. The finite volume code FDM3D¹¹ (Weiss and Constable, 2006) has been used for the comparison. FDM3D is restricted to tensor product grids with cellwise constant conductivity. For this reason, its coefficient matrix is identical with the matrix which could be derived using the finite difference method. The corresponding finite element matrix is obtained if the lowest order, curl-conforming hexahedral elements and the E -field formulation are used.

The computational domain $\Omega = [-500, +500]^3 \text{ m}^3$ is filled with seawater of conductivity $\sigma_1 = 3.3 \text{ S/m}$ for $z < 0$ and with sediments, $\sigma_2 = 1 \text{ S/m}$, for $z > 0$. Furthermore, $\mu_r = 1$ and $\varepsilon_r = 0$. Neglecting displacement currents can be justified for the small frequency $f = 1 \text{ Hz}$ used. FDM3D does not take displacement currents into account. The domain Ω is subdivided by a regular tensor product grid into N^3 hexahedral elements where $N = (10, 20, 30, 40, 50)$. This equals a grid spacing of $h = (100, 50, 33, 25, 20) \text{ m}$. The resulting approximation of the electric field by piecewise linear basis functions comprises $3N(N-1)^2 = (2\,430, 21\,660, 75\,690, 182\,520, 360\,150)$ degrees of freedom not including the vanishing boundary values.

For better comparison the coefficient matrix derived from FDM3D is divided by the volume of one of the cells of the equidistant tensor product grid. The matrix is also replaced by its complex conjugate since FDM3D and FEMSTER use different $e^{\pm i\omega t}$ -conventions. The matrix A can easily be split into the stiffness and mass matrices because they form the real and imaginary part, $A = S + iM$.

The matrix equation $Ax = b$ is solved for a unit right hand side vector using the MATLAB[®] inbuilt QMR routine with target relative residual $\|Ax - b\|/\|b\| = 10^{-8}$. Three choices of preconditioners are tested:

1. No preconditioner.
2. Jacobi preconditioner. A system with matrix $A^* = J^{-1}A$ is solved where $J = \text{diag}\{A\}$.
3. Mass matrix incomplete Cholesky preconditioner with drop tolerance 10^{-8} . A system with matrix $A^\circ = D^{-T}AD^{-1}$ is solved where only the (real) mass matrix part of A is factorized as $M = D^T D$.

While the mass matrix of the finite difference method is diagonal the finite element mass matrix is not. This motivates the mass matrix incomplete Cholesky preconditioner which transforms both matrices to the form $A^\circ = D^{-T}SD^{-1} + iI$ where I is the identity matrix.

Figure 3.15 shows the numbers of QMR iterations that have been determined for the finite difference and finite element coefficient matrices, and for the three choices of preconditioners. All six combinations exhibit the same rate of convergence as a function of the mesh size. However, the finite element matrices consistently require a larger number of iterations. This effect is reduced

¹¹<http://www.sandia.gov/comp-em-geop/>; retrieved on April 4, 2008

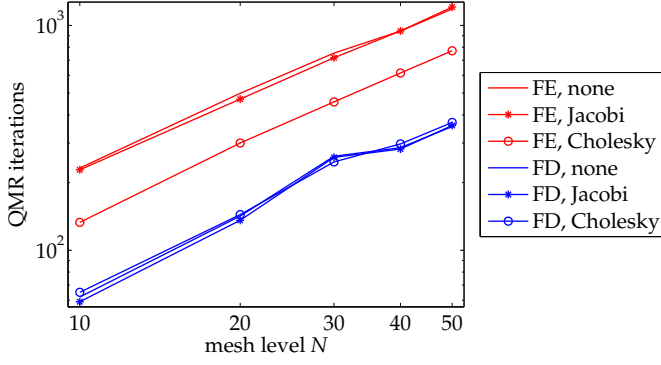


Figure 3.15: Comparison of the number of QMR iterations for finite difference (FD) and finite element (FE) system matrices using different preconditioners.

preconditioner	finite difference	finite element
none	148 (62)	737 (232)
Jacobi	148 (59)	737 (228)
Cholesky	145 (65)	401 (133)

Table 3.4: Spectral norm matrix condition number κ_2 for the coarsest grid ($N = 10$). The number of QMR iterations is given in parentheses.

markedly by the mass matrix incomplete Cholesky preconditioner. The same preconditioner has no significant effect for the finite difference matrices.

In order to examine further the convergence behavior of the QMR method, the spectra of the coefficient matrices of the coarsest grid have been computed and plotted in Figure 3.16. The eigenvalues are sorted according to their magnitude. The spectra of the unpreconditioned or Jacobi-preconditioned finite element matrices are more scattered than the spectra of the finite difference matrices. In particular the imaginary part of the unpreconditioned finite difference matrix only takes a couple of discrete values.

The spectra of the mass matrix incomplete Cholesky preconditioned matrices look very similar. By construction, the imaginary parts equal one in both cases. The real parts follow a comparable pattern but differ by their range of values. While the finite difference matrix has a spectral radius of 145 the finite element matrix has a spectral radius of 401. This indicates that the discrete curl-operator derived by the finite element method has a higher frequency content than its finite difference counterpart. The discrete curl-operator derived by the finite difference method may consequently be seen as an averaged or low-pass filtered version of the finite element operator.

The spectra of the mass matrix incomplete Cholesky preconditioned matrices also reveal that the kernel of the curl-operator, i. e., the rank deficit of the stiffness matrix is 729. Only the real part of eigenvalues 730 to 2430 is non-zero.

The spectral norm matrix condition number is defined as the ratio of the largest and smallest singular values. It is listed in Table 3.4 along with the number of QMR iterations. For this example, the number of QMR iterations correlates fairly well with the matrix condition number.

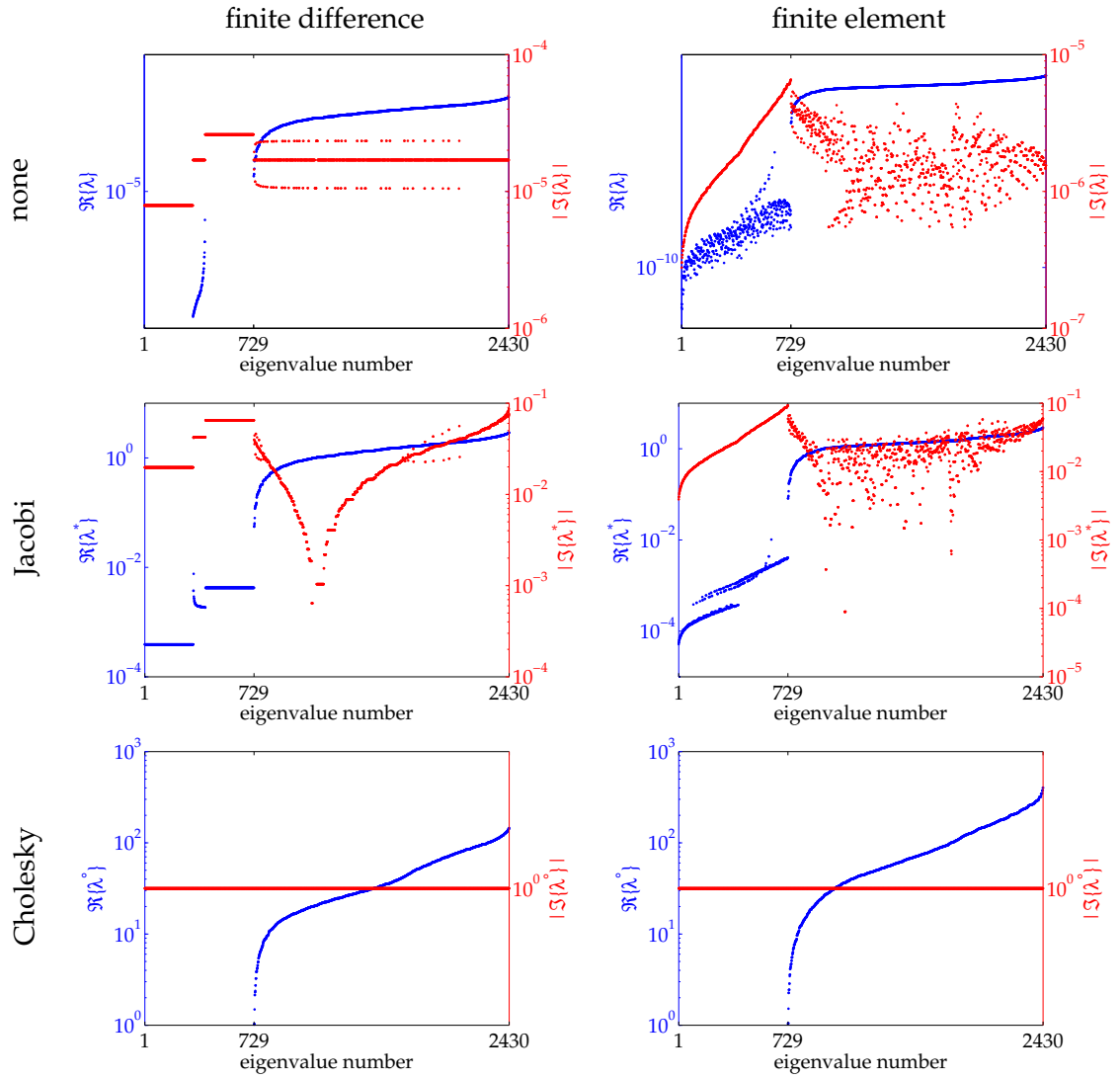


Figure 3.16: Eigenvalues of the unpreconditioned (top), Jacobi preconditioned (middle) and mass matrix incomplete Cholesky preconditioned (bottom) finite difference (left) and finite element (right) coefficient matrices. The eigenvalues are sorted by their absolute value.

3.5.4 Compatible polynomial spaces for the E - V formulation

The weak form of the E - V formulation involves the two function spaces $\mathcal{U} \subseteq H_{\text{curl}}(\Omega)$ and $\mathcal{V} \subseteq H_1(\Omega)$. Their finite dimensional approximation, the finite element spaces $\mathcal{U}_h \subseteq \mathcal{P}_{\text{curl}}(\Omega)$ and $\mathcal{V}_h \subseteq \mathcal{P}_1(\Omega)$ have to be chosen such that the range of the gradient operating on functions from \mathcal{V}_h spans the kernel of the curl-operator in \mathcal{U}_h . This compatibility condition basically reduces for the finite element spaces implemented in FEMSTER to choosing the correct combination of polynomial degrees for the spaces of finite element basis functions. The implication for the discrete problem is that the finite element system matrix is singular if the spaces are incompatible. A numerical example will illustrate this point.

The domain $\Omega = [-1, 1]^3 \text{ m}^3$ is discretized by a regular hexahedral grid with 2^3 elements, i. e., there is exactly one interior vertex. Ω is covered by a homogeneous medium of electrical conductivity $\sigma = 0.01 \text{ S/m}$ and relative magnetic permeability $\mu_r = 1$. The relative electrical permittivity is irrelevant because only frequency $f = 0$ is considered for this test problem. Vanishing tangential electric field components are imposed as a homogeneous Dirichlet boundary condition on $\partial\Omega$.

The electric field is approximated by piecewise quadratic basis functions ($p = 2$). This results in 108 degrees of freedom for E , excluding the fixed boundary values. Figure 3.17(a) shows the singular values of the finite element matrix resulting from the E -field formulation. The kernel of the curl-operator creates a matrix rank deficit of 27. In order to remove this kernel the E - V formulation is used. Figures 3.17(b) to (d) show the singular values of the finite element matrix where V has been approximated by piecewise linear, quadratic or cubic basis functions ($p = 1, 2, 3$). The system of linear equations is enlarged by respectively 1, 27, and 125 degrees of freedom for V and equations representing the equation of continuity.

Only in case (c) of a matching basis with quadratic basis functions ($p = 2$) for V the finite element matrix is regular. From an algebraic point of view, this agrees with the fact that a rank deficiency of 27 as observed for the matrix of Figure 3.17(a) can be remedied by taking additional 27 linearly independent equations into account.

From the function space point of view, this behavior reflects the exact sequence property of the underlying function spaces on the discrete level. If, on the one hand, V is chosen to be piecewise linear (Figure 3.17(b)), the gradient of V is contained in the kernel of the curl but it does not span the kernel completely. As E is constructed from piecewise quadratic polynomials, also the kernel of the curl consists of piecewise polynomials of degree two. If, on the other hand, V is chosen to be piecewise cubic (Figure 3.17(d)), the gradient of V is not contained in the kernel of the curl but spans a larger function space. This again results in a singular matrix. Only if V is chosen to be piecewise quadratic, in accordance with the approximation of E , the gradient of V is contained in the kernel of the curl and spans the kernel completely.

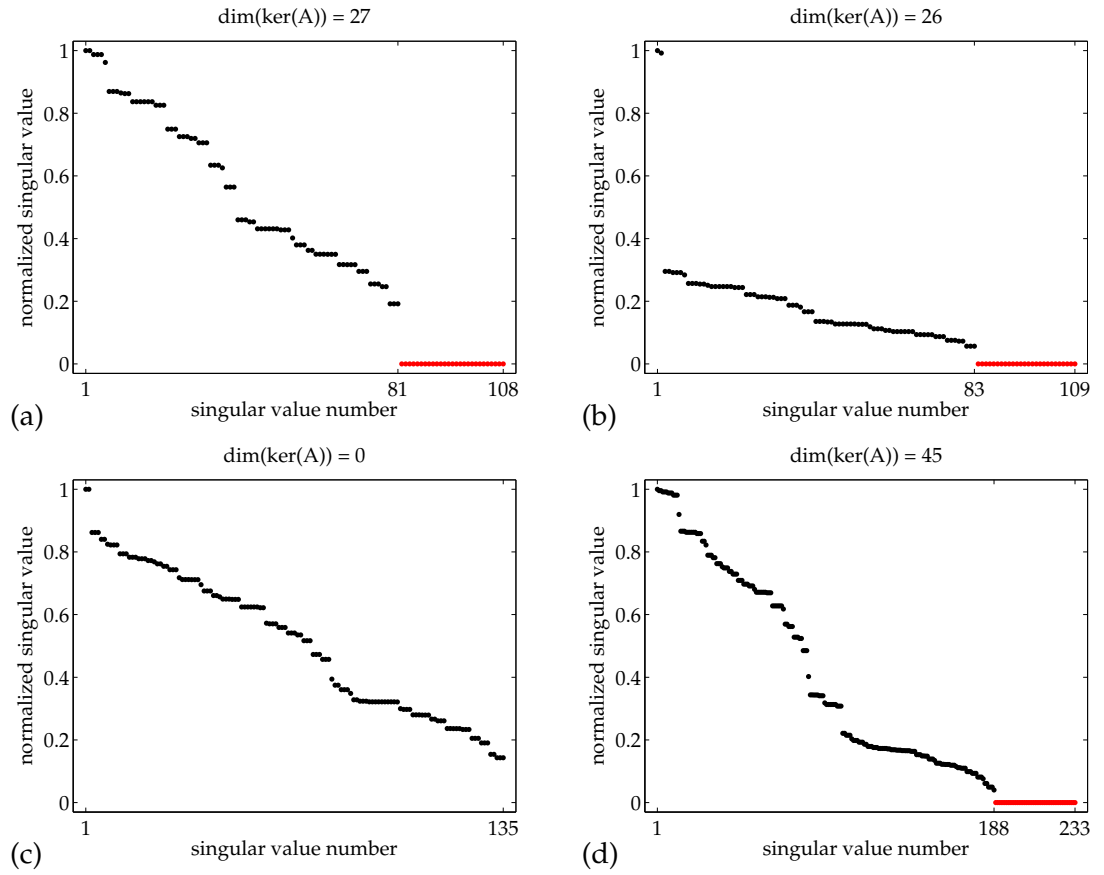


Figure 3.17: Singular values of the finite element system matrix A at frequency $\omega = 0$ for the E -field formulation (a) and the E - V formulation with V approximated by piecewise polynomials of degree $p = 1$ (b), $p = 2$ (c), $p = 3$ (d). E is approximated by piecewise polynomials of degree $p = 2$.

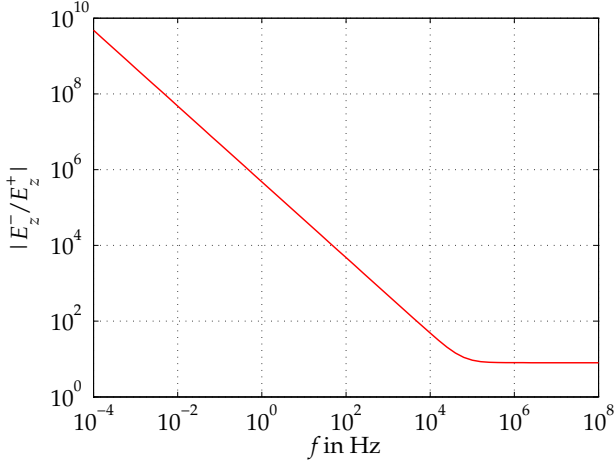


Figure 3.18: Ratio of the normal components of the electric field in air, E_z^- , and earth, E_z^+ , at the air–earth interface of the halfspaces test model. Continuity of the (complex) normal current flow through the air–earth interface requires that the normal component of the electric field is discontinuous.

3.5.5 Low frequency stability

The design of a frequency domain solver for Maxwell’s equations which is stable also for low frequencies has been the central point of the previous theoretical considerations. Now, the theory is going to be tested by a number of numerical examples. A test suite has been devised which combines two instances of constitutive parameter distributions, two types of sought solutions, and two different boundary condition type settings.

Test suite setup

The test problems are posed on the domain $\Omega = [-0.5, 0.5]^3 \text{ m}^3$ which is covered by

- a homogeneous *fullspace* with $\epsilon_r = 8$, $\mu_r = 1$, $\sigma = 0.01 \text{ S/m}$ or
- two homogeneous *halfspaces* with $\epsilon_r^+ = 8$, $\mu_r^+ = 1$, $\sigma^+ = 0.01 \text{ S/m}$ for $z > 0$ (earth) and $\epsilon_r^- = 1$, $\mu_r^- = 1$, $\sigma^- = 0$ for $z < 0$ (air).

The air–earth interface is a difficult test case because the continuity of the (complex) normal current flow through the earth’s surface implies a large jump in the normal electric field for low frequencies (Figure 3.18). There, the ratio E_z^-/E_z^+ is proportional to f^{-1} .

In order to be able to determine the solution accuracy, the source terms and boundary values are chosen such that the numerical solution is an approximation to a known solution. Two different analytical solutions are considered:

- The electric field corresponding to the *constant current density* $\mathbf{j} = (0, 0, 1) \text{ A/m}^2$,

$$\mathbf{E} = \frac{1}{\sigma - i\omega\epsilon} \mathbf{j} \quad (\text{fullspace}), \quad (3.21a)$$

$$\mathbf{E} = \begin{cases} \frac{1}{\sigma^- - i\omega\epsilon^-} \mathbf{j} & z < 0 \\ \frac{1}{\sigma^+ - i\omega\epsilon^+} \mathbf{j} & z > 0 \end{cases} \quad (\text{halfspaces}), \quad (3.21b)$$

represents the special case that the solution of the continuous problem, the piecewise constant electric field, is also contained in the finite element space. This test solution consequently excludes errors introduced by approximating the infinite dimensional function space $H_{\text{curl}}(\Omega)$ by the finite dimensional function space $\mathcal{P}_{\text{curl}}(\Omega)$. The electric fields (3.21a) and (3.21b) are curl-free. In order to satisfy the vector Helmholtz equation, the source current density in Ω has to be chosen according to $\mathbf{j}_s = -\mathbf{j}$.

- A plane wave travelling in positive z -direction represents the typical setup of a one-dimensional earth model in magnetotellurics. If the fields are normalized such that the horizontal magnetic field at $z = 0$ has unit amplitude, the electric field is expressed by

$$\mathbf{E} = Z(e^{ikz}, 0, 0) \quad (\text{fullspace}), \quad (3.21c)$$

$$\mathbf{E} = \begin{cases} \frac{Z^-}{1-R} (e^{ik^-z} + R e^{-ik^-z}, 0, 0) & z < 0 \\ Z^+ (e^{ik^+z}, 0, 0) & z > 0 \end{cases} \quad (\text{halfspaces}). \quad (3.21d)$$

$Z = \frac{\omega\mu}{k}$ denotes the complex wave impedance and $R = \frac{Z^+ - Z^-}{Z^+ + Z^-}$ the reflection coefficient. The plane wave is the prototype of a solution of the source free Maxwell's equations. Therefore, $\mathbf{j}_s = \mathbf{0}$ in Ω . As the fields approach the constant solution for low frequencies, the approximation error is expected to decrease with decreasing frequency.

Two sets of boundary conditions are chosen according to these known solutions:

- an inhomogeneous Dirichlet boundary condition is prescribed on Γ , i. e., the tangential electric field $\mathbf{n} \times \mathbf{E}$; or
- an inhomogeneous Neumann boundary condition is prescribed on Γ , i. e., the curl of the electric field $\mathbf{n} \times (\mu^{-1} \text{curl } \mathbf{E})$ which is basically the tangential magnetic field.

Numerical solutions have been computed for both a tetrahedral and a hexahedral mesh with 729 vertices each (Figure 3.19). While the hexahedral mesh is a regular tensor product grid of 8^3 cells the tetrahedral mesh is unstructured. Piecewise quadratic finite element basis functions ($p = 2$) have been used in both cases. A frequency range from 10^{-4} to 10^8 Hz is examined. The maximum element edge length 0.25 m implies a Nyquist frequency of 2.1×10^8 Hz which is well above the largest frequency used.

The system of linear equation was solved using MUMPS. A considerable number of cases involve coefficient matrices which are singular to working precision. The implementation of MUMPS allows for catching these cases even if the solver returns with an exit code, and continue the computation. This has been impossible with PARDISO which caused an irrecoverable segmentation fault and required program termination.

Matrix condition

Condition numbers measured in the 1-norm are shown as a function of frequency in Figures 3.20 and 3.21. The two figures differ by scaling the system of linear equations symmetrically prior to

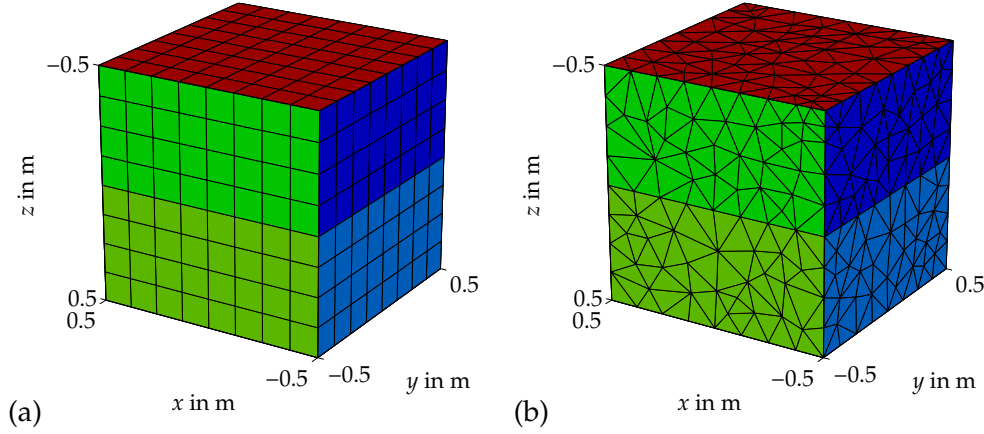


Figure 3.19: Hexahedral (a) and tetrahedral (b) meshes with 729 vertices each. Maximum edge lengths are 0.125 m (a) and 0.25 m (b).

solving as described in section 3.5.2. Each subfigure contains the results for three choices of the boundary value problem formulation:

- the E -field formulation;
- the E - V formulation with vanishing zeroth-order term for V , $\gamma = 0$, labelled ‘mixed, Laplace’; and
- the E - V formulation with non-trivial zeroth-order term for V , $\gamma = (\sigma - i\omega\epsilon)^2$, labelled ‘mixed, Helmholtz’.

The two cases of the E - V formulation are named by the Laplace- and Helmholtz-like boundary value problem that the dummy variable V implicitly satisfies.

Some curves appear to have no data at low frequencies. There, the condition number could not be computed because the matrix is singular to working precision and the linear equations solver returned a not-a-number solution. The condition number should be treated as infinity in these cases.

Note that the condition number is independent of the two analytical solutions. The same grids and constitutive parameters have been used in both cases. Only this part of the data has an impact on the coefficient matrix and, therefore, on the condition number. The two different solutions ‘constant current density’, equations (3.21a/b), and ‘plane wave’, equations (3.21c/d), are solely determined by differing boundary values which alter only the right hand side.

Figures 3.20 and 3.21 show that for the E -field formulation the matrix condition number increases with decreasing frequency, irrespective of the matrix scaling. The growing condition number is the numerical expression of the low frequency instability which has been predicted in Chapter 2. It has its origin in the non-uniqueness of the solution of the non-stabilized boundary value problem at frequency $\omega = 0$ that is caused by the non-trivial kernel of the curl-operator.

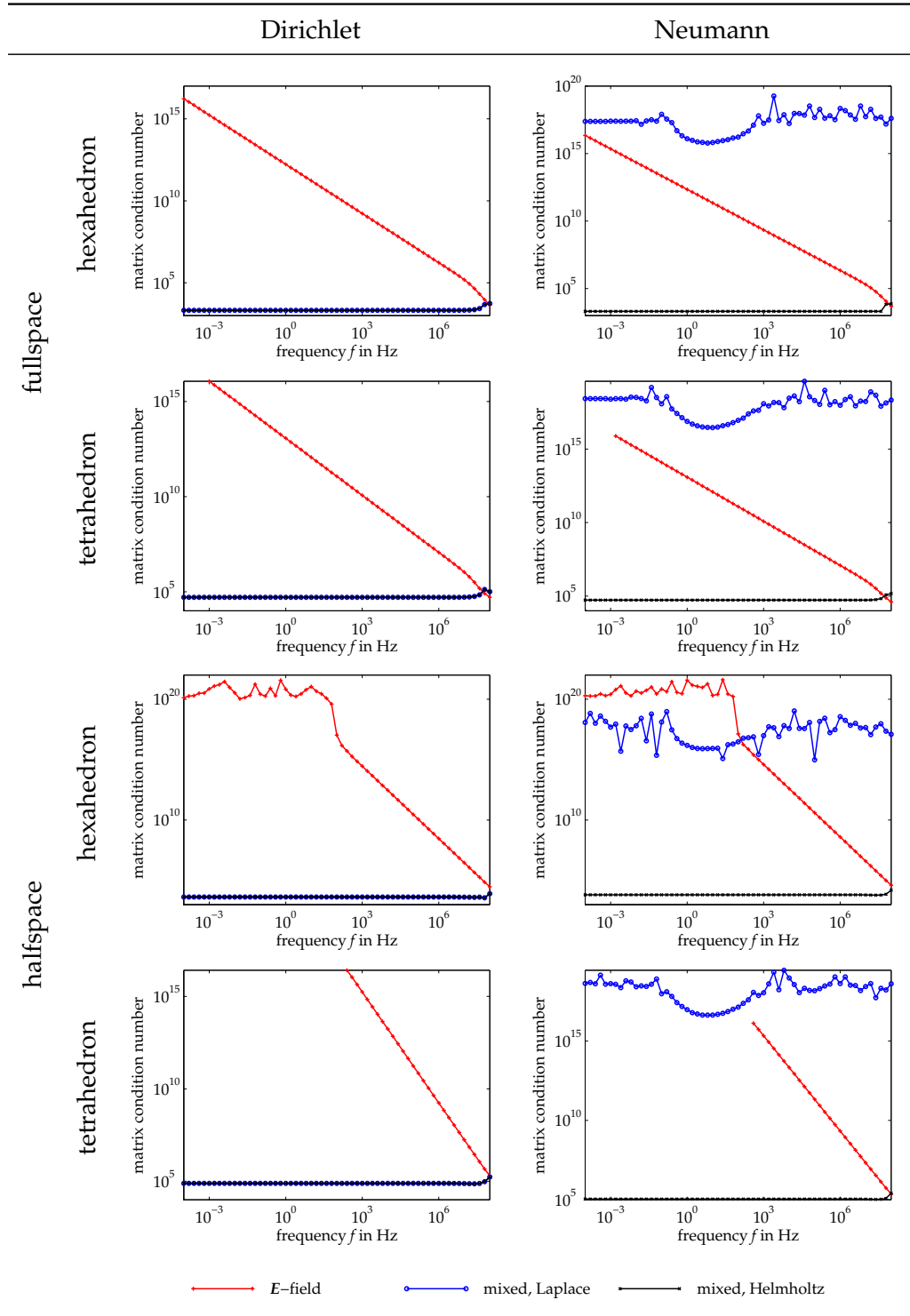


Figure 3.20: 1-norm matrix condition number for both test cases ‘constant current density’ and ‘plane wave’ with symmetric matrix scaling.

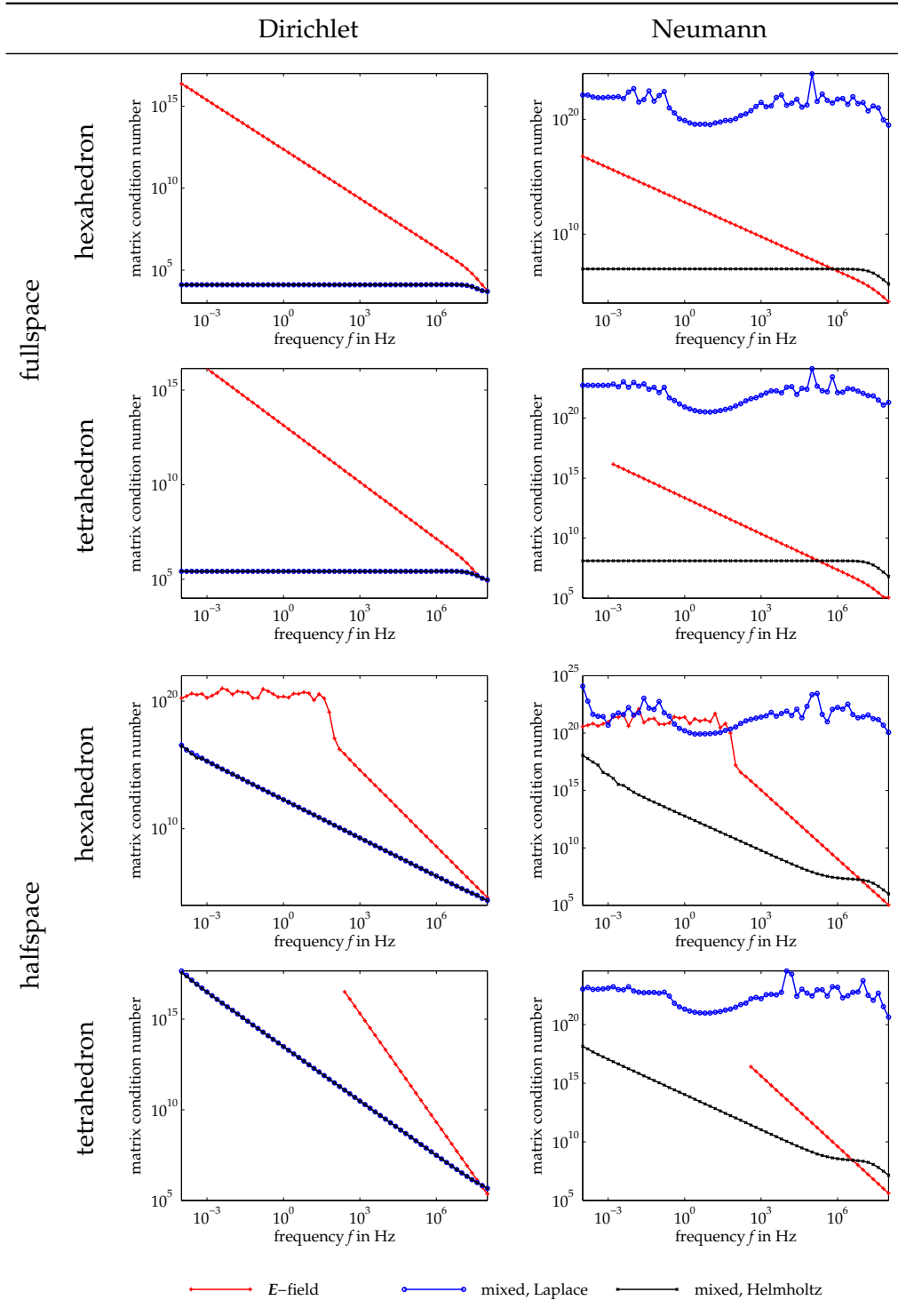


Figure 3.21: 1-norm matrix condition number for both test cases ‘constant current density’ and ‘plane wave’ without symmetric matrix scaling.

While the growth of $\kappa \propto \omega^{-1}$ for the fullspace model, $\kappa \propto \omega^{-2}$ for the halfspaces model. The faster increase in the inhomogeneous case can be explained by superposition of the low frequency instability observed also for the homogeneous case and the effect of an increasing parameter contrast as shown in Figure 3.18. Figures 3.20 and 3.21 reveal that the low frequency behavior can be improved for the fullspace model if the E - V formulation is used. The resulting matrix condition number is constant for the lower frequency range. Since the auxiliary field V implicitly satisfies a Laplace-like equation if $\gamma = 0$, it is not determined uniquely by the Neumann boundary condition. This fact is reflected by the matrix condition number on a level with the reciprocal machine precision of about 10^{16} . Only a non-vanishing γ , which renders the boundary value problem in terms of V Helmholtz-like, can stabilize the boundary value problem with an empty Dirichlet boundary part for low frequencies.

For the fullspace model the symmetric matrix scaling has only a minor effect. The constant level is obtained in both cases but the low frequency condition number of the scaled system is smaller. This does not hold for the halfspaces model. Compared to the E -field formulation the growth rate of the condition number of the E - V formulation is reduced by one for the unscaled system (Figure 3.21). However, the effect of the increasing parameter contrast is still present in the coefficient matrix. It can be removed if the symmetric matrix scaling is applied. As can be seen from Figure 3.20 the matrix has been successfully stabilized also for the high parameter contrast case.

A vital question is the particular choice of the parameter $\gamma \neq 0$ for the second variant of the E - V formulation. It must be considered in context with the action of the symmetric matrix scaling. If the coefficient matrix is subdivided into blocks according to equation (3.11j),

$$A = \begin{pmatrix} A^{(\Phi, \Phi)} & A^{(\Phi, \phi)} \\ A^{(\phi, \Phi)} & A^{(\phi, \phi)} \end{pmatrix}, \quad (3.22)$$

the blocks $A^{(\phi, \Phi)}$ and $A^{(\Phi, \phi)}$ scale like $(\sigma - i\omega\varepsilon)$ and the block $A^{(\phi, \phi)}$ like γ . The symmetric matrix scaling algorithm left and right multiplies the matrix A by diagonal matrices whose lower diagonal block, corresponding to the second block row and column of A , is in the order of $(\sigma - i\omega\varepsilon)^{-1}$. Since $A^{(\phi, \phi)}$ is an on-diagonal block it gets scaled by $(\sigma - i\omega\varepsilon)^{-2}$. Therefore, the choice $\gamma = (\sigma - i\omega\varepsilon)^2$ produces the desired effect and eliminates the influence of the highly discontinuous complex electric conductivity.

Solution error

The stability considerations discussed above relate to the matrix condition number. This quantity provides a useful means to point out potential problems with the actual solution of the discrete boundary value problem or system of linear equations. In order to gain confidence in this measure and to provide numerical evidence for the conclusions drawn from the condition number, the solution error for two instances of source and boundary data, according to equations (3.21a/b)

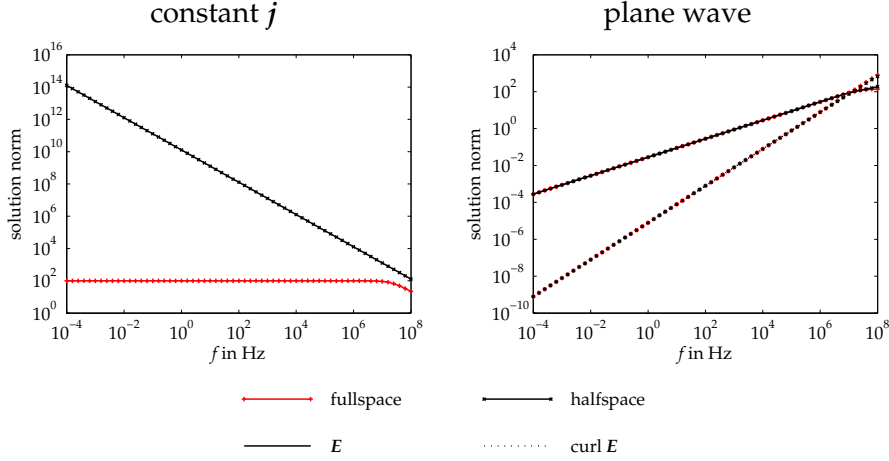


Figure 3.22: Solution norms $\|E\|$ and $\|\text{curl } E\|$ of the constant current density and the plane wave test case.

and (3.21c/d), is examined. The relative solution error is defined by

$$\delta \{E_h\} = \frac{\|E_h - E\|}{\|E\|} \quad \text{and} \quad (3.23a)$$

$$\delta \{\text{curl } E_h\} = \frac{\|\text{curl } E_h - \text{curl } E\|}{\|\text{curl } E\|} \quad (3.23b)$$

where $\|\cdot\|$ denotes the usual L_2 -norm on Ω . Since the curl of the constant current density electric field vanishes, equation (3.23b) cannot be applied in this case. The true solution norms, which are used to normalize the absolute solution error, are depicted in Figure 3.22. While the solution norm of the constant current density case approaches a constant level at low frequencies for the fullspace model, the norm is dominated by the air halfspace for the halfspaces model. This is in contrast to the plane wave test case where the norms of the electric field and of its curl are dominated by the earth halfspace. Therefore, the norms of the plane wave fullspace and halfspaces cases can only be distinguished at the highest frequencies considered. For most of the spectrum $\|E\| \propto \omega^{1/2}$ and $\|\text{curl } E\| \propto \omega$.

Figures 3.23 and 3.25 respectively show the relative solution errors for the constant current density and the plane wave test case where the symmetric matrix scaling has been used. The same quantities are depicted in Figures 3.24 and 3.26 where no matrix scaling was performed prior to calling the linear equations solver.

Comparison of Figures 3.20 and 3.23 reveals that for the constant current density solution the relative error exhibits virtually the same behavior as the matrix condition number. The error increases with decreasing frequency for the E -field formulation and lies in the order of the machine precision for the two variants of the E - V formulation. This is due to the fact that the solution of the continuous boundary value problem is piecewise constant and consequently does not suffer from the finite element approximation by a piecewise polynomial function.

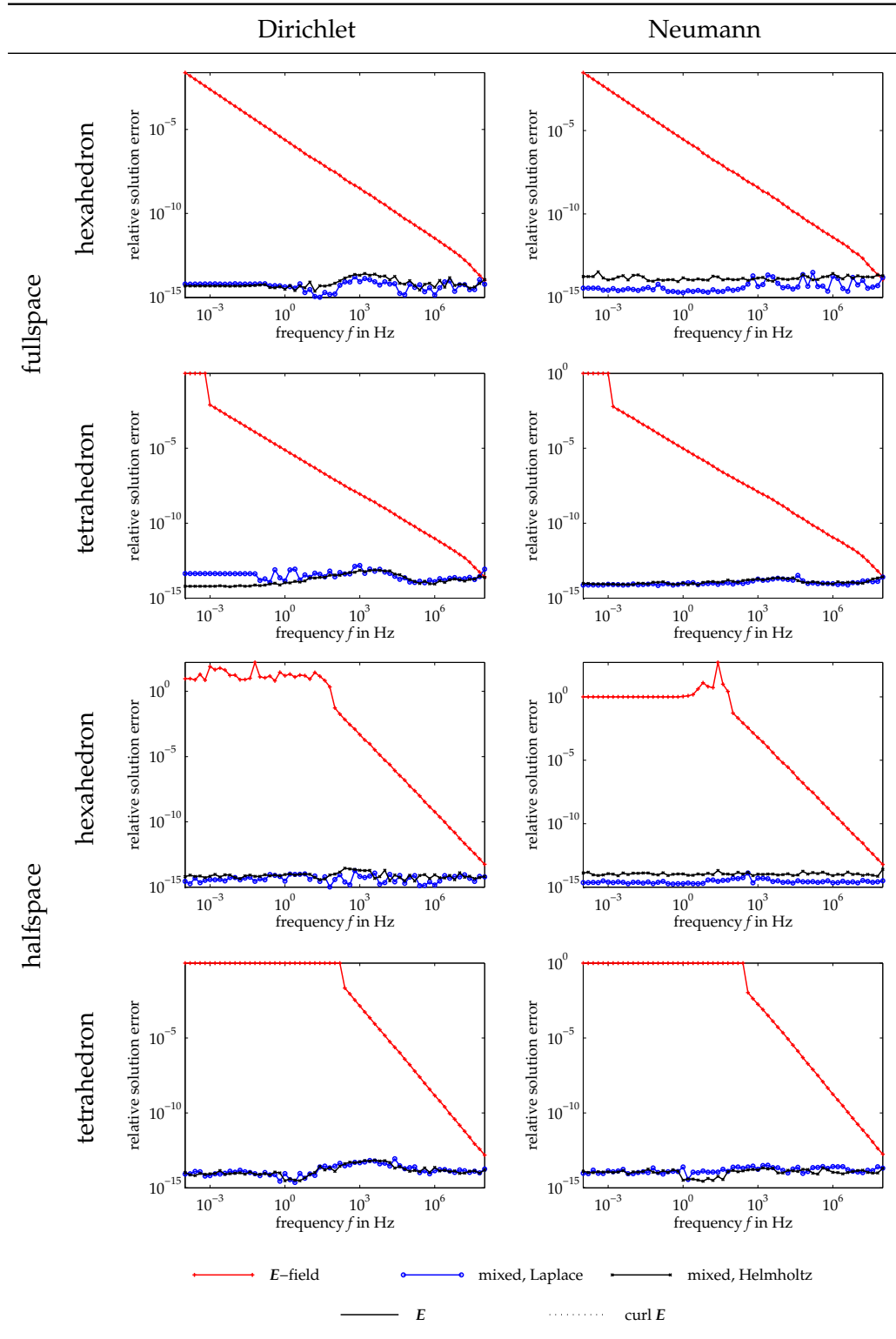


Figure 3.23: Relative solution error for test case ‘constant current density’ with symmetric matrix scaling.

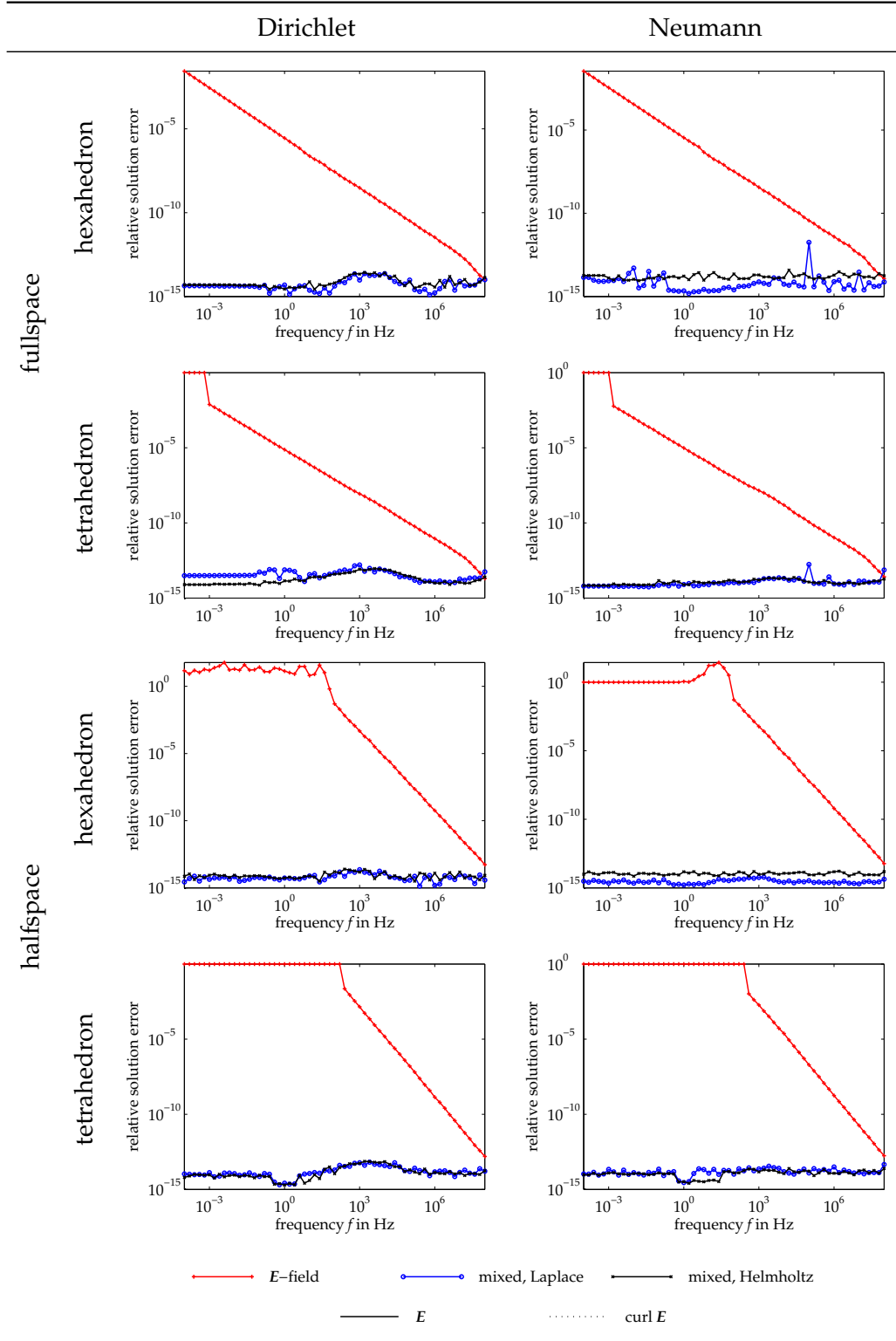


Figure 3.24: Relative solution error for test case ‘constant current density’ without symmetric matrix scaling.

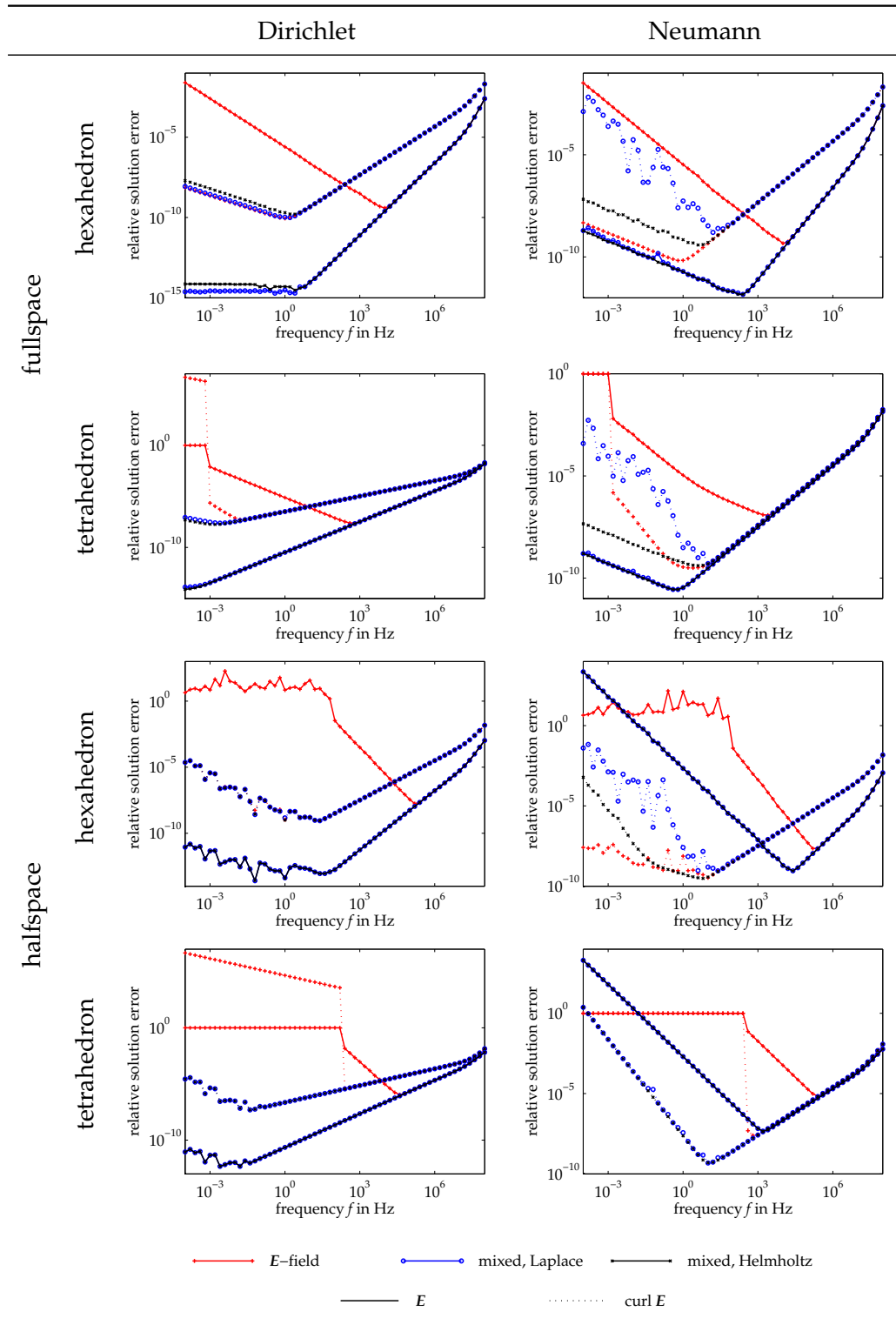


Figure 3.25: Relative solution error for test case ‘plane wave’ with symmetric matrix scaling; piecewise quadratic approximation ($p = 2$).

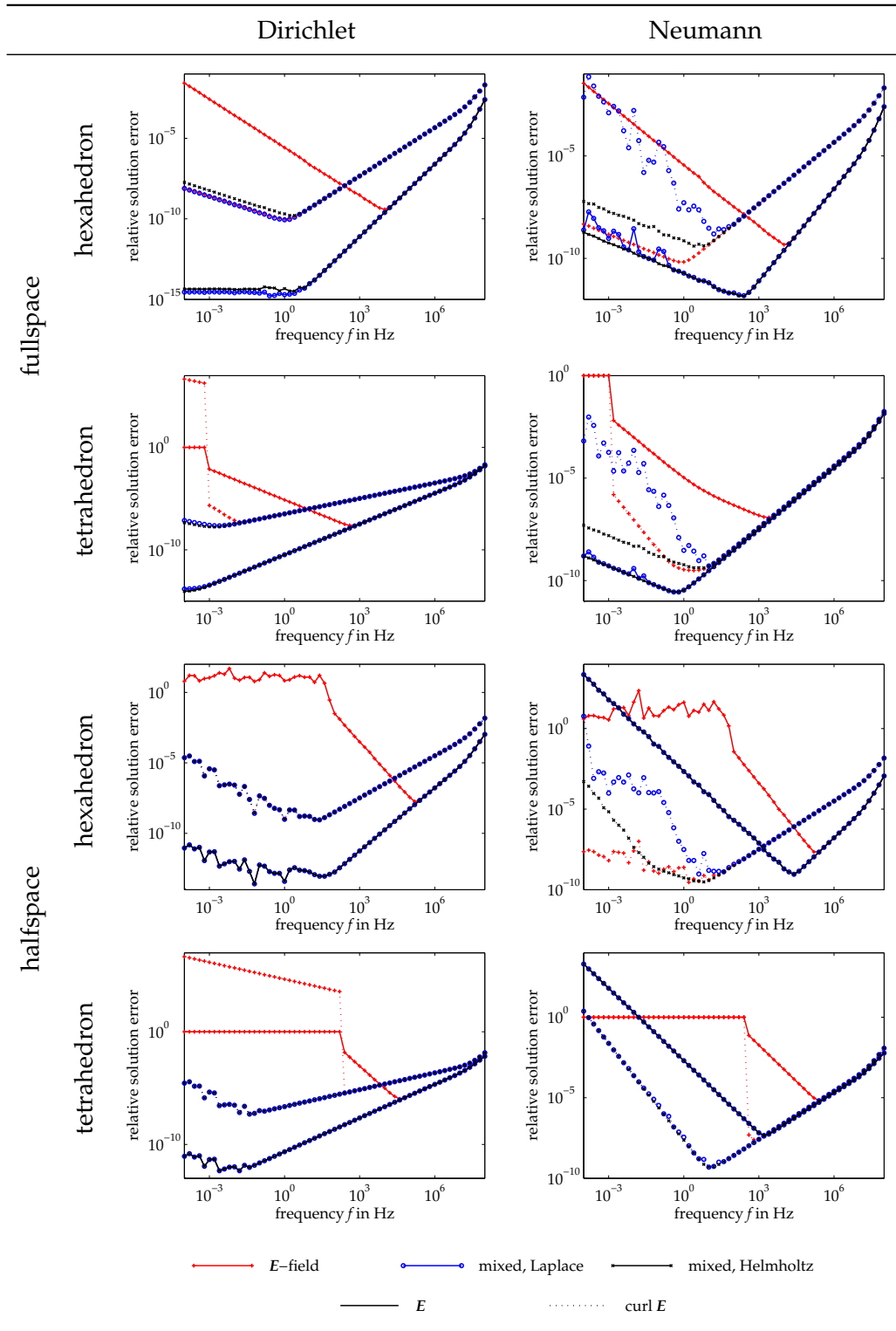


Figure 3.26: Relative solution error for test case ‘plane wave’ without symmetric matrix scaling; piecewise quadratic approximation ($p = 2$).

		$p = 1$		$p = 2$	
		Dirichlet	Neumann	Dirichlet	Neumann
hexahedron	fullspace	1.5/1.5	1.5/1.5	2.0/2.0	2.0/2.0
	halfspace	1.5/1.5	1.5/1.5	2.0/2.0	2.0/2.0
tetrahedron	fullspace	1.0/1.5	1.0/1.5	1.5/1.5	1.5/2.0
	halfspace	1.0/1.5	1.0/1.5	1.5/1.5	1.5/2.0

Table 3.5: The duplets m/n denote the frequency dependency of the *absolute* solution error according to $\|E_h - E\| \propto \omega^m$ and $\|\text{curl } E_h - \text{curl } E\| \propto \omega^n$ for the plane wave test case at higher frequencies (compare the *relative* solution error in Figures 3.25 to 3.28).

The relative error of the plane wave test case (Figures 3.25 and 3.26) looks different but is mostly consistent with the condition number of the scaled system. The differing frequency behavior can be explained by the approximation error of the complex exponential function by a piecewise polynomial which increases with increasing frequency. This effect can be observed in all instances of the plane wave test case at least for the upper part of the spectrum. In order to investigate this approximation property further, the relative solution error of a piecewise linear approximation is provided for comparison in Figures 3.27 and 3.28.

Table 3.5 summarizes the results of a polynomial fit of the absolute solution errors $\|E_h - E\|$ and $\|\text{curl } E_h - \text{curl } E\|$ as a function of frequency for the upwards sloping part of the curves in Figures 3.25 to 3.28. For the case of the hexahedral mesh the absolute error only depends on the polynomial degree irrespective of the boundary condition type or fullspace/halfspaces settings, and is equal for the norms of the field and its curl. Consequently, the frequency behavior of the relative errors (3.23a) and (3.23b) differ by a factor of $\omega^{1/2}$.

The absolute solution error for the tetrahedral mesh exhibits a less consistent frequency behavior. Some settings have a different slope for the error of the field and the error of its curl, some have the same. Those whose slopes differ in the absolute error have the same slope in the relative error. If the relative solution error as a function of frequency is interpreted as a measure for the rate of convergence of the finite element approximation, the electric field can be stated to converge either by the same degree or faster than its curl. Compared to the hexahedral mesh, the rate of convergence for the tetrahedral mesh is equal or lower. This effect may be an effect of the unstructured mesh whose edges are not aligned parallel to the direction of the field vector as it is the case with the hexahedral mesh.

Two features of the relative error plots obviously disagree with the prediction of the matrix condition number. First, the matrix condition number of the ‘mixed, Laplace’ test cases with Neumann boundary condition claims that the matrix is singular to working precision. However, the relative errors prove to be comparable to those of the ‘mixed, Helmholtz’ case. This effect is attributed to the robustness of the linear solver implemented in MUMPS. PARDISO produces the same result. The singular behaviour of the ‘mixed, Laplace’ test cases has its origin in the

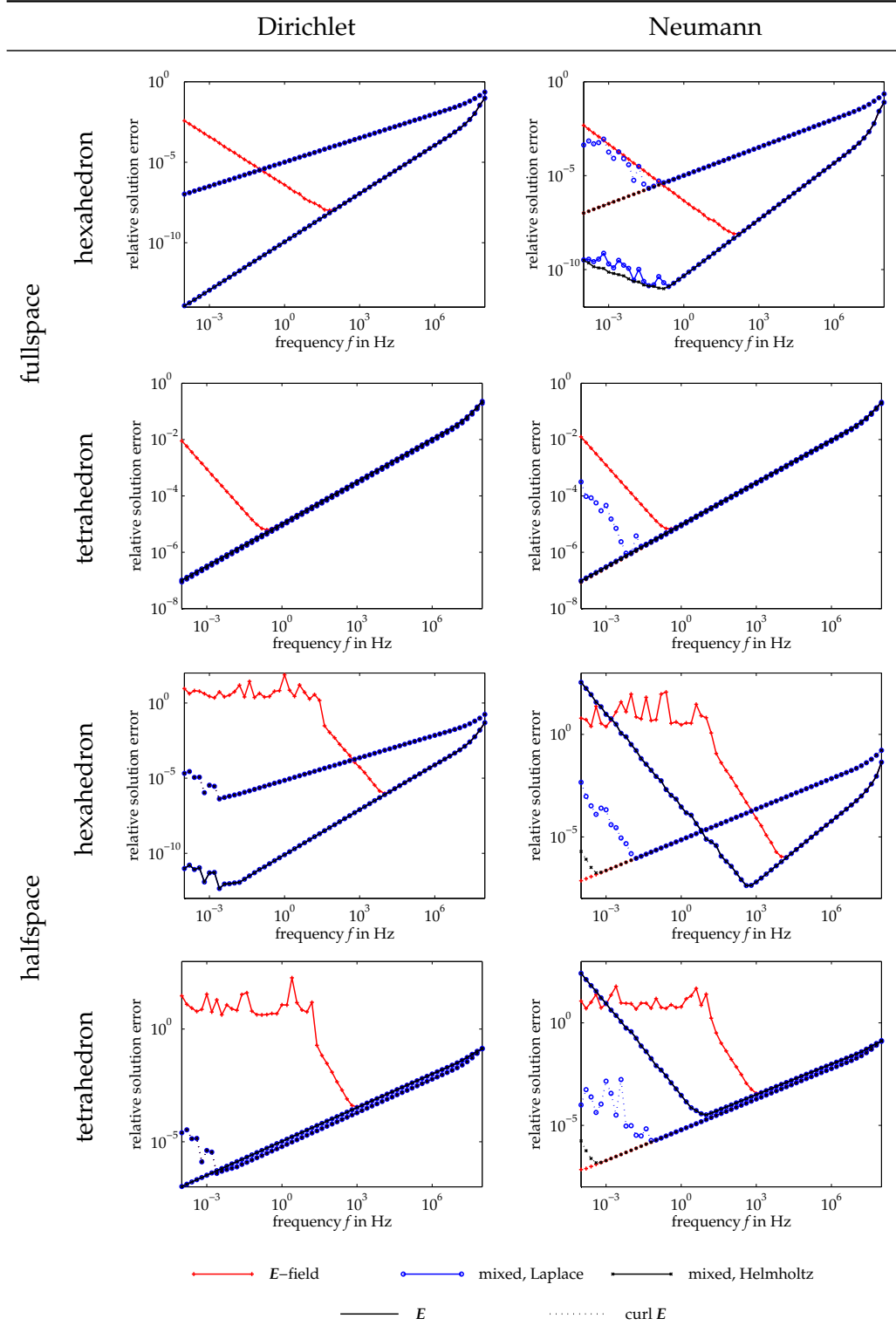


Figure 3.27: Relative solution error for test case ‘plane wave’ with symmetric matrix scaling; piecewise linear approximation ($p = 1$).

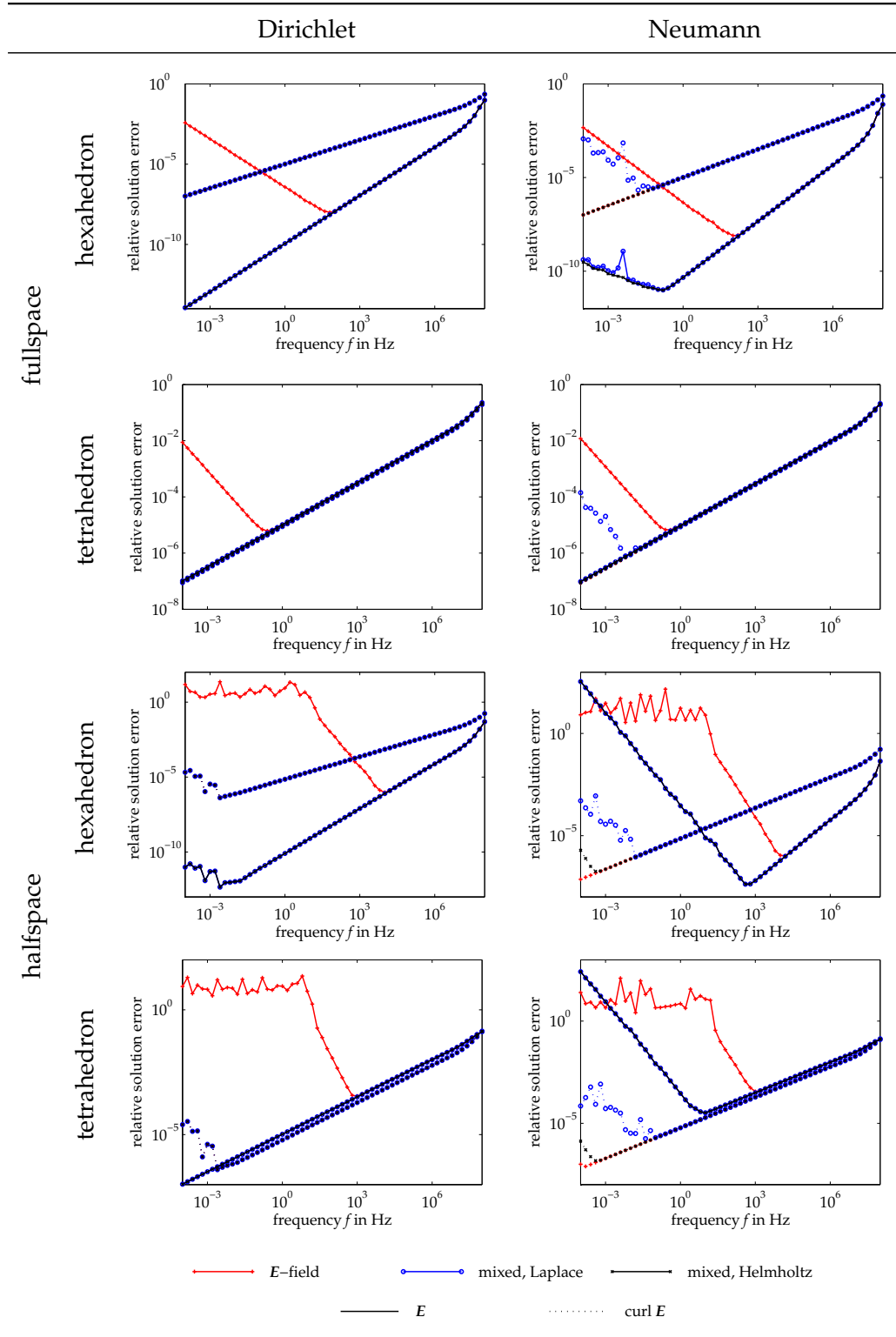


Figure 3.28: Relative solution error for test case ‘plane wave’ without symmetric matrix scaling; piecewise linear approximation ($p = 1$).

Laplace-like equation with a Neumann boundary condition which the scalar field V implicitly satisfies. V is determined non-uniquely. However, the relative solution error (3.23) does not account for V but only includes the electric field E which is determined uniquely.

Second, at low frequencies not only the relative errors of the E -field formulation increase with decreasing frequency as expected but also the relative errors of the E - V formulation. In the case of the halfspaces model and the Neumann boundary condition they even reach prohibitive values. At the same time, the relative solution errors of the unscaled system are almost identical to those of the scaled system. The symmetric scaling appears to have only an effect on the matrix condition and no effect on the relative solution error. On the one hand, this observation recommends the quality of the linear solver used. On the other hand, it questions the benefit of using the matrix scaling and demands an explanation.

If the matrix A is scaled symmetrically according to $\tilde{A} = SAS$, inevitable errors in the solution of the scaled system $\tilde{A}\tilde{x} = \tilde{b}$ are amplified when the solution of the original problem $x = S^{-1}\tilde{x}$ is finally computed. If the scaling matrix S contains very large and very small values, comparably small elements of the solution vector \tilde{x} , which are prone to numerical errors, might be enlarged and reduce the quality of the actual solution vector x . This amounts to the same effect as if the unscaled matrix equation had been solved, provided the linear equations solver is able to deal with the badly scaled matrix.

The origin of the numerical errors has to be sought in the data of the system of linear equations, namely in its linear coefficients and in the right hand side. The fact that the increasing relative errors are observed only for the plane wave test case points to the boundary values. They are subject to integration errors when the right hand side integrals for the Neumann boundary condition or the degrees of freedom fixed by the Dirichlet boundary condition are computed. The inferior low frequency solution quality of the Neumann boundary condition test cases supports the assumption of the boundary values being the origin of the errors. The norm of $\text{curl } E$ decreases to zero faster than the norm of E by a factor of $|k| \propto \omega^{1/2}$. The Neumann boundary data therefore gets very small at low frequencies compared to the Dirichlet boundary data of the same frequency and compared to the field to be computed within the domain. Errors of these tiny numbers eventually beset the solution quality.

Concluding, the matrix condition number has not proven to be the ultimate measure for solution stability. Yet, it has served as a valuable indicator during the development of a numerical solution strategy for Maxwell's equations with improved stability properties. The E - V formulation consistently gives more accurate results over a larger range of frequencies even for high contrast models. However, the solution remains susceptible to approximation errors of the boundary value problem input data.

For the examples and linear equations solvers considered, the symmetric matrix scaling has turned out to be of no significance for the solution accuracy. The matrix condition numbers of the scaled system and the halfspaces model are consistent only with the solution error of the constant current density test case but neither completely inconsistent nor consistent with the solution error of the plane wave test case.

Chapter 4

Enhanced concepts

The boundary value problems presented in Chapter 2 and their finite element solution described in Chapter 3 provide a straightforward approach to modelling electromagnetic phenomena in general and geophysical problems in particular. Stability considerations concerning the solution behavior with respect to low frequencies could be carried out within this framework without need for an overly complex notation. This chapter now introduces enhanced concepts which refine the physical modelling. The simple boundary value problems of Chapter 2 are extended in order to improve the overall solution quality and tailor the software to the particular requirements of geophysical model settings.

4.1 Scattered field problems

The electric field sought in the boundary value problems of Chapter 2 is caused by impressed current or charge densities within the domain or on its boundary, or by given field values on the boundary. This class of problems is termed total field problems in contrast to the problem class of scattered fields. The total field is the physical field which is present at a point within space. Exploiting linearity of Maxwell's equations, the total field can be split into an incident field part and a scattered field part. A scattered field problem now reduces the boundary value problem to the solution for the scattered field E_s only, given the incident field E_i .

From a numerical point of view this procedure is often advantageous because the known part of the total field does not need to be approximated numerically and, therefore, does not suffer approximation errors. The incident field magnitude is often significantly larger than the scattered field magnitude. In addition, the scattered field can be made more amenable to numerical approximation if the singular behavior of the electric field around point sources is exactly expressed by the incident field. This technique is also known as singularity removal. The incident field is sometimes called the primary or normal field and the scattered field the secondary or anomalous field.

In order to cover the most general case and to save space at the same time, only the E - V formulation is given in the following. The E -field formulation can easily be deduced by dropping certain terms and equations.

4.1.1 The boundary value problem

The total field is assumed to be a solution of boundary value problem (2.17) or its augmented equivalent (2.18); the incident field E_i to be a solution of boundary value problem (2.17) with a different set of constitutive parameters ϵ_i , μ_i and σ_i ,

$$\text{curl} \left(\mu_i^{-1} \text{curl} E_i \right) - i\omega(\sigma_i - i\omega\epsilon_i)E_i = i\omega j_s \quad \text{on } \Omega_i, \quad (4.1a)$$

$$- \text{div} (\sigma_i - i\omega\epsilon_i)E_i = \text{div} j_s \quad \text{on } \Omega_i, \quad (4.1b)$$

$$[n \times E_i]_\Sigma = 0 \quad \text{on } \Sigma_{i,j}, \quad (4.1c)$$

$$\left[n \times (\mu_i)^{-1} \text{curl} E_i \right]_\Sigma = i\omega j_f \quad \text{on } \Sigma_{i,j}, \quad (4.1d)$$

$$- [n \cdot (\sigma_i - i\omega\epsilon_i)E_i]_\Sigma = [n \cdot j_s]_\Sigma \quad \text{on } \Sigma_{i,j}, \quad (4.1e)$$

$$n \times E_i = n \times E_0 \quad \text{on } \Gamma_e, \quad (4.1f)$$

$$n \times \mu_i^{-1} \text{curl} E_i + i\omega n \times (\lambda_i (n \times E_i)) = i\omega n \times H_0 + i\omega j_f \quad \text{on } \Gamma_h \text{ and} \quad (4.1g)$$

$$n \cdot (\sigma_i - i\omega\epsilon_i)E_i + n \cdot \text{curl} (\lambda_i (n \times E_i)) = n \cdot \text{curl} H_0 - n \cdot j_s \quad \text{on } \Gamma_h. \quad (4.1h)$$

The source and exterior field terms of the total and the incident field problem are chosen to be identical. The constitutive parameters are usually assumed to follow a very simple pattern such that the incident field is analytically known. Since E_i is a given field only the set of Maxwell's equations is of interest which E_i satisfies. The additional terms and equations in the E - V formulation involving the auxiliary scalar field V vanish by construction.

The scattered field problem is derived by inserting the split field approach

$$E = E_i + E_s \quad (4.2)$$

into the total field problem (2.18). Note that the augmented form of the E - V formulation is used as the starting point because the final boundary value problem in terms of the scattered field will have to be solved numerically. Therefore, the algebraically balanced form, including the auxiliary scalar field V , is preferred. Finally, corresponding equations of boundary value problem (4.1) are subtracted from the total field problem. Using the definitions

$$\delta\epsilon = \epsilon_i - \epsilon, \quad (4.3a)$$

$$\delta\lambda = \lambda_i - \lambda, \quad (4.3b)$$

$$\delta\mu^{-1} = \mu_i^{-1} - \mu^{-1} \quad \text{and} \quad (4.3c)$$

$$\delta\sigma = \sigma_i - \sigma \quad (4.3d)$$

the scattered field E_s is sought as a solution of the boundary value problem

$$\begin{aligned} \text{curl} (\mu^{-1} \text{curl} E_s) - i\omega(\sigma - i\omega\epsilon)E_s \\ + (\sigma - i\omega\epsilon) \text{grad} V = \text{curl} (\delta\mu^{-1} \text{curl} E_i) \\ - i\omega(\delta\sigma - i\omega\delta\epsilon)E_i \quad \text{on } \Omega_i, \end{aligned} \quad (4.4a)$$

4.1 Scattered field problems

$$-\operatorname{div}(\sigma - i\omega\epsilon)E_s - \gamma V = -\operatorname{div}(\delta\sigma - i\omega\delta\epsilon)E_i \quad \text{on } \Omega_i, \quad (4.4b)$$

$$[\mathbf{n} \times E_s]_\Sigma = \mathbf{0} \quad \text{on } \Sigma_{i,j}, \quad (4.4c)$$

$$[V]_\Sigma = 0 \quad \text{on } \Sigma_{i,j}, \quad (4.4d)$$

$$\left[\mathbf{n} \times \mu^{-1} \operatorname{curl} E_s \right]_\Sigma = \left[\mathbf{n} \times \delta\mu^{-1} \operatorname{curl} E_i \right]_\Sigma \quad \text{on } \Sigma_{i,j}, \quad (4.4e)$$

$$-[\mathbf{n} \cdot (\sigma - i\omega\epsilon)E_s]_\Sigma = -[\mathbf{n} \cdot (\delta\sigma - i\omega\delta\epsilon)E_i]_\Sigma \quad \text{on } \Sigma_{i,j}, \quad (4.4f)$$

$$[\mathbf{n} \cdot (\sigma - i\omega\epsilon) \operatorname{grad} V]_\Sigma = 0 \quad \text{on } \Sigma_{i,j}, \quad (4.4g)$$

$$\mathbf{n} \times E_s = \mathbf{0} \quad \text{on } \Gamma_e, \quad (4.4h)$$

$$V = 0 \quad \text{on } \Gamma_e, \quad (4.4i)$$

$$\begin{aligned} \mathbf{n} \times \mu^{-1} \operatorname{curl} E_s + i\omega \mathbf{n} \times (\lambda(\mathbf{n} \times E_s)) \\ - \mathbf{n} \times (\lambda(\mathbf{n} \times \operatorname{grad} V)) = \mathbf{n} \times \delta\mu^{-1} \operatorname{curl} E_i \\ + i\omega \mathbf{n} \times (\delta\lambda(\mathbf{n} \times E_i)) \end{aligned} \quad \text{on } \Gamma_h, \quad (4.4j)$$

$$\begin{aligned} \mathbf{n} \cdot (\sigma - i\omega\epsilon) E_s + \mathbf{n} \cdot \operatorname{curl}(\lambda(\mathbf{n} \times E_s)) = \mathbf{n} \cdot (\delta\sigma - i\omega\delta\epsilon) E_i \\ + \mathbf{n} \cdot \operatorname{curl}(\delta\lambda(\mathbf{n} \times E_i)) \end{aligned} \quad \text{on } \Gamma_h, \quad (4.4k)$$

$$\mathbf{n} \cdot (\sigma - i\omega\epsilon) \operatorname{grad} V - \mathbf{n} \cdot \operatorname{curl}(\lambda(\mathbf{n} \times \operatorname{grad} V)) = 0 \quad \text{on } \Gamma_h. \quad (4.4l)$$

All source and exterior field terms cancel because they have been chosen identical for the the total field and the incident field. Sources of the scattered field are generated by the incident field in domains where the constitutive parameters deviate from those of the incident field boundary value problem. The sources are not restricted to the interior of the subdomains Ω_i . Differences of the constitutive parameters can also cause source terms at the interfaces $\Sigma_{i,j}$ between subdomains as well as on the Neumann boundary Γ_h . The Dirichlet boundary condition is chosen such that it is homogeneous in terms of the scattered field.

4.1.2 The weak form

The weak form of the scattered field problem is derived from the total field problem similarly to the previous section. Assume that the incident field is a solution of the weak equivalent of boundary value problem (4.1). This is the same as the weak form of the total field problem (2.31) where the constitutive parameters are replaced by their incident field values. Dropping all terms which involve the dummy variable V the incident field will satisfy the following variational problem:

Search $E_i \in \mathcal{U}_i$ such that

$$\begin{aligned} \int_{\Omega} \operatorname{curl} \bar{\Phi} \cdot (\mu_i^{-1} \operatorname{curl} E_i) d^3r - i\omega \int_{\Omega} \bar{\Phi} \cdot ((\sigma_i - i\omega\epsilon_i)E_i) d^3r + i\omega \int_{\Gamma_h} (\mathbf{n} \times \bar{\Phi}) \cdot (\lambda_i(\mathbf{n} \times E_i)) d^2r \\ = i\omega \int_{\Omega} \bar{\Phi} \cdot \mathbf{j}_s d^3r - i\omega \sum_{\substack{i,j=1 \\ i < j}}^n \int_{\Sigma_{i,j}} \bar{\Phi} \cdot \mathbf{j}_f d^2r - i\omega \int_{\Gamma_h} \bar{\Phi} \cdot (\mathbf{j}_f + \mathbf{n} \times H_0) d^2r \end{aligned} \quad (4.5a)$$

Chapter 4 Enhanced concepts

for all $\Phi \in \mathcal{U}_0$ and

$$\begin{aligned} \int_{\Omega} \text{grad } \bar{\phi} \cdot ((\sigma_i - i\omega \epsilon_i) E_i) d^3r - \int_{\Gamma_h} (\mathbf{n} \times \text{grad } \bar{\phi}) \cdot (\lambda_i (\mathbf{n} \times E_i)) d^2r \\ = - \int_{\Omega} \text{grad } \bar{\phi} \cdot \mathbf{j}_s d^3r + \int_{\Gamma_h} \text{grad } \bar{\phi} (\mathbf{n} \times \mathbf{H}_0) d^2r \end{aligned} \quad (4.5b)$$

for all $\phi \in \mathcal{V}_0$. The spaces of test and trial functions are defined by

$$\mathcal{U}_0 = \{ \Phi \in H_{\text{curl}}(\Omega) : \mathbf{n} \times \Phi = \mathbf{0} \text{ on } \Gamma_e \}, \quad (4.5c)$$

$$\mathcal{U}_i = \{ E_i \in H_{\text{curl}}(\Omega) : \mathbf{n} \times E_i = \mathbf{n} \times E_0 \text{ on } \Gamma_e \} \quad (4.5d)$$

$$\mathcal{V}_0 = \{ \phi \in H_1(\Omega) : \phi = 0 \text{ on } \Gamma_e \}, \quad (4.5e)$$

where

$$H_{\text{curl}}(\Omega) = \{ E_i \in (L_2(\Omega))^3 : \text{curl } E_i \in (L_2(\Omega))^3 \}, \quad (4.5f)$$

$$H_1(\Omega) = \{ \phi \in L_2(\Omega) : \text{grad } \phi \in L_2(\Omega) \} \quad (4.5g)$$

are the spaces of functions with a well-defined curl and gradient, respectively.

The variational problem in terms of the scattered field E_s is obtained by inserting the split field approach $E = E_i + E_s$ into the total field variational problem (2.31) and subtracting corresponding equations from (4.5). As before, all source terms cancel except for those involving the difference of the two sets of constitutive parameters.

Search $E_s \in \mathcal{U}_s$ and $V \in \mathcal{V}$ such that

$$\begin{aligned} \int_{\Omega} \text{curl } \bar{\Phi} \cdot (\mu^{-1} \text{curl } E_s) d^3r - i\omega \int_{\Omega} \bar{\Phi} \cdot ((\sigma - i\omega \epsilon) E_s) d^3r + \int_{\Omega} \bar{\Phi} \cdot ((\sigma - i\omega \epsilon) \text{grad } V) d^3r \\ + i\omega \int_{\Gamma_h} (\mathbf{n} \times \bar{\Phi}) \cdot (\lambda (\mathbf{n} \times E_s)) d^2r - \int_{\Gamma_h} (\mathbf{n} \times \bar{\Phi}) \cdot (\lambda (\mathbf{n} \times \text{grad } V)) d^2r \\ = \int_{\Omega} \text{curl } \bar{\Phi} \cdot (\delta \mu^{-1} \text{curl } E_i) d^3r - i\omega \int_{\Omega} \bar{\Phi} \cdot ((\delta \sigma - i\omega \delta \epsilon) E_i) d^3r \\ + i\omega \int_{\Gamma_h} (\mathbf{n} \times \bar{\Phi}) \cdot (\delta \lambda (\mathbf{n} \times E_i)) d^2r \end{aligned} \quad (4.6a)$$

for all $\Phi \in \mathcal{U}_0$ and

$$\begin{aligned} \int_{\Omega} \text{grad } \bar{\phi} \cdot ((\sigma - i\omega \epsilon) E_s) d^3r - \int_{\Omega} \bar{\phi} \gamma V d^3r - \int_{\Gamma_h} (\mathbf{n} \times \text{grad } \bar{\phi}) \cdot (\lambda (\mathbf{n} \times E_s)) d^2r \\ = \int_{\Omega} \text{grad } \bar{\phi} \cdot ((\delta \sigma - i\omega \delta \epsilon) E_i) d^3r - \int_{\Gamma_h} (\mathbf{n} \times \text{grad } \bar{\phi}) \cdot (\delta \lambda (\mathbf{n} \times E_i)) d^2r \end{aligned} \quad (4.6b)$$

for all $\phi \in \mathcal{V}_0$. The spaces of test and trial functions are defined by

$$\mathcal{U}_0 = \{ \Phi \in H_{\text{curl}}(\Omega) : \mathbf{n} \times \Phi = \mathbf{0} \text{ on } \Gamma_e \} \quad (4.6c)$$

$$\mathcal{U}_s = \mathcal{U}_0 \quad (4.6d)$$

$$\mathcal{V}_0 = \{\phi \in H_1(\Omega) : \phi = 0 \text{ on } \Gamma_e\} \quad (4.6e)$$

$$\mathcal{V} = \mathcal{V}_0 \quad (4.6f)$$

where

$$H_{\text{curl}}(\Omega) = \{E \in (L_2(\Omega))^3 : \text{curl } E \in (L_2(\Omega))^3\} \quad (4.6g)$$

$$H_1(\Omega) = \{V \in L_2(\Omega) : \text{grad } V \in L_2(\Omega)\} \quad (4.6h)$$

are the spaces of functions with a well-defined curl and gradient, respectively.

In contrast to the classical form of the scattered field formulation (4.4) source terms in the weak form (4.6) turn up only as volume integrals over Ω and as a boundary integral over Γ_h . The source terms at the interfaces $\Sigma_{i,j}$ (4.4e) and (4.4f) have been absorbed by the variational integrals as natural interface conditions.

4.1.3 Finite element solution

As in Chapter 3, the variational problem (4.6) forms the point of departure for the finite element method. The discrete problem is derived in a completely analogous way to Chapter 3. Therefore, only the final form of the resulting system of linear equations is given here. If the scattered electric field is expanded in terms of the finite element basis $\{\Phi_i\}_{i=1}^N$ as

$$E_{s,h}(\mathbf{r}) = \sum_{i=1}^N E_i \Phi_i(\mathbf{r}) \quad (4.7)$$

the unknown linear coefficients E_i and V_i are determined by

$$\sum_{i=1}^n a_{j,i}^{(\Phi,\Phi)} E_i + \sum_{i=1}^m a_{j,i}^{(\Phi,\phi)} V_i = f_j^{(\Phi)}, \quad j = 1, \dots, n, \quad (4.8a)$$

$$\sum_{i=1}^n a_{j,i}^{(\phi,\Phi)} E_i + \sum_{i=1}^m a_{j,i}^{(\phi,\phi)} V_i = f_j^{(\phi)}, \quad j = 1, \dots, m, \quad (4.8b)$$

where

$$\begin{aligned} a_{j,i}^{(\Phi,\Phi)} = & \int_{\Omega} \text{curl } \bar{\Phi}_j \cdot (\mu^{-1} \text{curl } \Phi_i) d^3r - i\omega \int_{\Omega} \bar{\Phi}_j \cdot ((\sigma - i\omega\epsilon) \Phi_i) d^3r \\ & + i\omega \int_{\Gamma_h} (\mathbf{n} \times \bar{\Phi}_j) \cdot (\lambda (\mathbf{n} \times \Phi_i)) d^2r, \end{aligned} \quad (4.8c)$$

$$a_{j,i}^{(\Phi,\phi)} = \int_{\Omega} \bar{\Phi}_j \cdot ((\sigma - i\omega\epsilon) \text{grad } \phi_i) d^3r - \int_{\Gamma_h} (\mathbf{n} \times \bar{\Phi}_j) \cdot (\lambda (\mathbf{n} \times \text{grad } \phi_i)) d^2r, \quad (4.8d)$$

$$a_{j,i}^{(\phi,\Phi)} = \int_{\Omega} \text{grad } \bar{\phi}_j \cdot ((\sigma - i\omega\epsilon) \Phi_i) d^3r - \int_{\Gamma_h} (\mathbf{n} \times \text{grad } \bar{\phi}_j) \cdot (\lambda (\mathbf{n} \times \Phi_i)) d^2r, \quad (4.8e)$$

$$a_{j,i}^{(\phi,\phi)} = - \int_{\Omega} \bar{\phi}_j \gamma \phi_i d^3r \quad (4.8f)$$

and

$$f_j^{(\Phi)} = \int_{\Omega} \text{curl } \bar{\Phi}_j \cdot (\delta \mu^{-1} \text{curl } E_i) d^3r - i\omega \int_{\Omega} \bar{\Phi}_j \cdot ((\delta \sigma - i\omega \delta \epsilon) E_i) d^3r \\ + i\omega \int_{\Gamma_h} (\mathbf{n} \times \bar{\Phi}_j) \cdot (\delta \lambda (\mathbf{n} \times E_i)) d^2r - \sum_{i=n+1}^N a_{j,i}^{(\Phi, \Phi)} E_i - \sum_{i=m+1}^M a_{j,i}^{(\Phi, \phi)} V_i, \quad (4.8g)$$

$$f_j^{(\phi)} = \int_{\Omega} \text{grad } \bar{\phi}_j \cdot ((\delta \sigma - i\omega \delta \epsilon) E_i) d^3r \\ - \int_{\Gamma_h} (\mathbf{n} \times \text{grad } \bar{\phi}_j) \cdot (\delta \lambda (\mathbf{n} \times E_i)) d^2r - \sum_{i=n+1}^N a_{j,i}^{(\phi, \Phi)} E_i - \sum_{i=m+1}^M a_{j,i}^{(\phi, \phi)} V_i. \quad (4.8h)$$

The Dirichlet boundary conditions for E_s and V require that $E_i = 0$ for $i = n + 1, \dots, N$ and $V_i = 0$ for $i = m + 1, \dots, M$.

Note that the coefficient matrices of both the total and the scattered field discrete problem are identical. The total field variational problem (2.31) and the scattered field variational problem (4.6) differ only by their source terms and boundary values and, therefore, the derived systems of linear equations only by different right hand side vectors.

4.1.4 Incident fields

Three of the most important types of incident fields have been integrated into the finite element software suite, the electric and magnetic dipole as well as the plane wave.

The electric and magnetic dipole are prototypes for most of the sources used in active electromagnetic methods. The approximation of the real source geometry by an ideal point source is valid if the fields are considered far enough from the source. This model assumption always needs to be remembered. The electromagnetic fields of the electric and magnetic dipole have a compact form solution for the case of a homogeneous fullspace. The fields of an electric dipole at \mathbf{r}_s excited by source current density \mathbf{j}_s are given by (Nolting, 1997)

$$\mathbf{E} = \frac{Z}{4\pi} \frac{e^{ikr}}{r^2} \left((\mathbf{j}_s - (\mathbf{n} \cdot \mathbf{j}_s) \mathbf{n}) ikr + (\mathbf{j}_s - 3(\mathbf{n} \cdot \mathbf{j}_s) \mathbf{n}) \left(\frac{1}{ikr} - 1 \right) \right), \quad (4.9a)$$

$$\mathbf{H} = \frac{1}{4\pi} \frac{e^{ikr}}{r^2} (\mathbf{n} \times \mathbf{j}_s) (ikr - 1) \quad (4.9b)$$

where $r = |\mathbf{r} - \mathbf{r}_s|$, $\mathbf{n} = (\mathbf{r} - \mathbf{r}_s)/r$ and $Z = \omega\mu/k$. Equations (4.9a) and (4.9b) are a solution of Maxwell's equations with source current density $\mathbf{j}_s(\mathbf{r}) = \mathbf{j}_s \delta(\mathbf{r} - \mathbf{r}_s)$ where $\delta(\mathbf{r} - \mathbf{r}_s)$ denotes the Dirac delta distribution. Similarly, the fields of a magnetic dipole at \mathbf{r}_s with magnetic dipole moment \mathbf{m} are given by

$$\mathbf{E} = \frac{ikZ}{4\pi} \frac{e^{ikr}}{r^2} (\mathbf{n} \times \mathbf{m}) (ikr - 1), \quad (4.10a)$$

$$\mathbf{H} = -\frac{ik}{4\pi} \frac{e^{ikr}}{r^2} \left((\mathbf{m} - (\mathbf{n} \cdot \mathbf{m}) \mathbf{n}) ikr + (\mathbf{m} - 3(\mathbf{n} \cdot \mathbf{m}) \mathbf{n}) \left(\frac{1}{ikr} - 1 \right) \right). \quad (4.10b)$$

4.2 Absorbing boundaries – The perfectly matched layer

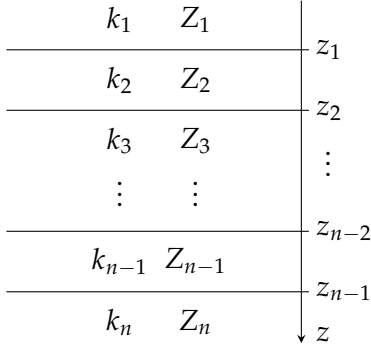


Figure 4.1: Horizontally stratified earth which consists of n layers (including the upper and lower halfspaces).

If the magnetic dipole is assumed to be the approximation of a single loop circular coil with radius R , the coil's axis determines the direction of vector \mathbf{m} and $|\mathbf{m}| = \pi R^2 I$ where I denotes the current flowing through the coil.

Equations (4.9) and (4.10) are only valid for an isotropic and homogeneous fullspace. They are, nevertheless, preferred to the much more complicated formulae for a layered medium which involve Hankel integrals (Løseth, 2007). The numerical evaluation of these integrals is computationally expensive compared to the simple expressions of the fullspace case.

In contrast to the dipole field solution, the plane wave solution of Maxwell's equations for a horizontally stratified earth reduces to a very compact form. Denote by k_i and Z_i the complex wavenumber and the intrinsic complex wave impedance of layer i ($i = 1, \dots, n$; Figure 4.1). Further, denote the depth of the layer interfaces by z_i and let $z_0 = z_1$. Then, the fields of a plane wave travelling along the z -axis, i. e., perpendicular to the stack of layers can be expressed within layer i by

$$\mathbf{E}_i = Z_i \left(a_i e^{ik_i(z-z_{i-1})} + b_i e^{-ik_i(z-z_{i-1})} \right) \mathbf{E}_0, \quad (4.11a)$$

$$\mathbf{H}_i = \left(a_i e^{ik_i(z-z_{i-1})} - b_i e^{-ik_i(z-z_{i-1})} \right) \mathbf{H}_0 \quad (4.11b)$$

where \mathbf{E}_0 and \mathbf{H}_0 define the horizontal field vectors. They satisfy $\mathbf{n} \cdot \mathbf{E}_0 = 0$, $\mathbf{n} \cdot \mathbf{H}_0 = 0$ and $\mathbf{H}_0 = \mathbf{n} \times \mathbf{E}_0$ if $\mathbf{n} = (0, 0, 1)^T$ is the propagation direction. The coefficients a_i and b_i are derived in Appendix E and turn out to be independent of z . If they are precomputed the fields can be evaluated for arbitrary z according to equations (4.11a) and (4.11b) very fast. Note that due to the one-dimensional model assumptions the fields do not depend on the x - and y -coordinates. The plane wave solution for a layered medium is the typical incident field pattern for modelling magnetotellurics.

4.2 Absorbing boundaries – The perfectly matched layer

All electromagnetic methods of geophysics probe part of the earth either with active sources placed within or near the target under investigation like, e. g., GPR and TEM or with passive sources

placed far away like, e. g., MT or VLF. In each case, the electromagnetic field introduced by the source and distorted by the ground structure is not confined to a closed volume but penetrates all space. The field of a finite source obeys the Sommerfeld radiation condition, i. e., it decays to zero as the distance from the source approaches infinity.

Translated into mathematical terms, the boundary value problem describing the electromagnetic phenomena is naturally posed on an infinite domain, in fact, the \mathbb{R}^3 . Numerical simulation with the finite element method requires a finite domain. Therefore, an artificial boundary Γ needs to be introduced that defines the simulation volume $\Omega \subsetneq \mathbb{R}^3$. Suitable boundary conditions have to be posed on the boundary $\Gamma = \partial\Omega$. Their effect on the fields has to be equivalent to that of the Sommerfeld radiation condition for the original infinite domain problem. This means, the field approaches and penetrates the boundary as if there was no boundary. If the field is considered to be decomposed into the superposition of plane waves with all possible propagation directions, the boundary must be able to pass all partial waves coming from within the simulation volume and block all waves coming from outside. This can be formally described by the so called one way wave equation, a pseudodifferential equation (Trefethen, 1996): Consider the vector Helmholtz equation of an isotropic and homogeneous medium

$$\left(\frac{1}{c^2} \frac{\partial^2}{\partial t^2} - \frac{\partial^2}{\partial x^2} - \frac{\partial^2}{\partial y^2} - \frac{\partial^2}{\partial z^2} \right) \mathbf{E} = \mathbf{0} \quad (4.12)$$

where c denotes the phase velocity. Any plane wave $\mathbf{E} = \hat{\mathbf{E}} e^{i(k_x x + k_y y + k_z z - \omega t)}$ solves equation (4.12) if k_x, k_y, k_z and ω satisfy the dispersion relation

$$k_z = \pm \frac{1}{c} \sqrt{\omega^2 - c^2 k_x^2 - c^2 k_y^2}. \quad (4.13)$$

The plus sign corresponds to waves travelling in positive z -direction, the minus sign to waves travelling in negative z -direction. At an artificial planar boundary with a $+z$ -directed outward normal vector the desired outgoing waves are characterized by positive k_z . These waves could be extracted by a differential operator with an associated dispersion relation

$$k_z = + \frac{1}{c} \sqrt{\omega^2 - c^2 k_x^2 - c^2 k_y^2}. \quad (4.14)$$

Unfortunately, such a differential equation does not exist. A number of absorbing boundary conditions can be derived from (4.14) if the square root is approximated by rational functions. Neglecting the k_x and k_y terms leads to the dispersion relation $k_z = \omega/c$ which corresponds to the simple differential equation

$$\left(\frac{1}{c} \frac{\partial}{\partial t} - \frac{\partial}{\partial z} \right) \mathbf{E} = \mathbf{0}. \quad (4.15)$$

This zeroth order absorbing boundary condition is exact for waves incident at a right angle onto the x - y -plane but causes reflections for oblique incidences, i. e., if k_x and k_y do not vanish.

4.2 Absorbing boundaries – The perfectly matched layer

Higher order absorbing boundary conditions involve higher order derivatives of space and time. In other words, they may require more regular solutions than the wave equation within Ω . Their benefit, however, is a lower reflectivity for a wider range of oblique incidences.

The problem could be treated mathematically rigorously by coupling the finite element solution of the interior problem with an integral equations solution of the exterior problem. This approach, however, has several drawbacks: The implementation is rather involved since two numerical methods have to be implemented. The key problem of the integral equation method is finding an appropriate Green's function. Take, e. g., a problem where some objects are imbedded within a layered earth structure. This layered earth has to be taken into account for computing the Green's function, i. e., the field of a point source placed at an arbitrary position within the earth. The Green's function depends on the particular model structure. Therefore, this approach might be beneficial for a certain class of models and special cases but is not very general.

Simple boundary conditions are applicable directly to the finite element method and are easier implemented. One possibility to improve their poor quality for obliquely incident wave fields is moving the boundary further away from the simulation volume of interest. The size of this sponge layer can be reduced if loss is added to the material properties. While this approach has been used for a long time, an revolutionary improvement has been suggested by Berenger in 1994. He modified the set of Maxwell's equations such that the sponge layer has optimal properties in a certain sense: Waves traversing the layer are exponentially damped. And, there is no reflection at the interface between the simulation volume and the sponge layer. That's why his approach is called the perfectly matched layer (PML). A number of different derivations of the PML equations (in contrast to the usual Maxwell's equations) have been made, since (Berenger, 1994; Chew and Weedon, 1995; Rappaport, 1995; Sacks, Kingsland, Lee, and Lee, 1995; Fang and Wu, 1995; Gedney, 1996; Zhao and Cangellaris, 1996; Teixeira and Chew, 1997; Petropoulos, 2000). It turns out that the PML can be seen as a refined combination of both simple approaches – moving away the boundary and adding loss – if a complex coordinate stretching is applied to Maxwell's equations.

Concerning finite element algorithmic development, the PML is implemented most easily using an anisotropic media set of equations. They will be derived using the complex coordinate stretching argument in the next section. Some properties of the PML will be examined before the chapter is finished by a simple example.

4.2.1 Construction of a perfectly matched layer

The starting point for all considerations is the boundary value problem (boundary value problem) which is posed on an infinite domain $\Omega^* \subseteq \mathbb{R}^3$. A Sommerfeld radiation condition determines the solution behavior far away from any sources. Ω^* can have a boundary Γ^* where problem dependent boundary conditions are imposed like, e. g., PEC or symmetry boundary conditions. In order to be able to compute a finite element approximation to the boundary value problem solution the infinite domain Ω^* is subdivided into three disjoint parts, a Maxwell domain Ω_{Maxwell} , a PML domain Ω_{PML} and the remainder $\Omega_\infty = \Omega^* \setminus \Omega$. The Maxwell and PML domains are chosen

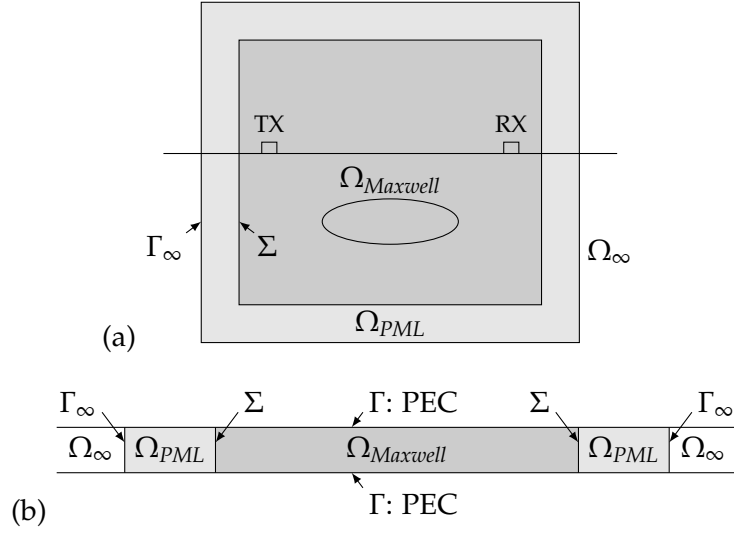


Figure 4.2: Examples of PML applications: (a) a buried object within the earth, (b) a waveguide.

as finite subsets of Ω^* such that their union $\Omega = \Omega_{Maxwell} \cup \Omega_{PML}$ forms the finite computational domain. See Figure 4.2 for two examples.

The boundary of the computational domain Ω can consist of up to two parts. The first one, $\Gamma \subseteq \Gamma^*$, is the restriction of Γ^* to $\bar{\Omega}$. The same boundary conditions apply for the boundary value problems posed on Ω^* and Ω . The second part will be denoted by $\Gamma_\infty = \bar{\Omega} \cap \bar{\Omega}_\infty$. Γ_∞ is an artificial boundary which cuts the finite computational domain out of the infinite domain Ω^* . New boundary conditions have to be introduced on Γ_∞ that replace and approximate the Sommerfeld radiation condition of the original problem. The interior boundary $\Sigma = \bar{\Omega}_{Maxwell} \cap \bar{\Omega}_{PML}$ separates the Maxwell and the PML domain.

It is reasonable to assume that the solution is only needed at a finite and discrete set of points of interest within Ω^* . The Maxwell domain $\Omega_{Maxwell}$ has to be large enough to contain these points of interest as well as all sources and relevant structures that contribute to the wavefield at the points of interest. This condition is easily met for bounded scatterers. Unbounded structures like, e. g., the layered halfspace will have to be cut somewhere and, consequently, introduce diffraction points at the boundary. In this case, a suitable balance has to be found which minimizes the domain size on the one hand and, on the other hand, constrains solution errors introduced by cutting the boundary through reflectors.

The PML domain Ω_{PML} is a buffer which moves away the boundary of the computational domain Γ_∞ from the Maxwell domain and, thus, reduces solution errors caused by the approximate boundary conditions. In addition, Maxwell's equations are modified in Ω_{PML} such that no reflections occur at the Maxwell–PML domain interface Σ and that the solution decays rapidly away from Σ . Consequently, the influence of the boundary condition imposed on Γ_∞ further decreases.

The construction of a PML can be divided into three steps.

1. Define the PML domain $\Omega_{PML} \subset \Omega^*$ which acts as a sponge layer between $\Omega_{Maxwell}$ and Ω_∞ .

4.2 Absorbing boundaries – The perfectly matched layer

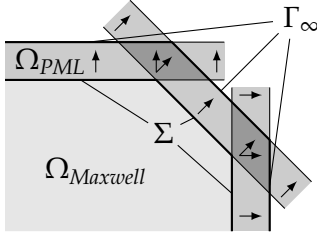


Figure 4.3: The PMLs of adjacent boundary faces of $\Omega_{Maxwell}$ overlap. The arrows indicate the stretching direction.

2. Define a complex coordinate stretching on the PML domain. Maxwell's equations are assumed to be valid for fields defined over these complex coordinates while the constitutive parameters maintain their values from the original problem defined on Ω^* .
3. Rewrite Maxwell's equations from complex to real coordinates. This yields the classical system of Maxwell's equations with modified, anisotropic constitutive parameters within the PML.

These steps will be made more precise in the following.

PML geometry

The derivation of the PML equations will be restricted to the case of a PML in Cartesian coordinates. Since coordinate surfaces in Cartesian coordinates are planar, the Maxwell–PML domain interface Σ is assumed to be composed of planar faces, in particular of polygons. If $\Gamma = \emptyset$, the Maxwell domain is a polyhedron. This assumption has the nice consequence that $\Omega_{Maxwell}$ can be triangulated by standard finite element meshes with rectilinear elements.

Now, the PML domain can be constructed in the following manner: A planar layer of constant thickness L_i is attached to the i -th polygonal subdomain of Σ . The layer not only covers its originating boundary face but extends to the right and left such that layers of adjacent subdomains overlap and create a boundary Γ_∞ parallel to Σ (Figure 4.3). Γ_∞ can be seen as an extrusion of Σ . The distance between Σ and Γ_∞ is at least $\min_i L_i$. A complex coordinate stretching will be applied within the i -th layer in the direction of the i -th face normal vector. Within the overlap regions, the individual stretchings of all layers involved will contribute to the total stretching. The stretching is discussed in the next section.

Complex coordinate stretching

The idea behind the complex coordinate stretching can be illustrated by considering an one-dimensional, scalar wave function $u(x) = u_0 \cos kx$. If the wavenumber k is real, the wave propagates with constant amplitude u_0 along the real x -axis. This corresponds to the black, horizontal line in Figure 4.4 which gives a color encoded picture of $u(x)$ for $x \in \mathbb{C}$. The wave is damped if u is defined on a path $\tilde{x}(x)$ in the upper complex plane like the one shown by the green line in Figure 4.4, $u(\tilde{x}) = u_0 e^{-kx_{\Im}} \cos kx_{\Re}$. The mapping $x \mapsto \tilde{x}$ is assumed to be bijective and called a complex coordinate stretching.

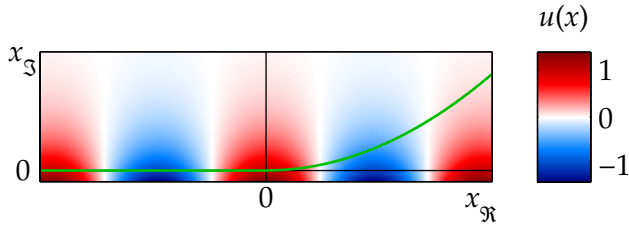


Figure 4.4: Continuation of a harmonic wave $u(x) = \cos kx$, $k, x \in \mathbb{R}$, into the complex plane. The PML extension of Maxwell's equations replaces the path along the real axis by a path within the upper complex plane, marked by the green line.

This motivates the following complex coordinate transform $\mathbb{R}^3 \ni \mathbf{r} \mapsto \tilde{\mathbf{r}} \in \mathbb{C}^3$ for a Cartesian PML:

$$\tilde{\mathbf{r}}(\mathbf{r}) = \mathbf{r} + \sum_{k=1}^l S_k((\mathbf{r} - \mathbf{r}_k)^T \mathbf{n}_k) \mathbf{n}_k \quad (4.16a)$$

where

$$S_k(t) = \int_0^t s_k(\tau) d\tau \quad (4.16b)$$

and $s_k(t)$, $\mathbb{R} \ni t \mapsto s_k(t) \in \mathbb{C}$, is the k -th, frequency dependent, so-called stretching function which is applied along the direction of vector \mathbf{n}_k . If the Maxwell–PML domain interface Σ consists of l planar faces with normal vectors \mathbf{n}_k , l different layers are attached to Σ to form the PML domain and l corresponding stretching functions s_k are defined. For each PML subdomain, however, the summation in (4.16a) only involves those layers which actually overlap within the subdomain. The quantity $t = (\mathbf{r} - \mathbf{r}_k)^T \mathbf{n}_k$ measures the distance from the plane through \mathbf{r}_k . This point and the normal vector \mathbf{n}_k define the plane which is tangent to the k -th polygonal Maxwell–PML domain interface part.

A short calculation shows that the Jacobian of the mapping (4.16a) $\mathbf{J} = \partial \tilde{\mathbf{r}}_i / \partial r_j$ reads

$$\mathbf{J} = \mathbf{I} + \sum_{k=1}^l s_k((\mathbf{r} - \mathbf{r}_k)^T \mathbf{n}_k) \mathbf{n}_k \mathbf{n}_k^T \quad (4.17)$$

where \mathbf{I} denotes the identity matrix.

Throughout this work, all choices of the stretching function $s_k(t)$ will be covered by the definition

$$s_k(t) = a_k t^{m_k} + \frac{i}{\omega + c_k} b_k t^{n_k} \quad (4.18)$$

where $a_k, b_k \in \mathbb{R}$, $c_k \in \mathbb{C}$, $m_k, n_k \in \mathbb{N}$, $0 \leq t \leq L_k$ and L_k is the thickness of the k -th PML. The stretching function is a polynomial of t with bounded coefficients provided that $\omega \neq c_k$. If $m_k, n_k > 0$, $s_k(t)$ vanishes at $t = 0$. Equation (4.18) reduces to some important cases for particular sets of the PML parameters:

- $a_k = 0$, $\omega_k = 0$ is the standard PML stretching (Rappaport, 1995; Fang and Wu, 1995);

4.2 Absorbing boundaries – The perfectly matched layer

- $a_k = 0$, $\omega_k \in i\mathbb{R}$ is the complex frequency shifted (CFS) PML stretching (Kuzuoglu and Mittra, 1996);
- $b_k = 0$ is a physical stretching of the PML cells.

The classical definition of the electric field E as the mapping $\mathbb{R}^3 \ni \mathbf{r} \mapsto E(\mathbf{r}) \in \mathbb{C}^3$ is now extended to a transformed electric field $\mathbb{C}^3 \ni \tilde{\mathbf{r}} \mapsto \tilde{E}(\tilde{\mathbf{r}}) \in \mathbb{C}^3$ and similar for the magnetic field H , the electric flux density D , the magnetic flux density B and the electric current density j . Analogously to E, H, D, B, j which are a solution to Maxwell's equations combined with constitutive equations $\tilde{E}, \tilde{H}, \tilde{D}, \tilde{B}, \tilde{j}$ are to satisfy Maxwell's equations written in the transformed coordinates $\tilde{\mathbf{r}}$,

$$\tilde{\text{curl}} \tilde{E} = i\omega \tilde{B}, \quad (4.19a)$$

$$\tilde{\text{curl}} \tilde{H} = \tilde{j} - i\omega \tilde{D}, \quad (4.19b)$$

$$\tilde{\text{div}} \tilde{B} = 0, \quad (4.19c)$$

$$\tilde{\text{div}}(\tilde{j} - i\omega \tilde{D}) = 0 \quad (4.19d)$$

with constitutive equations

$$\tilde{B} = \tilde{\mu} \tilde{H}, \quad (4.19e)$$

$$\tilde{D} = \tilde{\epsilon} \tilde{E}, \quad (4.19f)$$

$$\tilde{j} = \tilde{\sigma} \tilde{E}. \quad (4.19g)$$

The tilde over the operators curl and div denotes differentiation with respect to the stretched coordinates. For the PML domain, the constitutive parameters are assumed to maintain their values from the original problem defined on Ω^* ,

$$\tilde{\epsilon}(\tilde{\mathbf{r}}) \equiv \epsilon(\mathbf{r}), \quad (4.19h)$$

$$\tilde{\mu}(\tilde{\mathbf{r}}) \equiv \mu(\mathbf{r}), \quad (4.19i)$$

$$\tilde{\sigma}(\tilde{\mathbf{r}}) \equiv \sigma(\mathbf{r}) \quad (4.19j)$$

for $\mathbf{r} \in \Omega_{PML}$ and $\tilde{\mathbf{r}} = \tilde{\mathbf{r}}(\mathbf{r})$. The PML has been designed as a buffer zone where the wave field leaving the Maxwell domain is extinguished. This implies that the PML is source free and does not generate a new wave field which can propagate back into the Maxwell domain. Therefore, all source terms are restricted to the Maxwell domain and have been dropped in equations (4.19a) to (4.19g).

Anisotropic PML equations

Equations (4.19a) to (4.19g) are now rewritten in terms of the real coordinates. To do this, the finite element techniques can be applied which are used for mappings between reference and actual elements. First, note that per definition and by the assumption on $s_i(t)$ the mapping $\mathbf{r} \mapsto \tilde{\mathbf{r}}$ is

continuously differentiable, invertible and surjective. Therefore, Corollary 3.58 of Monk (2003) can be used to rewrite the curl of a vector function Φ with well-defined curl

$$\tilde{\text{curl}} \tilde{\Phi} = \frac{1}{\det J} J^T \text{curl} \Phi \quad \text{if} \quad \tilde{\Phi} = J^{-1} \Phi \quad (4.20a)$$

where J denotes the Jacobian matrix with entries $J_{i,j} = \partial \tilde{r}_i / \partial r_j$. Similarly, Lemma 3.59 gives for another vector field Ψ with well-defined divergence

$$\tilde{\text{div}} \tilde{\Psi} = \frac{1}{\det J} \text{div} \Psi \quad \text{if} \quad \tilde{\Psi} = \frac{1}{\det J} J^T \Psi. \quad (4.20b)$$

While the fields \tilde{E} and \tilde{H} transform according to (4.20a), the flux densities D , B and j transform according to (4.20b). Now, the transform pairs for the constitutive parameters can be derived as follows:

$$\begin{aligned} \tilde{D} &= \tilde{\epsilon} \tilde{E} \\ \frac{1}{\det J} J^T D &= \epsilon J^{-1} E \\ D &= (\det J) J^{-T} \epsilon J^{-1} E \end{aligned}$$

and similarly for μ and σ . If new constitutive parameters are defined by

$$\hat{\epsilon} = (\det J) J^{-T} \epsilon J^{-1}, \quad (4.21a)$$

$$\hat{\mu} = (\det J) J^{-T} \mu J^{-1}, \quad (4.21b)$$

$$\hat{\sigma} = (\det J) J^{-T} \sigma J^{-1} \quad (4.21c)$$

the system of partial differential equations (4.19a) to (4.19d) with constitutive equations (4.19e) to (4.19g) is equivalent to

$$\text{curl} E = i\omega B, \quad (4.22a)$$

$$\text{curl} H = j - i\omega D, \quad (4.22b)$$

$$\text{div} B = 0, \quad (4.22c)$$

$$\text{div}(j - i\omega D) = 0 \quad (4.22d)$$

with constitutive equations

$$B = \hat{\mu} H, \quad (4.22e)$$

$$D = \hat{\epsilon} E, \quad (4.22f)$$

$$j = \hat{\sigma} E. \quad (4.22g)$$

To prove this, straightforward application of the transform pairs (4.20a) and (4.20b) shows that

$$\begin{aligned} \text{curl} E &= i\omega B \\ (\det J) J^{-T} \tilde{\text{curl}} \tilde{E} &= i\omega (\det J) J^{-T} \tilde{B} \\ \tilde{\text{curl}} \tilde{E} &= i\omega \tilde{B} \end{aligned}$$

4.2 Absorbing boundaries – The perfectly matched layer

and similarly for the other curl equation. Furthermore,

$$\begin{aligned}\operatorname{div} \mathbf{B} &= 0 \\ (\det \mathbf{J}) \tilde{\operatorname{div}} \tilde{\mathbf{B}} &= 0 \\ \tilde{\operatorname{div}} \tilde{\mathbf{B}} &= 0\end{aligned}$$

and similarly for the other divergence equations. It has been assumed that $\det \mathbf{J} \neq 0$, i. e., that \mathbf{J} is invertible for all $\mathbf{r} \in \Omega_{PML}$ which follows from the assumption that $\tilde{\mathbf{r}}(\mathbf{r})$ is invertible.

The partial differential equations (4.19a) to (4.19d) and the constitutive equations (4.19e) to (4.19g) can be combined and reduce to the PML equations in complex coordinates $\tilde{\mathbf{r}}(\mathbf{r})$, $\mathbf{r} \in \Omega_{PML}$,

$$\tilde{\operatorname{curl}} \tilde{\mathbf{E}} = i\omega \tilde{\boldsymbol{\mu}} \tilde{\mathbf{H}}, \quad (4.23a)$$

$$\tilde{\operatorname{curl}} \tilde{\mathbf{H}} = (\tilde{\boldsymbol{\sigma}} - i\omega \tilde{\boldsymbol{\varepsilon}}) \tilde{\mathbf{E}}, \quad (4.23b)$$

$$\tilde{\operatorname{div}} \tilde{\boldsymbol{\mu}} \tilde{\mathbf{H}} = 0, \quad (4.23c)$$

$$\tilde{\operatorname{div}}(\tilde{\boldsymbol{\sigma}} - i\omega \tilde{\boldsymbol{\varepsilon}}) \tilde{\mathbf{E}} = 0 \quad (4.23d)$$

where the constitutive parameters are chosen according to equations (4.19h) to (4.19j). Combination of equations (4.22a) to (4.22d) and (4.22e) to (4.22g) produces the equivalent formulation in real coordinates $\mathbf{r} \in \Omega_{PML}$,

$$\operatorname{curl} \mathbf{E} = i\omega \hat{\boldsymbol{\mu}} \mathbf{H}, \quad (4.24a)$$

$$\operatorname{curl} \mathbf{H} = (\hat{\boldsymbol{\sigma}} - i\omega \hat{\boldsymbol{\varepsilon}}) \mathbf{E}, \quad (4.24b)$$

$$\operatorname{div} \hat{\boldsymbol{\mu}} \mathbf{H} = 0, \quad (4.24c)$$

$$\operatorname{div}(\hat{\boldsymbol{\sigma}} - i\omega \hat{\boldsymbol{\varepsilon}}) \mathbf{E} = 0. \quad (4.24d)$$

The constitutive parameters are defined by equations (4.21a) to (4.21c). If a solution $\{\tilde{\mathbf{E}}, \tilde{\mathbf{H}}\}$ of equations (4.23a) to (4.23d) is known, the fields $\{J\tilde{\mathbf{E}}, J\tilde{\mathbf{H}}\}$, defined by the transform pair (4.20a), will satisfy equations (4.24a) to (4.24d).

From this point on, the usual theory for Maxwell's equations applies except for the fact that the real-valued, oftentimes isotropic constitutive parameters are replaced by complex-valued, anisotropic ones. Note that the definitions (4.21a) to (4.21c) preserve symmetry of the constitutive parameter tensors. The PML constitutive parameters $\hat{\boldsymbol{\varepsilon}}$, $\hat{\boldsymbol{\mu}}$, $\hat{\boldsymbol{\sigma}}$ are symmetric tensors if the corresponding Maxwell constitutive parameters $\boldsymbol{\varepsilon}$, $\boldsymbol{\mu}$, $\boldsymbol{\sigma}$ are symmetric tensors.

4.2.2 Properties of a uniaxial PML

The properties of the electromagnetic field within the PML are most easily revealed if a plane wave incident onto the planar interface between the Maxwell domain and its PML extension is examined. Since only one interface is considered there is only one complex stretching function and the PML is therefore called uniaxial. For simplicity only the case of a homogeneous and isotropic medium is

inspected. The Maxwell domain is assumed to cover the halfspace $z < 0$ and the PML domain the halfspace $z > 0$. The complex coordinate transform (4.16) for this particular case simplifies to

$$\tilde{\mathbf{r}}(\mathbf{r}) = \mathbf{r} + S(z) \mathbf{e}_z \quad \text{for } z > 0 \quad (4.25)$$

where the stretching is performed along the direction of the third unit vector \mathbf{e}_z . The Jacobian of $\tilde{\mathbf{r}}(\mathbf{r})$ takes the explicit form

$$\mathbf{J} = \mathbf{I} + s(z) \mathbf{e}_z \mathbf{e}_z^T = \begin{pmatrix} 1 & 0 & 0 \\ 0 & 1 & 0 \\ 0 & 0 & 1 + s(z) \end{pmatrix} \quad (4.26)$$

where $s(z) = S'(z)$. The introduction of function $d(z)$ according to

$$\tilde{z}(z) = z + S(z) = z d(z) \quad (4.27a)$$

for $z > 0$ will be useful in the following. Using definitions (4.16) and (4.18), $d(z)$ can be written as

$$\begin{aligned} d(z) &= 1 + \frac{1}{z} \int_0^z s(t) dt \\ &= 1 + \frac{az^m}{m+1} + \frac{i}{\omega + c} \frac{bz^n}{n+1} \\ &= 1 + \frac{az^m}{m+1} + \frac{c_{\Im}}{(\omega + c_{\Re})^2 + c_{\Im}^2} \frac{bz^n}{n+1} + i \frac{\omega + c_{\Re}}{(\omega + c_{\Re})^2 + c_{\Im}^2} \frac{bz^n}{n+1}. \end{aligned} \quad (4.27b)$$

One dimensional wave propagation

If the plane wave propagates along the z -axis it encounters the Maxwell–PML domain interface at a right angle. Without loss of generality, the electric field is assumed to be polarized parallel to the y -axis and can be expressed by

$$\mathbf{E}(\mathbf{r}) = E(z) \mathbf{e}_y \quad (4.28a)$$

where

$$E(z) = E_0 \begin{cases} \exp \{ikz\}, & z \leq 0, \\ \exp \{ik\tilde{z}(z)\}, & z > 0. \end{cases} \quad (4.28b)$$

The electric field of two instances of a PML is depicted for $z \geq 0$ in panels (a) of Figures 4.5 and 4.6.

The electric field expression can be reinterpreted if a modified wavenumber is introduced,

$$E(z) = E_0 \exp \{i\tilde{k}z\} \quad (4.29a)$$

with

$$\tilde{k} = \tilde{k}(z) = \begin{cases} k, & z \leq 0, \\ k d(z), & z > 0. \end{cases} \quad (4.29b)$$

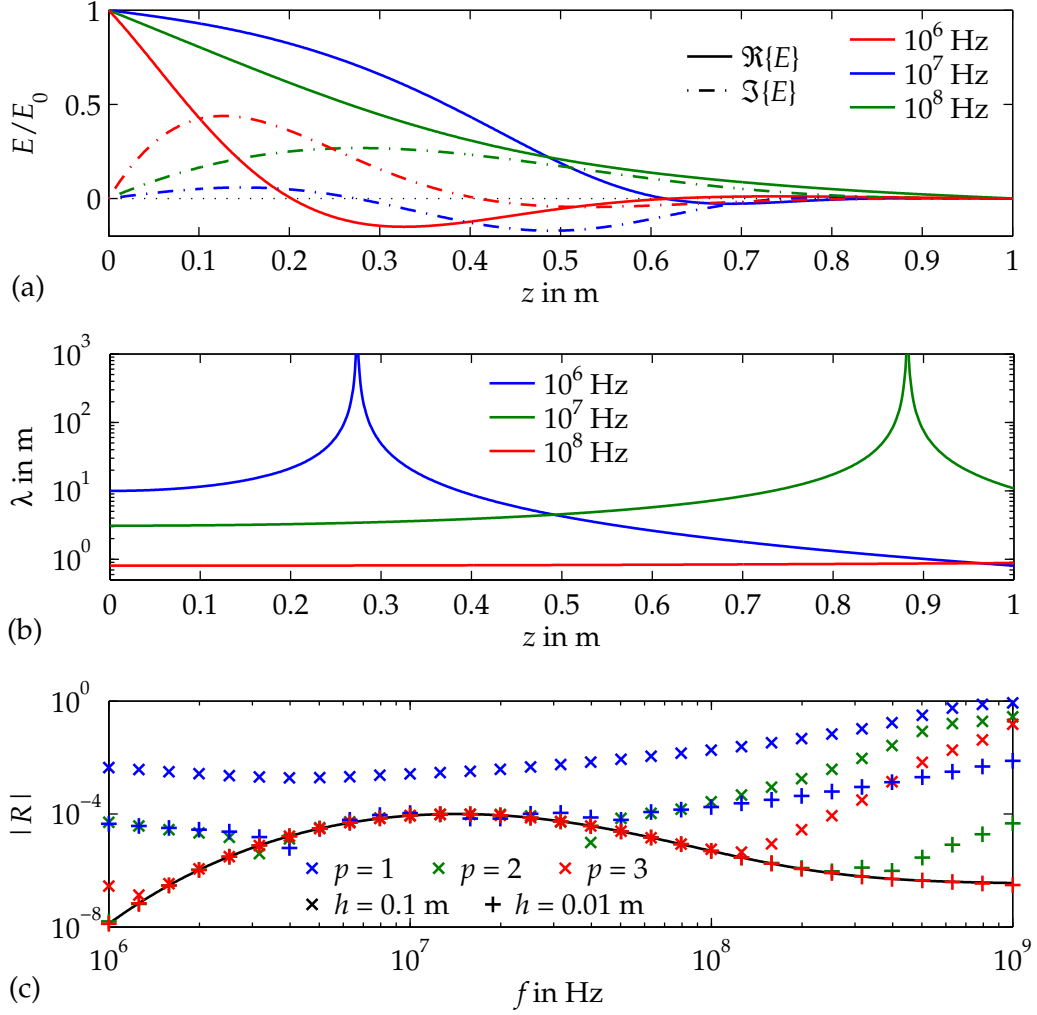


Figure 4.5: Plane wave traversing a uniaxial PML with $\mu_r = 1$, $\epsilon_r = 8$, $\sigma = 0.1$ S/m, $L = 1$ m, $a = 0$, $b = 2.53 \times 10^8$ Hz/m², $c = 0$, $n = 2$.

(a) Electric field $E = E(z) \mathbf{e}_y$. (b) Wavelength $\lambda(z)$. (c) Reflection coefficient $R(f)$ calculated analytically (line) and numerically (symbols) for two grid spacings h and three polynomial degrees p of the finite element basis functions.

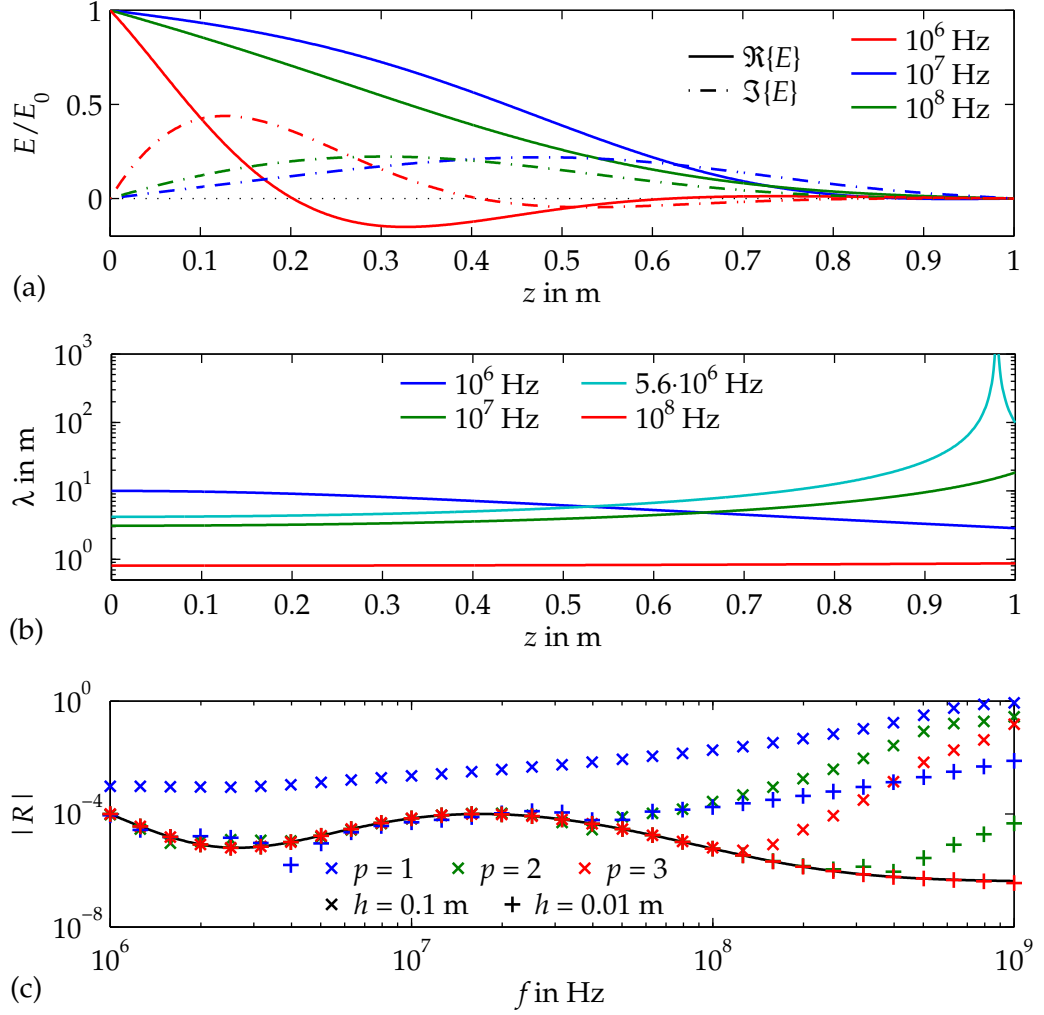


Figure 4.6: Plane wave traversing a uniaxial CFS PML with $\mu_r = 1$, $\varepsilon_r = 8$, $\sigma = 0.1$ S/m, $L = 1$ m, $a = 0$, $b = 2.27 \times 10^8$ Hz/m², $c_{\Re} = 0$, $c_{\Im} = 2\pi \times 2.30 \times 10^6$ Hz, $n = 2$.

(a) Electric field $E = E(z) \mathbf{e}_y$. (b) Wavelength $\lambda(z)$. (c) Reflection coefficient $R(f)$ calculated analytically (line) and numerically (symbols) for two grid spacings h and three polynomial degrees p of the finite element basis functions.

4.2 Absorbing boundaries – The perfectly matched layer

Equation (4.29a) describes a plane wave defined for $z \in \mathbb{R}$ with a non-constant wavenumber $\tilde{k}(z)$. The imaginary part of \tilde{k} ,

$$\tilde{k}_{\Im} = k_{\Im} + \frac{az^m}{m+1}k_{\Im} + \frac{bz^n}{n+1} \frac{c_{\Im}k_{\Im} + (\omega + c_{\Re})k_{\Re}}{(\omega + c_{\Re})^2 + c_{\Im}^2} \quad \text{for } z > 0, \quad (4.30a)$$

determines the damping of the wave. If $\tilde{k}_{\Im} > 0$, the wave is exponentially damped. The first summand k_{\Im} is the normal damping coefficient which is present in all conductive media. The other two terms are introduced by the PML extension and add to the normal damping if $a \geq 0$ or $b \geq 0$ and $c_{\Im}k_{\Im} + (\omega + c_{\Re})k_{\Re} \geq 0$. Note that $\tilde{k}_{\Im} = k_{\Im}$ at $z = 0$ and the PML damping increases monotonically as a function of z if $m, n > 0$. The real part of \tilde{k} ,

$$\tilde{k}_{\Re} = k_{\Re} + \frac{az^m}{m+1}k_{\Re} + \frac{bz^n}{n+1} \frac{c_{\Im}k_{\Re} - (\omega + c_{\Re})k_{\Im}}{(\omega + c_{\Re})^2 + c_{\Im}^2} \quad \text{for } z > 0, \quad (4.30b)$$

determines wave propagation which is more frequently described by, e. g., phase velocity $v = \omega / \tilde{k}_{\Re}$ or wavelength $\lambda = 2\pi / \tilde{k}_{\Re}$. The general form (4.30b) includes some important special cases which deserve a closer examination. In order to ensure exponential damping, $b > 0$ and $c_{\Im} \geq 0$ is assumed throughout the following.

Standard PML: $a = 0$ and $c = 0$ reduce \tilde{k}_{\Re} to

$$\tilde{k}_{\Re} = k_{\Re} - \frac{bz^n}{n+1} \frac{k_{\Im}}{\omega} \quad \text{for } z > 0. \quad (4.31)$$

For a dielectric, $k_{\Im} = 0$ and the propagation constant is the same within the Maxwell and the PML domain. Within a conductive medium, \tilde{k}_{\Re} is a decreasing function of z which assumes negative values for $z > z_c$ where

$$z_c = \sqrt[n]{\frac{n+1}{b} \frac{\omega}{k_{\Im}/k_{\Re}}}. \quad (4.32)$$

Consequently, the phase velocity and the wavenumber are increasing functions of z as long as $z < z_c$. They have a pole at $z = z_c$. An infinite phase velocity is of course a non-physical phenomenon which is introduced by the non-physical PML extension of Maxwell's equations. For $z > z_c$ the phase velocity and wavenumber are negative. Their absolute values are monotonically decreasing functions of z which decay to zero as z approaches infinity. This can be seen in panel (b) of Figure 4.5 for frequencies 10^6 Hz and 10^7 Hz. Since the poles of the wavelength are caused by a root of the complex wavenumber real part, they coincide with a zero crossing of the electric field imaginary part shown in panel (a) above. The field itself does not look suspicious. The dubious behavior of phase velocity and wavelength can be relaxed for the complex frequency shifted (CFS) PML. This modification has been introduced by Kuzuoglu and Mittra (1996) in order to obtain anisotropic constitutive parameters which satisfy the Kramers-Kronig relations and to render the PML extension of Maxwell's equations causal. The standard PML is not causal.

CFS PML: $a = 0$ and $c_{\Re} = 0$ reduce \tilde{k}_{\Re} to

$$\tilde{k}_{\Re} = k_{\Re} + \frac{bz^n}{n+1} \frac{c_{\Im}k_{\Re} - \omega k_{\Im}}{\omega^2 + c_{\Im}^2} \quad \text{for } z > 0. \quad (4.33)$$

If, on the one hand, $c_{\Im} > \omega k_{\Im}/k_{\Re}$, wavelength and phase velocity are decreasing functions of z . This holds especially for dielectric media if $c_{\Im} > 0$. A smaller wavelength will have to be taken care of by a finer mesh within the PML domain if the boundary value problem is solved numerically. If, on the other hand, $0 < c_{\Im} < \omega k_{\Im}/k_{\Re}$, wavelength and phase velocity are increasing functions of z as long as $z < z_c$ where

$$z_c = \sqrt[n]{\frac{n+1}{b} \frac{\omega^2 + c_{\Im}^2}{\omega k_{\Im}/k_{\Re} - c_{\Im}}}. \quad (4.34)$$

Compared to the standard PML which is depicted in Figure 4.5, the range of critical frequencies where the wavelength has a pole can be reduced considerably by introducing the imaginary frequency shift. This fact can be seen in panel (b) of Figure 4.6.

For monofrequent problems it is possible to render the propagation constant the same for both the Maxwell and the PML domain by choosing $c_{\Im} = \omega k_{\Im}/k_{\Re}$. In contrast to the standard PML this property can be achieved also for conductive media but only at a single frequency.

Reflection coefficient for orthogonal incidence

So far, only the outgoing wave has been considered. If the PML domain is terminated at $z = L$, the boundary condition imposed there gives rise to a reflection and an incoming wave. In the simplest case, the PML is terminated by a homogeneous Dirichlet boundary condition for the tangential electric field, i. e., the computational domain is enclosed by a PEC surface. Then the electric field is given by

$$E(z) = E_0 (\exp \{i\tilde{k}z\} - R \exp \{-i\tilde{k}z\}) \quad \text{for } z \leq L \quad (4.35a)$$

where

$$R = \exp \{2i\tilde{k}L\} \quad (4.35b)$$

is the reflection coefficient of the truncated PML. At the interface, $E(0) = E_0(1 - R)$. The magnitude of R is determined by \tilde{k}_{\Im} ,

$$\begin{aligned} |R| &= \exp \{-2\tilde{k}_{\Im}L\} \\ &= \exp \{-2k_{\Im}L\} \exp \left\{ -2 \left(\frac{aL^{m+1}}{m+1} k_{\Im} + \frac{bL^{n+1}}{n+1} \frac{c_{\Im}k_{\Im} + (\omega + c_{\Re})k_{\Re}}{(\omega + c_{\Re})^2 + c_{\Im}^2} \right) \right\}. \end{aligned} \quad (4.36)$$

The first exponential term is the natural damping of the Maxwell medium which depends on the electric conductivity. The second exponential term describes the influence of the PML extension, the complex coordinate stretching.

4.2 Absorbing boundaries – The perfectly matched layer

The frequency dependency of R is depicted in panel (c) of Figures 4.5 and 4.6. Its analytically computed values according to equation (4.37) are shown as a solid line. Both instances of the PML have been designed such that $R(f) \leq 10^{-4}$ for $10^6 \text{ Hz} \leq f \leq 10^9 \text{ Hz}$. In order to assess the accuracy of the finite element implementation the problem has been solved numerically with two grid spacings $h = 0.1 \text{ m}$ and 0.01 m and a piecewise polynomial approximation of E of degrees $p = 1, 2$ and 3 . The numerical results are shown in the figures as symbols. The reflection coefficient is extracted from the total field numerical solution by computing $R = 1 - E(0)/E_0$. Note that the finest resolution $h = 0.01 \text{ m}$ with $p = 3$ involves 300 degrees of freedom for E_y within the PML if only the discretization with respect to z is considered. However, only this very fine mesh reproduces the analytical reflection coefficient sufficiently well. There are significant differences between the analytically and numerically computed reflection coefficients for the coarser approximations at least at the low and high frequencies. This can partly be explained by the fact that the numerical approximation has to recover the field with an accuracy of R . Consequently, larger values of R will be recovered better than lower values which occur at high and for the standard PML also at low frequencies. The higher frequency part also suffers from the smaller wavelengths which are poorly sampled by the coarser mesh and lower polynomial degrees.

In practice, the PML will not be sampled that densely. The additional number of degrees of freedom spent for the PML domain solution should not exceed a reasonable factor of the number of degrees of freedom for the solution of interest in the Maxwell domain. Even the coarse grid spacing $h = 0.1 \text{ m}$, which subdivides the PML into 10 elements in z -direction, combined with a piecewise linear approximation of the electric field appears to cut the edge of this assumption. As a conclusion, the theoretical reflection coefficient (4.37) can be used to get an order of magnitude estimation for the actual effect of the truncated PML but will rarely be realized in practice. The dominating influence is supposed to be the approximation error of the finite element solution.

Polynomial stretching

The spatial variation of the stretching function (4.18) is a polynomial of the form bz^n . Interestingly enough, the reflection coefficient of the truncated PML (4.36) only depends on the integral value $\int_0^L bz^n dz = bL^{n+1}/(n+1)$. In theory, a PML can be constructed using polynomials of arbitrary degree such that the same reflection coefficient is obtained. Discretization errors will make a difference in practice if the solution varies too rapidly with a polynomial stretching of a high degree.

In order to achieve a smooth transition of the constitutive parameters between the Maxwell and the PML domain, $n > 0$ has to be assumed. If $n = 0$ the PML stretching function is piecewise constant and renders the Jacobian (4.17) of the coordinate transform (4.16) discontinuous and, according to their definition (4.21), also the anisotropic constitutive parameters. The PML thus created will suffer from physical reflections at the interfaces where the constitutive parameters are discontinuous. This effect is demonstrated in Figure 4.7.

The figure depicts three instances of the polynomial stretching bz^n with $n = 1, 2, 3$ in panel (a).

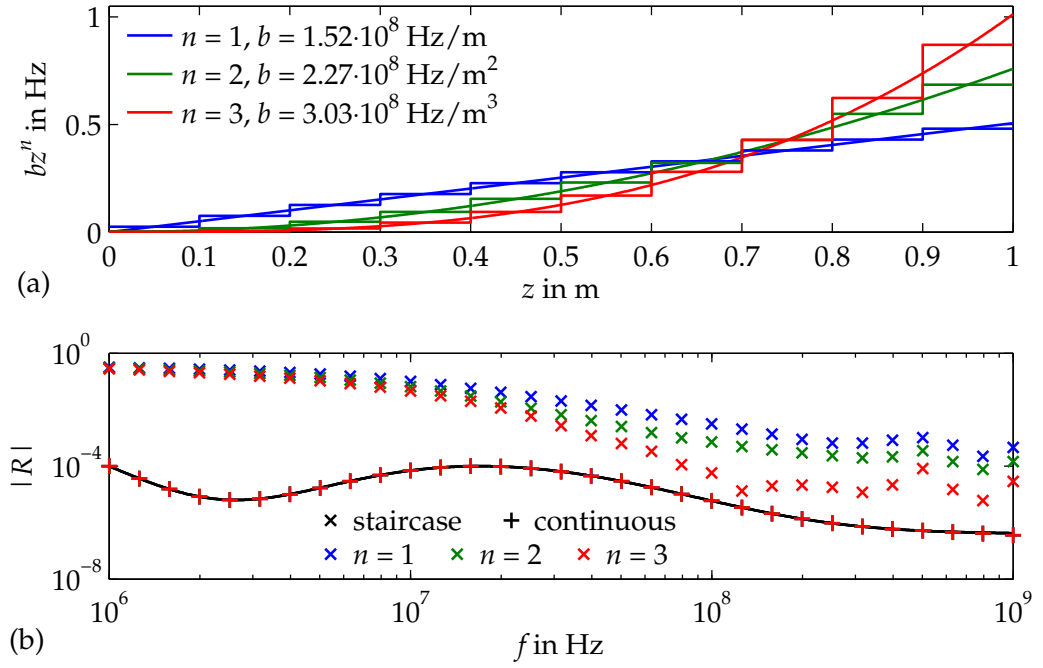


Figure 4.7: (a) Spatial component bz^n of the stretching function $s(z)$ for $n = 1, 2, 3$ and its staircase approximation. (b) Corresponding reflection coefficient of a CFS PML computed numerically with grid spacing $h = 0.01$ m and a cubic finite element basis ($p = 3$). The remaining CFS PML parameters are $L = 1$ m, $a = 0$, $c_{\Re} = 0$, $c_{\Im} = 2\pi \times 2.30 \times 10^6$ Hz, $\mu_r = 1$, $\epsilon_r = 8$, $\sigma = 0.1$ S/m.

They have been chosen such that they yield the same reflection coefficient. Panel (b) shows that the analytically and numerically computed reflection coefficients agree very well for the spatial discretization of $h = 0.01$ m and the piecewise cubic finite element basis used. If the continuous stretching function is approximated by a piecewise constant, ‘staircase’ function as shown in panel (a) the numerically determined reflection coefficient shown in panel (b) clearly deviates from the continuous case, as predicted. The extremely fine discretization practically excludes numerical errors and identifies the physical reflections at the material discontinuities as the origin of the poor performance of the staircase PML.

The staircase PML is of some practical relevance, though. It is usually used in finite difference approximations of Maxwell’s equations where constitutive parameters are assumed to be piecewise constant. This assumption is relaxed for the finite element approximation where constitutive parameters enter the variational integrals. Their spatial variation is accommodated by using numerical quadrature when the integrals are evaluated. Concluding, PMLs for the finite element method are better constructed using continuous stretching functions ($n > 0$).

Anisotropy

The isotropic constitutive parameters of the Maxwell domain are transformed to anisotropic parameters within the PML domain. According to equations (4.21) and (4.26),

$$\begin{aligned}\hat{\eta} &= \eta (\det J) J^{-T} J^{-1} \\ &= \eta \begin{pmatrix} 1 + s(z) & 0 & 0 \\ 0 & 1 + s(z) & 0 \\ 0 & 0 & \frac{1}{1+s(z)} \end{pmatrix}\end{aligned}\tag{4.37}$$

where η is used as a placeholder for ε , μ and σ . This particular form of an anisotropic medium has been considered in section 2.5 of Chapter 2. Setting $M = (\det J) J^{-T} J^{-1}$ reveals that the uniaxial PML extension of an isotropic Maxwell medium does not distinguish between two polarizations with distinct wavenumbers as it is the case with a generally anisotropic medium. The two wavenumbers are identical but their values very well depend on the propagation direction.

In any boundary value problem discussed so far the constitutive parameter tensors have been assumed to possess eigenvalues bounded from below and above. This guarantees that the integrals defining the finite element matrix entries are bounded as well. In Chapters 2 and 3 the electric conductivity had been assumed to be non-zero in order to have a non-vanishing contribution of the integral $\int_{\Omega} \text{grad } \bar{\phi} \cdot (\sigma - i\omega\varepsilon) E d^3r$ also in the static limit $\omega \rightarrow 0$. Following this concept, the eigenvalues of the anisotropic PML constitutive parameters should be bounded for low frequencies as well. As PMLs are usually applied to models describing wave propagation the notion of ‘low frequency’ differs somewhat from the low frequencies considered in Chapter 3. Nevertheless, the idea of bounded constitutive parameters might prove to be beneficial for numerical accuracy as well.

Returning to the uniaxial PML, the critical eigenvalue of $\hat{\eta}$ according to (4.37) is

$$\begin{aligned} \frac{1}{|1+s(z)|} &= \frac{1}{\left|1 + az^m + \frac{i}{\omega+c}bz^n\right|} \\ &= \frac{1}{\sqrt{\left(1 + az^m + \frac{c_{\Im}}{(\omega+c_{\Re})^2+c_{\Im}^2}bz^n\right)^2 + \left(\frac{\omega+c_{\Re}}{(\omega+c_{\Re})^2+c_{\Im}^2}bz^n\right)^2}} \end{aligned} \quad (4.38a)$$

For the standard PML, $a = 0$, $b > 0$ and $c = 0$,

$$\frac{1}{|1+s(z)|} = \frac{1}{\sqrt{1 + \left(\frac{bz^n}{\omega}\right)^2}} = \frac{\omega}{\sqrt{\omega^2 + (bz^n)^2}} \xrightarrow{\omega \rightarrow 0} 0. \quad (4.38b)$$

Introduction of an imaginary frequency shift c_{\Im} with the CFS PML, $a = 0$, $b > 0$, $c_{\Re} = 0$ and $c_{\Im} > 0$, establishes a non-zero lower bound,

$$\frac{1}{|1+s(z)|} = \frac{1}{\sqrt{\left(1 + \frac{c_{\Im}}{\omega^2+c_{\Im}^2}bz^n\right)^2 + \left(\frac{\omega}{\omega^2+c_{\Im}^2}bz^n\right)^2}} \xrightarrow{\omega \rightarrow 0} \left| \frac{c_{\Im}}{c_{\Im} + bz^n} \right| \quad (4.38c)$$

for a PML domain of finite extension, $z < \infty$.

From a numerical point of view the anisotropy factor ρ of the constitutive parameter tensors is of interest. It is defined as the ratio of the largest and smallest eigenvalue of $\hat{\eta}$ and takes the form

$$\rho = \frac{1}{|1+s(z)|^2} \quad (4.39)$$

if $a > 0$ in equation (4.18). Similarly to a model with highly discontinuous constitutive parameters a highly anisotropic medium causes large variations of the numerical values present in the finite element matrices and deteriorates the system matrix condition. This has been shown in section 3.5.5 of Chapter 3 for the case of a strong contrast in the electric conductivity.

Figure 4.8 illustrates this effect for the case of the anisotropic PML medium. The standard PML of Figure 4.5 and the CFS PML of Figure 4.6 are compared. Panel (a) shows the corresponding anisotropy factors which differ markedly only at lower frequencies. The finite element system matrix condition number has been computed for a piecewise polynomial approximation of the electric field of degrees $p = 1, 2$ and 3. Differing matrix condition numbers for the two PML instances can only be observed visually at low frequencies, in agreement with the anisotropy factor. The inferior matrix condition number of the standard PML is not significant for the frequency range considered.

Reflection coefficient for oblique incidence

A plane wave propagating within the x - z plane at angle φ measured from the positive z -axis (Figure 4.9) is described by the expression $\exp\{ik(x \sin \varphi + z \cos \varphi)\}$. The one-dimensional model

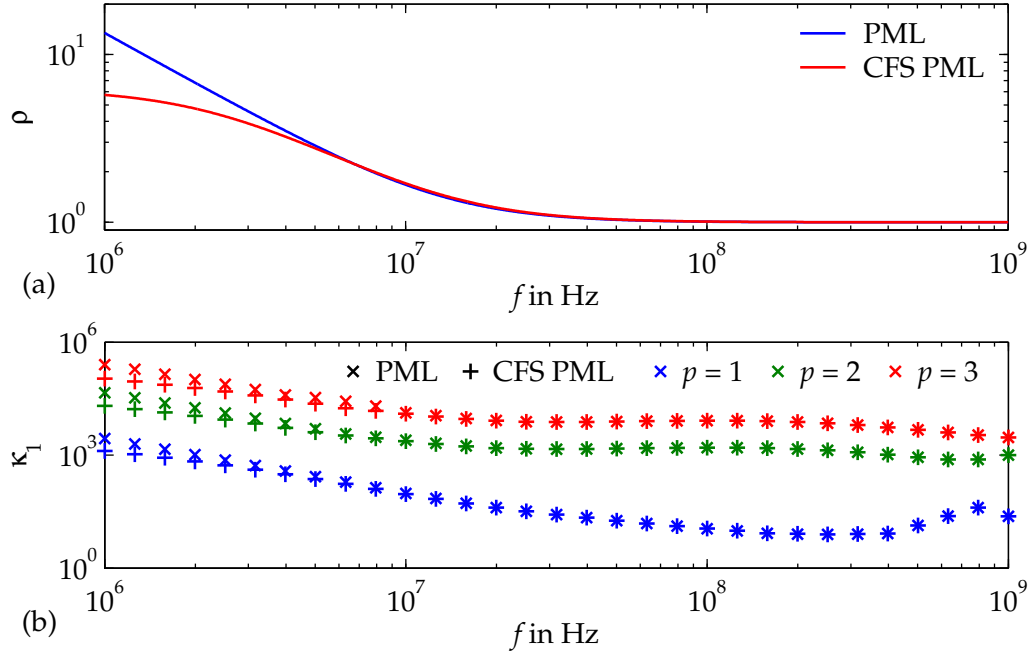


Figure 4.8: (a) Anisotropy factor $\rho(f)$ of the PML of Figure 4.5 and of the CFS PML of Figure 4.6. (b) 1-norm condition number of the system matrix for grid spacing $h = 0.1$ m and three polynomial degrees p of the finite element basis functions.

structure permits the decomposition of the wavefield into two independent modes. If the definition of the PML electric and magnetic fields, wavenumber and stretching function are extended to the Maxwell domain by

$$\tilde{\mathbf{E}}(\mathbf{r}) = \begin{cases} \mathbf{E}(\mathbf{r}), & z \leq 0, \\ \tilde{\mathbf{E}}(\tilde{\mathbf{r}}(\mathbf{r})), & 0 < z \leq L, \end{cases} \quad (4.40a)$$

$$\tilde{\mathbf{H}}(\mathbf{r}) = \begin{cases} \mathbf{H}(\mathbf{r}), & z \leq 0, \\ \tilde{\mathbf{H}}(\tilde{\mathbf{r}}(\mathbf{r})), & 0 < z \leq L, \end{cases} \quad (4.40b)$$

$$\tilde{k}(z) = \begin{cases} k, & z \leq 0, \\ k d(z), & 0 < z \leq L, \text{ and} \end{cases} \quad (4.40c)$$

$$\tilde{s}(z) = \begin{cases} 0, & z \leq 0, \\ s(z), & 0 < z \leq L, \end{cases} \quad (4.40d)$$

the notation of the electromagnetic fields can be compacted. The extended PML electric and magnetic fields satisfy the usual Maxwell's equation within the Maxwell domain and Maxwell's equations in stretched coordinates within the PML domain. Therefore, the electric field in real coordinates is obtained for the PML domain by the transformation (4.20a), $\mathbf{E} = \mathbf{J}\tilde{\mathbf{E}}$. The Jacobian of

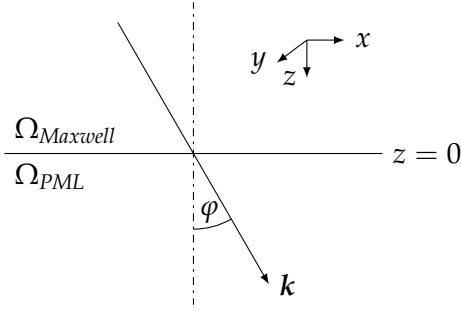


Figure 4.9: Propagation direction of a plane wave travelling within the x - z -plane and incident on the Maxwell–PML domain interface at angle φ .

the uniaxial PML (4.26) only affects the z -components which are related by $E_z = (1 + s(z))\tilde{E}_z$. The same applies to the magnetic field.

Now, the electromagnetic fields in real coordinates are sought according to the following approach:

Transverse electric (TE) mode

$$H_x(x, z) = -H_0 e^{ikx \sin \varphi} \left(e^{i\tilde{k}(z)z \cos \varphi} + R e^{-i\tilde{k}(z)z \cos \varphi} \right) \cos \varphi \quad (4.41a)$$

$$E_y(x, z) = E_0 e^{ikx \sin \varphi} \left(e^{i\tilde{k}(z)z \cos \varphi} - R e^{-i\tilde{k}(z)z \cos \varphi} \right) \quad (4.41b)$$

$$H_z(x, z) = H_0 (1 + \tilde{s}(z)) e^{ikx \sin \varphi} \left(e^{i\tilde{k}(z)z \cos \varphi} + R e^{-i\tilde{k}(z)z \cos \varphi} \right) \sin \varphi \quad (4.41c)$$

Transverse magnetic (TM) mode

$$E_x(x, z) = E_0 e^{ikx \sin \varphi} \left(e^{i\tilde{k}(z)z \cos \varphi} - R e^{-i\tilde{k}(z)z \cos \varphi} \right) \cos \varphi \quad (4.42a)$$

$$H_y(x, z) = H_0 e^{ikx \sin \varphi} \left(e^{i\tilde{k}(z)z \cos \varphi} + R e^{-i\tilde{k}(z)z \cos \varphi} \right) \quad (4.42b)$$

$$E_z(x, z) = -E_0 (1 + \tilde{s}(z)) e^{ikx \sin \varphi} \left(e^{i\tilde{k}(z)z \cos \varphi} + R e^{-i\tilde{k}(z)z \cos \varphi} \right) \sin \varphi \quad (4.42c)$$

The fields can easily be shown to satisfy Maxwell's equations in real coordinates if the constants E_0 and H_0 are related by $H_0 = Y E_0$ where Y is the complex wave admittance. E_0 and H_0 are independent constants for each mode. Note that \tilde{k} only appears in the exponential in terms of z and not in the exponential in terms of x because \tilde{k} absorbs the PML function $d(z)$ which is only present in the stretched coordinate $\tilde{z}(z)$.

The reflection coefficient R needs to be determined by the boundary condition which terminates the PML domain at $z = L$.

PEC boundary condition: If the tangential electric field is made to vanish on the boundary,

$$\mathbf{n} \times \mathbf{E} = \mathbf{0} \quad (4.43a)$$

at $z = L$ where $\mathbf{n} = (0, 0, 1)^T$, the reflection coefficient is given by

$$R = e^{2i\tilde{k}(L)L \cos \varphi} = R_0^{\cos \varphi} \quad (4.43b)$$

4.2 Absorbing boundaries – The perfectly matched layer

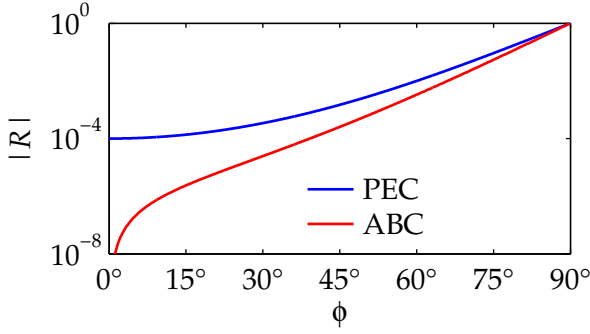


Figure 4.10: Reflection coefficient R of a PML, which is terminated by a Dirichlet boundary condition (PEC) or by an absorbing boundary condition (ABC), as a function of the angle of incidence ϕ .

for both modes. It is related to the reflection coefficient with orthogonal incidence $R_0 = R(\phi = 0)$ by the power of $\cos \phi$.

ABC boundary condition: If a first order absorbing boundary condition is applied (Jin and Chew, 1996),

$$\mathbf{n} \times \mathbf{H} + \mathbf{n} \times \left(\tilde{\mathbf{k}} (\omega \hat{\mu})^{-1} \mathbf{n} \times \mathbf{E} \right) = \mathbf{0} \quad (4.44a)$$

at $z = L$ where $\mathbf{n} = (0, 0, 1)^T$, the reflection coefficient is given by

$$R = \frac{1 - \cos \phi}{1 + \cos \phi} e^{2i\tilde{\mathbf{k}}(L)L \cos \phi} = \frac{1 - \cos \phi}{1 + \cos \phi} R_0^{\cos \phi} \quad (4.44b)$$

for both modes. Of course, $R = 0$ for $\phi = 0$ because a plane wave incident at a right angle onto the boundary satisfies the absorbing boundary condition of zeroth order exactly. Here, R_0 also denotes the reflection coefficient with orthogonal incidence of a PEC boundary condition truncated PML.

The angular dependency of the reflection coefficients R according to equations (4.43b) and (4.44b) is depicted in Figure 4.10 for $R_0 = 10^{-4}$. Not surprisingly, the absorbing boundary condition outperforms the PEC boundary condition and produces unwanted reflections of lower magnitude for all angles of incidence.

4.2.3 The PML in three dimensions – An example

In order to demonstrate the use of the PML technique in three dimensions a simple test example has been devised as follows. The computational domain is the cube $\Omega = [0, 0.7]^3 \text{ m}^3$ whose intersection with the sphere $\mathcal{S} = \{\mathbf{r} : |\mathbf{r}| \leq 0.1 \text{ m}\}$ of radius 0.1 m and placed at the origin has been removed (Figure 4.11(a)). The electric field of a vertical electric dipole (VED) placed at the origin is to be computed within the Maxwell domain $\Omega_{\text{Maxwell}} = [0, 0.5]^3 \text{ m}^3 \setminus \mathcal{S}$. The electric dipole field is coupled into the computational domain by prescribing the tangential electric field on the spherical surface $\partial\mathcal{S}$. This construction avoids the source singularity at the origin. For symmetry reasons, the tangential components of the magnetic field are made to vanish on the planar faces $x, y = 0$ by imposing a homogeneous Neumann boundary condition in terms of the electric field. Similarly,

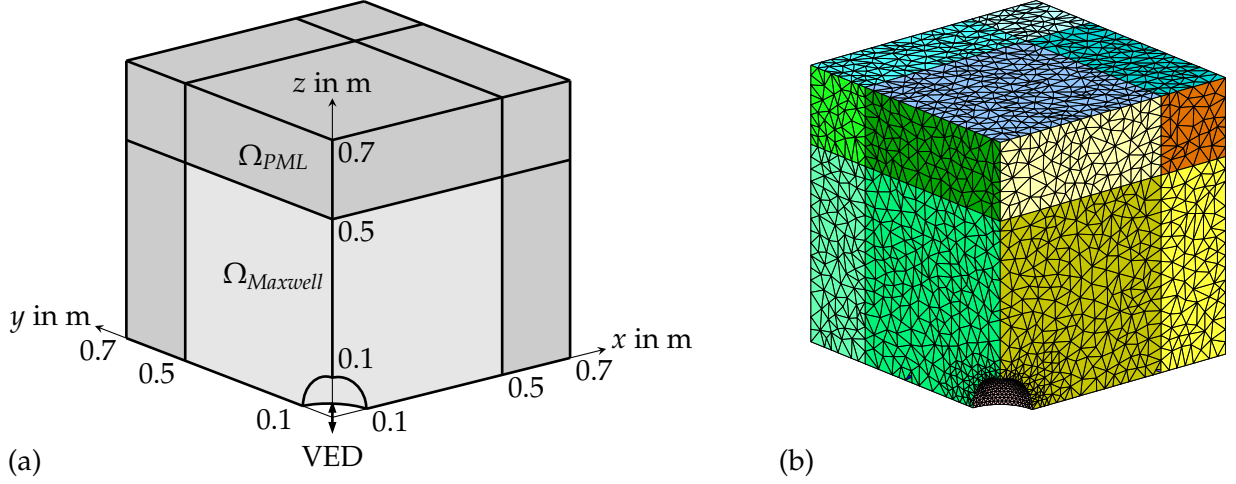


Figure 4.11: Geometry of the 3-D PML test model (a) and its boundary mesh (b).

a homogeneous Dirichlet boundary condition is imposed on the plane $z = 0$ which requires that the tangential electric field components vanish. The remaining boundary part Γ_∞ at $x, y, z = 0.7$ m is subject either to a homogeneous Dirichlet, i. e., PEC boundary condition or to a mixed, i. e., absorbing boundary condition of the first order.

The PML domain $\Omega_{PML} = \Omega \setminus \Omega_{Maxwell}$ serves as a buffer zone which reduces the influence of the approximate nature of the boundary conditions on Γ_∞ . The volume ratio between $\Omega_{Maxwell}$ and Ω_{PML} is 1 : 1.75. The computational domain is triangulated by a tetrahedral mesh which consists of 48 658 elements (Figure 4.11(b)). They split into 19 174 elements for $\Omega_{Maxwell}$ and 29 484 elements for Ω_{PML} (ratio 1 : 1.54). A piecewise quadratic approximation of the electric field results in a total number of 320 810 degrees of freedom for the E -field formulation.

For comparison the electric field has been computed for a homogeneous medium covering both $\Omega_{Maxwell}$ and Ω_{PML} . This case can be seen as the special choice $s_k(t) \equiv 0$ for all uniaxial PML stretching functions within Ω_{PML} . Panels (a) and (b) of Figure 4.12 show the relative solution error for constitutive parameters $\mu_r = 1$, $\epsilon_r = 8$, $\sigma = 0.1$ S/m and frequency $f = 10^8$ Hz. These values result in a wavelength of $\lambda = 0.8$ m. Therefore, the boundary Γ_∞ is placed in the near-field of the dipole. The relative errors have been computed according to equations (3.23a) and (3.23b) of Chapter 3 for each element K , i. e., the norm is evaluated elementwise, $\|u\| = \int_K u d^3r$.

Comparison of panels (a) and (b) clearly reveals that the absorbing boundary condition approximates the field behavior at the boundary far better than the PEC boundary condition. Panels (c) and (d) show the corresponding relative solution errors which have been computed for a PML stretching function (4.18) with parameters $a = 0$, $b = 3.9 \times 10^9$ Hz/m, $c_{\mathfrak{R}} = 0$, $c_{\mathfrak{I}} = 2\pi \times 4.8 \times 10^6$ Hz and $n = 1$. The theoretical reflection coefficient of a PEC boundary condition terminated PML of thickness $L = 0.2$ m for orthogonal incidence is, according to equation (4.36), $|R_0| = 1.8 \times 10^{-2}$. This value suffices to improve the solution accuracy markedly within the complete Maxwell domain as can be seen by comparison of panels (a) and (c) as well as (b) and (d). Similarly to the

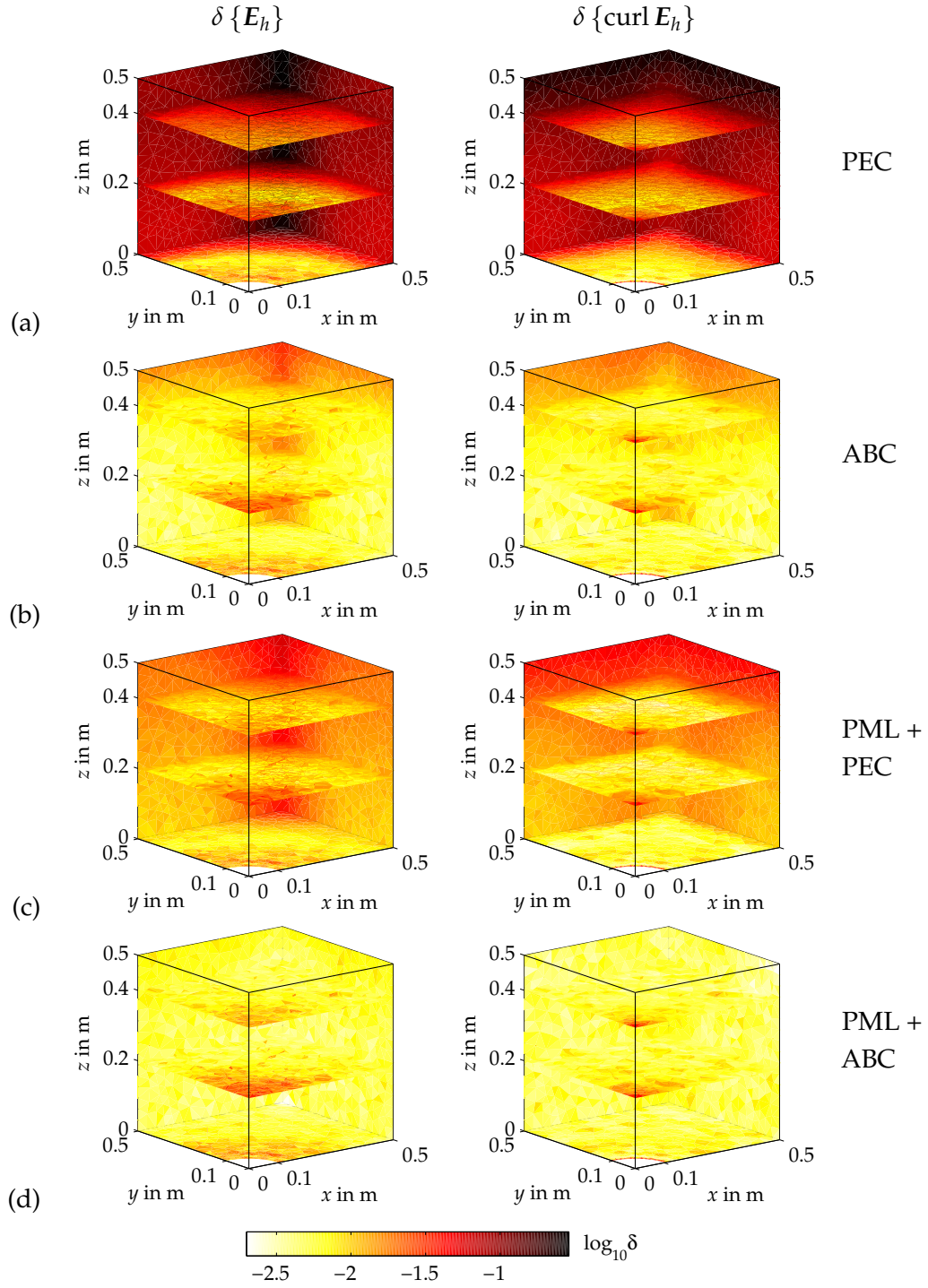


Figure 4.12: Relative L_2 -norm error δ of the electrical field E and its curl calculated elementwise. (a), (b): Ω_{PML} and $\Omega_{Maxwell}$ have identical constitutive parameters. (c), (d): Complex coordinate stretching applied in Ω_{PML} . (a), (c): PEC boundary condition on Γ_∞ . (b), (d): Absorbing boundary condition on Γ_∞ .

result of the trivial PML stretching function the ABC terminated PML performs better than the PEC terminated PML. While in case (b) the errors are higher near the edges where the planes $x, y, z = 0.5$ m intersect, the PML case (d) reduces the error to about the same level of about 1% across all planes $x, y, z = 0.5$ m.

This observation agrees well with the integral expansion of the VED electric field in terms of plane waves propagating in all directions (Chew, 1995). Within the x - y plane at $z = 0$ the electric field can be expressed at the first approximation by a plane wave travelling in the radial direction. The ABC accounts best for this field behavior along the x - and y -coordinate axes where the propagation direction is parallel to the boundary normal vector. At $x, y = 0.7$ m the ABC of the first order gives rise to a reflected field since the outer normal vectors on the boundary are $(1, 0, 0)$ and $(0, 1, 0)$ but the propagation direction is $(1/\sqrt{2}, 1/\sqrt{2}, 0)$. The electric field has a non-negligible component normal to the boundary and is therefore poorly approximated by the ABC.

For $z > 0$, especially at the upper boundary part $z = 0.7$ m, the plane wave expansion contains significant contributions from non-radial propagation directions. Figure 4.12(b) shows that here the ABC introduces errors. The PML significantly improves the solution quality also within this part of the Maxwell domain even though the PML reflection coefficient is predicted by equation (4.44b) to approach unity for slanting angles of incidence.

Comparison of the two columns in Figure 4.12 discloses that the relative error of the electric field and the relative error of its curl assume about the same level. They follow a similar behavior for all the four combinations of PML and boundary condition settings.

As a final note, the elevated relative error along the z -axis is explained by approximation errors of the vertical electric field component which dominates at $x = y = 0$. Here, the solution is very sensitive with respect to projection errors introduced by the Dirichlet boundary condition on $\partial\mathcal{S}$. The source field is coupled into the computational domain by prescribing the tangential electric field on the surface $\partial\mathcal{S}$ of the spherical exclusion while the dominating field component at $x = y = 0$, $z = 0.1$ m is normal to the boundary.

Chapter 5

Application – Marine controlled source electromagnetics

The software suite presented in Chapter 3 has been designed as versatile as possible in order to cover a broad range of geophysical applications. Here, only one application, marine controlled source electromagnetics (CSEM), will be considered and illustrated by two models. Marine CSEM has recently gained considerable attention as a method which is potentially able to detect and quantify marine hydrocarbon deposits (Constable and Weiss, 2006; Weiss and Constable, 2006). Even though the data acquisition technique has reached a satisfactory level of quality data interpretation tools are still under development, in particular with regard to sophisticated 3-D modelling and inversion software. The finite volume code FDM3D by C. Weiss (Weiss and Constable, 2006) is one of the simulation tools available. However, it is limited to rectilinear tensor product grids and a first order finite difference approximation of the spatial derivatives. The first example of this chapter will compare simulation results computed for the canonical disk model (Weiss and Constable, 2006) with FDM3D and with the finite element software of this work. The geometric flexibility of the finite element software is demonstrated in a second example by a model involving seafloor topography which is compared to a model with a flat seafloor.

Along with the geophysical application this chapter provides examples for the scattered field approach and the adaptive mesh refinement using a local error indicator, techniques which have been introduced in the previous chapters. The incident field is always the electric field of a horizontal electric dipole situated within a homogeneous fullspace filled with sea water. The adaptive mesh refinement proceeds in two stages: During the first stage less accurate solutions are computed on a sequence of locally refined meshes with finite element basis functions of lower degree, $p = 1$. A direct solver provided by PARDISO is used to solve the system of linear equations for these smaller problem sizes. The non-normalized error indicator (3.16) is preferred to the normalized one (3.18) in order to resolve the large gradient of the fields near the source. For a mesh consisting of n elements denote by η_{K_i} the local error indicator of element K_i , $i = 1, \dots, n$, and enumerate the elements such that $\eta_{K_1} \geq \eta_{K_2} \geq \dots \geq \eta_{K_n}$. Then, element η_{K_i} is selected for refinement if

$$\eta_{K_i} \geq \alpha_1 \max_{j=1, \dots, n} \eta_{K_j} \quad \text{or} \quad i \geq \alpha_2 n. \quad (5.1)$$

The values $\alpha_1 = 0.1$ and $\alpha_2 = 0.001$ have been used for the examples presented here.

During the second stage of the adaptive mesh refinement process the actual solution is computed on the finest grid using higher order basis functions, $p = 3$ for the canonical disk model and $p = 2$

model	DOFs	QMR iterations
canonical disk, finite volume	4 518 780	1 146
canonical disk, finite element ($p = 3$)	2 199 111	111 975
flat seafloor, finite element ($p = 2$)	755 762	29 574
topography, finite element ($p = 2$)	3 444 676	45 813

Table 5.1: Summary of the marine CSEM numerical examples. DOFs is the number of degrees of freedom used to approximate the electric field.

for the topography model. The large number of degrees of freedom (Table 5.1) and the limited computational resources necessitated the use of the QMR algorithm. The number of QMR iterations required to reduce the residual norm to 10^{-8} times the right hand side vector norm (Table 5.1) are almost prohibitive. Apart from the differing finite element and finite difference matrix properties discussed in section 3.5.3 of Chapter 3 the largely different number of QMR iterations are attributed to two causes. The higher order polynomial approximation appears to decelerate QMR convergence. This can easily be seen from Table 5.1 by comparing the number of QMR iterations for the finite element solutions. Even though less degrees of freedom are used for the canonical disk model the number of QMR iterations with cubic polynomials is considerably larger than the number of QMR iterations for the topography model with quadratic polynomials. The other cause for the slower convergence of the QMR method is seen in the unstructured and locally highly refined finite element mesh if compared to the large but orthogonal and almost equidistant finite difference grid.

5.1 Canonical disk model

The canonical disk model (Figure 5.1) has been introduced by Weiss and Constable (2006). It serves as a simplified model of a resistive hydrocarbon deposit which is located in a conductive, marine environment consisting of two layers of sea water and sea bed. The electric field of a horizontal electric dipole radiating at frequency 1 Hz and placed 100 m above the sea floor has been computed by FDM3D using a tensor product grid of size $161 \times 161 \times 61$ and by FEMSTER using adaptive mesh refinement. The initial tetrahedral mesh contains 79 616 elements and is depicted in Figure 5.2(a). It has been refined adaptively in eight steps. The final mesh shown in Figure 5.2(b) consists of 118 534 elements. The vicinity of point $\mathbf{r} = (-3 \text{ km}, 0, 0)$ has been subject to the mesh refinement. This point lies directly beneath the transmitter on the seafloor. Here, the secondary sources are strongest since they scale with some power of the inverse distance from the primary source at $\mathbf{r} = (-3 \text{ km}, 0, -100 \text{ m})$.

The scattered electric field computed by FDM3D is depicted at four slices through the computational volume in Figures 5.3, 5.5, 5.7 and 5.9. The corresponding results computed by FEMSTER using a piecewise cubic approximation are given in Figures 5.4, 5.6, 5.8 and 5.10. Each figure consists of six subfigures which respectively show the absolute value (modulus, abbreviation mod)

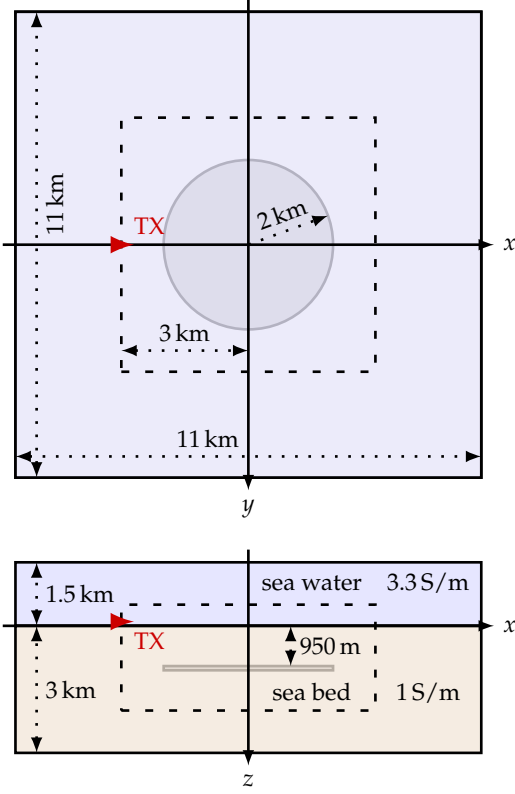


Figure 5.1: Geometry of the canonical disk model (Weiss and Constable, 2006). The disk has a height of 100 m and a conductivity of 0.01 S/m. An x -directed electric dipole TX radiating with frequency 1 Hz is placed 100 m above the seafloor. Scattered electric field values are plotted in Figures 5.3 to 5.10 for the subdomain enclosed by the dashed rectangle.

as well as the phase (argument, abbreviation \arg) of the three complex vector components of the electric field. Note that only the scattered field part is plotted in order to better illustrate the effect of the sea bed and the disk.

Comparison of the results computed by FDM3D and FEMSTER shows that the non-zero components of the field generally agree very well. For symmetry reasons the y -component of the electric field vanishes within the x - z plane at $y = 0$ km (Figures 5.5 and 5.6). Approximation and interpolation errors introduced by the finite difference and finite element method produce an electric field whose y -component is smaller by orders of magnitude compared to the non-vanishing x - and z -components but which is not exactly zero. While the regular structure of the finite difference grid yields a smoother picture of E_y the unstructured finite element mesh produces a speckled pattern, especially in the phase. The residual magnitude of the zero component is reduced to a lower level on the orthogonal finite difference grid than on the unstructured finite element mesh. This is not surprisingly since the evaluation of the field on the tetrahedral mesh is subject to interpolation errors which originate in the distribution of the degrees of freedom on the non-orthogonal edges and faces of a tetrahedron while the interpolation of one vector component on the orthogonal finite difference grid involves only degrees of freedom defined in the same coordinate direction.

There is one interesting difference in the x - y plane at $z = 1$ km which cuts horizontally through the center of the disk. The horizontal components of the scattered electric field computed by FEMSTER (Figure 5.10) rarely show an influence of the disk but only the response of the sea bed

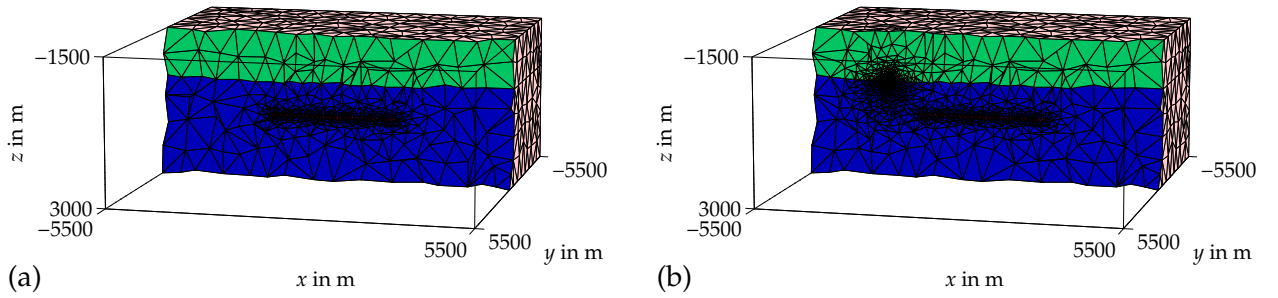


Figure 5.2: Canonical disk model. (a) Initial volume mesh and (b) final volume mesh after eight steps of mesh refinement. Side view on a slice at $y = 0$ m.

homogeneous halfspace. This is best seen in the phases which have a concentric shape around the vertical axis through the transmitter location. The disk expresses itself within this plane only in the vertical component. This is in contrast to the results of FDM3D (Figure 5.9) where the disk is visible in all three field components. In order to understand this difference it is instructive to compare the results with the two vertical slices cut through the center of the disk (Figures 5.3 to 5.6). The phase of the non-zero horizontal field components above and below the disk differ by 180° . This implies that the horizontal field components change their direction along an arbitrary vertical line from top, $z = 950$ m, to bottom, $z = 1050$ m, of the disk. Consequently, they must be zero somewhere in-between. The results of the finite element approximation in Figure 5.10 now reveal that the horizontal field components vanish approximately at $z = 1000$ m. The finite difference results do not show this feature because they are computed with lower accuracy within the disk. Both the finite difference grid and the finite element mesh spatially discretize the disk by one cell/element in height. However, the finite difference approximation is of first order and the horizontal field components are computed by linear interpolation between their values at the top and bottom faces of the disk. The finite element approximation consists of a cubic polynomial which interpolates not only between the horizontal field components on the boundary of the disk but also involves degrees of freedom within the disk's interior with non-vanishing horizontal components. This results in a locally higher solution accuracy compared to the finite difference solution.

A speckled pattern occurs in Figure 5.10 in the horizontal components around the disk's rim and at $x > 2$ km. It points at the inherent interpolation error of the unstructured tetrahedral mesh and the rather coarse mesh size away from the primary source and the disk. The average edge length of elements at the right margin of the plotted slice at $x = 3$ km is about 700 m and should be compared to the finite difference grid spacing of 100 m in vertical and 68.75 m in horizontal direction.

5.1 Canonical disk model

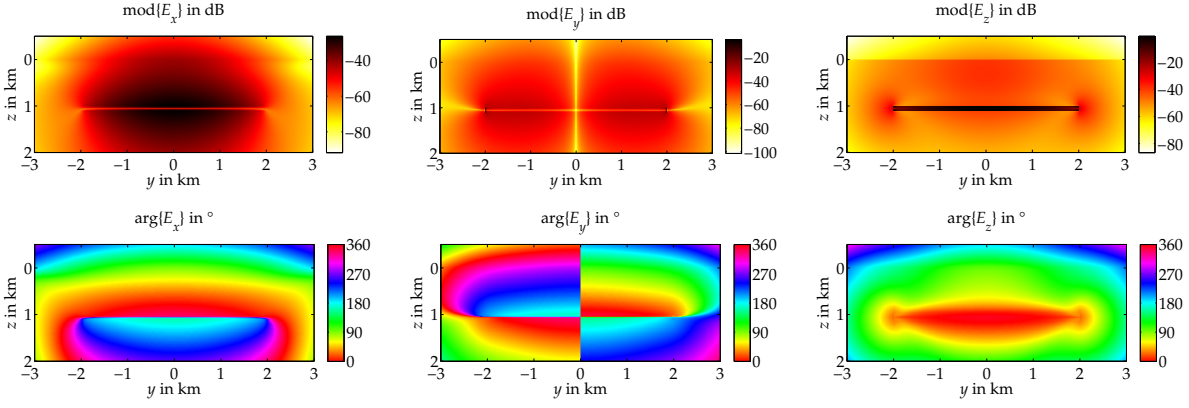


Figure 5.3: Canonical disk model, finite volume solution. Scattered electric field in y - z -plane at $x = 0$ km.

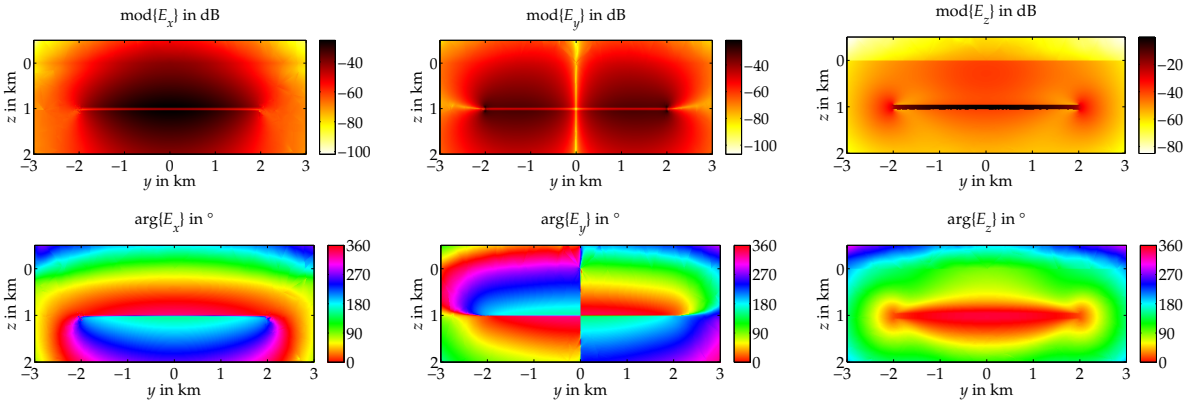


Figure 5.4: Canonical disk model, finite element solution. Scattered electric field in y - z -plane at $x = 0$ km.

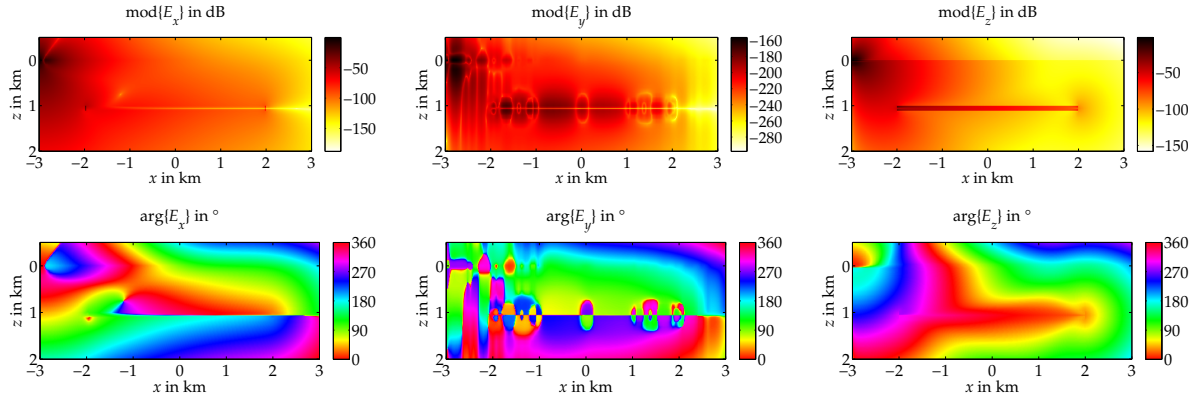


Figure 5.5: Canonical disk model, finite volume solution. Scattered electric field in x - z -plane at $y = 0$ km.

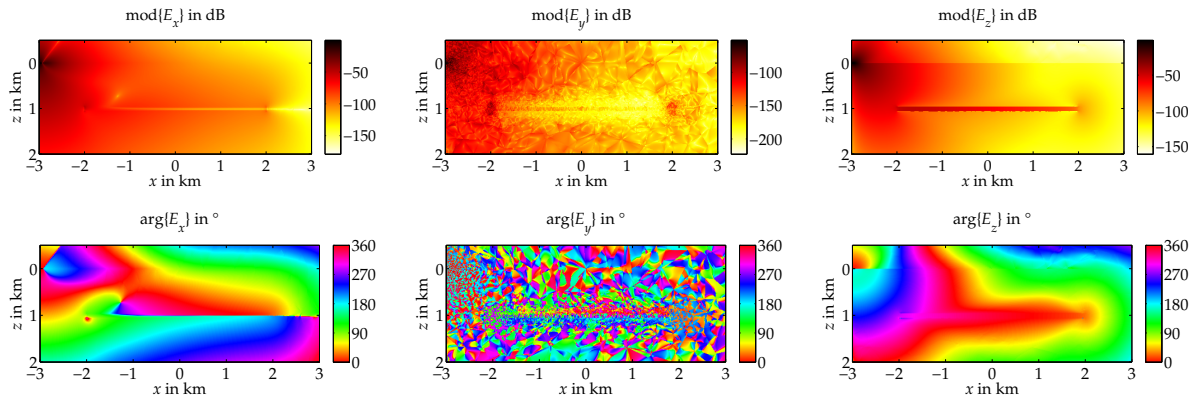


Figure 5.6: Canonical disk model, finite element solution. Scattered electric field in x - z -plane at $y = 0$ km.

5.1 Canonical disk model

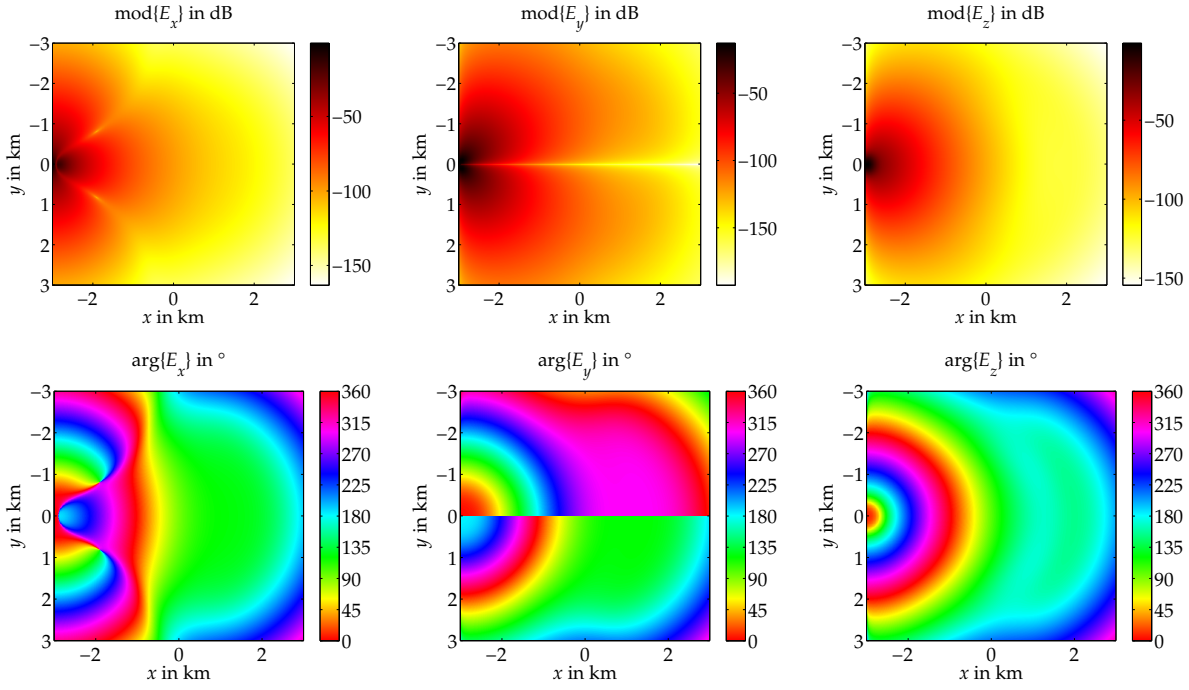


Figure 5.7: Canonical disk model, finite volume solution. Scattered electric field in x - y -plane at $z = +0$ km.

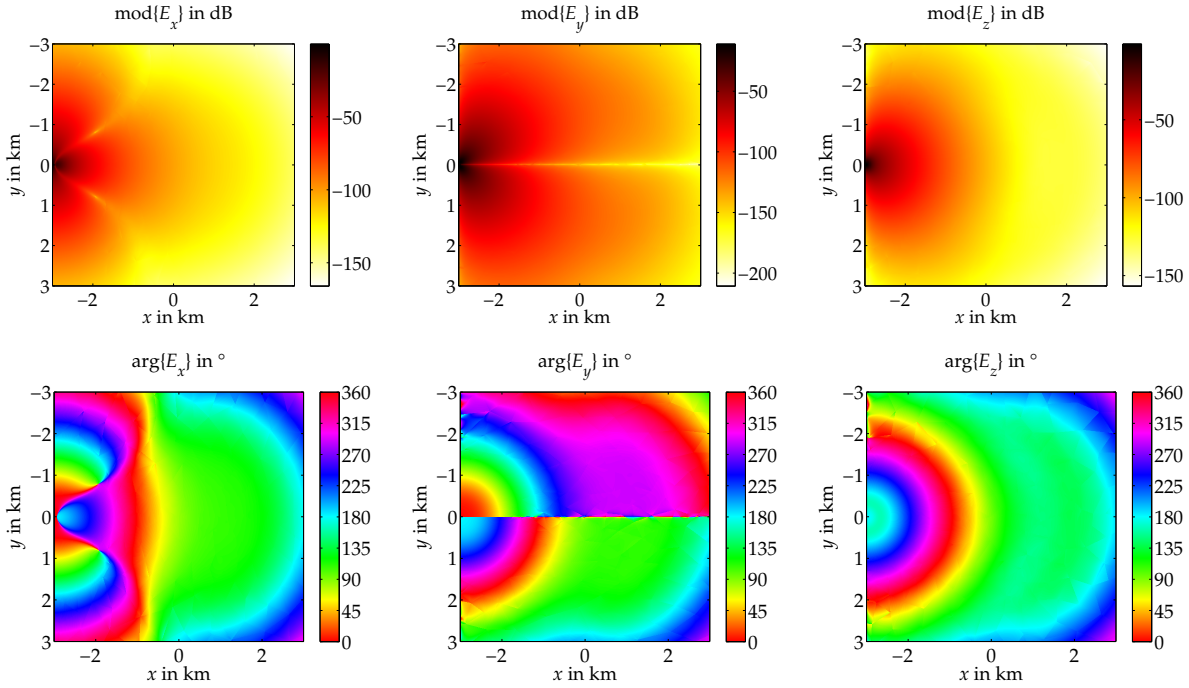


Figure 5.8: Canonical disk model, finite element solution. Scattered electric field in x - y -plane at $z = +0$ km.

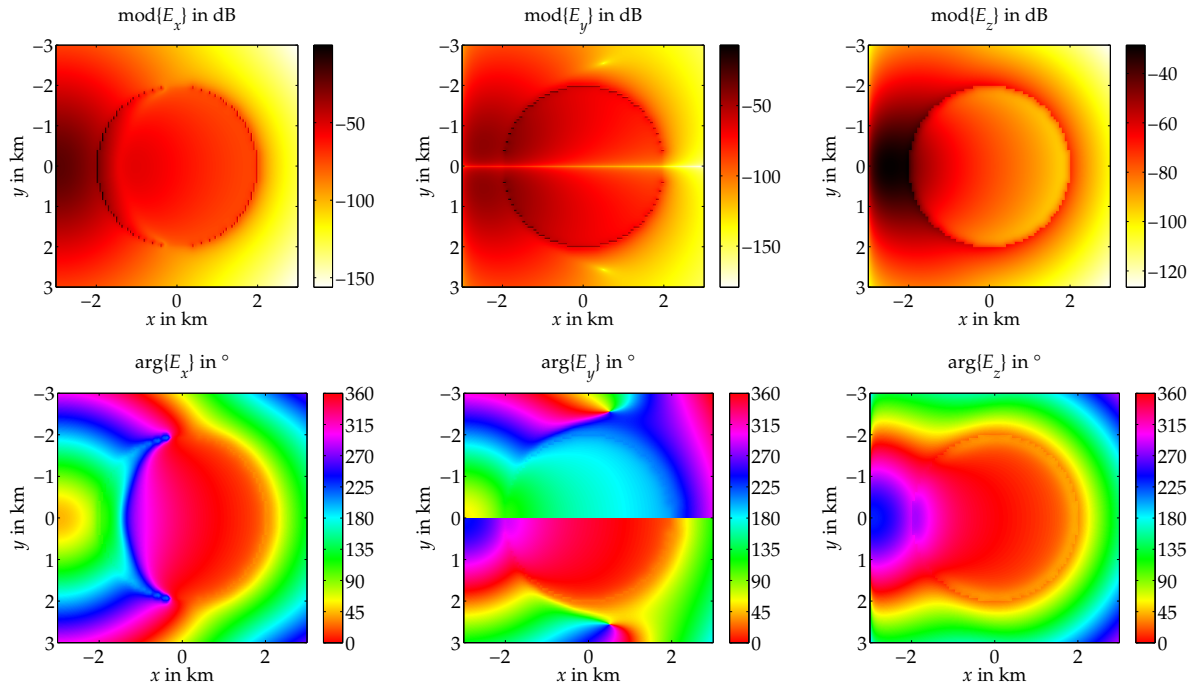


Figure 5.9: Canonical disk model, finite volume solution. Scattered electric field in x - y -plane at $z = 1$ km.

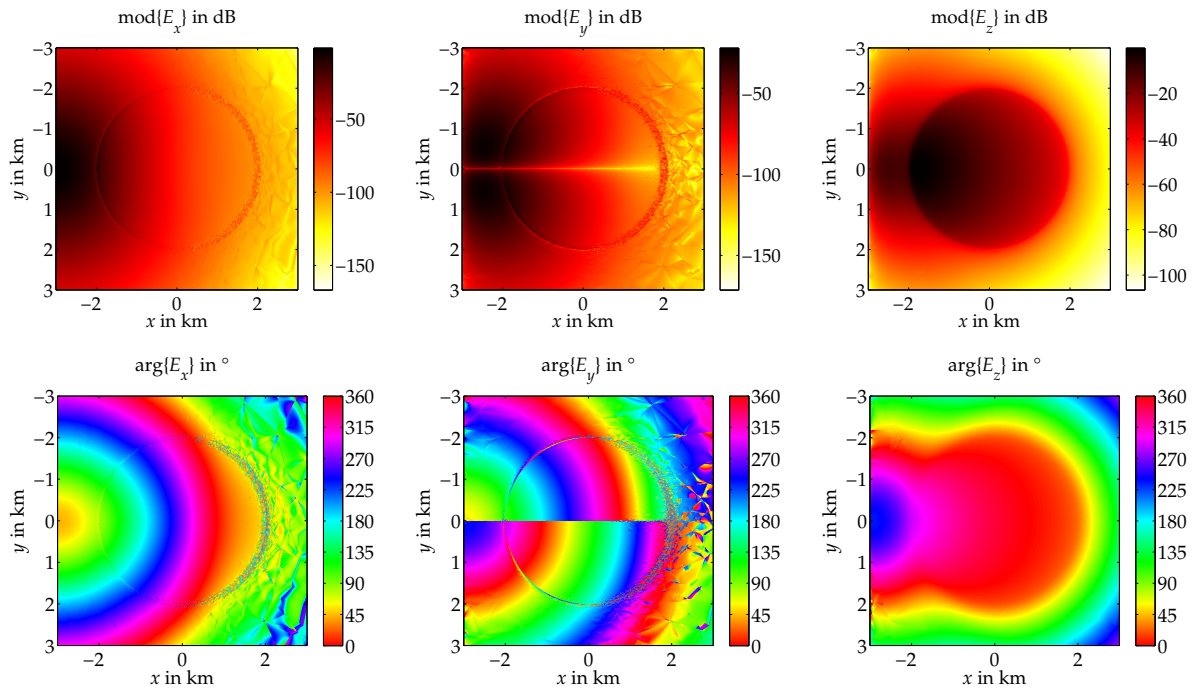


Figure 5.10: Canonical disk model, finite element solution. Scattered electric field in x - y -plane at $z = 1$ km.

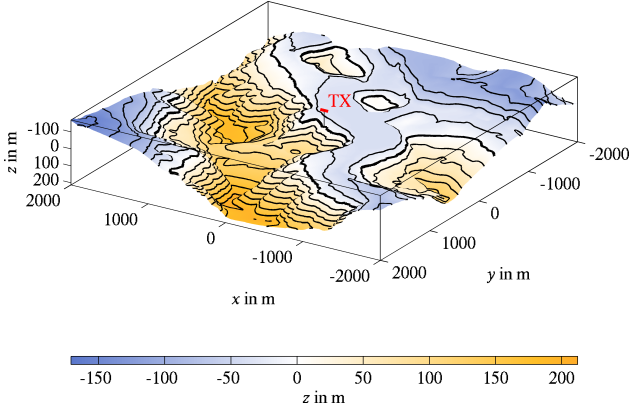


Figure 5.11: Seafloor bathymetry of the topography model, $2 \times$ vertical exaggeration. An x -directed electric dipole TX is placed 100 m above the seafloor.

5.2 Seafloor topography

One of the problems realistic marine CSEM simulations have to face is the consideration of seafloor topography. Bathymetric data can be incorporated into the model most naturally as a surface triangulation of the seafloor. In contrast to a typical finite difference, i. e., tensor product grid which samples the seafloor in a staircase-like manner the seafloor can be represented as a continuous surface by an unstructured tetrahedral mesh. The example considered here is constructed from a synthetic bathymetry data set provided by the INRIA Gamma team¹. The bathymetry is depicted in Figure 5.11. It divides the computational volume $\Omega = \{(x, y, z) : -2 \text{ km} \leq x, y \leq 2 \text{ km}, -1.5 \text{ km} \leq z \leq 2.5 \text{ km}\}$ into two halfspaces representing sea water and the sea bed. The electrical conductivity has been chosen as in the previous section, 3.3 S/m for sea water and 1 S/m for the sea bed sediments. An x -directed electric dipole TX radiating with frequency 1 Hz is placed 100 m above the seafloor at $x = y = 0$ and $z = -100 \text{ m}$.

In order to quantify the accuracy of the solution and to qualitatively estimate the distortion of the electromagnetic field by the seafloor topography a second, flat seafloor model is considered for comparison. Both models have been spatially discretized using the adaptive mesh refinement strategy presented in Chapter 3. The initial mesh of the flat seafloor model is shown in Figure 5.12(a) and the final mesh after eight steps of mesh refinement in Figure 5.12(b). The meshes respectively contain 16 545 and 118 793 elements. Similarly, Figure 5.13 shows the initial and final mesh of the topography model. Here, only five steps of mesh refinement were required to enlarge the number of elements from 380 809 to 542 425 elements. The considerably larger number of elements in the initial mesh is a consequence of the relatively dense surface triangulation of the bathymetry data set with a regular grid spacing of 250 m in x - and y -direction. Similarly to the canonical disk model the mesh is refined directly beneath the primary source at the seafloor where the secondary sources and, consequently, the scattered field assumes its maximum magnitude.

This can be seen from the bottom rows of Figures 5.14 and 5.15 which respectively depict the norm of the electric and magnetic field plotted on three orthogonal planes through the origin. The relative solution error of a piecewise quadratic approximation of E and H as defined by

¹<http://www-c.inria.fr/gamma/download/affichage.php?dir=RELIEF/&name=mmal25pm>

equation (3.23a) in Chapter 3 is plotted above in the top row. The slices are restricted to the subvolume $[-500, 500]^3 \text{ m}^3$. The relative error within this smaller portion of the computational volume is mostly less than 1%. Only the x - z - and x - y -plane views of the relative error of \mathbf{H} in Figure 5.15 contain pronounced regions where it is significantly larger. However, this is an artifact of the relative measure used. The norm of the magnetic field which normalizes the absolute solution error has a pronounced minimum which exactly coincides with the maximum of the relative error. A smaller field magnitude is naturally reconstructed less accurately by the finite element approximation.

The reference solution for the horizontal electric dipole in a two-layered medium has been implemented according to Sommerfeld (1964). The Hankel integrals are evaluated numerically using the digital filter algorithm of Anderson (1989).

Figures 5.15 to 5.27 finally show slices of the electric and magnetic fields for the seafloor and the topography model in the three planes defined by $x = 0$, $y = 0$ and $z = 0$. Comparison of corresponding field components and slices between both models nicely illustrates how the seafloor topography distorts the symmetric shape of the electromagnetic fields. In particular the field components which vanish for the one-dimensional flat seafloor model gain significant values from the three-dimensional geometry of the topography model.

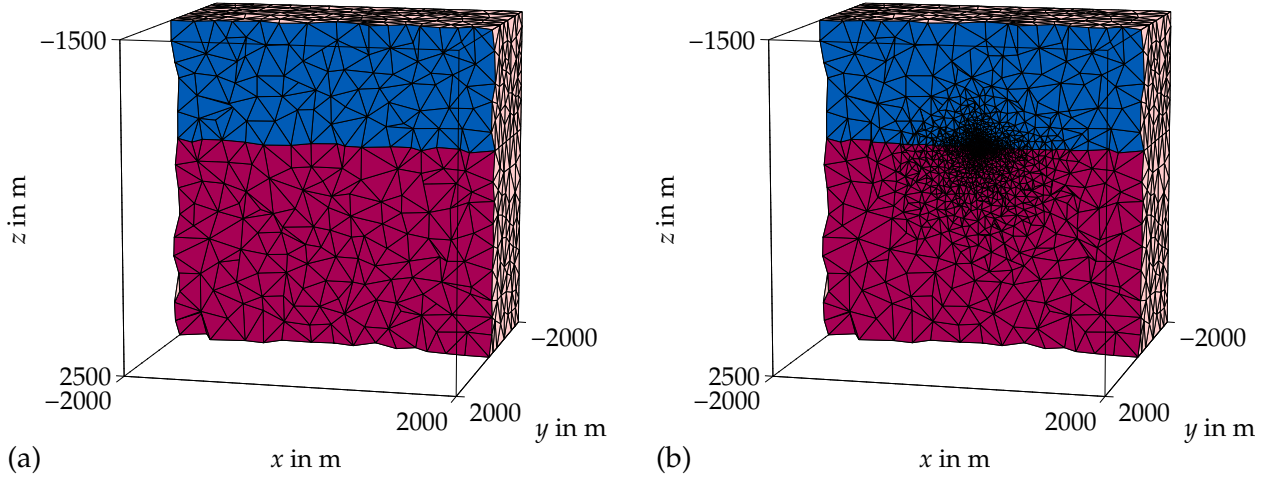


Figure 5.12: Flat seafloor model. (a) Initial volume mesh and (b) final volume mesh after eight steps of mesh refinement. Side view on a slice at $y = 0$ m.

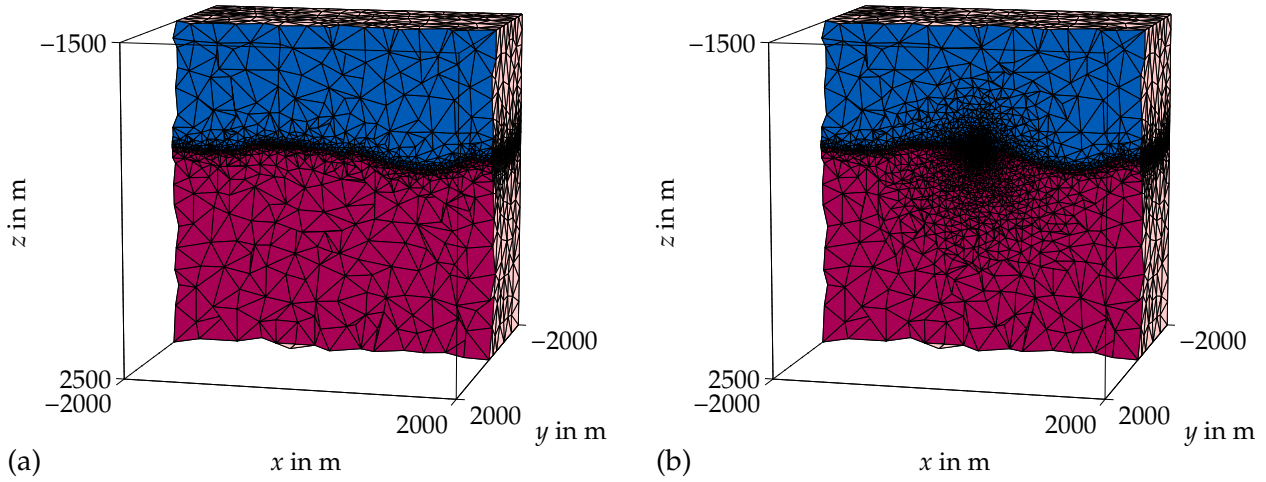


Figure 5.13: Topography model. (a) Initial volume mesh and (b) final volume mesh after five steps of mesh refinement. Side view on a slice at $y = 0$ m.

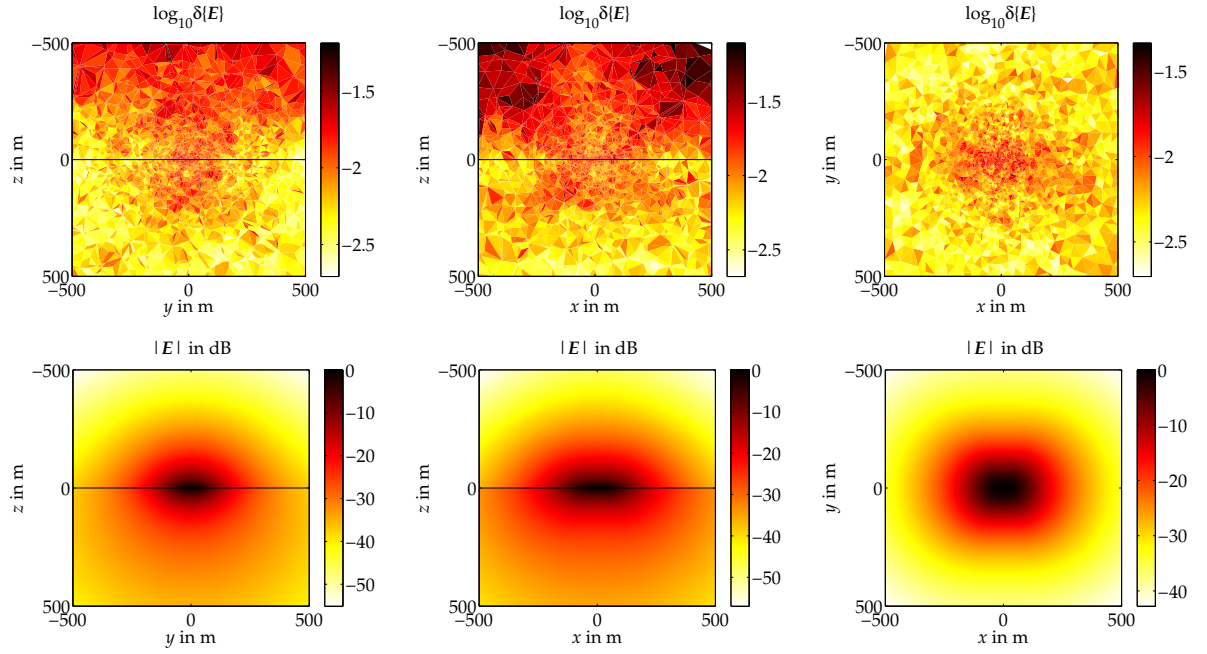


Figure 5.14: Flat seafloor model. Relative error (top row) and norm (bottom row) of the scattered electric field in y - z -plane at $x = 0$ m (left column), x - z -plane at $y = 0$ m (middle column), x - y -plane at $z = +0$ m (right column).

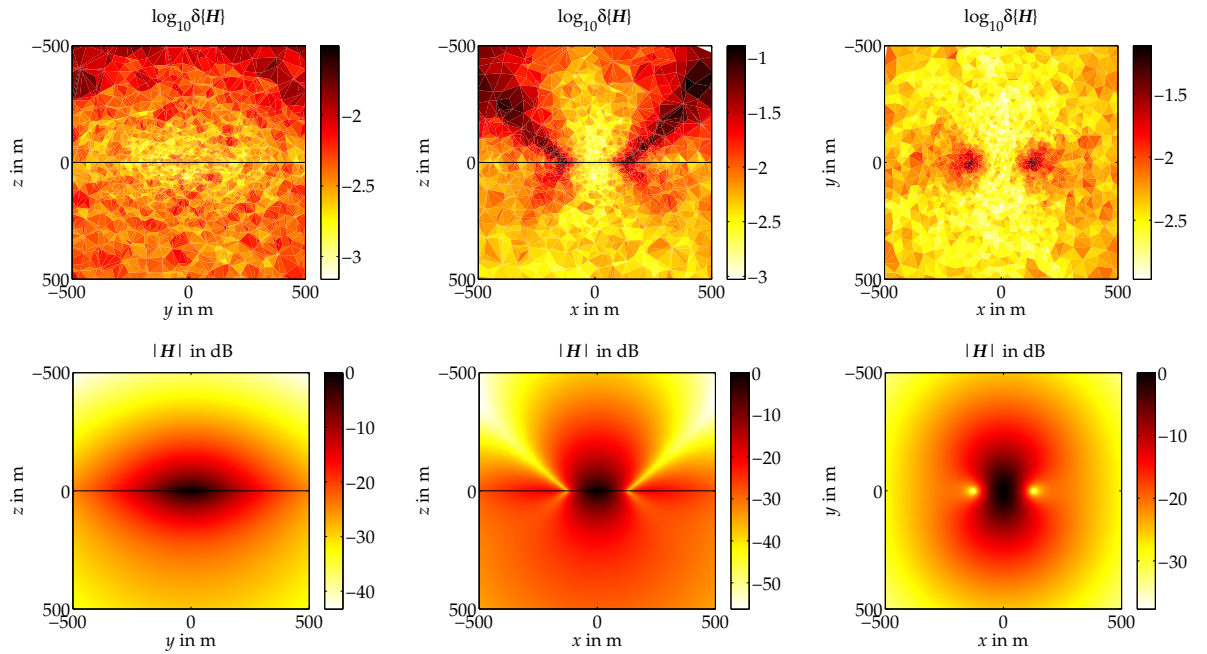


Figure 5.15: Flat seafloor model. Relative error (top row) and norm (bottom row) of the scattered magnetic field in y - z -plane at $x = 0$ m (left column), x - z -plane at $y = 0$ m (middle column), x - y -plane at $z = +0$ m (right column).

5.2 Seafloor topography

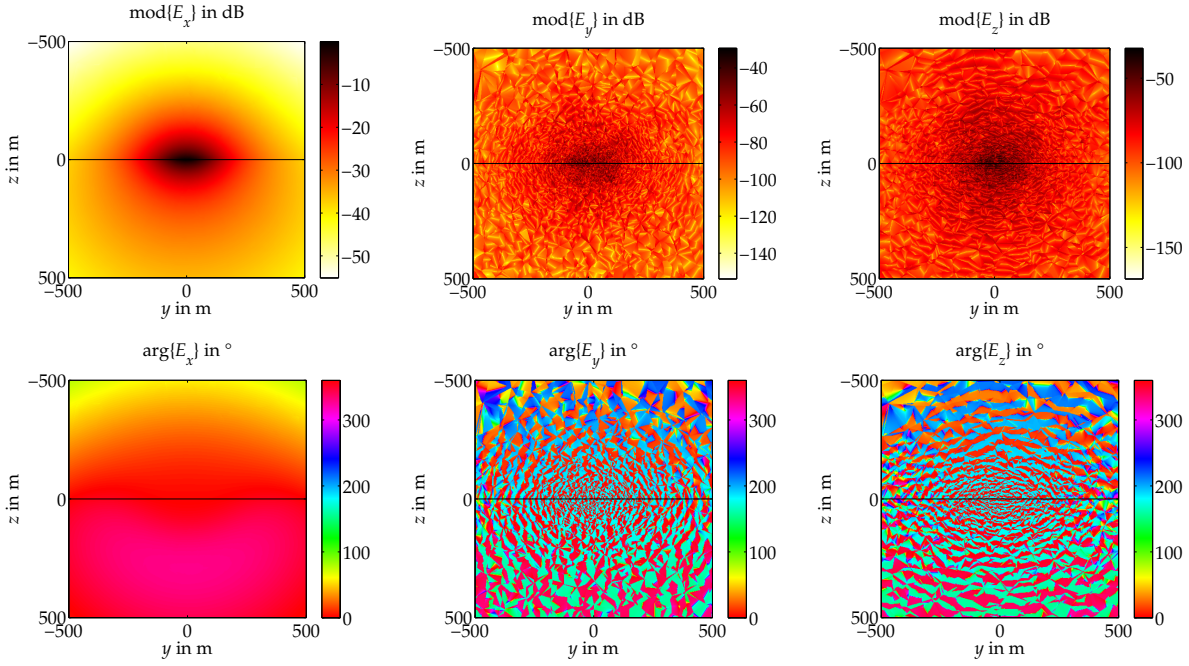


Figure 5.16: Flat seafloor model. Scattered electric field in y - z -plane at $x = 0$ m. The black line represents the seafloor.

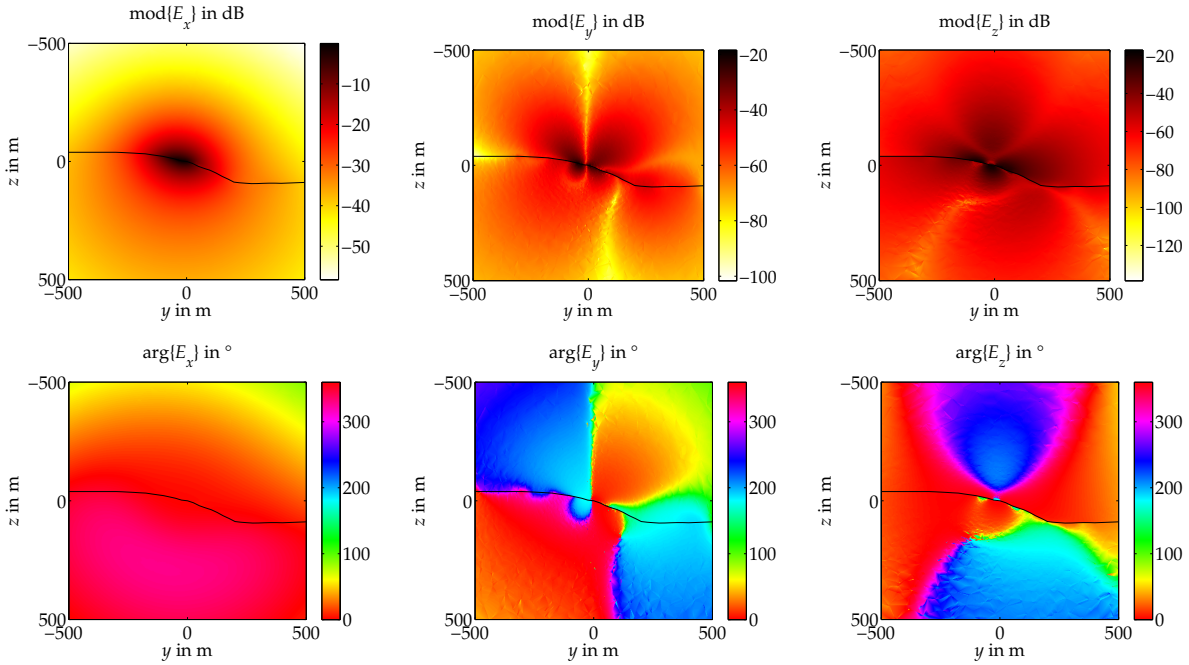


Figure 5.17: Topography model. Scattered electric field in y - z -plane at $x = 0$ m. The black line represents the seafloor.

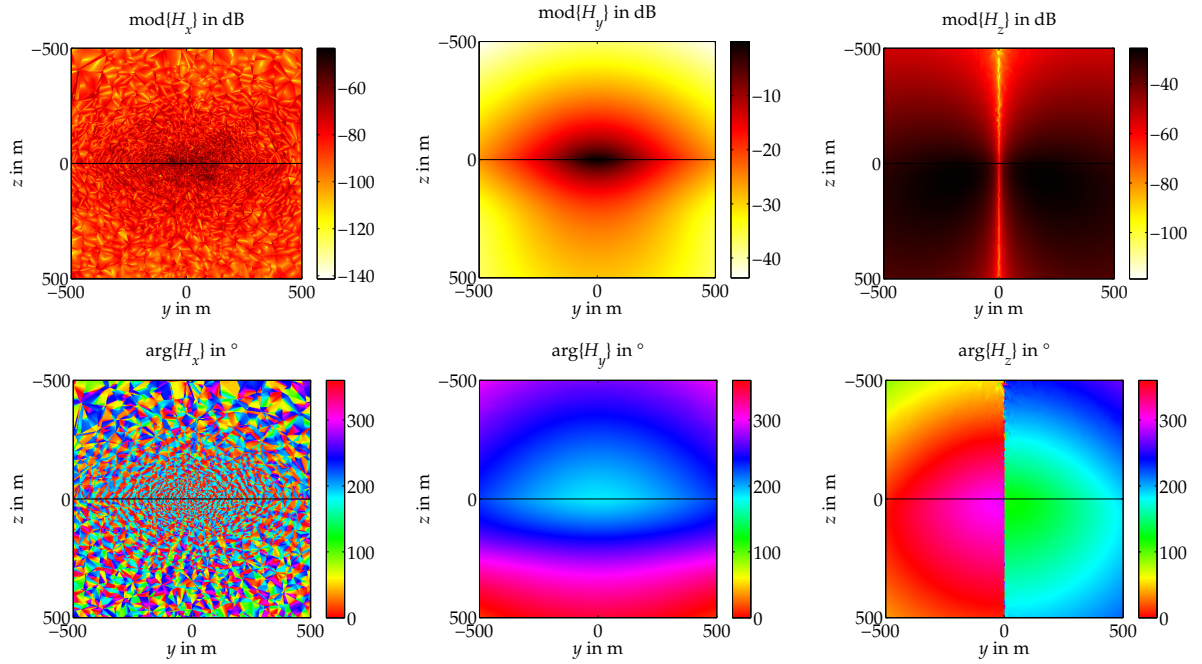


Figure 5.18: Flat seafloor model. Scattered magnetic field in y - z -plane at $x = 0$ m. The black line represents the seafloor.

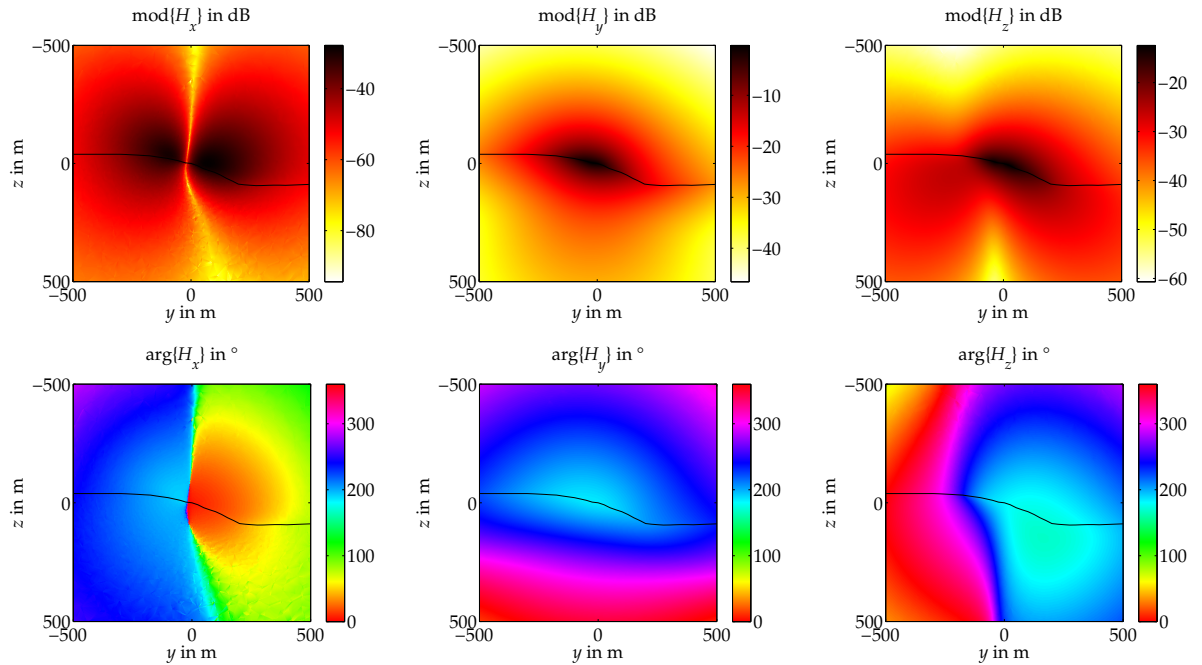


Figure 5.19: Topography model. Scattered magnetic field in y - z -plane at $x = 0$ m. The black line represents the seafloor.

5.2 Seafloor topography

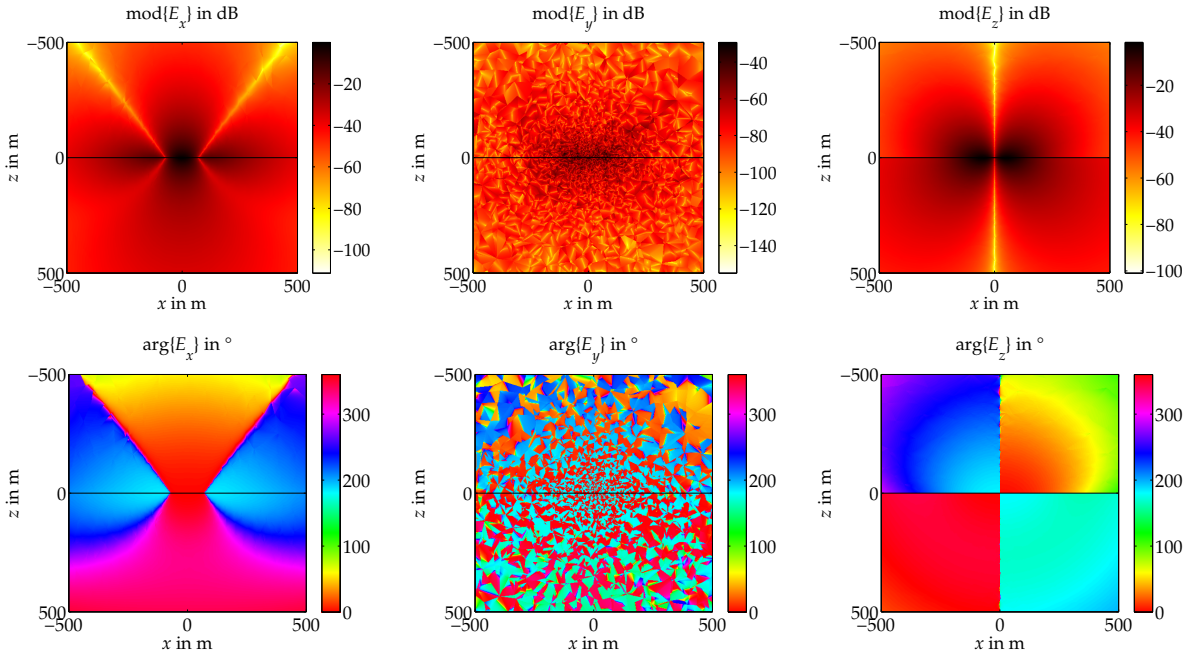


Figure 5.20: Flat seafloor model. Scattered electric field in x - z -plane at $y = 0$ m. The black line represents the seafloor.

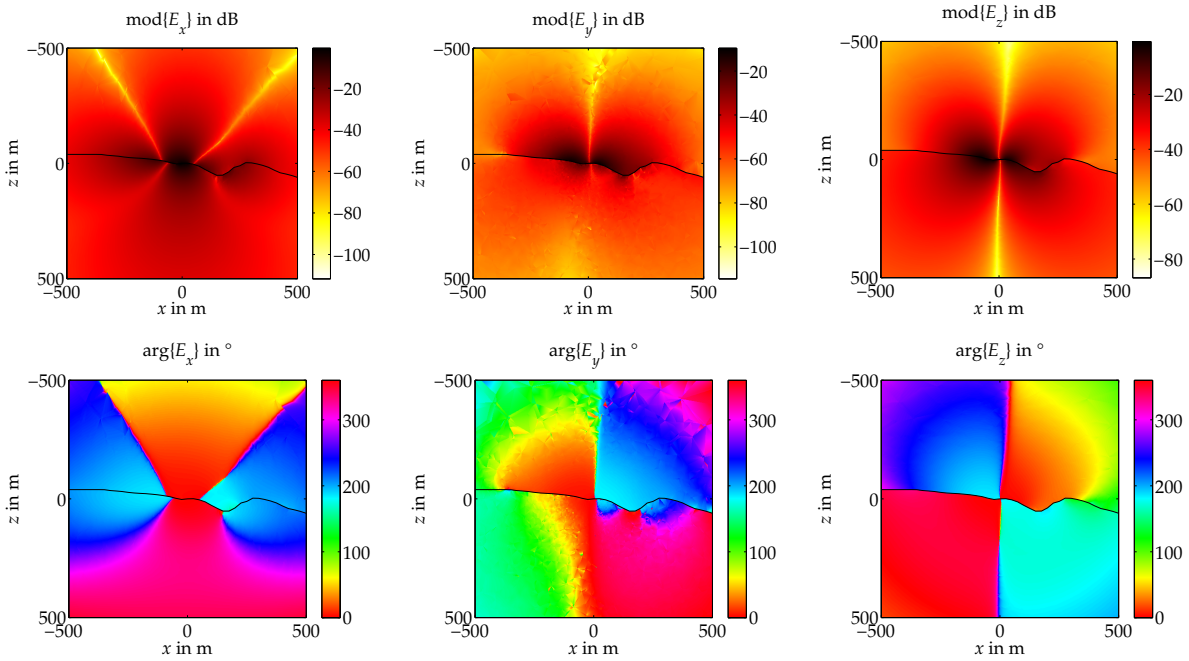


Figure 5.21: Topography model. Scattered electric field in x - z -plane at $y = 0$ m. The black line represents the seafloor.

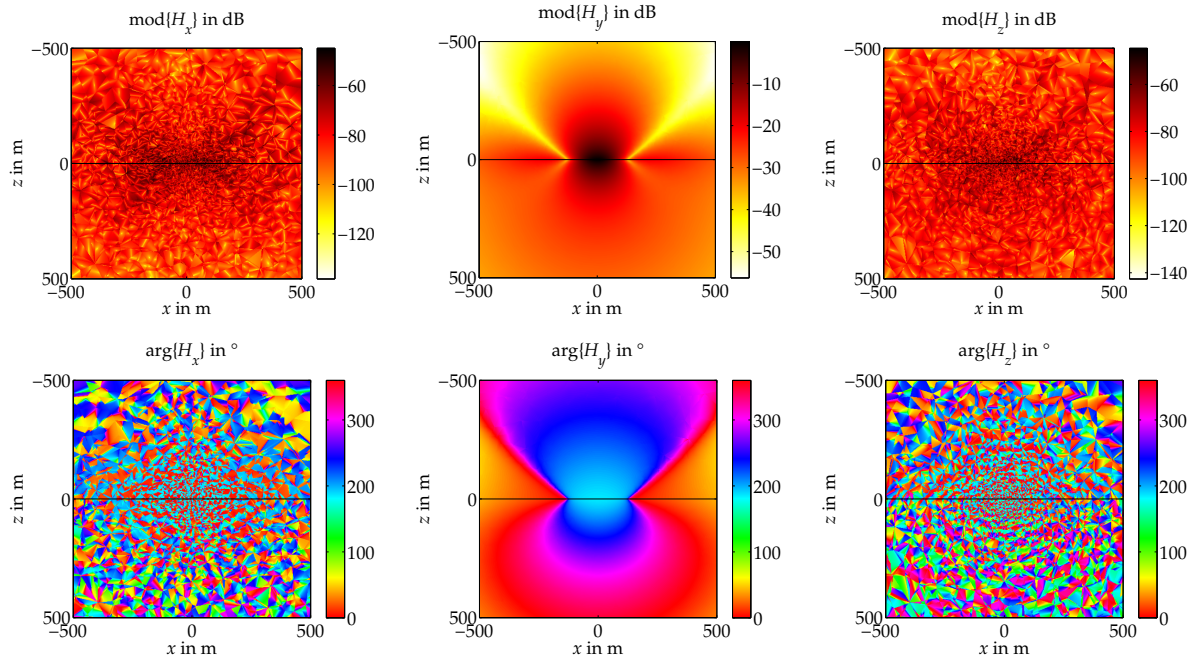


Figure 5.22: Flat seafloor model. Scattered magnetic field in x - z -plane at $y = 0$ m. The black line represents the seafloor.

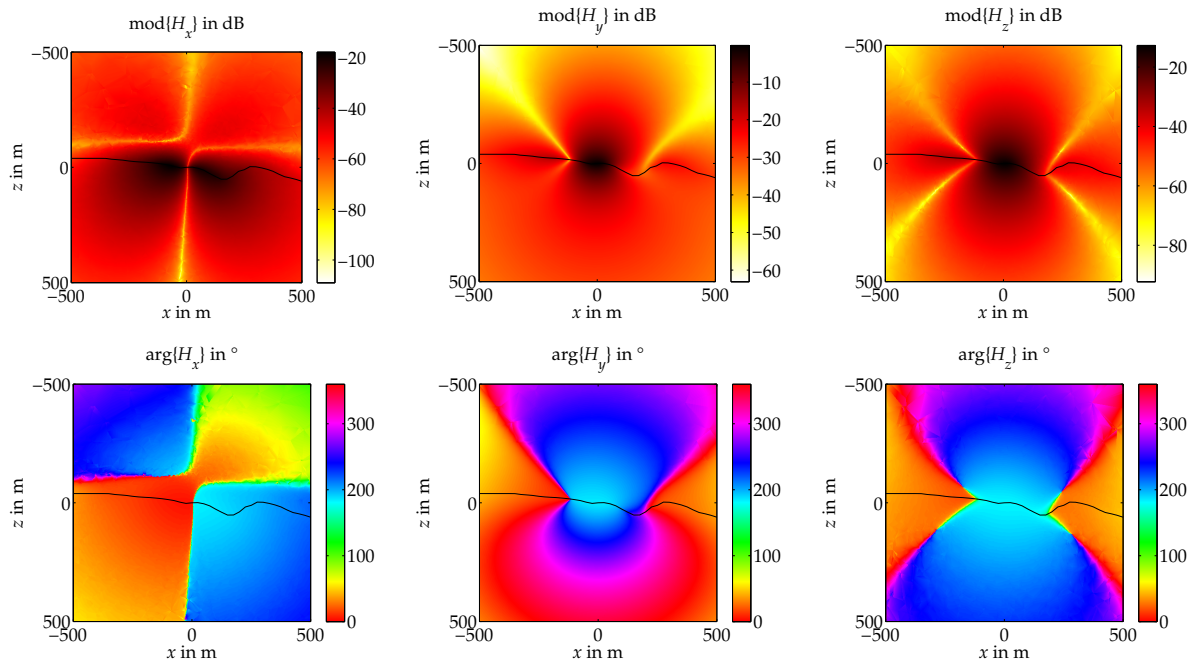


Figure 5.23: Topography model. Scattered magnetic field in x - z -plane at $y = 0$ m. The black line represents the seafloor.

5.2 Seafloor topography

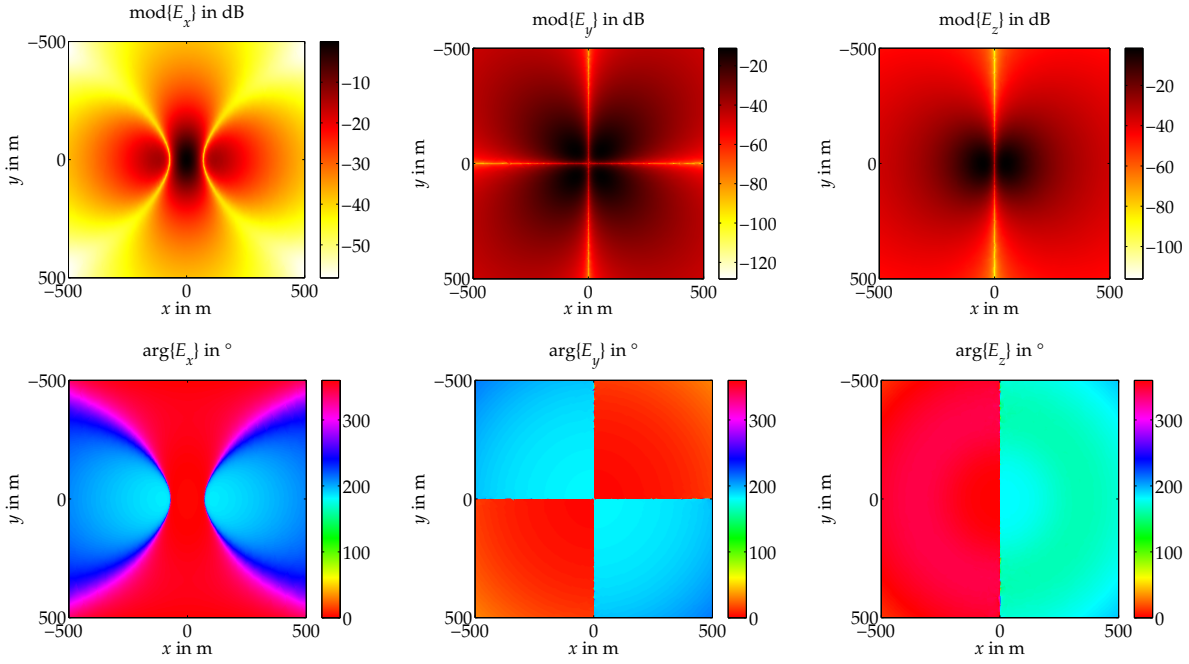


Figure 5.24: Flat seafloor model. Scattered electric field in x - y -plane at $z = +0$ m. The black line represents the seafloor.

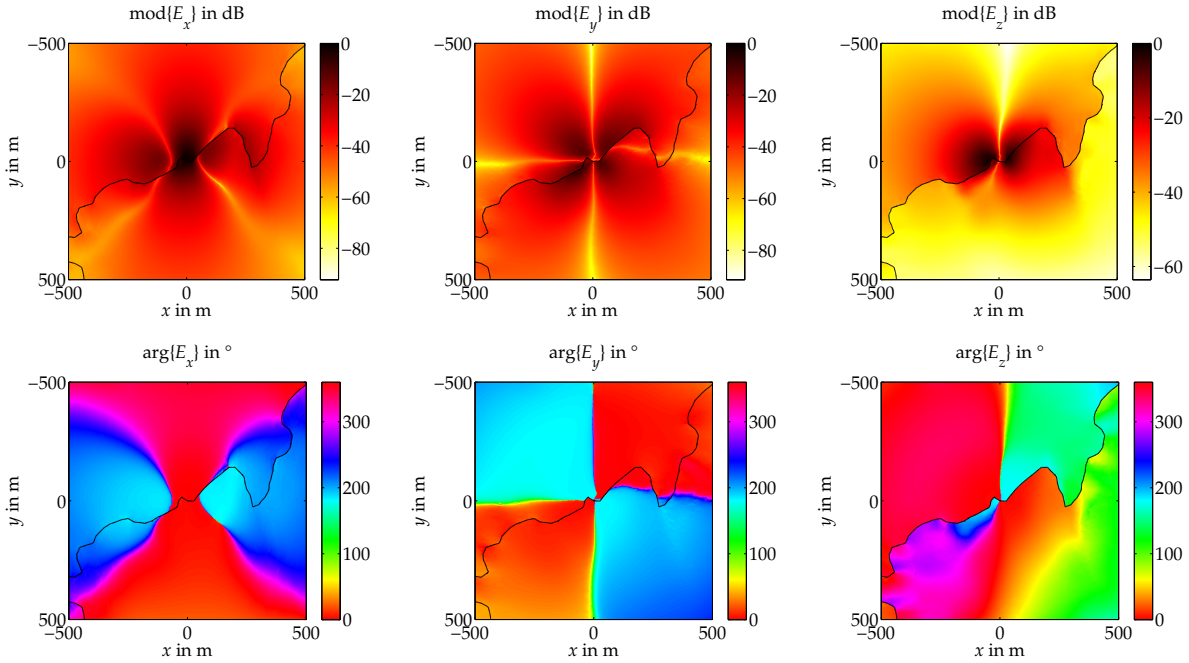


Figure 5.25: Topography model. Scattered electric field in x - y -plane at $z = 0$ m. The black line represents the seafloor.

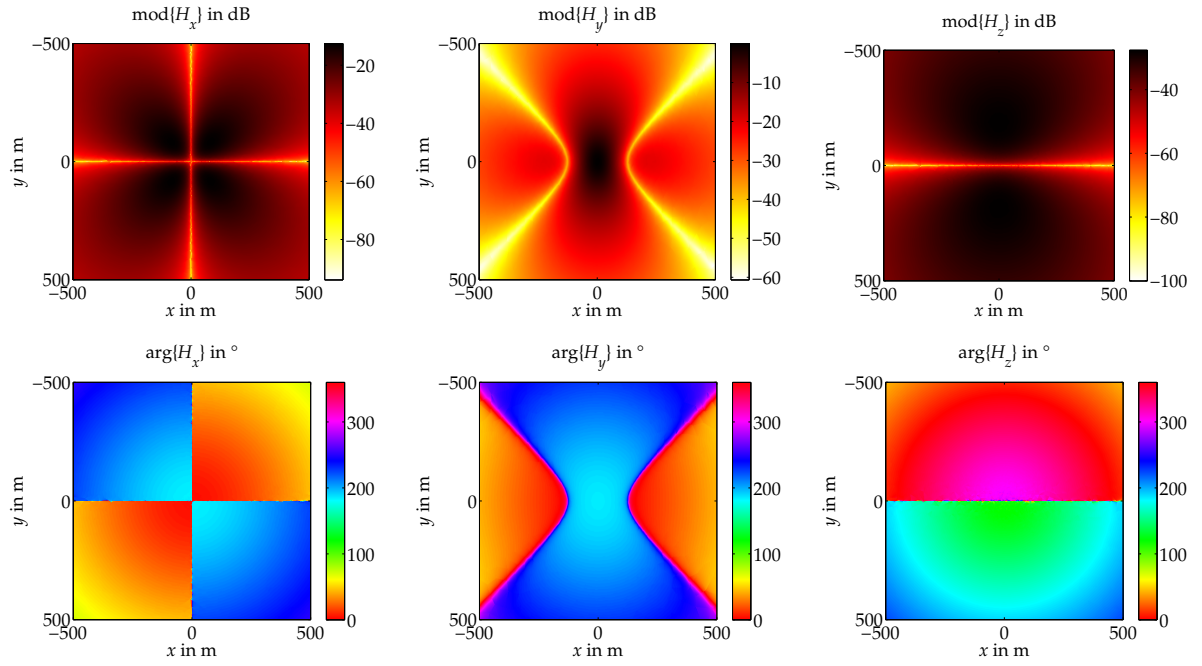


Figure 5.26: Flat seafloor model. Scattered magnetic field in x - y -plane at $z = +0$ m. The black line represents the seafloor.

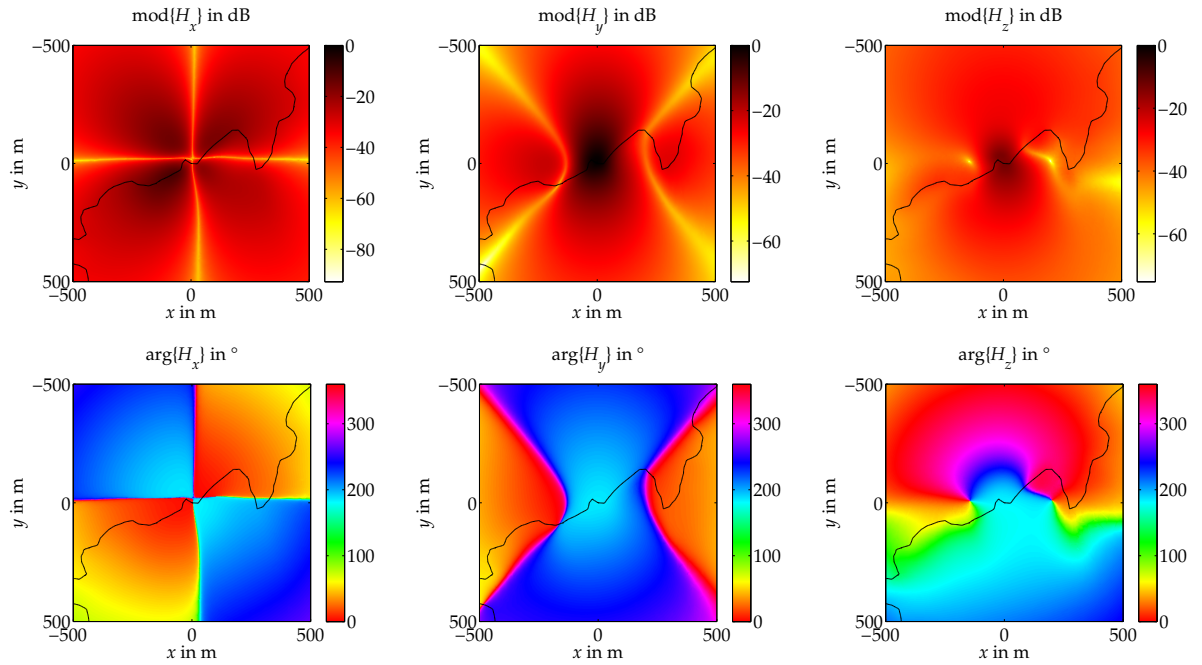


Figure 5.27: Topography model. Scattered magnetic field in x - y -plane at $z = 0$ m. The black line represents the seafloor.

Chapter 6

Summary and outlook

A finite element software has been developed which solves Maxwell's equations for time-harmonic problems. The complete Maxwell system is considered including both conduction and displacement currents in order to model inductive as well as wave propagation phenomena. The implementation allows for constitutive parameters which may be isotropic or anisotropic, homogeneous or polynomial functions of space. In addition, an anisotropic constitutive parameters formulation of the perfectly matched layer in Cartesian coordinates has been implemented. The most important incident field patterns for the scattered field approach which are relevant for geophysical applications are provided, namely, the electric and magnetic dipole in fullspace as well as the plane wave in a horizontally stratified earth. The finite element core supplies polynomial base functions of practically arbitrary order for both tetrahedral and hexahedral elements. Combined with mesh generators any geometric shape can be accounted for by unstructured meshes. An *a posteriori* error indicator forms the basis for adaptive mesh refinement. Implementation of such a powerful finite element code would have been impossible without the use of existing software modules. Third party libraries or programs include the finite element core FEMSTER, the mesh generators NETGEN and TETGEN, the direct solvers for the system of linear equations PARDISO and MUMPS, and MATLAB® for visualization.

The finite element solver bases on either the vector Helmholtz equation in terms of the electric field E or its extension by the continuity equation. Stability considerations of the low frequency behavior of the electric field lead to the introduction of a mixed formulation in terms of both the electric field and an auxiliary scalar variable V . The vector Helmholtz equation alone suffers from the large kernel of the curl-operator which spoils the solution for low frequencies. The kernel can be removed if the continuity equation is explicitly taken into account. In order to obtain an algebraically balanced problem, the auxiliary scalar variable V has been introduced. The augmented problem was designed such that the symmetry property of the coefficient matrix of the discrete problem pertaining to the vector Helmholtz equation alone is retained for the coefficient matrix of the augmented discrete problem.

The derivation of the E - V formulation necessitated two assumptions which do not apply to the E -field formulation. First, a stable implementation could only be achieved for conducting media, $\sigma > 0$ within all of the computational domain, because the continuity equation vanishes in a dielectric at $\omega = 0$. Replacing the continuity equation by a non-vanishing divergence condition within the dielectric subdomain leads to technical problems which are due to the finite element

function spaces used (Appendix B). This assumption can be relaxed in practice as long as the frequency is bounded away from zero.

Second, the computational domain was assumed to be simply connected with not more than one connected Dirichlet boundary part. This excludes, e. g., the case of the parallel plate capacitor where the two plate electrodes are represented by two disconnected Dirichlet, PEC boundary patches. An generalization for more than one connected Dirichlet boundary part can be found in Appendix C. However, the design paradigm of a symmetric extension that is equivalent to the vector Helmholtz equation boundary value problem implies that the augmented formulation does not contain additional source terms. The parallel plate capacitor would indeed extend the class of physical models beyond the limit of the E -field formulation since a non-vanishing integral current flow through all but one of the Dirichlet boundary patches, i. e., through one of the plates would have to be prescribed and introduce a new source term. Investigation of non-symmetric mixed formulations and the comparison with mixed vector and scalar potential approaches (Haber et al., 2000; Mitsuhashi and Uchida, 2004) offers a line of future research.

The theoretical considerations concerning the kernel of the curl-operator and the low frequency stability have been supported by a number of numerical experiments. They give empirical evidence for the improved stability of the E - V formulation at low frequencies. The solution of a boundary value problem using a stable operator is still susceptible to errors of the data, in particular of the boundary values. If alternate types of boundary conditions can be devised which model one and the same physical problem the particular choice might influence solution stability and needs to be carefully considered. An improper set of boundary conditions appears to give rise to elevated solution errors for part of the numerical example given in Appendix C. According to this observation the influence of unstructured meshes on the convergence rate of the finite element method should be further investigated.

Another open question remains the solver for the system of linear equations. Most experiments have been carried out using a direct solver. The memory requirement for the storage of the matrix factors is still the limiting factor for the simulation of three-dimensional problems, even on recent computers. Experiments with a QMR solver proved to be discouraging and resulted in a far slower convergence than for a finite difference/volume discretization of the same problem setup. The poor convergence might be accelerated if a suitable preconditioner can be found. However, storage and operational costs of the construction of a non-trivial preconditioner and of its application to an iterative solver need to be carefully weighed against the costs of a direct solver.

The finite element software has primarily been developed as a versatile simulation tool. Its application has been successfully demonstrated by two examples from marine CSEM. Simulation of other geophysical methods like MT, airborne EM or even GPR measurements for more or less complicated earth models only waits to be carried out. In future, the software can also serve as a forward operator for an inversion scheme. Nevertheless, the efficient computation of sensitivities still needs to be investigated and should be closely seen in context with the inverse problem solution strategy. So far, only the sensitivity equation method (McGillivray and Oldenburg, 1990) has been implemented as a straightforward extension of the boundary value problem finite element solution

(Appendix D). If the system of linear equations is solved directly the matrix factorization can be exploited in order to compute sensitivities without much overhead. The sensitivity equation method is best suited for sensitivity studies for models with a moderate number of model parameters. The typical parameterization of a three-dimensional inverse model, however, involves tens or hundreds of thousands cells for each of which a system of linear equations needs to be solved. Even if only the forward and backwards substitution phases need to be carried out, this method is impractical and unfavorable compared to the adjoint fields method (McGillivray and Oldenburg, 1990) as long as the number of receiver locations times the number of measured field components is significantly smaller than the number of cells.

Chapter 6 Summary and outlook

Appendices

A Formulary

This section collects a number of useful vector and integral identities which frequently occur within the main part of this work.

A.1 Vector identities

For a scalar function u , a vector function \mathbf{u} and a unit vector \mathbf{n} , $\|\mathbf{n}\| = 1$, the following equalities hold, provided the functions are smooth enough:

$$\operatorname{curl} \operatorname{grad} u = \mathbf{0}, \quad (\text{A.1a})$$

$$\operatorname{div} \operatorname{curl} \mathbf{u} = 0, \quad (\text{A.1b})$$

$$\mathbf{n} \cdot (\mathbf{n} \times \mathbf{u}) = 0, \quad (\text{A.1c})$$

$$(\mathbf{n} \times \mathbf{u}) \times \mathbf{n} = \mathbf{u} - (\mathbf{n} \cdot \mathbf{u}) \mathbf{n}, \quad (\text{A.1d})$$

$$\boldsymbol{\phi} \cdot (\mathbf{n} \times \mathbf{u}) = -(\mathbf{n} \times \boldsymbol{\phi}) \cdot \mathbf{u}. \quad (\text{A.1e})$$

In addition to the well known volume differential operators grad , curl and div , a set of differential operators can be defined on surfaces. The following relations between surface and volume differential operators are taken from Buffa, Costabel, and Sheen (2002). Let Ω be a Lipschitz domain with smooth boundary Γ whose outer normal vector is denoted by \mathbf{n} . For a scalar function $u \in H_1(\Omega)$, the surface gradient and the surface vector curl are related to the volume gradient by

$$\operatorname{grad}_\Gamma u = (\mathbf{n} \times \operatorname{grad} u) \times \mathbf{n} \quad \text{and} \quad (\text{A.1f})$$

$$\operatorname{curl}_\Gamma u = -\mathbf{n} \times \operatorname{grad} u. \quad (\text{A.1g})$$

The surface scalar curl and the surface divergence of a vector field $\mathbf{u} \in H_{\operatorname{curl}}(\Omega)$ are related to the volume curl by

$$\operatorname{curl}_\Gamma ((\mathbf{n} \times \mathbf{u}) \times \mathbf{n}) = \mathbf{n} \cdot \operatorname{curl} \mathbf{u} \quad \text{and} \quad (\text{A.1h})$$

$$\operatorname{div}_\Gamma (\mathbf{n} \times \mathbf{u}) = -\mathbf{n} \cdot \operatorname{curl} \mathbf{u}. \quad (\text{A.1i})$$

Note that there are two types of curl-operators defined for surfaces. The surface vector curl (A.1g) maps scalar fields onto vector fields and the surface scalar curl (A.1h) vector fields onto scalar fields. This distinction should be evident from the different argument types in equations (A.1g) and (A.1h).

A.2 Integral identities

Let $\Omega \in \mathbb{R}^3$. For functions $\mathbf{u} \in H_{\text{div}}(\Omega)$ and $\phi \in H_1(\Omega)$ the following Green's theorem holds (Monk, 2003, Theorem 3.24)

$$\int_{\Omega} \phi \operatorname{div} \mathbf{u} d^3r = - \int_{\Omega} \operatorname{grad} \phi \cdot \mathbf{u} d^3r + \int_{\partial\Omega} \phi (\mathbf{n} \cdot \mathbf{u}) d^2r \quad (\text{A.2})$$

and for functions $\mathbf{u}, \Phi \in H_{\text{curl}}(\Omega)$ (Monk, 2003, Theorem 3.31)

$$\int_{\Omega} \Phi \cdot \operatorname{curl} \mathbf{u} d^3r = \int_{\Omega} \operatorname{curl} \Phi \cdot \mathbf{u} d^3r + \int_{\partial\Omega} ((\mathbf{n} \times \Phi) \times \mathbf{n}) \cdot (\mathbf{n} \times \mathbf{u}) d^2r. \quad (\text{A.3})$$

The double cross product $(\mathbf{n} \times \Phi) \times \mathbf{n}$ ensures that the trace of $\Phi \in H_{\text{curl}}(\Omega)$ on $\partial\Omega$ belongs to an appropriate function space. For practical purposes it is sufficient to use the form

$$\int_{\Omega} \Phi \cdot \operatorname{curl} \mathbf{u} d^3r = \int_{\Omega} \operatorname{curl} \Phi \cdot \mathbf{u} d^3r + \int_{\partial\Omega} \Phi \cdot (\mathbf{n} \times \mathbf{u}) d^2r \quad (\text{A.3}^*)$$

which formally follows from equation (A.3) by expanding the double cross product according to (A.1d) and making use of the vector identity (A.1c).

Equalities (A.2) to (A.3*) apply to volume integrals. Another integral identity is required for the transformation of surface integrals. Let Σ be a surface in \mathbb{R}^3 with normal vector \mathbf{n} . Denote the outer normal vector on the boundary $\partial\Sigma$ by \mathbf{v} where $\mathbf{n} \cdot \mathbf{v} = 0$. A tangential vector on $\partial\Sigma$ is uniquely defined by $\boldsymbol{\tau} = \mathbf{n} \times \mathbf{v}$. Using the notation of the surface differential operators introduced above, Stoke's theorem (Monk, 2003, Corollary 3.21) can be stated as

$$\int_{\Sigma} \phi \operatorname{curl}_{\Sigma} \hat{\mathbf{u}} d^2r = \int_{\Sigma} \operatorname{curl}_{\Sigma} \phi \cdot \hat{\mathbf{u}} d^2r + \int_{\partial\Sigma} \phi \boldsymbol{\tau} \cdot \hat{\mathbf{u}} dr \quad (\text{A.4})$$

where $\hat{\mathbf{u}} = (\mathbf{n} \times \mathbf{u}) \times \mathbf{n}$ and ϕ are continuously differentiable functions on Σ . Relaxing the regularity assumptions on $\hat{\mathbf{u}}$ and ϕ and inserting the expressions (A.1g) and (A.1h) leads to the proposition that

$$\int_{\Sigma} \phi \mathbf{n} \cdot \operatorname{curl} \mathbf{u} d^2r = - \int_{\Sigma} (\mathbf{n} \times \operatorname{grad} u) \cdot ((\mathbf{n} \times \mathbf{u}) \times \mathbf{n}) d^2r + \int_{\partial\Sigma} \phi \boldsymbol{\tau} \cdot ((\mathbf{n} \times \mathbf{u}) \times \mathbf{n}) dr$$

for functions $\mathbf{u} \in H_{\text{curl}}(\Omega)$ and $\phi \in H_1(\Omega)$. Expansion of the double cross product, the vector identity $\mathbf{n} \cdot (\mathbf{n} \times \operatorname{grad} \phi) = 0$ and the orthogonality $\mathbf{n} \cdot \boldsymbol{\tau} = 0$ finally yield

$$\int_{\Sigma} \phi \mathbf{n} \cdot \operatorname{curl} \mathbf{u} d^2r = \int_{\Sigma} \operatorname{grad} \phi \cdot (\mathbf{n} \times \mathbf{u}) d^2r + \int_{\partial\Sigma} \phi \boldsymbol{\tau} \cdot \mathbf{u} dr. \quad (\text{A.4}^*)$$

B The mixed dielectric and conductive media case – A counterexample

The weak form of the E - V formulation has been derived in Chapter 2 under the assumption of a non-vanishing electric conductivity, $\sigma \neq 0$ in Ω . The rationale of this assumption will be given here. Note that in the following the inequality $\boldsymbol{\eta} \neq 0$ is to be understood for a tensor $\boldsymbol{\eta}$ in the sense of its non-vanishing eigenvalues.

The crucial point when stabilizing the vector Helmholtz equation of the E -field formulation for low frequencies is the proper choice of the divergence condition. The choice of $\text{div}(\sigma - i\omega\epsilon)E$ is consistent with the vector Helmholtz equation and eliminates the charge density as a variable. The complex current density $(\sigma - i\omega\epsilon)E$ is non-zero for all frequencies including $\omega = 0$ if, and only if, $\sigma \neq 0$. For a dielectric, where $\sigma \equiv 0$, the divergence condition vanishes at $\omega = 0$ and can consequently not be used to eliminate the kernel of the curl-operator. A dielectric requires that a divergence condition involving $\text{div} \epsilon E$ is enforced. This condition is non-trivial also at $\omega = 0$. The derivation of the weak form of the divergence condition leads to a technical problem if the domain contains both dielectric and conductive subdomains. A simple example will illustrate this issue.

Consider the domain Ω which is subdivided into two subdomains Ω_1 and Ω_2 as depicted in Figure B.1 such that the constitutive parameters are smooth within each subdomain and may be discontinuous at the interface Σ . The outer boundary of Ω will not be of interest during the following considerations. Denote by \mathbf{n} the surface normal vector on Σ pointing from Ω_1 to Ω_2 . The constitutive parameters and the electric field within each subdomain are marked by subscripts 1 and 2. In order to get a complete picture, all three possible combinations of a vanishing/non-vanishing conductivity within each of the subdomains will be examined in turn. For the sake of simplicity, the domain is assumed to be source free ($\mathbf{j}_s = \mathbf{0}$, $\mathbf{j}_f = \mathbf{0}$, $\rho = 0$).

$\sigma_1 \neq 0, \sigma_2 \neq 0$: The electric field has to satisfy the continuity equations and conditions

$$-\text{div}(\sigma_1 - i\omega\epsilon_1)E_1 = 0 \quad \text{in } \Omega_1, \quad (\text{B.1a})$$

$$-\text{div}(\sigma_2 - i\omega\epsilon_2)E_2 = 0 \quad \text{in } \Omega_2, \quad (\text{B.1b})$$

$$\mathbf{n} \cdot (\sigma_1 - i\omega\epsilon_1)E_1 = \mathbf{n} \cdot (\sigma_2 - i\omega\epsilon_2)E_2 \quad \text{on } \Sigma. \quad (\text{B.1c})$$

Multiplication by a test function ϕ and integration over Ω yields

$$\begin{aligned} & - \int_{\Omega_1} \bar{\phi} \text{div}(\sigma_1 - i\omega\epsilon_1)E_1 d^3r - \int_{\Omega_2} \bar{\phi} \text{div}(\sigma_2 - i\omega\epsilon_2)E_2 d^3r \\ &= \int_{\Omega_1} \text{grad } \bar{\phi} \cdot (\sigma_1 - i\omega\epsilon_1)E_1 d^3r + \int_{\Omega_2} \text{grad } \bar{\phi} \cdot (\sigma_2 - i\omega\epsilon_2)E_2 d^3r \\ & \quad - \int_{\Sigma} \bar{\phi} (\mathbf{n} \cdot (\sigma_1 - i\omega\epsilon_1)E_1 - \mathbf{n} \cdot (\sigma_2 - i\omega\epsilon_2)E_2) d^2r. \end{aligned} \quad (\text{B.2a})$$

Appendices

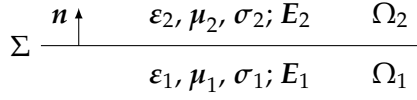


Figure B.1: Interface between two subdomains.

Note the opposite signs of the two terms in the surface integral. The normal vector \mathbf{n} is outward pointing for Ω_1 but inward pointing for Ω_2 . The surface integral vanishes thanks to the interface condition (B.1c). Combining the integrals leads to

$$\int_{\Omega} \bar{\phi} \operatorname{div} (\sigma - i\omega\epsilon) E d^3r = \int_{\Omega} \operatorname{grad} \bar{\phi} \cdot (\sigma - i\omega\epsilon) E d^3r \quad (\text{B.2b})$$

where

$$E = \begin{cases} E_1 & \text{in } \Omega_1, \\ E_2 & \text{in } \Omega_2 \end{cases} \quad (\text{B.2c})$$

and similarly for σ and ϵ . The continuity condition at Σ has been absorbed into the volume integral on the right hand side and will be enforced in the weak sense. The right hand side integral is well-defined if $\phi \in H_1(\Omega)$ and $E \in H_{\operatorname{curl}}(\Omega)$.

$\sigma_1 \equiv 0, \sigma_2 \equiv 0$: The electric field has to satisfy the continuity equations and conditions

$$-\operatorname{div} \epsilon_1 E_1 = 0 \quad \text{in } \Omega_1, \quad (\text{B.3a})$$

$$-\operatorname{div} \epsilon_2 E_2 = 0 \quad \text{in } \Omega_2, \quad (\text{B.3b})$$

$$\mathbf{n} \cdot \epsilon_1 E_1 = \mathbf{n} \cdot \epsilon_2 E_2 \quad \text{on } \Sigma. \quad (\text{B.3c})$$

Analogously to the previous case, multiplication by a test function ϕ and integration over Ω yields

$$\begin{aligned} & - \int_{\Omega_1} \bar{\phi} \operatorname{div} \epsilon_1 E_1 d^3r - \int_{\Omega_2} \bar{\phi} \operatorname{div} \epsilon_2 E_2 d^3r \\ &= \int_{\Omega_1} \operatorname{grad} \bar{\phi} \cdot \epsilon_1 E_1 d^3r + \int_{\Omega_2} \operatorname{grad} \bar{\phi} \cdot \epsilon_2 E_2 d^3r - \int_{\Sigma} \bar{\phi} (\mathbf{n} \cdot \epsilon_1 E_1 - \mathbf{n} \cdot \epsilon_2 E_2) d^2r. \end{aligned} \quad (\text{B.4a})$$

The surface integral again vanishes thanks to the interface condition (B.3c). Combining the integrals leads to

$$\int_{\Omega} \bar{\phi} \operatorname{div} \epsilon E d^3r = \int_{\Omega} \operatorname{grad} \bar{\phi} \cdot \epsilon E d^3r. \quad (\text{B.4b})$$

The continuity condition at Σ has been absorbed into the volume integral on the right hand side and will be enforced in the weak sense. The right hand side integral is well-defined if $\phi \in H_1(\Omega)$ and $E \in H_{\operatorname{curl}}(\Omega)$.

$\sigma_1 \equiv 0, \sigma_2 \neq 0$: The electric field has to satisfy the continuity equations and conditions

$$-\operatorname{div} \varepsilon_1 E_1 = 0 \quad \text{in } \Omega_1, \quad (\text{B.5a})$$

$$-\operatorname{div} (\sigma_2 - i\omega \varepsilon_2) E_2 = 0 \quad \text{in } \Omega_2, \quad (\text{B.5b})$$

$$-i\omega \mathbf{n} \cdot \varepsilon_1 E_1 = \mathbf{n} \cdot (\sigma_2 - i\omega \varepsilon_2) E_2 \quad \text{on } \Sigma. \quad (\text{B.5c})$$

If equation (B.5a) is considered as special case of equation (B.1a) the factor $-i\omega$ can and must be dropped in order to obtain a non-vanishing partial differential equation at $\omega = 0$. This factor is retained in the continuity condition (B.5c) which is a special case of equation (B.1a) and turns out to be the obstacle when deriving the weak form. Multiplication by a test function ϕ and integration over Ω yields

$$\begin{aligned} & - \int_{\Omega_1} \bar{\phi} \operatorname{div} \varepsilon_1 E_1 d^3r - \int_{\Omega_2} \bar{\phi} \operatorname{div} (\sigma_2 - i\omega \varepsilon_2) E_2 d^3r \\ &= \int_{\Omega_1} \operatorname{grad} \bar{\phi} \cdot \varepsilon_1 E_1 d^3r + \int_{\Omega_2} \operatorname{grad} \bar{\phi} \cdot (\sigma_2 - i\omega \varepsilon_2) E_2 d^3r \\ & \quad - \int_{\Sigma} \bar{\phi} (\mathbf{n} \cdot \varepsilon_1 E_1 - \mathbf{n} \cdot (\sigma_2 - i\omega \varepsilon_2) E_2) d^2r. \end{aligned} \quad (\text{B.6a})$$

Now, the surface integral does not vanish any more because the two terms differ by the factor of $-i\omega$ compared to the interface condition (B.5c). The definition of a composite parameter according to

$$\boldsymbol{\eta} = \begin{cases} \varepsilon_1 & \text{in } \Omega_1 \text{ and} \\ \sigma_2 - i\omega \varepsilon_2 & \text{in } \Omega_2 \end{cases} \quad (\text{B.6b})$$

allows for the combination of the volume integrals like in (B.2b) or (B.4b). Making use of (B.5c) leads to

$$\int_{\Omega} \bar{\phi} \operatorname{div} \boldsymbol{\eta} E d^3r = \int_{\Omega} \operatorname{grad} \bar{\phi} \cdot \boldsymbol{\eta} E d^3r - (1 + i\omega) \int_{\Sigma} \bar{\phi} \mathbf{n} \cdot \varepsilon_1 E_1 d^2r. \quad (\text{B.6c})$$

The continuity condition at Σ has not been absorbed into the volume integral on the right hand side but leaves a surface integral. If $\phi \in H_1(\Omega)$ and $E \in H_{\operatorname{curl}}(\Omega)$, only the right hand side volume integral is well-defined but not the surface integral. The normal trace of $\varepsilon_1 E_1$ on Σ is not well-defined for $E \in H_{\operatorname{curl}}(\Omega)$ even if ε_1 is a scalar and $\mathbf{n} \cdot \varepsilon_1 E_1 = \varepsilon_1 \mathbf{n} \cdot E_1$.

In conclusion, a variational form of the E - V formulation which is stable for $\omega \rightarrow 0$ cannot be found for the case of a mixed dielectric and conductive medium using the standard procedure. Enforcing different types of continuity equations within separate subdomains leads to a surface integral which cannot be made vanish by the physically correct interface condition. This surface integral is not well-defined since the standard function space $H_{\operatorname{curl}}(\Omega)$ does not provide the required regularity for the electric field.

C Removing a non-trivial normal cohomology space

C.1 The continuous problem

The E - V formulation has been introduced in Chapter 2 under the assumption that the Dirichlet boundary part Γ_e consists of exactly one connected but possibly empty part. If it is composed of $J > 1$ connected parts $\Gamma_{e,j}$, $j = 1, \dots, J$, the kernel of the curl-operator is not only spanned by functions $\text{grad } V$, where $V \in H_1(\Omega)$ and $V = 0$ on Γ_e , but by additional $J - 1$ functions spanning the normal cohomology space

$$K_N = \left\{ V_i \in H^1(\Omega) : \text{div}(\sigma - i\omega\epsilon) \text{grad } V_i = 0 \text{ in } \Omega \text{ and } V_i = \delta_{i,j} \text{ on } \Gamma_{e,j}, i = 1, \dots, J-1, j = 1, \dots, J \right\}. \quad (\text{C.1})$$

Its definition has been extended to non-zero frequencies in comparison to definition (2.16). While the first, infinite dimensional part of the kernel has been removed in Chapter 2 by enforcing the continuity equation within Ω , the normal cohomology space can be annihilated by additional boundary conditions. According to the dimension of K_N , the net current flow through $J - 1$ of the J Dirichlet boundary parts can be prescribed,

$$\int_{\Gamma_{e,j}} \mathbf{n} \cdot (\mathbf{j}_s + (\sigma - i\omega\epsilon)\mathbf{E}) d^2r = I_{s,j} \quad \text{for } j = 1, \dots, J-1, \quad (\text{C.2})$$

where $I_{s,j}$ denotes an exterior current entering the domain Ω through $\Gamma_{e,j}$. Note that the nature of the integral boundary condition allows for a locally varying normal current flow $\mathbf{n} \cdot (\mathbf{j}_s + (\sigma - i\omega\epsilon)\mathbf{E})$ which might even be positive on one part of $\Gamma_{e,j}$ and negative on another.

The net current flow through $\Gamma_{e,J}$ is not independent but follows from the continuity equation. It balances the current flow through $\partial\Omega \setminus \Gamma_{e,J}$,

$$0 = \int_{\Omega} \text{div}(\mathbf{j}_s + (\sigma - i\omega\epsilon)\mathbf{E}) d^3r = \int_{\partial\Omega} \mathbf{n} \cdot (\mathbf{j}_s + (\sigma - i\omega\epsilon)\mathbf{E}) d^2r,$$

hence,

$$-\int_{\Gamma_{e,J}} \mathbf{n} \cdot (\mathbf{j}_s + (\sigma - i\omega\epsilon)\mathbf{E}) d^2r = \int_{\Gamma_h} \mathbf{n} \cdot (\mathbf{j}_s + (\sigma - i\omega\epsilon)\mathbf{E}) d^2r + \sum_{j=1}^{J-1} I_{s,j}. \quad (\text{C.3})$$

In order to show that the additional boundary conditions (C.2) completely remove the kernel of the curl-operator, the boundary value problem (2.15) in terms of V is extended to the case of $J > 1$. The boundary condition (2.15d), $V = \text{const.}$ on Γ_e , translates to $V = C_j$ on $\Gamma_{e,j}$, $j = 1, \dots, J$, where $C_j \in \mathbb{C}$ are unknown constants. The kernel is spanned by functions $\mathbf{E} = \text{grad } V$ where V satisfies

$$\text{div } \sigma \text{ grad } V = 0 \quad \text{on } \Omega_i, \quad (\text{C.4a})$$

$$[V] = 0 \quad \text{on } \Sigma_{i,j}, \quad (\text{C.4b})$$

$$[\mathbf{n} \cdot \sigma \text{ grad } V] = 0 \quad \text{on } \Sigma_{i,j}, \quad (\text{C.4c})$$

$$V = C_j \quad \text{on } \Gamma_{e,j}, j = 1, \dots, J \quad (\text{C.4d})$$

$$\mathbf{n} \cdot \boldsymbol{\sigma} \text{ grad } V = 0 \quad \text{on } \Gamma_h. \quad (\text{C.4e})$$

The solution of this boundary value problem can be constructed by

$$V = \sum_{j=1}^J C_j \psi_j \quad (\text{C.5a})$$

where the functions ψ_j are a solution of boundary value problem (C.4) with $C_i = \delta_{i,j}$, $i, j = 1, \dots, J$. By construction,

$$\sum_{j=1}^J \psi_j \equiv 1 \quad (\text{C.5b})$$

holds on Γ_e . Since (C.4) is a potential problem, the maximum principle can be applied to proof that (C.5b) also holds in Ω and on Γ_h . This gives rise to the following decomposition

$$\begin{aligned} V &= \sum_{j=1}^{J-1} C_j \psi_j + C_J \psi_J \\ &= \sum_{j=1}^{J-1} C_j \psi_j + C_J \left(1 - \sum_{j=1}^{J-1} \psi_j \right) \\ &= C_J + \sum_{j=1}^{J-1} (C_j - C_J) \psi_j. \end{aligned} \quad (\text{C.5c})$$

Now, the boundary conditions (C.2) with $\mathbf{E} = \text{grad } V$, $\omega = 0$ and vanishing source terms require that V also satisfies

$$\int_{\Gamma_{e,j}} \mathbf{n} \cdot \boldsymbol{\sigma} \text{ grad } V \, d^2r = 0 \quad \text{for } j = 1, \dots, J-1. \quad (\text{C.5d})$$

Insertion of (C.5c) yields a system of linear equations

$$\begin{pmatrix} \int_{\Gamma_{e,1}} \mathbf{n} \cdot \boldsymbol{\sigma} \text{ grad } \psi_1 \, d^2r & \dots & \int_{\Gamma_{e,1}} \mathbf{n} \cdot \boldsymbol{\sigma} \text{ grad } \psi_{J-1} \, d^2r \\ \vdots & & \vdots \\ \int_{\Gamma_{e,J-1}} \mathbf{n} \cdot \boldsymbol{\sigma} \text{ grad } \psi_1 \, d^2r & \dots & \int_{\Gamma_{e,J-1}} \mathbf{n} \cdot \boldsymbol{\sigma} \text{ grad } \psi_{J-1} \, d^2r \end{pmatrix} \begin{pmatrix} C_1 - C_J \\ \vdots \\ C_{J-1} - C_J \end{pmatrix} = \begin{pmatrix} 0 \\ \vdots \\ 0 \end{pmatrix} \quad (\text{C.5e})$$

in terms of the unknown constants C_j . Its coefficient matrix is regular because the functions ψ_j , $j = 1, \dots, J-1$, are linearly independent. Equation (C.5e) consequently has only the trivial solution and $C_1 = \dots = C_{J-1} = C_J$. Consequently, $V \equiv C_J$ in Ω and its gradient vanishes. This completes the proof that the boundary conditions (C.2), in addition to the equation of continuity, remove the kernel of the curl-operator completely and stabilize the \mathbf{E} -field formulation for low frequencies.

The E - V formulation

Straightforward extension of the E - V formulation as presented in Chapter 2 to the case of a non-trivial normal cohomology space is most easily performed within the framework of the weak form. In section 2.3 of Chapter 2, the equation of continuity had been tested against all functions $\phi \in H^1(\Omega)$ with $\phi = 0$ on Γ_e . This set of test functions is exhaustive only if Γ_e consists of one connected, possibly empty, part, i. e., if $J \leq 1$. If $J > 1$, $J - 1$ additional test functions are required which correspond to the dimension of the normal cohomology space and the number of integral boundary conditions (C.2). Alas, choosing arbitrary but fixed functions $\psi_j \in H^1(\Omega)$, $j = 1, \dots, J - 1$, with $\psi_j = \delta_{i,j}$ on $\Gamma_{e,i}$, $i = 1, \dots, J$, the continuity equation is integrated as given by equations (2.28) to (2.30) where the test function ϕ is replaced by ψ_j . The only difference occurs with the boundary integrals which additionally give rise to a contribution from the j -th Dirichlet boundary part, where $\psi_j \equiv 1$. Similarly to equation (2.30),

$$\begin{aligned} - \sum_{i=1}^n \int_{\partial\Omega_i} \bar{\psi}_j \mathbf{n} \cdot (\mathbf{j}_s + (\sigma - i\omega\epsilon)\mathbf{E}) d^2r \\ = I_{s,j} - \int_{\Gamma_h} \text{grad } \bar{\psi}_j \cdot (\mathbf{n} \times \mathbf{H}_0) d^2r - \int_{\Gamma_h} (\mathbf{n} \times \text{grad } \bar{\psi}_j) \cdot (\lambda(\mathbf{n} \times \mathbf{E})) d^2r \end{aligned} \quad (\text{C.6a})$$

holds because

$$\begin{aligned} \int_{\Gamma_e} \bar{\psi}_j \mathbf{n} \cdot (\mathbf{j}_s + (\sigma - i\omega\epsilon)\mathbf{E}) d^2r &= \int_{\Gamma_{e,j}} \mathbf{n} \cdot (\mathbf{j}_s + (\sigma - i\omega\epsilon)\mathbf{E}) d^2r \\ &= I_{s,j}. \end{aligned} \quad (\text{C.6b})$$

In order to obtain a symmetric system, the vector Helmholtz equation is supplemented by the terms

$$\sum_{j=1}^{J-1} C_j \int_{\Omega} \bar{\Phi} \cdot ((\sigma - i\omega\epsilon) \text{grad } \psi_j) d^3r, \quad (\text{C.7a})$$

$$- \sum_{j=1}^{J-1} C_j \int_{\Gamma_h} (\mathbf{n} \times \bar{\Phi}) \cdot (\lambda(\mathbf{n} \times \text{grad } \psi_j)) d^2r \quad (\text{C.7b})$$

and the continuity equation by

$$- \sum_{j=1}^{J-1} C_j \int_{\Omega} \bar{\phi} \gamma \psi_j d^3r \quad (\text{C.7c})$$

which enlarge the unknown quantities of the boundary value problem by the $J - 1$ constants $C_j \in \mathbb{C}$, $j = 1, \dots, J - 1$. Now, the weak form of the E - V formulation reads

Search $\mathbf{E} \in \mathcal{U}$, $V \in \mathcal{V}$ and, if $J > 1$, constants $C_1, \dots, C_{J-1} \in \mathbb{C}$ such that

$$\int_{\Omega} \text{curl } \bar{\Phi} \cdot (\mu^{-1} \text{curl } \mathbf{E}) d^3r - i\omega \int_{\Omega} \bar{\Phi} \cdot ((\sigma - i\omega\epsilon) \mathbf{E}) d^3r$$

$$\begin{aligned}
 & + \int_{\Omega} \bar{\Phi} \cdot ((\sigma - i\omega\varepsilon) \operatorname{grad} V) \, d^3r + \sum_{j=1}^{J-1} C_j \int_{\Omega} \bar{\Phi} \cdot ((\sigma - i\omega\varepsilon) \operatorname{grad} \psi_j) \, d^3r \\
 & + i\omega \int_{\Gamma_h} (\mathbf{n} \times \bar{\Phi}) \cdot (\lambda (\mathbf{n} \times \mathbf{E})) \, d^2r - \int_{\Gamma_h} (\mathbf{n} \times \bar{\Phi}) \cdot (\lambda (\mathbf{n} \times \operatorname{grad} V)) \, d^2r \\
 & - \sum_{j=1}^{J-1} C_j \int_{\Gamma_h} (\mathbf{n} \times \bar{\Phi}) \cdot (\lambda (\mathbf{n} \times \operatorname{grad} \psi_j)) \, d^2r \\
 & = i\omega \int_{\Omega} \bar{\Phi} \cdot \mathbf{j}_s \, d^3r - i\omega \sum_{\substack{i,j=1 \\ i < j}}^n \int_{\Sigma_{i,j}} \bar{\Phi} \cdot \mathbf{j}_f \, d^2r - i\omega \int_{\Gamma_h} \bar{\Phi} \cdot (\mathbf{j}_f + \mathbf{n} \times \mathbf{H}_0) \, d^2r \quad (\text{C.8a})
 \end{aligned}$$

for all $\Phi \in \mathcal{U}_0$,

$$\begin{aligned}
 & \int_{\Omega} \operatorname{grad} \bar{\phi} \cdot ((\sigma - i\omega\varepsilon) \mathbf{E}) \, d^3r - \int_{\Omega} \bar{\phi} \gamma V \, d^3r - \sum_{j=1}^{J-1} C_j \int_{\Omega} \bar{\phi} \gamma \psi_j \, d^3r \\
 & - \int_{\Gamma_h} (\mathbf{n} \times \operatorname{grad} \bar{\phi}) \cdot (\lambda (\mathbf{n} \times \mathbf{E})) \, d^2r = - \int_{\Omega} \operatorname{grad} \bar{\phi} \cdot \mathbf{j}_s \, d^3r + \int_{\Gamma_h} \operatorname{grad} \bar{\phi} \cdot (\mathbf{n} \times \mathbf{H}_0) \, d^2r \quad (\text{C.8b})
 \end{aligned}$$

for all $\phi \in \mathcal{V}_0$ and, if $J > 1$,

$$\begin{aligned}
 & \int_{\Omega} \operatorname{grad} \bar{\psi}_j \cdot ((\sigma - i\omega\varepsilon) \mathbf{E}) \, d^3r - \int_{\Omega} \bar{\psi}_j \gamma V \, d^3r - \sum_{j=1}^{J-1} C_j \int_{\Omega} \bar{\psi}_j \gamma \psi_j \, d^3r \\
 & - \int_{\Gamma_h} (\mathbf{n} \times \operatorname{grad} \bar{\psi}_j) \cdot (\lambda (\mathbf{n} \times \mathbf{E})) \, d^2r \\
 & = I_{s,j} - \int_{\Omega} \operatorname{grad} \bar{\psi}_j \cdot \mathbf{j}_s \, d^3r + \int_{\Gamma_h} \operatorname{grad} \bar{\psi}_j \cdot (\mathbf{n} \times \mathbf{H}_0) \, d^2r \quad (\text{C.8c})
 \end{aligned}$$

for $j = 1, \dots, J-1$ where $\psi_j \in \mathcal{V}_j$ is fixed. The spaces of test and trial functions are defined by

$$\mathcal{U}_0 = \{\Phi \in H_{\operatorname{curl}}(\Omega) : \mathbf{n} \times \Phi = \mathbf{0} \text{ on } \Gamma_e\}, \quad (\text{C.8d})$$

$$\mathcal{U} = \{\mathbf{E} \in H_{\operatorname{curl}}(\Omega) : \mathbf{n} \times \mathbf{E} = \mathbf{n} \times \mathbf{E}_0 \text{ on } \Gamma_e\}, \quad (\text{C.8e})$$

$$\mathcal{V}_0 = \{\phi \in H_1(\Omega) : \phi = 0 \text{ on } \Gamma_e\}, \quad (\text{C.8f})$$

$$\mathcal{V}_j = \{\psi_j \in H_1(\Omega) : \psi_j = \delta_{i,j} \text{ on } \Gamma_{e,i}, i = 1, \dots, J\}, \quad (\text{C.8g})$$

$$\mathcal{V} = \mathcal{V}_0 \quad (\text{C.8h})$$

where

$$H_{\operatorname{curl}}(\Omega) = \{\mathbf{E} \in (L_2(\Omega))^3 : \operatorname{curl} \mathbf{E} \in (L_2(\Omega))^3\}, \quad (\text{C.8i})$$

$$H_1(\Omega) = \{V \in L_2(\Omega) : \operatorname{grad} V \in L_2(\Omega)\} \quad (\text{C.8j})$$

are the spaces of functions with a well-defined curl and gradient, respectively.

Appendices

Note that in contrast to the infinite number of test functions ϕ and the infinite dimension of the trial function space $H_1(\Omega)$, the number of test functions ψ_j and the number of unknown constants C_j is finite. This corresponds to the decomposition of the kernel of the curl-operator into an infinite dimensional part and its finite dimensional orthogonal complement using the $H_{\text{curl}}(\Omega)$ inner product, called the normal cohomology space.

If the variational problem (C.8) is to be a valid extension of the E -field formulation (2.27), all V and C_1, \dots, C_{J-1} have to be identical to zero. Inserting $\Phi = \text{grad } \phi$ and $\Phi = \text{grad } \psi_j$ as test functions in equation (C.8a), and using equations (C.8b) and (C.8c) produces the following boundary value problem:

Search $V \in \mathcal{V}$ and, if $J > 1$, constants $C_1, \dots, C_{J-1} \in \mathbb{C}$ such that

$$\begin{aligned} \int_{\Omega} \text{grad } \bar{\phi} \cdot ((\sigma - i\omega\epsilon) \text{grad } \tilde{V}) \, d^3r - i\omega \int_{\Omega} \bar{\phi} \gamma \tilde{V} \, d^3r \\ - \int_{\Gamma_h} (\mathbf{n} \times \text{grad } \bar{\phi}) \cdot (\lambda (\mathbf{n} \times \text{grad } \tilde{V})) \, d^2r = 0 \end{aligned} \quad (\text{C.9a})$$

holds for all $\phi \in \mathcal{V}_0$ and

$$\begin{aligned} \int_{\Omega} \text{grad } \bar{\psi}_j \cdot ((\sigma - i\omega\epsilon) \text{grad } \tilde{V}) \, d^3r - i\omega \int_{\Omega} \bar{\psi}_j \gamma \tilde{V} \, d^3r \\ - \int_{\Gamma_h} (\mathbf{n} \times \text{grad } \bar{\psi}_j) \cdot (\lambda (\mathbf{n} \times \text{grad } \tilde{V})) \, d^2r = I_{s,j} \end{aligned} \quad (\text{C.9b})$$

for $j = 1, \dots, J-1$ where $\psi_j \in \mathcal{V}_j$ is fixed and \tilde{V} is defined by

$$\tilde{V} = V + \sum_{j=1}^{J-1} C_j \psi_j. \quad (\text{C.9c})$$

The solution of this boundary value problem only vanishes if $I_{s,j} = 0$ for all $j = 1, \dots, J-1$. This requirement is not surprising at all. The net current flow $I_{s,j}$ through the Dirichlet boundary part $\Gamma_{e,j}$ has no analogue in the E -field formulation (2.27). It introduces a new source term into the E - V formulation. Both formulations can only be equivalent if $I_{s,j} = 0$.

Even if this assumption is met the class of problems covered by the E - V formulation (C.8) is enlarged by a number of important applications. Buried metallic objects can be modelled by a PEC surface, for example. However, current emitting electrodes which could be modelled by a PEC surface with non-zero net current flow lead to a non-vanishing auxiliary field \tilde{V} . The ensuing solution E of (C.8) does not satisfy Maxwell's equations any more.

There is one exception. boundary value problem (C.9) in terms of \tilde{V} can only derived from (C.8) if $\omega \neq 0$. If $\omega = 0$, insertion of $\Phi = \text{grad } \phi$ and $\Phi = \text{grad } \psi_j$ as test functions into equation (C.8a) produces a boundary value problem identical to (C.9) except for vanishing source terms, $I_{s,j} = 0$ for

all $j = 1, \dots, J-1$. Equations (C.8b) and (C.8b) have not been used. Consequently, $\tilde{V} \equiv 0$ for $\omega = 0$ and E is a valid solution of the static Maxwell's equations. boundary value problem (C.9) could be used, e. g., to compute the electric field of direct current problem settings with electrodes of finite extension. The numerical solution of the general boundary value problem (C.9) covering all frequencies is, of course, far more expensive than the solution of a zero or low frequency specialized boundary value problem in terms of the electric scalar potential only.

C.2 The discrete problem

Finite element approximation

The discrete problem is derived by the finite element method as described in Chapter 3. Basically, the infinite dimensional function spaces $H_{\text{curl}}(\Omega)$ and $H_1(\Omega)$ are approximated by finite dimensional, piecewise polynomial spaces $\mathcal{P}_{\text{curl}}(\Omega)$ and $\mathcal{P}_1(\Omega)$. The weak form (C.8) consequently reads

Search $E_h \in \mathcal{U}_h$, $V_h \in \mathcal{V}_h$ and, if $J > 1$, constants $C_1, \dots, C_{J-1} \in \mathbb{C}$ such that

$$\begin{aligned} & \int_{\Omega} \text{curl } \overline{\Phi}_h \cdot (\mu^{-1} \text{curl } E_h) d^3r - i\omega \int_{\Omega} \overline{\Phi}_h \cdot ((\sigma - i\omega\epsilon) E_h) d^3r \\ & + \int_{\Omega} \overline{\Phi}_h \cdot ((\sigma - i\omega\epsilon) \text{grad } V_h) d^3r + \sum_{j=1}^{J-1} C_j \int_{\Omega} \overline{\Phi}_h \cdot ((\sigma - i\omega\epsilon) \text{grad } \psi_j) d^3r \\ & + i\omega \int_{\Gamma_h} (\mathbf{n} \times \overline{\Phi}_h) \cdot (\lambda (\mathbf{n} \times E_h)) d^2r - \int_{\Gamma_h} (\mathbf{n} \times \overline{\Phi}_h) \cdot (\lambda (\mathbf{n} \times \text{grad } V_h)) d^2r \\ & - \sum_{j=1}^{J-1} C_j \int_{\Gamma_h} (\mathbf{n} \times \overline{\Phi}_h) \cdot (\lambda (\mathbf{n} \times \text{grad } \psi_j)) d^2r \\ & = i\omega \int_{\Omega} \overline{\Phi}_h \cdot \mathbf{j}_s d^3r - i\omega \sum_{\substack{i,j=1 \\ i < j}}^n \int_{\Sigma_{i,j}} \overline{\Phi}_h \cdot \mathbf{j}_f d^2r - i\omega \int_{\Gamma_h} \overline{\Phi}_h \cdot (\mathbf{j}_f + \mathbf{n} \times \mathbf{H}_0) d^2r \quad (\text{C.10a}) \end{aligned}$$

for all $\Phi_h \in \mathcal{U}_{h,0}$,

$$\begin{aligned} & \int_{\Omega} \text{grad } \overline{\phi}_h \cdot ((\sigma - i\omega\epsilon) E_h) d^3r - \int_{\Omega} \overline{\phi}_h \gamma V_h d^3r - \sum_{j=1}^{J-1} C_j \int_{\Omega} \overline{\phi}_h \gamma \psi_j d^3r \\ & - \int_{\Gamma_h} (\mathbf{n} \times \text{grad } \overline{\phi}_h) \cdot (\lambda (\mathbf{n} \times E_h)) d^2r \\ & = - \int_{\Omega} \text{grad } \overline{\phi}_h \cdot \mathbf{j}_s d^3r + \int_{\Gamma_h} \text{grad } \overline{\phi}_h \cdot (\mathbf{n} \times \mathbf{H}_0) d^2r \quad (\text{C.10b}) \end{aligned}$$

for all $\phi_h \in \mathcal{V}_{h,0}$ and, if $J > 1$,

Appendices

$$\begin{aligned}
& \int_{\Omega} \text{grad } \bar{\psi}_j \cdot ((\sigma - i\omega\varepsilon) \mathbf{E}_h) d^3r - \int_{\Omega} \bar{\psi}_j \gamma V_h d^3r - \sum_{j=1}^{J-1} C_j \int_{\Omega} \bar{\psi}_j \gamma \psi_j d^3r \\
& - \int_{\Gamma_h} (\mathbf{n} \times \text{grad } \bar{\psi}_j) \cdot (\lambda (\mathbf{n} \times \mathbf{E}_h)) d^2r \\
& = I_{s,j} - \int_{\Omega} \text{grad } \bar{\psi}_j \cdot \mathbf{j}_s d^3r + \int_{\Gamma_h} \text{grad } \bar{\psi}_j \cdot (\mathbf{n} \times \mathbf{H}_0) d^2r \quad (\text{C.10c})
\end{aligned}$$

for $j = 1, \dots, J-1$ where $\psi_j \in \mathcal{V}_{h,j}$ is fixed. The spaces of test and trial functions are defined by

$$\mathcal{U}_{h,0} = \{\mathbf{\Phi}_h \in \mathcal{P}_{\text{curl}}(\Omega) : \mathbf{n} \times \mathbf{\Phi}_h = \mathbf{0} \text{ on } \Gamma_e\}, \quad (\text{C.10d})$$

$$\mathcal{U}_h = \{\mathbf{E}_h \in \mathcal{P}_{\text{curl}}(\Omega) : \mathbf{n} \times \mathbf{E}_h = \mathbf{n} \times \mathbf{E}_0 \text{ on } \Gamma_e\}, \quad (\text{C.10e})$$

$$\mathcal{V}_{h,0} = \{\phi_h \in \mathcal{P}_1(\Omega) : \phi_h = 0 \text{ on } \Gamma_e\}, \quad (\text{C.10f})$$

$$\mathcal{V}_{h,j} = \{\psi_j \in \mathcal{P}_1(\Omega) : \psi_j = \delta_{i,j} \text{ on } \Gamma_{e,i}, i = 1, \dots, J\}, \quad (\text{C.10g})$$

$$\mathcal{V}_h = \mathcal{V}_{h,0} \quad (\text{C.10h})$$

where

$$\mathcal{P}_{\text{curl}}(\Omega) = \{\mathbf{E}_h \in (L_2(\Omega))^3 : \text{curl } \mathbf{E}_h \in (L_2(\Omega))^3, \mathbf{E}_h|_K \text{ polynomial}\}, \quad (\text{C.10i})$$

$$\mathcal{P}_1(\Omega) = \{V_h \in L_2(\Omega) : \text{grad } V_h \in L_2(\Omega), V_h|_K \text{ polynomial}\} \quad (\text{C.10j})$$

are the spaces of elementwise polynomial functions with a well-defined curl and gradient, respectively.

If $\{\mathbf{\Phi}_i\}_{i=1}^N$ forms a basis of $\mathcal{P}_{\text{curl}}(\Omega)$ and $\{\phi_i\}_{i=1}^M$ a basis of $\mathcal{P}_1(\Omega)$, the finite element approximation of the electric field \mathbf{E} and the auxiliary field V can be expressed by

$$\mathbf{E}_h(\mathbf{r}) = \sum_{i=1}^N E_i \mathbf{\Phi}_i(\mathbf{r}) \quad \text{and} \quad (\text{C.11a})$$

$$V_h(\mathbf{r}) = \sum_{i=1}^M V_i \phi_i(\mathbf{r}). \quad (\text{C.11b})$$

The basis functions are sorted such that the set $\{\mathbf{\Phi}_i\}_{i=1}^n, n \leq N$, forms a basis of $\mathcal{U}_{h,0}$, i.e., $\mathbf{n} \times \mathbf{\Phi}_i = \mathbf{0}$, $i = 1, \dots, n$, on Γ_e , and the set $\{\phi_i\}_{i=1}^m, m \leq M$, forms a basis of $\mathcal{V}_{h,0}$, i.e., $\phi_i = 0$, $i = 1, \dots, m$, on Γ_e . The coefficients E_i and V_i of the remaining basis functions $\mathbf{\Phi}_i, i = n+1, \dots, N$, and $\phi_i, i = m+1, \dots, M$, have to be fixed in order to ensure $\mathbf{E}_h \in \mathcal{U}_h$ and $V_h \in \mathcal{V}_h$, i.e., to enforce the Dirichlet boundary conditions.

Since the additional test functions $\psi_j, j = 1, \dots, J-1$, are arbitrary but fixed functions from $H_1(\Omega)$ the approximation of $H_1(\Omega)$ by $\mathcal{P}_1(\Omega)$ is irrelevant for ψ_j . Therefore, the assumption $\psi_j \in \mathcal{P}_1(\Omega)$ allows for a basis function expansion of the form

$$\psi_j(\mathbf{r}) = \sum_{i=1}^M \alpha_{i,j} \phi_i(\mathbf{r}) \quad (\text{C.12a})$$

where the coefficients $\alpha_{i,j}$ have to be chosen such that $\psi_j = \delta_{i,j}$ on $\Gamma_{e,i}$ for $i = 1, \dots, J$. Given the linear mapping \mathcal{A}_i which maps the scalar field V onto its degrees of freedom V_i the coefficients $\alpha_{i,j}$ are determined by

$$\alpha_{i,j} = \mathcal{A}_i\{H_j\} \quad \text{where} \quad H_j(\mathbf{r}) = \begin{cases} 1 & \text{if } \mathbf{r} \in \Gamma_{e,j}, \\ 0 & \text{if } \mathbf{r} \in \overline{\Omega} \setminus \Gamma_{e,j} \end{cases} \quad (\text{C.12b})$$

for $i = 1, \dots, M, j = 1, \dots, J - 1$. The projection (C.12b) is exact, i. e., $\psi_j \equiv 1$ on $\Gamma_{e,j}$ for any reasonable finite element space $\mathcal{P}_1(\Omega)$ which contains the constant function.

Inserting the trial functions (C.11a) and (C.11b) into the variational integrals (C.10a), (C.10b) and (C.10c), and taking the j -th basis function Φ_j, ϕ_j, ψ_j , respectively, as the test function produces the j -th row of a system of linear equations in terms of the unknown linear coefficients E_i, V_i and C_i ,

$$\sum_{i=1}^n a_{j,i}^{(\Phi,\Phi)} E_i + \sum_{i=1}^m a_{j,i}^{(\Phi,\phi)} V_i + \sum_{i=1}^{J-1} a_{j,i}^{(\Phi,\psi)} C_i = f_j^{(\Phi)}, \quad j = 1, \dots, n, \quad (\text{C.13a})$$

$$\sum_{i=1}^n a_{j,i}^{(\phi,\Phi)} E_i + \sum_{i=1}^m a_{j,i}^{(\phi,\phi)} V_i + \sum_{i=1}^{J-1} a_{j,i}^{(\phi,\psi)} C_i = f_j^{(\phi)}, \quad j = 1, \dots, m, \quad (\text{C.13b})$$

$$\sum_{i=1}^n a_{j,i}^{(\psi,\Phi)} E_i + \sum_{i=1}^m a_{j,i}^{(\psi,\phi)} V_i + \sum_{i=1}^{J-1} a_{j,i}^{(\psi,\psi)} C_i = f_j^{(\psi)}, \quad j = 1, \dots, J - 1, \quad (\text{C.13c})$$

where

$$\begin{aligned} a_{j,i}^{(\Phi,\Phi)} = & \int_{\Omega} \text{curl } \overline{\Phi}_j \cdot \left(\mu^{-1} \text{curl } \Phi_i \right) d^3r - i\omega \int_{\Omega} \overline{\Phi}_j \cdot ((\sigma - i\omega\epsilon)\Phi_i) d^3r \\ & + i\omega \int_{\Gamma_h} (\mathbf{n} \times \overline{\Phi}_j) \cdot (\lambda(\mathbf{n} \times \Phi_i)) d^2r, \end{aligned} \quad (\text{C.13d})$$

$$a_{j,i}^{(\Phi,\phi)} = \int_{\Omega} \overline{\Phi}_j \cdot ((\sigma - i\omega\epsilon) \text{grad } \phi_i) d^3r - \int_{\Gamma_h} (\mathbf{n} \times \overline{\Phi}_j) \cdot (\lambda(\mathbf{n} \times \text{grad } \phi_i)) d^2r, \quad (\text{C.13e})$$

$$\begin{aligned} a_{j,i}^{(\Phi,\psi)} = & \int_{\Omega} \overline{\Phi}_j \cdot ((\sigma - i\omega\epsilon) \text{grad } \psi_i) d^3r - \int_{\Gamma_h} (\mathbf{n} \times \overline{\Phi}_j) \cdot (\lambda(\mathbf{n} \times \text{grad } \psi_i)) d^2r \\ = & \sum_{k=m+1}^M a_{j,k}^{(\Phi,\phi)} \alpha_{k,i}, \end{aligned} \quad (\text{C.13f})$$

$$a_{j,i}^{(\phi,\Phi)} = \int_{\Omega} \text{grad } \overline{\phi}_j \cdot ((\sigma - i\omega\epsilon)\Phi_i) d^3r - \int_{\Gamma_h} (\mathbf{n} \times \text{grad } \overline{\phi}_j) \cdot (\lambda(\mathbf{n} \times \Phi_i)) d^2r, \quad (\text{C.13g})$$

$$a_{j,i}^{(\phi,\phi)} = - \int_{\Omega} \overline{\phi}_j \gamma \phi_i d^3r \quad (\text{C.13h})$$

Appendices

$$\begin{aligned}
a_{j,i}^{(\phi,\psi)} &= - \int_{\Omega} \bar{\phi}_j \gamma \psi_i d^3r \\
&= \sum_{k=m+1}^M a_{j,k}^{(\phi,\phi)} \alpha_{k,i},
\end{aligned} \tag{C.13i}$$

$$\begin{aligned}
a_{j,i}^{(\psi,\Phi)} &= \int_{\Omega} \text{grad } \bar{\psi}_j \cdot ((\sigma - i\omega\epsilon) \Phi_i) d^3r - \int_{\Gamma_h} (\mathbf{n} \times \text{grad } \bar{\psi}_j) \cdot (\lambda (\mathbf{n} \times \Phi_i)) d^2r \\
&= \sum_{l=m+1}^M \alpha_{l,j} a_{l,i}^{(\phi,\Phi)},
\end{aligned} \tag{C.13j}$$

$$\begin{aligned}
a_{j,i}^{(\psi,\phi)} &= - \int_{\Omega} \bar{\psi}_j \gamma \phi_i d^3r \\
&= \sum_{l=m+1}^M \alpha_{l,j} a_{l,i}^{(\phi,\phi)},
\end{aligned} \tag{C.13k}$$

$$\begin{aligned}
a_{j,i}^{(\psi,\psi)} &= - \int_{\Omega} \bar{\psi}_j \gamma \psi_i d^3r \\
&= \sum_{k,l=m+1}^M \alpha_{l,j} a_{l,k}^{(\phi,\phi)} \alpha_{k,i}
\end{aligned} \tag{C.13l}$$

and

$$\begin{aligned}
f_j^{(\Phi)} &= i\omega \int_{\Omega} \bar{\Phi}_j \cdot \mathbf{j}_s d^3r - i\omega \sum_{\substack{i,j=1 \\ i < j}}^n \int_{\Sigma_{i,j}} \bar{\Phi}_j \cdot \mathbf{j}_f d^2r - i\omega \int_{\Gamma_h} \bar{\Phi}_j \cdot (\mathbf{j}_f + \mathbf{n} \times \mathbf{H}_0) d^2r \\
&\quad - \sum_{i=n+1}^N a_{j,i}^{(\Phi,\Phi)} E_i - \sum_{i=m+1}^M a_{j,i}^{(\Phi,\phi)} V_i,
\end{aligned} \tag{C.13m}$$

$$\begin{aligned}
f_j^{(\phi)} &= - \int_{\Omega} \text{grad } \bar{\phi}_j \cdot \mathbf{j}_s d^3r + \int_{\Gamma_h} \text{grad } \bar{\phi}_j \cdot (\mathbf{n} \times \mathbf{H}_0) d^2r \\
&\quad - \sum_{i=n+1}^N a_{j,i}^{(\phi,\Phi)} E_i - \sum_{i=m+1}^M a_{j,i}^{(\phi,\phi)} V_i,
\end{aligned} \tag{C.13n}$$

$$\begin{aligned}
f_j^{(\psi)} &= -I_{s,j} - \int_{\Omega} \text{grad } \bar{\psi}_j \cdot \mathbf{j}_s d^3r + \int_{\Gamma_h} \text{grad } \bar{\psi}_j \cdot (\mathbf{n} \times \mathbf{H}_0) d^2r \\
&\quad - \sum_{i=n+1}^N a_{j,i}^{(\psi,\Phi)} E_i - \sum_{i=m+1}^M a_{j,i}^{(\psi,\phi)} V_i \\
&= -I_{s,j} + \sum_{l=m+1}^M \alpha_{l,j} f_l^{(\phi)}.
\end{aligned} \tag{C.13o}$$

Summarizing all equations the overall system of linear equations reads in matrix notation as follows

$$\begin{pmatrix}
 a_{1,1}^{(\Phi,\Phi)} & \dots & a_{1,n}^{(\Phi,\Phi)} & a_{1,1}^{(\Phi,\phi)} & \dots & a_{1,m}^{(\Phi,\phi)} & a_{1,1}^{(\Phi,\psi)} & \dots & a_{1,J-1}^{(\Phi,\psi)} \\
 \vdots & & \vdots & \vdots & & \vdots & \vdots & & \vdots \\
 a_{n,1}^{(\Phi,\Phi)} & \dots & a_{n,n}^{(\Phi,\Phi)} & a_{n,1}^{(\Phi,\phi)} & \dots & a_{n,m}^{(\Phi,\phi)} & a_{n,1}^{(\Phi,\psi)} & \dots & a_{n,J-1}^{(\Phi,\psi)} \\
 a_{1,1}^{(\phi,\Phi)} & \dots & a_{1,n}^{(\phi,\Phi)} & a_{1,1}^{(\phi,\phi)} & \dots & a_{1,m}^{(\phi,\phi)} & a_{1,1}^{(\phi,\psi)} & \dots & a_{1,J-1}^{(\phi,\psi)} \\
 \vdots & & \vdots & \vdots & & \vdots & \vdots & & \vdots \\
 a_{m,1}^{(\phi,\Phi)} & \dots & a_{m,n}^{(\phi,\Phi)} & a_{m,1}^{(\phi,\phi)} & \dots & a_{m,m}^{(\phi,\phi)} & a_{m,1}^{(\phi,\psi)} & \dots & a_{m,J-1}^{(\phi,\psi)} \\
 a_{1,1}^{(\psi,\Phi)} & \dots & a_{1,n}^{(\psi,\Phi)} & a_{1,1}^{(\psi,\phi)} & \dots & a_{1,m}^{(\psi,\phi)} & a_{1,1}^{(\psi,\psi)} & \dots & a_{1,J-1}^{(\psi,\psi)} \\
 \vdots & & \vdots & \vdots & & \vdots & \vdots & & \vdots \\
 a_{J-1,1}^{(\psi,\Phi)} & \dots & a_{J-1,n}^{(\psi,\Phi)} & a_{J-1,1}^{(\psi,\phi)} & \dots & a_{J-1,m}^{(\psi,\phi)} & a_{J-1,1}^{(\psi,\psi)} & \dots & a_{J-1,J-1}^{(\psi,\psi)}
 \end{pmatrix} \times \begin{pmatrix} E_1 \\ \vdots \\ E_n \\ V_1 \\ \vdots \\ V_m \\ C_1 \\ \vdots \\ C_{J-1} \end{pmatrix} = \begin{pmatrix} f_1^{(\Phi)} \\ \vdots \\ f_n^{(\Phi)} \\ f_1^{(\phi)} \\ \vdots \\ f_m^{(\phi)} \\ f_1^{(\psi)} \\ \vdots \\ f_{J-1}^{(\psi)} \end{pmatrix}. \quad (\text{C.13p})$$

This system of equations is the straightforward extension of system (3.11i) to the case of a boundary with $J > 1$ connected Dirichlet parts by $J - 1$ additional unknowns and equations. The matrix in (C.13i) has the same properties as the matrix in (3.11i).

C.3 Numerical experiments

Similar to the numerical experiments described in section 3.5 of Chapter 3, additional numerical tests have been devised in order to give numerical evidence for the correctness of the theoretical considerations outlined in the previous sections.

Dimension of the normal cohomology space

In section 3.5.4 the compatibility of the polynomial spaces which are used to approximate E and V had been examined by the singular decomposition of the finite element system matrix. This experiment is now extended to the case of a Dirichlet boundary which consists of two disjoint parts.

Appendices

As in Chapter 3, the domain $\Omega = [-1, 1]^3 \text{ m}^3$ is discretized by a regular hexahedral grid with 2^3 elements, i. e., there is exactly one interior vertex. Ω is covered by a homogeneous medium of electrical conductivity $\sigma = 0.01 \text{ S/m}$ and relative magnetic permeability $\mu_r = 1$. The relative electrical permittivity is irrelevant because only frequency $f = 0$ is considered for this test problem. Here, vanishing tangential electric field components are imposed as a homogeneous Dirichlet boundary condition only on the two $+z$ - and $-z$ -directed boundary faces of $\partial\Omega$. A homogeneous Neumann boundary condition is imposed on the $\pm x$ - and $\pm y$ -directed boundary faces. Therefore, the Dirichlet boundary part Γ_e consists of two disjoint parts.

The electric field E and the scalar field V are approximated by piecewise quadratic basis functions ($p = 2$). This results in 220 degrees of freedom for E and 76 degrees of freedom for V , excluding the fixed boundary values. Note that, compared to the experiment in section 3.5.4, the different setup of boundary conditions leads to a different number of degrees of freedom.

The kernel of the curl-operator now not only consists of the gradient of a scalar field V which vanishes on Γ_e , but contains one additional function which can be fixed by prescribing the electric current flow through one of the Dirichlet boundary parts. Figure C.1 displays the singular values of the resulting finite element system matrices if only the E -field formulation is used (a), or if the E - V formulation is used and the total current flow is prescribed through none (b), one (c) or both (d) Dirichlet boundary parts.

Only case (c) results in a regular finite element system matrix. The rank deficiency of 76 caused by the kernel of the curl-operator is resolved by enhancing the discrete problem by 76 additional equations reflecting the equation of continuity. Therefore, the well posed problem has 296 degrees of freedom, subdivided into 220 for the electric field and 76 for the scalar field. If in case (b) a scalar field is considered which vanishes on all of Γ_e , there are only additional 75 equations. The total current flow through one of the boundaries is required as one additional condition to render the problem well-posed. If the current flow is prescribed for the second Dirichlet boundary part as well, the resulting system is again singular. The additional equation is not linearly independent of the others.

Low frequency stability

In order to show that the E - V formulation is stable at low frequencies also for the case of a non-trivial cohomology space, the numerical experiment described in section 3.5.5 of Chapter 3 has been repeated. The test suite is extended by a third set of boundary conditions which is a mixture of the purely Dirichlet or purely Neumann boundary conditions considered there. Here, the inhomogeneous Dirichlet boundary condition is prescribed only on the two $+z$ - and $-z$ -directed boundary faces and the inhomogeneous Neumann boundary condition on the $\pm x$ - and $\pm y$ -directed boundary faces. Therefore, the Dirichlet boundary part Γ_e consists of two disjoint parts and an integral boundary condition of the type (C.2) is applied on the $-z$ -directed boundary face $\Gamma_{e,1}$. The mixture of Dirichlet and Neumann boundary conditions will shortly be called the mixed boundary case in the following. This should not be confused with an actual mixed boundary condition.

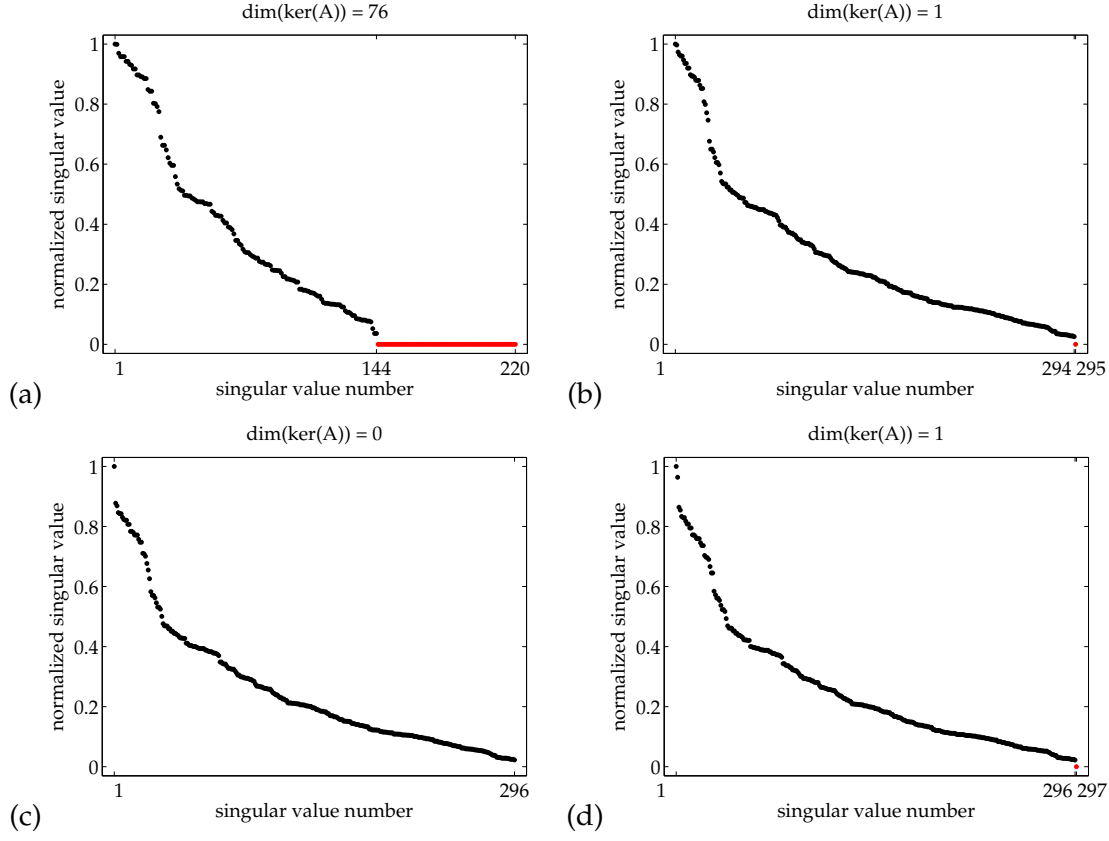


Figure C.1: Singular values of the finite element system matrix A at frequency $\omega = 0$ for the E -field formulation (a) and the E - V formulation where the total current flow is prescribed through none (b), one (c) and two (d) of the two disjoint Dirichlet boundary parts.

The 1-norm matrix condition number for the finite element matrices is depicted as a function of frequency in Figures C.2 and C.3 and should be compared to Figures 3.20 and 3.21. The condition number of the mixed boundary case exhibits the same behavior like the condition number of the Dirichlet boundary case. Since the Dirichlet boundary part is not empty, the finite element matrix of the E - V formulation ‘Laplace, mixed’ does not show the singular behavior of the Neumann boundary condition case.

The relative solution error of the constant current density test case is depicted in Figures C.4 and C.5. It agrees well with the relative solution error for the other boundary condition types in Figures 3.23 and 3.24. The electric field of the constant current density is a special case of the E - V formulation (C.10). Since $I_{s,1} = -1 \text{ A} \neq 0$ the auxiliary scalar field V does not vanish. However, the property $\text{curl } E \equiv 0$ renders $E = -\text{grad } V / i\omega$ the correct solution of Maxwell’s equations.

The plane wave test case satisfies the assumption $I_{s,1} = 0$. Figures C.6/C.7 and C.8/C.9 show the relative solution error for a piecewise quadratic and linear approximation. Their counterparts for the other boundary conditions are depicted in Figures 3.25/3.26 and 3.27/3.28. The relative errors

Appendices

of the mixed boundary case compare best with the Neumann boundary case of Chapter 3. There is one exception. The relative error of the electric field is bounded from below by circa 10^{-3} for the tetrahedral mesh. The error bound is of the same order of magnitude for both the fullspace and the halfspace model as well as for $p = 1$ and 2. However, the relative error of the curl agrees with the results of the Neumann boundary condition. This indicates that E is spoiled by the gradient of a scalar field whose origin seems to be connected with the unstructured tetrahedral mesh since the effect is not observed with the hexahedral mesh. Examination of the numerical solution indeed shows that the electric field computed on the tetrahedral mesh has a non-physical, constant and non-vanishing z -component. This component is proportional to the total electric field energy within Ω and, therefore, produces a frequency independent solution error level.

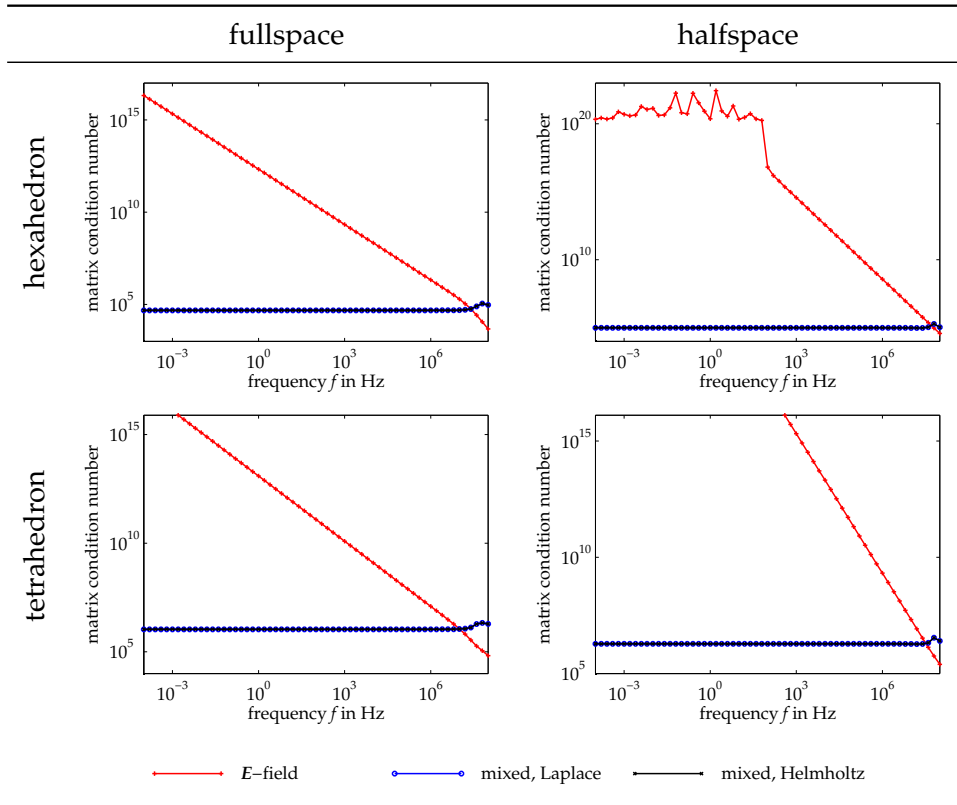


Figure C.2: 1-norm matrix condition number for both test cases ‘constant current density’ and ‘plane wave’ with symmetric matrix scaling; mixed boundary case, Dirichlet and Neumann boundary conditions.

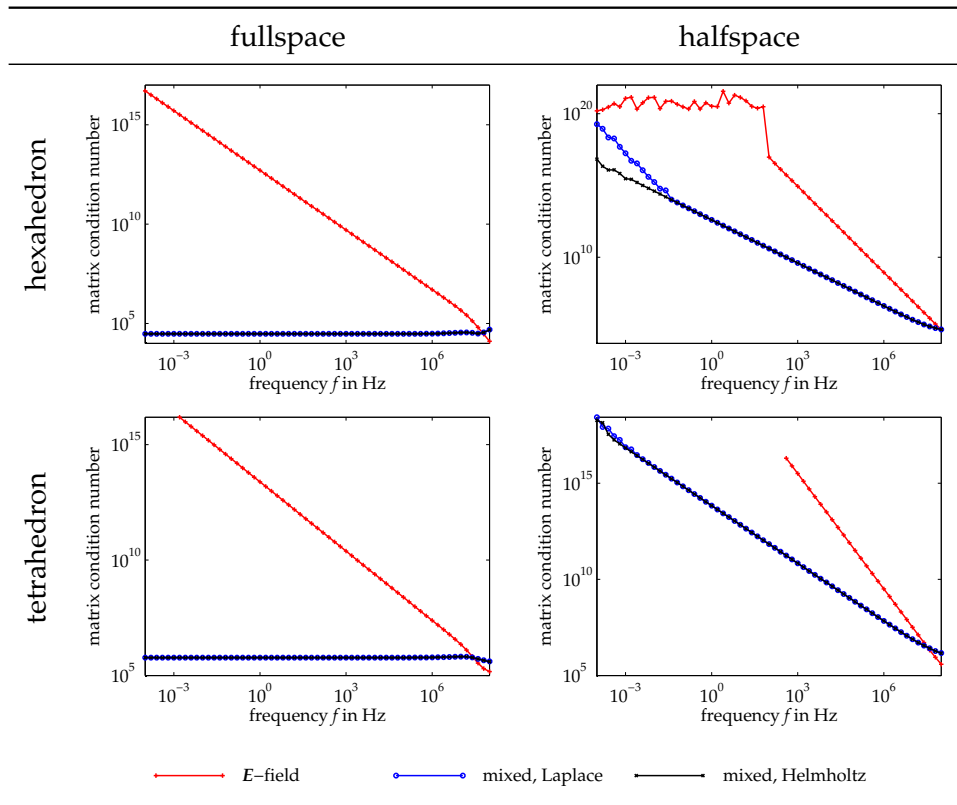


Figure C.3: 1-norm matrix condition number for both test cases 'constant current density' and 'plane wave' without symmetric matrix scaling; mixed boundary case, Dirichlet and Neumann boundary conditions.

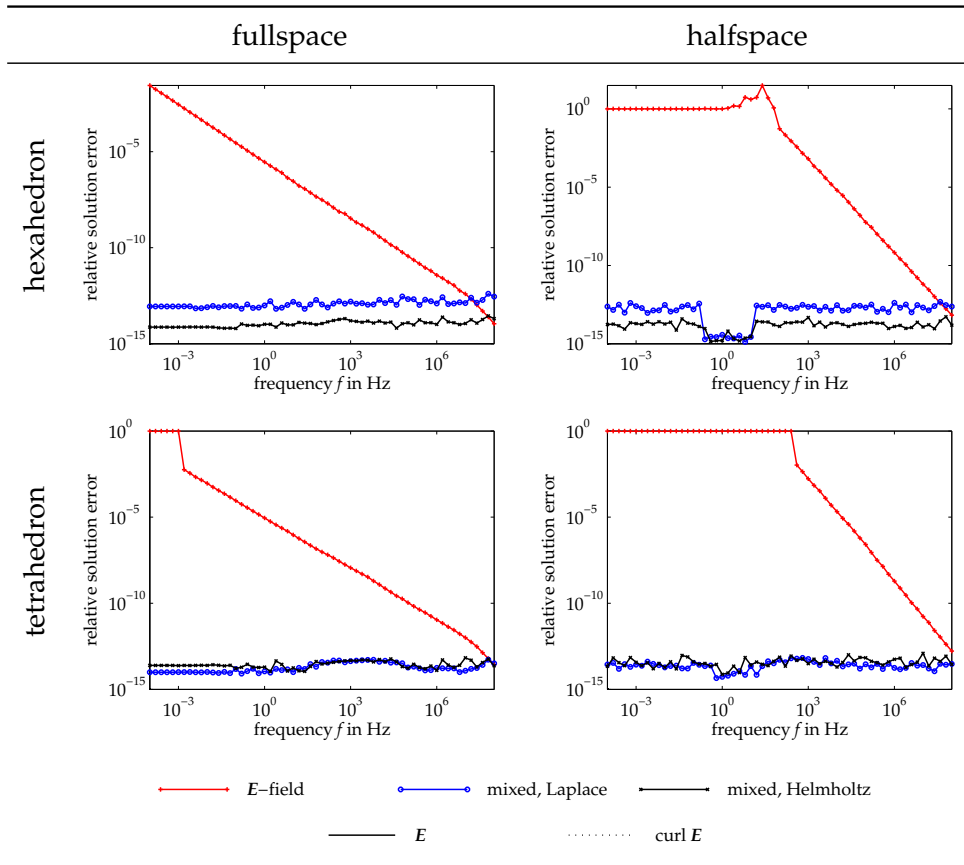


Figure C.4: Relative solution error for test case 'constant current density' with symmetric matrix scaling; mixed boundary case, Dirichlet and Neumann boundary conditions.

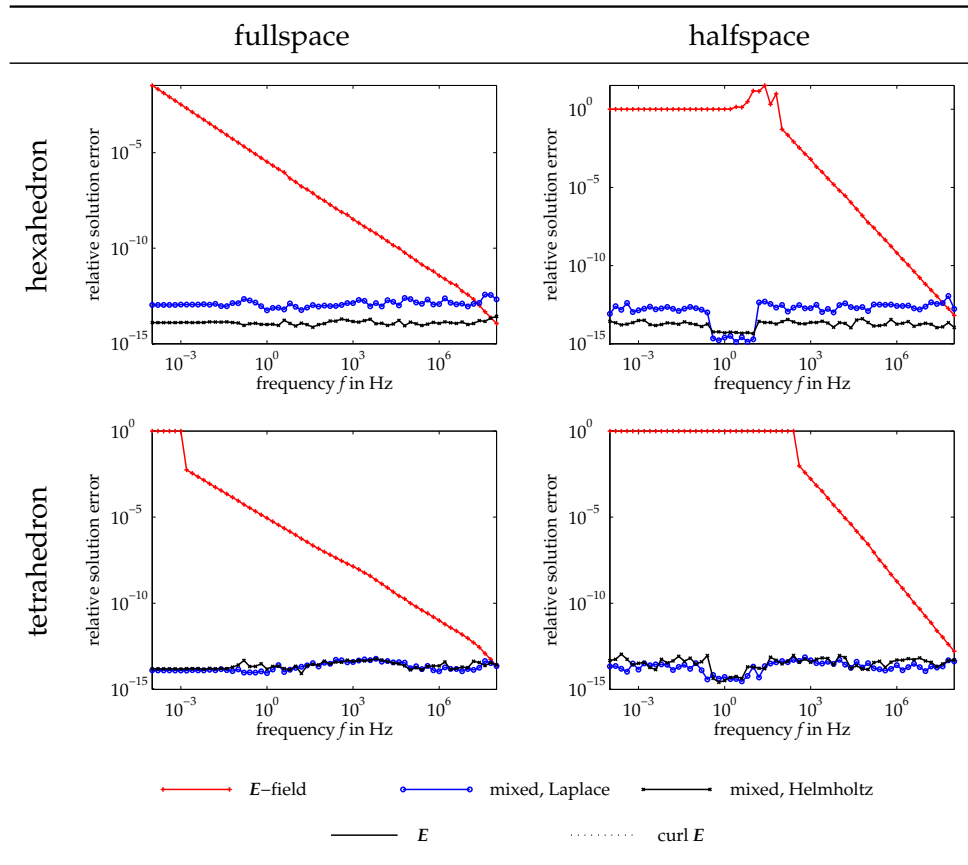


Figure C.5: Relative solution error for test case ‘constant current density’ without symmetric matrix scaling; mixed boundary case, Dirichlet and Neumann boundary conditions.

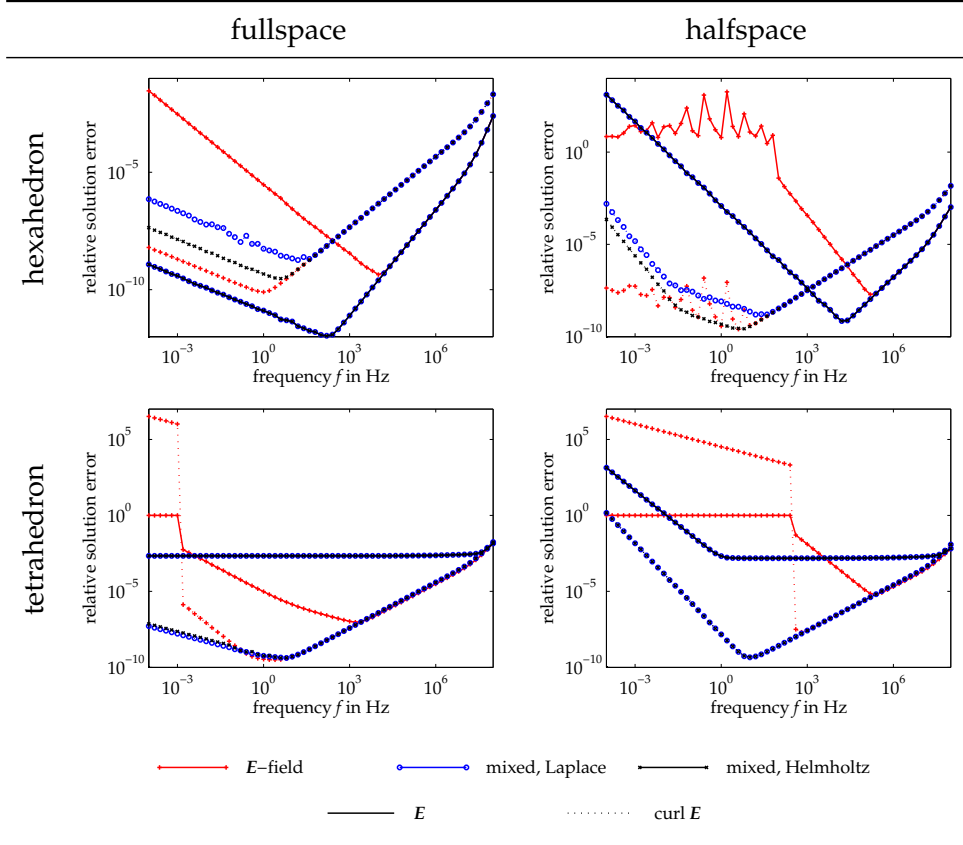


Figure C.6: Relative solution error for test case ‘plane wave’ with symmetric matrix scaling; piecewise quadratic approximation ($p = 2$); mixed boundary case, Dirichlet and Neumann boundary conditions.

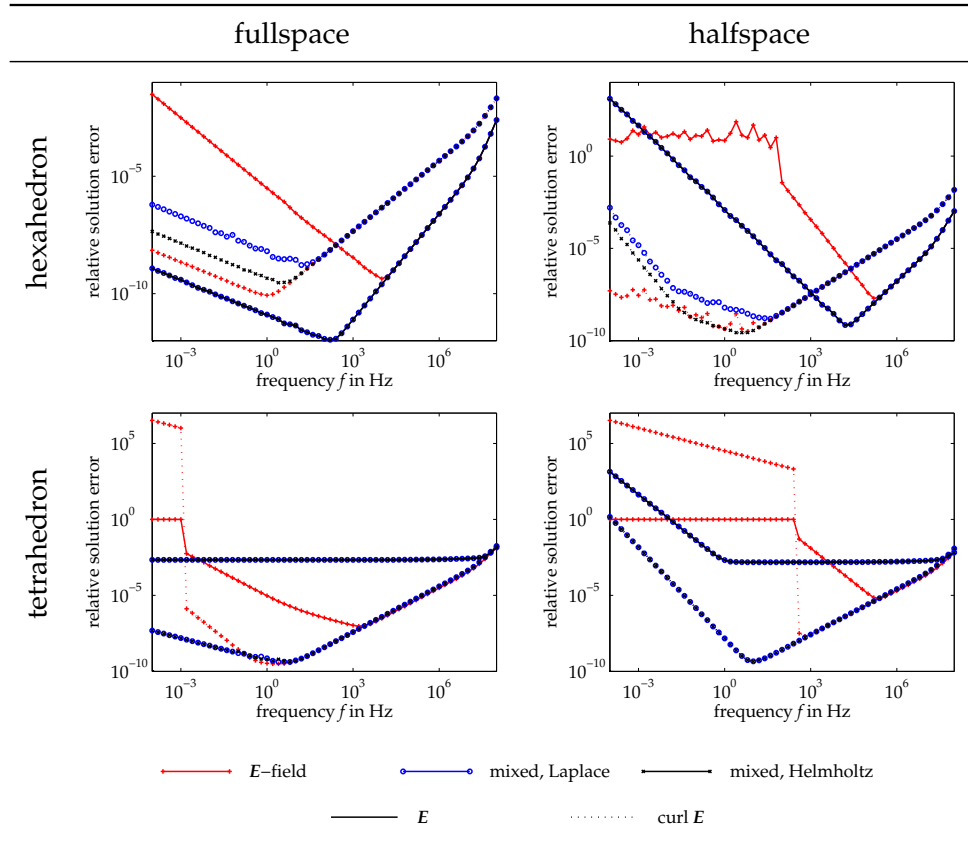


Figure C.7: Relative solution error for test case ‘plane wave’ without symmetric matrix scaling; piecewise quadratic approximation ($p = 2$); mixed boundary case, Dirichlet and Neumann boundary conditions.

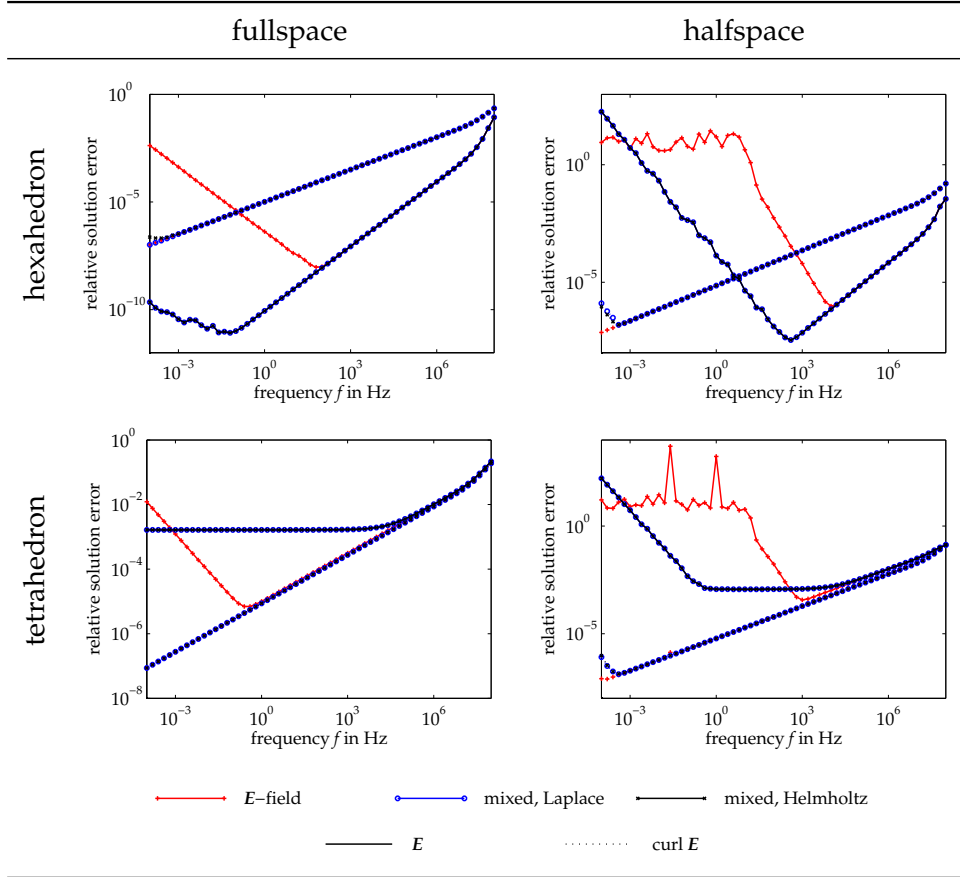


Figure C.8: Relative solution error for test case ‘plane wave’ with symmetric matrix scaling; piecewise linear approximation ($p = 1$); mixed boundary case, Dirichlet and Neumann boundary conditions.

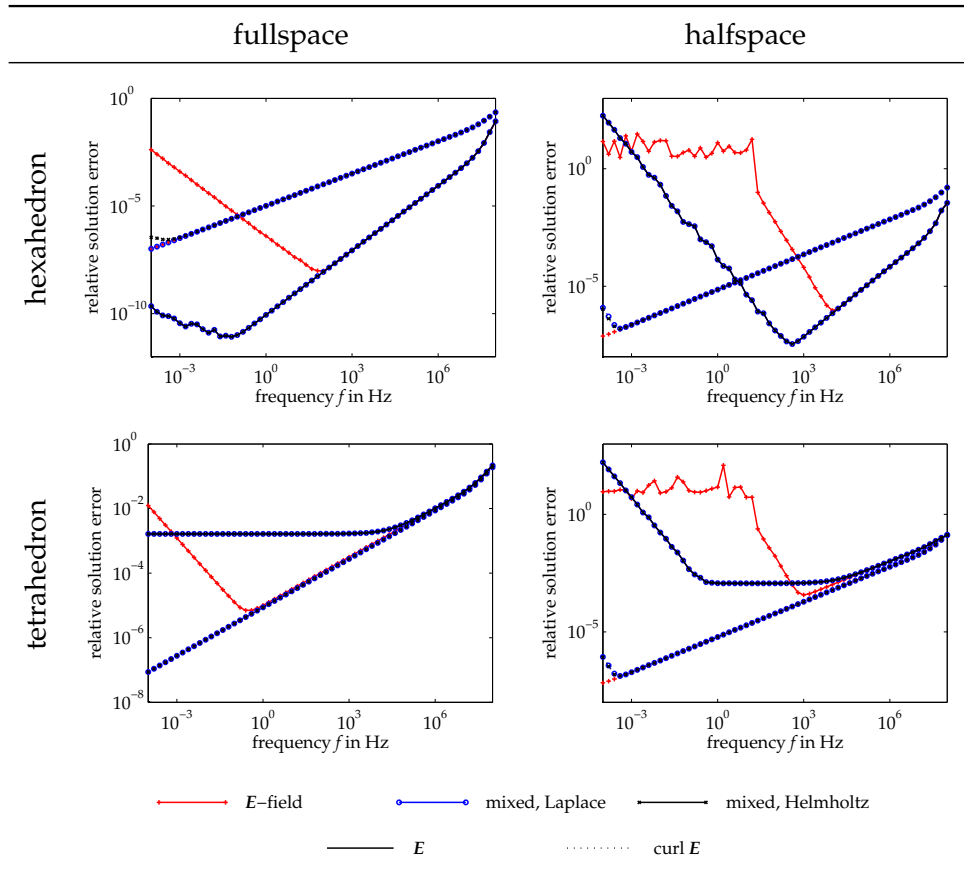


Figure C.9: Relative solution error for test case ‘plane wave’ without symmetric matrix scaling; piecewise linear approximation ($p = 1$); mixed boundary case, Dirichlet and Neumann boundary conditions.

D Sensitivity calculation

Given the data of one of the boundary value problems of Chapter 2, i. e., constitutive parameters, frequency, source terms and boundary values, an approximate solution of the boundary value problem is computed using the numerical techniques described in Chapter 3. The solution can be interpreted as a non-linear function of the data and consequently be partially differentiated with respect to the data. This differentiation leads to the concept of sensitivity which is generally understood as the derivative of a physical field with respect to the value of some constitutive parameter within a subvolume of the computational domain.

Computation of sensitivities can easily be appended to the solution of the boundary value problem using the sensitivity equation approach (McGillivray and Oldenburg, 1990). The sensitivity is sought as the solution of a boundary value problem which is identical to the boundary value problem in terms of the electric field except for modified source terms. Therefore, a system of linear equations is to be solved for the electric field and the sensitivities which has the same coefficient matrix but different right hand sides. The sensitivities can be computed quite efficiently if the system of linear equations is solved directly and the matrix factorization can be reused.

Recall that the electric field E is approximated by an expansion in terms of piecewise polynomial vector finite element basis functions Φ_i as

$$E_h(\mathbf{r}) = \sum_{i=1}^N E_i \Phi_i(\mathbf{r}). \quad (\text{D.1})$$

While the coefficients $E_i \in \mathbb{C}$, $i = 1, \dots, n$, are determined by a system of linear equations

$$\sum_{i=1}^n a_{j,i} E_i = f_j, \quad j = 1, \dots, n, \quad (\text{D.2a})$$

where

$$\begin{aligned} a_{j,i} = & \int_{\Omega} \text{curl } \overline{\Phi}_j \cdot \left(\mu^{-1} \text{curl } \Phi_i \right) d^3r - i\omega \int_{\Omega} \overline{\Phi}_j \cdot ((\sigma - i\omega\epsilon) \Phi_i) d^3r \\ & + i\omega \int_{\Gamma_h} (\mathbf{n} \times \overline{\Phi}_j) \cdot (\lambda (\mathbf{n} \times \Phi_i)) d^2r, \end{aligned} \quad (\text{D.2b})$$

$$\begin{aligned} f_j = & i\omega \int_{\Omega} \overline{\Phi}_j \cdot \mathbf{j}_s d^3r - i\omega \sum_{\substack{i,j=1 \\ i < j}}^n \int_{\Sigma_{i,j}} \overline{\Phi}_j \cdot \mathbf{j}_f d^2r - i\omega \int_{\Gamma_h} \overline{\Phi}_j \cdot (\mathbf{j}_f + \mathbf{n} \times \mathbf{H}_0) d^2r \\ & - \sum_{i=n+1}^N a_{j,i} E_i, \end{aligned} \quad (\text{D.2c})$$

the remaining coefficients $E_i \in \mathbb{C}$, $i = n+1, \dots, N$, are fixed by the Dirichlet boundary condition according to

$$E_i = \mathcal{A}_i \{E_0\}. \quad (\text{D.3})$$

Appendices

The sensitivity of the electric field with respect to an arbitrary, scalar parameter is formally described by the derivative $S := \partial E / \partial \eta$. This translates into the finite element approximation (D.1) as a dependency of the basis function expansion coefficients E_i on η ,

$$S_h(\mathbf{r}) = \sum_{i=1}^N S_i \Phi_i(\mathbf{r}), \quad (\text{D.4})$$

where $S_i := \partial E_i / \partial \eta$. The coefficients $S_i, i = n+1, \dots, N$ vanish if the Dirichlet boundary condition is assumed to be independent of η .

Application of the derivative $\partial / \partial \eta$ to the system of linear equations (D.2) and making use of the chain rule, a similar system of equations has to be solved in terms of coefficients $S_i \in \mathbb{C}, i = 1, \dots, n$,

$$\sum_{i=1}^n a_{j,i} S_i = g_j, \quad j = 1, \dots, n, \quad (\text{D.5a})$$

where

$$\begin{aligned} a_{j,i} = & \int_{\Omega} \text{curl } \bar{\Phi}_j \cdot \left(\mu^{-1} \text{curl } \Phi_i \right) d^3r - i\omega \int_{\Omega} \bar{\Phi}_j \cdot \left((\sigma - i\omega\epsilon) \Phi_i \right) d^3r \\ & + i\omega \int_{\Gamma_h} (\mathbf{n} \times \bar{\Phi}_j) \cdot (\lambda (\mathbf{n} \times \Phi_i)) d^2r, \\ g_j = & i\omega \int_{\Omega} \bar{\Phi}_j \cdot \frac{\partial \mathbf{j}_s}{\partial \eta} d^3r - i\omega \sum_{\substack{i,j=1 \\ i < j}}^n \int_{\Sigma_{i,j}} \bar{\Phi}_j \cdot \frac{\partial \mathbf{j}_f}{\partial \eta} d^2r \\ & - i\omega \int_{\Gamma_h} \bar{\Phi}_j \cdot \left(\frac{\partial \mathbf{j}_f}{\partial \eta} + \mathbf{n} \times \frac{\partial \mathbf{H}_0}{\partial \eta} \right) d^2r \\ & - \sum_{i=1}^N E_i \left\{ - \int_{\Omega} \text{curl } \bar{\Phi}_j \cdot \left(\frac{\partial \mu}{\partial \eta} \mu^{-2} \text{curl } \Phi_i \right) d^3r \right. \\ & \quad - i\omega \int_{\Omega} \bar{\Phi}_j \cdot \left(\left(\frac{\partial \sigma}{\partial \eta} - i\omega \frac{\partial \epsilon}{\partial \eta} \right) \Phi_i \right) d^3r \\ & \quad \left. + i\omega \int_{\Gamma_h} (\mathbf{n} \times \bar{\Phi}_j) \cdot \left(\frac{\partial \lambda}{\partial \eta} (\mathbf{n} \times \Phi_i) \right) d^2r \right\}. \end{aligned} \quad (\text{D.5b})$$

$$(\text{D.5c})$$

Note that the sum in equation (D.5c) involves all E_1, \dots, E_N , including the Dirichlet boundary values, while the system of linear equations (D.5a) includes only S_1, \dots, S_n .

As an example, consider the sensitivity of the electric field with respect to conductivity σ . Assume that the domain Ω consists of a number of subdomains such that σ is constant within each subdomain, $\sigma = \sigma_k$ on Ω_k . Then, the finite element approximation to $S = \partial E / \partial \sigma_k$ is computed

according to equations (D.5) where the right hand side reduces to

$$g_j = i\omega \sum_{i=1}^N E_i \left\{ \int_{\Omega_k} \overline{\Phi_j} \cdot \Phi_i d^3r - \frac{i}{2} \int_{\Gamma_h \cap \Omega_k} (\mathbf{n} \times \overline{\Phi_j}) \cdot \left(\frac{1}{k} (\mathbf{n} \times \Phi_i) \right) d^2r \right\} \quad (\text{D.5c}^*)$$

if $\lambda = k(\omega\mu)^{-1}$ and $k = \sqrt{i\omega\mu(\sigma - i\omega\varepsilon)}$. The sensitivity of the other electromagnetic fields can be derived using the expansion (D.4). For example, if

$$\frac{\partial \mathbf{E}_h}{\partial \sigma_k} = \sum_{i=1}^N S_i \Phi_i(\mathbf{r}) \quad (\text{D.6a})$$

then, by $\text{curl } \mathbf{E}_h = i\omega \mathbf{B}_h$,

$$\frac{\partial \mathbf{B}_h}{\partial \sigma_k} = \frac{1}{i\omega} \sum_{i=1}^N S_i \text{curl } \Phi_i(\mathbf{r}). \quad (\text{D.6b})$$

One practical aspect of the proposed method requires a note of caution. Even though the storage of the degrees of freedom E_i , $i = 1, \dots, N$, appears undemanding, the storage of the degrees of freedom S_i , $i = 1, \dots, N$ quickly becomes prohibitive if sensitivities are to be calculated for all subdomains Ω_k of a typical 3-D inverse problem parameterization. Therefore, the post-processing step, evaluation of the sensitivity for all receiver positions, needs to be integrated into the finite element solution stage such that the degrees of freedom need not be stored.

E Plane wave within a horizontally stratified earth

A plane wave travelling in positive z -direction is assumed to impinge upon a stack of horizontal layers with homogeneous constitutive parameters (Figure E.1). The electromagnetic field expressions (4.11a) and (4.11b) satisfy Maxwell's equations within each layer if the coefficients a_i and b_i are independent of z . Without loss of generality, the fields can be assumed to be polarized according to

$$\mathbf{E}_i = (E_i(z), 0, 0)^T, \quad (\text{E.1a})$$

$$\mathbf{H}_i = (0, H_i(z), 0)^T \quad (\text{E.1b})$$

where

$$E_i(z) = Z_i \left(a_i e^{ik_i(z-z_{i-1})} + b_i e^{-ik_i(z-z_{i-1})} \right), \quad (\text{E.1c})$$

$$H_i(z) = a_i e^{ik_i(z-z_{i-1})} - b_i e^{-ik_i(z-z_{i-1})} \quad (\text{E.1d})$$

and $\|\mathbf{E}_0\| = \|\mathbf{H}_0\| = 1$ has been set in equations (4.11a) and (4.11b). For the first layer, $z_0 = z_1$. The coefficients a_i and b_i can be determined by enforcing the continuity of the tangential field components at the interfaces and by taking boundary conditions into account. The following definitions will be useful:

$$Y_i = \frac{k_i}{\omega \mu_i} \quad i = 1, \dots, n, \quad (\text{E.2a})$$

$$Z_i = \frac{\omega \mu_i}{k_i} = \frac{1}{Y_i} \quad i = 1, \dots, n, \quad (\text{E.2b})$$

$$R_i = \frac{Y_i - Y_{i+1}}{Y_i + Y_{i+1}} = \frac{Z_{i+1} - Z_i}{Z_{i+1} + Z_i} \quad i = 1, \dots, n-1, \quad (\text{E.2c})$$

$$r_i = \frac{b_i}{a_i} \quad i = 1, \dots, n-1, \quad (\text{E.2d})$$

$$h_1 = 0, \quad (\text{E.2e})$$

$$h_i = z_i - z_{i-1} \quad i = 2, \dots, n-1. \quad (\text{E.2f})$$

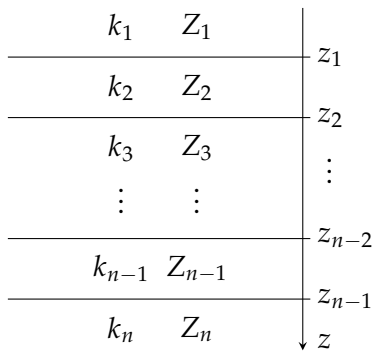


Figure E.1: Horizontally stratified earth which consists of n layers including the upper and the lower halfspace.

Y_i , Z_i , R_i , r_i and h_i are respectively the intrinsic wave admittance, the intrinsic wave impedance, the intrinsic reflection coefficient of the interface between two layers, the generalized reflection coefficient and the layer thickness. Since the wave is assumed to be travelling in positive z -direction

$$b_n = 0 \quad (\text{E.3})$$

has to be enforced in order to eliminate the upgoing wave within the last layer. Now, continuity of the tangential field components requires that

$$\begin{aligned} E_{i-1}(z_{i-1}) &= E_i(z_{i-1}) \\ Z_{i-1} \left(a_{i-1} e^{ik_{i-1}h_{i-1}} + b_{i-1} e^{-ik_{i-1}h_{i-1}} \right) &= Z_i (a_i + b_i) \\ Z_{i-1} a_{i-1} \left(e^{2ik_{i-1}h_{i-1}} + r_{i-1} \right) e^{-ik_{i-1}h_{i-1}} &= Z_i a_i (1 + r_i) \end{aligned} \quad (\text{E.4a})$$

and

$$\begin{aligned} H_{i-1}(z_{i-1}) &= H_i(z_{i-1}) \\ a_{i-1} e^{ik_{i-1}h_{i-1}} - b_{i-1} e^{-ik_{i-1}h_{i-1}} &= a_i - b_i \\ a_{i-1} \left(e^{2ik_{i-1}h_{i-1}} - r_{i-1} \right) e^{-ik_{i-1}h_{i-1}} &= a_i (1 - r_i) \end{aligned} \quad (\text{E.4b})$$

hold for all layer interfaces z_1, \dots, z_{n-1} . Division of equation (E.4b) by equation (E.4a) yields a recursion formula of the form $r_{i-1} = r_{i-1}(r_i)$. First, at $z = z_{n-1}$ for $i = n$

$$r_n = 0 \quad (\text{E.5a})$$

follows from equation (E.3) and

$$\begin{aligned} \frac{1}{Z_{n-1}} \frac{e^{2ik_{n-1}h_{n-1}} - r_{n-1}}{e^{2ik_{n-1}h_{n-1}} + r_{n-1}} &= \frac{1}{Z_n} \\ r_{n-1} &= \frac{Z_n - Z_{n-1}}{Z_n + Z_{n-1}} e^{2ik_{n-1}h_{n-1}} \\ &= R_{n-1} e^{2ik_{n-1}h_{n-1}}. \end{aligned} \quad (\text{E.5b})$$

Next, at $z = z_{i-1}$ for $i = n-1, \dots, 2$,

$$\begin{aligned} \frac{1}{Z_{i-1}} \frac{e^{2ik_{i-1}h_{i-1}} - r_{i-1}}{e^{2ik_{i-1}h_{i-1}} + r_{i-1}} &= \frac{1}{Z_i} \frac{1 - r_i}{1 + r_i} \\ Z_i(1 + r_i) \left(e^{2ik_{i-1}h_{i-1}} - r_{i-1} \right) &= Z_{i-1}(1 - r_i) \left(e^{2ik_{i-1}h_{i-1}} + r_{i-1} \right) \\ r_{i-1} &= \frac{Z_i(1 + r_i) - Z_{i-1}(1 - r_i)}{Z_i(1 + r_i) + Z_{i-1}(1 - r_i)} e^{2ik_{i-1}h_{i-1}} \\ &= \frac{Z_i - Z_{i-1} + (Z_i + Z_{i-1}) r_i}{Z_i + Z_{i-1} + (Z_i - Z_{i-1}) r_i} e^{2ik_{i-1}h_{i-1}} \\ &= \frac{R_{i-1} + r_i}{1 + R_{i-1} r_i} e^{2ik_{i-1}h_{i-1}}. \end{aligned} \quad (\text{E.5c})$$

Appendices

The coefficient r_1 computed at the last step of the upward recursion (E.5) determines the fields within the topmost layer up to the factor a_1 . a_1 is fixed by enforcing that the horizontal magnetic field has unit amplitude at $z = z_1$,

$$\begin{aligned} H_1(z_1) &= a_1(1 - r_1) = 1 \\ a_1 &= \frac{1}{1 - r_1}. \end{aligned} \quad (\text{E.6a})$$

This condition is usually employed in magnetotelluric modelling where the topmost layer is the air halfspace and $z_1 = 0$ represents the air–earth interface. The other coefficients a_i are computed by a downward recursion of the form $a_i = a_i(a_{i-1})$ which is derived from the interface conditions by multiplication of equation (E.4b) with Z_{i-1} and adding equation (E.4a). For $i = 2, \dots, n - 1$

$$\begin{aligned} 2a_{i-1}Z_{i-1}e^{ik_{i-1}h_{i-1}} &= a_i(Z_i + Z_{i-1} + (Z_i - Z_{i-1})r_i) \\ a_{i-1}(1 - R_{i-1})e^{ik_{i-1}h_{i-1}} &= a_i(1 + R_{i-1}r_i) \\ a_i &= a_{i-1} \frac{1 - R_{i-1}}{1 + R_{i-1}r_i} e^{ik_{i-1}h_{i-1}} \end{aligned} \quad (\text{E.6b})$$

and for $i = n - 1$

$$a_n = a_{n-1}(1 - R_{n-1})e^{ik_{n-1}h_{n-1}}. \quad (\text{E.6c})$$

Finally,

$$b_i = a_i r_i \quad (\text{E.7})$$

for $i = 1, \dots, n$. Summarizing, the coefficients a_i and b_i in equations (E.1c) and (E.1d) can be computed according to the following sequence:

$$\begin{aligned} i = n : & \quad r_i = 0 \\ i = n - 1 : & \quad r_i = R_i e^{2ik_i h_i} \\ i = n - 2, \dots, 2 : & \quad r_i = \frac{R_i + r_{i+1}}{1 + R_i r_{i+1}} e^{2ik_i h_i} \\ i = 1 : & \quad r_i = \frac{R_i + r_{i+1}}{1 + R_i r_{i+1}} \\ i = 1 : & \quad a_i = \frac{1}{1 - r_i} \\ i = 2 : & \quad a_i = a_{i-1} \frac{1 - R_{i-1}}{1 + R_{i-1} r_i} \\ i = 3, \dots, n - 1 : & \quad a_i = a_{i-1} \frac{1 - R_{i-1}}{1 + R_{i-1} r_i} e^{ik_{i-1} h_{i-1}} \\ i = n : & \quad a_i = a_{i-1}(1 - R_{i-1})e^{ik_{i-1} h_{i-1}} \\ i = 1, \dots, n : & \quad b_i = a_i r_i \end{aligned} \quad (\text{E.8})$$

Note that only the three parameters intrinsic wave admittance Z_i , wavenumber k_i and layer interface depth z_i shown in Figure E.1 are required to compute the electromagnetic fields according to equations (E.1) and (E.8).

Bibliography

- Adhidjaja, J. I., and Hohmann, G. W. (1989). A finite-difference algorithm for the transient electromagnetic response of a three-dimensional body. *Geophysical Journal International*, 98(2), 233–242.
- Ainsworth, M., and Oden, J. T. (2000). *A posteriori error estimation in finite element analysis*. New York, Weinheim: Wiley.
- Amestoy, P. R., Duff, I. S., Koster, J., and L'Excellent, J.-Y. (2001). A fully asynchronous multifrontal solver using distributed dynamic scheduling. *SIAM Journal on Matrix Analysis and Applications*, 23(1), 15–41.
- Amestoy, P. R., Duff, I. S., and L'Excellent, J.-Y. (2000). Multifrontal parallel distributed symmetric and unsymmetric solvers. *Computer Methods in Applied Mechanics and Engineering*, 184(2-4), 501–520.
- Amestoy, P. R., Guermouche, A., L'Excellent, J.-Y., and Pralet, S. (2006). Hybrid scheduling for the parallel solution of linear systems. *Parallel Computing*, 32(2), 136–156.
- Amrouche, C., Bernardi, C., Dauge, M., and Girault, V. (1998). Vector potentials in three-dimensional non-smooth domains. *Mathematical Methods in the Applied Sciences*, 21(9), 823–864.
- Andersen, L. S., and Volakis, J. L. (1998). Hierarchical tangential vector finite elements for tetrahedra. *IEEE microwave and guided wave letters*, 8(3), 127–129.
- Anderson, W. L. (1989). A hybrid fast Hankel transform algorithm for electromagnetic modeling. *Geophysics*, 54(2), 263–266.
- Avdeev, D. B., Kuvshinov, A. V., Pankratov, O. V., and Newman, G. A. (1997). High-performance three-dimensional electromagnetic modelling using Neumann series. Wide-band numerical solution and examples. *Journal of Geomagnetism and Geoelectricity*, 49(11-12), 1519–1539.
- Badea, E. A., Everett, M. E., Newman, G. A., and Biro, O. (2001). Finite-element analysis of controlled-source electromagnetic induction using Coulomb-gauged potentials. *Geophysics*, 66(3), 786–799.
- Barret, R., Berry, M., Chan, T., Demmel, J., Donato, J., Dongarra, J., et al. (1994). *Templates for the solution of linear systems: Building blocks for iterative methods*. Philadelphia: SIAM.
- Beck, R., and Hiptmair, R. (1999). Multilevel solution of the time-harmonic Maxwell's equations based on edge elements. *International Journal for Numerical Methods in Engineering*, 45(7), 901–920.
- Berenger, J. P. (1994). A perfectly matched layer for the absorption of electromagnetic waves. *Journal of Computational Physics*, 114(2), 185–200.
- Bergmann, T., Robertsson, J. O. A., and Holliger, K. (1998). Finite-difference modeling of electromagnetic wave propagation in dispersive and attenuating media. *Geophysics*, 63(3), 856–867.

Bibliography

- Börner, R.-U., Ernst, O. G., and Spitzer, K. (2008). Fast 3D simulation of transient electromagnetic fields by model reduction in the frequency domain using Krylov subspace projection. *Geophysical Journal International*, 173(3), 766–780.
- Bossavit, A. (1998). *Computational electromagnetism: Variational formulations, complementarity, edge elements*. San Diego: Academic Press.
- Braess, D., and Schöberl, J. (2008). Equilibrated residual error estimator for edge elements. *Mathematics of Computation*, 77(262), 651–672.
- Bray, T., Paoli, J., Sperberg-McQueen, C. M., Maler, E., and Yergeau, F. (2006). *Extensible Markup Language (XML) 1.0* (4th ed.). World Wide Web Consortium (W3C). Available from <http://www.w3.org/TR/2006/REC-xml-20060816>
- Buffa, A., Costabel, M., and Sheen, D. (2002). On traces for $\mathbf{H}(\text{curl}, \Omega)$ in Lipschitz domains. *Journal of Mathematical Analysis and Applications*, 276(2), 845–867.
- Bureau international des poids et mesures (BIPM). (2006). *Le système international d'unités (SI)* [The International System of Units (SI)] (8th ed.). Sèvres: Organisation intergouvernementale de la Convention du Mètre.
- Castillo, P., Rieben, R., and White, D. (2005). FEMSTER: An object oriented class library of high-order discrete differential forms. *ACM Transactions on Mathematical Software*, 31(4), 425–457.
- Chen, Y. H., Chew, W. C., and Oristaglio, M. L. (1997). Application of perfectly matched layers to the transient modeling of subsurface EM problems. *Geophysics*, 62(6), 1730–1736.
- Chew, W. C. (1995). *Waves and fields in inhomogeneous media*. Piscataway, NJ: IEEE Press.
- Chew, W. C., and Weedon, W. H. (1995). A 3-D perfectly matched medium from modified Maxwell's equations with stretched coordinates. *Microwave and Optical Technology Letters*, 7(13), 599–604.
- Ciarlet, P. G. (1978). *The finite element method for elliptic problems*. Amsterdam: North-Holland.
- Coggon, J. H. (1971). Electromagnetic and electrical modeling by the finite element method. *Geophysics*, 36(1), 132–155.
- Constable, S., and Weiss, C. J. (2006). Mapping thin resistors and hydrocarbons with marine EM methods: Insights from 1D modeling. *Geophysics*, 71(2), G43–G51.
- Demkowicz, L. (2003). hp-adaptive finite elements for time-harmonic Maxwell equations. In M. Ainsworth, P. Davies, D. Duncan, P. Martin, and B. Rynne (Eds.), *Topics in computational wave propagation: Direct and inverse problems*. Berlin: Springer.
- Demkowicz, L., and Vardapetyan, L. (1998). Modeling of electromagnetic absorption/scattering problems using hp-adaptive finite elements. *Computer Methods in Applied Mechanics and Engineering*, 152(1-2), 103–124.
- Dongarra, J. (2000). Sparse matrix storage formats. In Z. Bai, J. Demmel, J. Dongarra, A. Ruhe, and H. van der Vorst (Eds.), *Templates for the solution of algebraic eigenvalue problems: A practical guide*. Philadelphia: SIAM.
- Druskin, V. L., and Knizhnerman, L. A. (1999). New spectral Lanczos decomposition method for induction modeling in arbitrary 3-D geometry. *Geophysics*, 64(3), 701–706.

- Fang, J., and Wu, Z. (1995). Generalized perfectly matched layer—An extension of Berenger's perfectly matched layer boundary condition. *IEEE Microwave and Guided Wave Letters*, 5(12), 451–453.
- Freund, R. W., and Nachtigal, N. M. (1994). An implementation of the QMR method based on coupled two-term recurrences. *SIAM Journal on Scientific Computing*, 15(2), 313–337.
- Gedney, S. D. (1996). An anisotropic perfectly matched layer-absorbing medium for the truncation of FDTD lattices. *IEEE Transactions on Antennas and Propagation*, 44(12), 1630–1639.
- Girault, V., and Raviart, P.-A. (1986). *Finite element methods for Navier-Stokes equations – Theory and algorithms*. Berlin, Heidelberg: Springer.
- Graglia, R. D., Wilton, D. R., and Peterson, A. F. (1997). Higher order interpolatory vector bases for computational electromagnetics. *IEEE Transactions on Antennas and Propagation*, 45(3), 329–342.
- Haber, E., and Ascher, U. M. (2001). Fast finite volume simulation of 3D electromagnetic problems with highly discontinuous coefficients. *SIAM Journal on Scientific Computing*, 22(6), 1943–1961.
- Haber, E., Ascher, U. M., Aruliah, D. A., and Oldenburg, D. W. (2000). Fast simulation of 3D electromagnetic problems using potentials. *Journal of Computational Physics*, 163(1), 150–171.
- Haber, E., and Heldmann, S. (2007). An octree multigrid method for quasi-static Maxwell's equations with highly discontinuous coefficients. *Journal of Computational Physics*, 223(2), 783–796.
- Higham, N. J., and Tisseur, F. (2000). A block algorithm for matrix 1-norm estimation, with an application to 1-norm pseudospectra. *SIAM Journal on Matrix Analysis and Applications*, 21(4), 1185–1201.
- Hiptmair, R. (2001). Higher order Whitney forms. *Progress In Electromagnetics Research*, 32, 271–299.
- Hiptmair, R. (2002). Finite elements in computational electromagnetism. *Acta Numerica*, 11(1), 237–339.
- Hohmann, G. W. (1975). Three-dimensional induced polarization and electromagnetic modeling. *Geophysics*, 40(2), 309–324.
- Izsák, F., Harutyunyan, D., and Vegt, J. J. W. van der. (2008). Implicit a posteriori error estimates for the Maxwell equations. *Mathematics of Computation*, 77(263), 1355–1386.
- Jiang, B.-N., Wu, J., and Povinelli, L. A. (1996). The origin of spurious solutions in computational electromagnetics. *Journal of Computational Physics*, 125(1), 104–123.
- Jin, J. (1993). *The finite element method in electromagnetics*. New York: John Wiley & Sons.
- Jin, J., and Chew, W. C. (1996). Combining PML and ABC for finite element analysis of scattering problems. *Microwave and Optical Technology Letters*, 12(4), 192–197.
- Kuzuoglu, M., and Mittra, R. (1996). Frequency dependence of the constitutive parameters of causal perfectly matched anisotropic absorbers. *IEEE Microwave and Guided Wave Letters*, 6(12), 447–449.
- Landau, L. D., and Lifschitz, E. M. (1980). *Lehrbuch der Theoretischen Physik. Band VIII: Elektrodynamik der Kontinua* [Textbook on theoretical physics. Volume VIII: Electrodynamics of continua] (3rd ed.). Berlin: Akademie-Verlag.

Bibliography

- Løseth, L. O. (2007). *Modelling of controlled source electromagnetic data*. PhD thesis, Norwegian University of Science and Technology, Faculty of Natural Sciences and Technology, Trondheim, Norway.
- Mackie, R. L., Madden, T. R., and Wannamaker, P. E. (1993). Three-dimensional magnetotelluric modeling using difference equations – Theory and comparisons to integral equation solutions. *Geophysics*, 58(2), 215–226.
- McGillivray, P. R., and Oldenburg, D. W. (1990). Methods for calculating Fréchet derivatives and sensitivities for the non-linear inverse problem: a comparative study. *Geophysical Prospecting*, 38(5), 499–524.
- Message Passing Interface Forum. (2008). *MPI: A message-passing interface standard: Version 1.3*. Available from <http://www.mpi-forum.org>
- Mitsuhata, Y., and Uchida, T. (2004). 3D magnetotelluric modeling using the T- Ω finite-element method. *Geophysics*, 69(1), 108–119.
- Mogi, T. (1996). Three-dimensional modeling of magnetotelluric data using finite element method. *Journal of Applied Geophysics*, 35(2-3), 185–189.
- Monk, P. (2003). *Finite element methods for Maxwell's equations*. New York: Oxford University Press.
- Mur, G., and Hoop, A. T. de. (1985). A finite-element method for computing three-dimensional electromagnetic fields in inhomogeneous media. *IEEE Transactions on Magnetics*, 21(6), 2188–2191.
- Nédélec, J.-C. (1980). Mixed finite elements in \mathbb{R}^3 . *Numerische Mathematik*, 35(3), 315–341.
- Nédélec, J.-C. (1986). A new family of mixed finite elements in \mathbb{R}^3 . *Numerische Mathematik*, 50(1), 57–81.
- Newman, G. A., and Alumbaugh, D. L. (1995). Frequency-domain modelling of airborne electromagnetic responses using staggered finite differences. *Geophysical Prospecting*, 43(8), 1021–1042.
- Newman, G. A., Hohmann, G. W., and Anderson, W. L. (1986). Transient electromagnetic response of a three-dimensional body in a layered earth. *Geophysics*, 51(8), 1608–1627.
- Nicaise, S., and Creusé, E. (2003). A posteriori error estimation for the heterogeneous Maxwell equations on isotropic and anisotropic meshes. *Calcolo*, 40(4), 249–271.
- Nolting, W. (1997). *Grundkurs Theoretische Physik. Band 3: Elektrodynamik* [Basic course theoretical physics. Volume 3: Electrodynamics] (5th ed.). Braunschweig, Wiesbaden: Vieweg.
- OpenMP Architecture Review Board. (2008). *OpenMP application program interface: Version 3.0 May 2008*. Available from <http://www.openmp.org>
- Petropoulos, P. G. (2000). Reflectionless sponge layers as absorbing boundary conditions for the numerical solution of maxwell equations in rectangular, cylindrical, and spherical coordinates. *SIAM Journal on Applied Mathematics*, 60(3), 1037–1058.
- Pridmore, D. F., Hohmann, G. W., Ward, S. H., and Sill, W. R. (1981). An investigation of finite-element modeling for electrical and electromagnetic data in three dimensions. *Geophysics*, 46(7), 1009–1024.

- Rappaport, C. M. (1995). Perfectly matched absorbing boundary conditions based on anisotropic lossy mapping of space. *IEEE Microwave and Guided Wave Letters*, 5(3), 90–92.
- Reddy, I. K., Rankin, D., and Phillips, R. J. (1977). Three-dimensional modeling in magnetotelluric and magnetic variational sounding. *Geophysical Journal of the Royal Astronomical Society*, 51(2), 313–325.
- Rieben, R. N. (2004). *A novel high order time domain vector finite element method for the simulation of electromagnetic device*. PhD thesis, University of California at Davis, Livermore, CA. Available from <https://e-reports-ext.llnl.gov/pdf/309818.pdf>
- Roberts, R. L., and Daniels, J. J. (1997). Modeling near-field GPR in three dimensions using the FDTD method. *Geophysics*, 62(4), 1114–1126.
- Ruiz, D. (2001). *A scaling algorithm to equilibrate both rows and columns norms in matrices* (Tech. Rep.). Didcot, Oxfordshire, UK: Rutherford Appleton Laboratory.
- Saad, Y. (1996). *Iterative methods for sparse linear systems*. Boston: PWS Publishing Company.
- Sacks, Z. S., Kingsland, D. M., Lee, R., and Lee, J. F. (1995). A perfectly matched anisotropic absorber for use as an absorbing boundary condition. *IEEE Transactions on Antennas and Propagation*, 43(12), 1460–1463.
- Schenk, O., and Gärtner, K. (2004). Solving unsymmetric sparse systems of linear equations with PARDISO. *Journal of Future Generation Computer Systems*, 20(3), 475–487.
- Schenk, O., and Gärtner, K. (2006). On fast factorization pivoting methods for symmetric indefinite systems. *Electronic Transactions on Numerical Analysis*, 23, 158–179.
- Schenk, O., Gärtner, K., and Fichtner, W. (2000). Efficient sparse LU factorization with left-right looking strategy on shared memory multiprocessors. *BIT Numerical Mathematics*, 40(1), 158–176.
- Schöberl, J. (2008). *NETGEN – Automatic mesh generator*. Johannes Kepler University Linz, Austria. Available from <http://www.hpfem.jku.at/netgen>
- Si, H. (2007). *TetGen: A quality tetrahedral mesh generator and 3D Delaunay triangulator*. Weierstrass Institute for Applied Analysis and Stochastics, Berlin, Germany. Available from <http://tetgen.berlios.de>
- Smith, J. T. (1996). Conservative modeling of 3-D electromagnetic fields. *Geophysics*, 61(5), 1308–1324.
- Sommerfeld, A. (1964). *Vorlesungen über Theoretische Physik. Band III: Elektrodynamik* [Lectures on theoretical physics. Volume III: Electrodynamics] (4th ed.). Leipzig: Akademische Verlagsgesellschaft Geest & Portig K.-G.
- Stroustrup, B. (1997). *The C++ programming language* (3rd ed.). Reading, MA: Addison-Wesley.
- Teixeira, F. L., and Chew, W. C. (1997). Systematic derivation of anisotropic PML absorbing media in cylindrical and spherical coordinates. *IEEE Microwave and Guided Wave Letters*, 7(11), 371–373.
- Teixeira, F. L., Chew, W. C., Straka, M., Oristaglio, M. L., and Wang, T. (1998). Finite-difference time-domain simulation of ground penetrating radar on dispersive, inhomogeneous, and conductive soils. *IEEE Transactions on Geoscience and Remote Sensing*, 36(8), 1928–1937.

Bibliography

- Trefethen, L. N. (1996). *Finite difference and spectral methods for ordinary and partial differential equations*. Unpublished textbook, Cornell University, Ithaca, NY, USA. Available from <http://web.comlab.ox.ac.uk/oucl/work/nick.trefethen/pdetext.html>
- Veillard, D. (1999). *The XML C parser and toolkit of Gnome*. Available from <http://xmlsoft.org>
- Verfürth, R. (1996). *A review of a posteriori error estimation and adaptive mesh-refinement techniques*. Chichester, Stuttgart: Wiley-Teubner.
- Wang, T., and Tripp, A. C. (1996). FDTD simulation of EM wave propagation in 3-D media. *Geophysics*, 61(1), 110–120.
- Wannamaker, P. E. (1991). Advances in 3D magnetotelluric modelling using integral equations. *Geophysics*, 56(11), 1716–1728.
- Wannamaker, P. E., Hohmann, G. W., and SanFilipo, W. A. (1984). Electromagnetic modeling of three-dimensional bodies in layered earths using integral equations. *Geophysics*, 49(1), 60–74.
- Webb, J. P. (1999). Hierarchical vector basis functions of arbitrary order for triangular and tetrahedral finite elements. *IEEE Transactions on Antennas and Propagation*, 47(8), 1244–1253.
- Weidelt, P. (1975). Electromagnetic induction in three-dimensional structures. *Geophysical Journal of the Royal Astronomical Society*, 41(1), 85–109.
- Weiss, C. J., and Constable, S. (2006). Mapping thin resistors and hydrocarbons with marine EM methods, Part II – Modeling and analysis in 3D. *Geophysics*, 71(6), G321–G332.
- Whitney, H. (1957). *Geometric integration theory*. Princeton: Princeton University Press.
- Xiong, Z., and Tripp, A. C. (1997). 3-D electromagnetic modeling for near-surface targets using integral equations. *Geophysics*, 62(4), 1097–1106.
- Yee, K. S. (1966). Numerical solution of initial boundary value problems involving Maxwell's equations in isotropic media. *IEEE Transactions on Antennas and Propagation*, 14(3), 302–309.
- Zanoubi, M. R., Jin, J. M., Donepudi, K. C., and Chew, W. C. (1999). A spectral Lanczos decomposition method for solving 3-D low-frequency electromagnetic diffusion by the finite-element method. *IEEE Transactions on Antennas and Propagation*, 47(2), 242–248.
- Zhao, L., and Cangellaris, A. C. (1996). GT-PML: Generalized theory of perfectly matched layers and its application to the reflectionless truncation of finite-difference time-domain grids. *IEEE Transactions on Microwave Theory and Techniques*, 44(12), 2555–2563.
- Zyserman, F. I., and Santos, J. E. (2000). Parallel finite element algorithm with domain decomposition for three-dimensional magnetotelluric modelling. *Journal of Applied Geophysics*, 44(4), 337–351.